Water Penetration in Solid Clay Brick Masonry and its Mitigation by Repointing

Kahangi, Mohammad

2024

Document Version:
Publisher's PDF, also known as Version of record

Link to publication

Citation for published version (APA):
Kahangi, M. (2024). *Water Penetration in Solid Clay Brick Masonry and its Mitigation by Repointing*. Department of Building and Environmental Technology, Lund University.

Total number of authors:
1

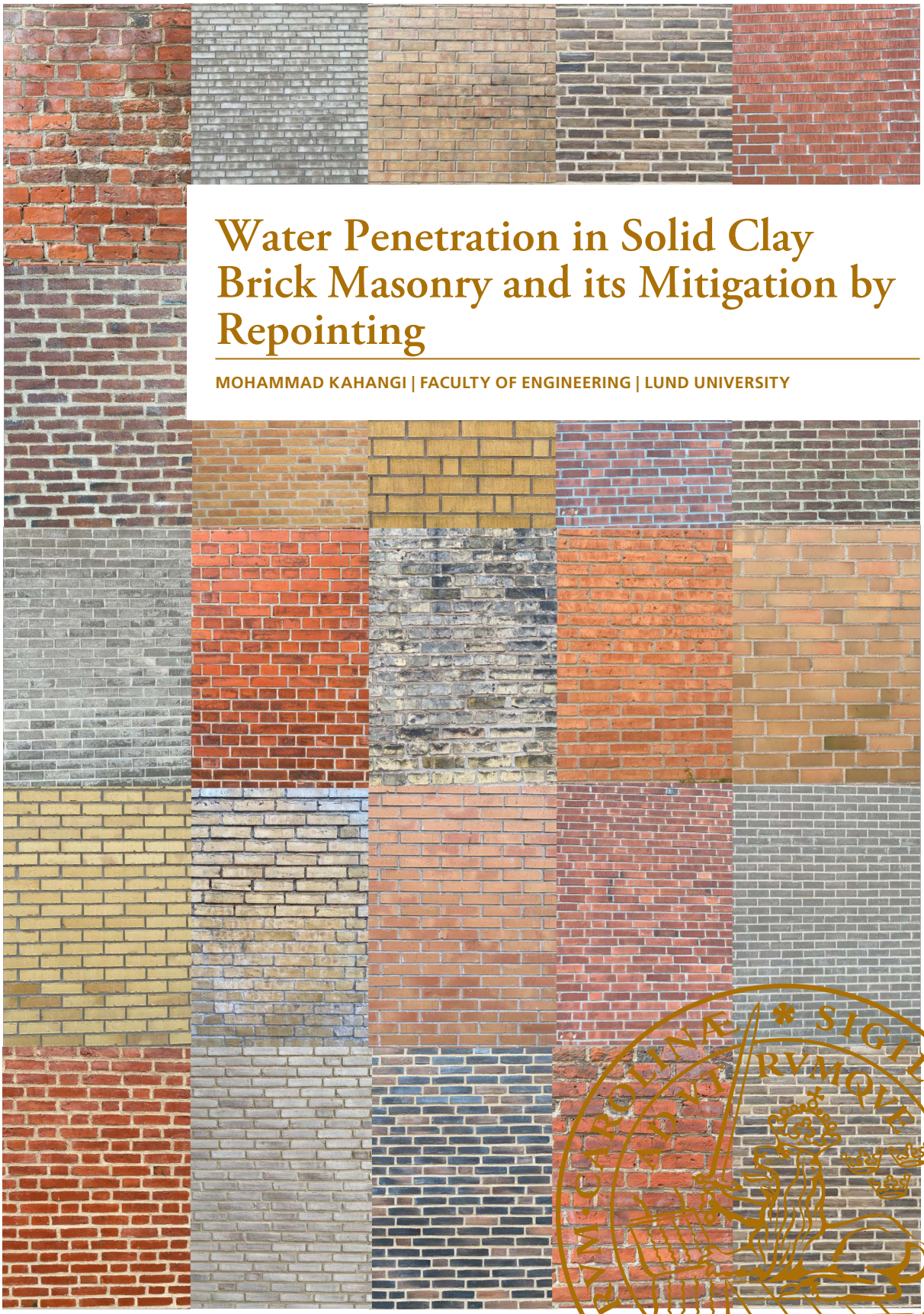

Water Penetration in Solid Clay Brick Masonry and its Mitigation by Repointing

MOHAMMAD KAHANGI | FACULTY OF ENGINEERING | LUND UNIVERSITY

Water Penetration in Solid Clay Brick Masonry and its Mitigation by Repointing

Mohammad Kahangi | Faculty of Engineering | Lund University

Water Penetration in Solid Clay Brick Masonry and its Mitigation by Repointing

by Mohammad Kahangi

LUND UNIVERSITY

DOCTORAL DISSERTATION

Doctoral dissertation for the degree of Doctor of Philosophy (Ph.D.) at the Faculty of Engineering at Lund University to be publicly defended on the 13th of September 2024, at 10:15 in the lecture hall V:A, Department of Building & Environmental Technology, V-Huset, John Ericssons väg 1, Lund

Faculty opponent
Professor Tore Kvande
Norwegian University of Science and Technology

Organization
LUND UNIVERSITY
Department of Building and Environmental Technology
Division of Structural Engineering
Box 118, SE–221 00 LUND, Sweden

Document name
DOCTORAL DISSERTATION

Date of disputation
2024-09-13

Author(s)
Mohammad Kahangi

Sponsoring organization
SBUF & TMPB

Title and subtitle
Water Penetration in Solid Clay Brick Masonry and its Mitigation by Repointing

Abstract

Clay brick masonry façades are widely used because of their extended durability and aesthetic appeal. They also offer good protection against wind-driven rain (WDR), one of the most common moisture sources in Northern Europe. In clay brick masonry, WDR is associated with elevated water content and the possibility of water penetration, which may negatively impact the hygrothermal performance of building envelopes. Maintenance measures are thus recommended to address elevated moisture content and water penetration associated with WDR, where repointing is a commonly used maintenance technique. Presently, in Sweden, repointing is typically scheduled every 40–50 years from the construction of the building, regardless of the condition of the façade. Given that repointing is a labor-intensive and expensive undertaking, there is a pressing need for a systematic approach to evaluating the necessity for repointing based on rational grounds.

Within this Ph.D. project, a new laboratory test setup is developed to study water absorption and penetration in clay brick masonry. The key feature is to enable uniform water spray exposure at considerably lower water spray rates than in existing test setups while continuously recording both the amount of absorbed and penetrated water. The developed test setup is used in four experimental campaigns to study the interaction of clay brick masonry exposed to water spray.

In the first two experimental campaigns, two series of clay brick masonry specimens without known cracks, built with two different types of bricks and three different mortar joint profiles, are exposed to water spraying. The obtained results indicate that in clay brick masonry without known cracks, water penetration starts when the masonry is nearly saturated (average moisture content above 90% saturation level). As there is a lack of consensus regarding the quantity of WDR penetration through clay brick masonry claddings and the appropriate methodology for incorporating penetration in hygrothermal analyses, a novel water penetration criterion in clay brick masonry is introduced.

As cracks provide low resistance pathways for water penetration, clay brick masonry specimens with different crack widths, created artificially, are exposed to water spray in the third campaign. Subsequently, in the fourth campaign, specimens tested in the third campaign were repointed and tested once again to study the effect of repointing on water absorption and penetration in clay brick masonry. The results indicate a reasonable correlation between the crack width and the average water penetration rate. Further, a strong correlation is observed between the saturation level and the start of water penetration; the larger the crack width, the lower the saturation level at the start of water penetration. The obtained results suggest that repointing can effectively reduce water penetration in cracked clay brick masonry.

Finally, the experimental results are implemented in hygrothermal simulations, providing an understanding of scenarios where repointing may mitigate moisture risks in building envelopes. The results of the simulations suggest that repointing has the potential to notably decrease the mold risk of timber frame walls and reduce the moisture content of autoclaved aerated concrete (AAC) walls. The positive effects of repointing are particularly pronounced when the brick veneer exhibits signs of poor workmanship or visible cracks, especially when walls are exposed to high WDR loads.

Keywords: **clay brick masonry, cracked masonry, repointing, wind-driven rain (WDR), water absorption, water penetration, damp patches**

Classification system and/or index terms (if any)

ISRN
LUTVDG/TVBK-1059/24-SE(129)

Language
English

ISSN and key title
0349-4969

ISBN 978-91-8104-062-3 (print)
ISBN 978-91-8104-063-0 (electronic)

Recipient's notes

Number of pages 123

Price

Security classification

Signature

Date 2024-07-10

Water Penetration in Solid Clay Brick Masonry and its Mitigation by Repointing

by Mohammad Kahangi

LUND
UNIVERSITY

Cover photo by Mohammad Kahangi

Faculty of Engineering
Department of Building & Environmental Technology
Division of Structural Engineering

Report TVBK-1059
ISBN 978-91-8104-062-3 (print)
ISBN 978-91-8104-063-0 (electronic)
ISSN 0349-4969
ISRN LUTVDG/TVBK-1059/24-SE(129)

Printed in Sweden, V-huset, Lund University
Lund 2024

Table of Contents

Acknowledgments

I would like to express my deepest gratitude to my supervisor, Dr. Miklós Molnár, for his exceptional guidance and support throughout my study. He is a generous, supportive, caring, and intelligent person whom I admire the most and appreciate working with. I consider him the best academic father, and I am forever grateful for his mentorship and guidance. Thank you for being a source of inspiration for my growth and success. Thank you sincerely for all your encouragement, exceptional guidance, sharing your knowledge, and always providing valuable feedback that has played an instrumental role in shaping my academic journey.

I am also deeply grateful to my co-supervisor, Dr. Jonas Niklewski, for his invaluable input, programming skills, and expertise in image analysis. His friendship, patience, and contributions have been truly invaluable to the project. I will always cherish our meaningful and insightful discussions throughout this journey. Thank you for being there to listen and provide support whenever I needed to vent. Your presence has made a significant difference, and I am truly grateful to have you by my side. Thank you for being such a remarkable friend and colleague.

I extend my gratitude to my co-supervisor, Tekn Lic. Tomas Gustavsson, for consistently offering valuable insights on masonry and providing constructive feedback. Thank you for sharing practical examples and extensive knowledge in the field. I would also like to express my appreciation to my co-supervisor, Dr. Akram Abdul Hamid, who joined me during the second half of my Ph.D. journey. Thank you for enhancing my understanding of building physics and assisting me in exploring numerical simulations more deeply.

I would like to extend my thanks to my co-supervisor, Dr. Ivar Björnsson, for his excellent guidance and support during this project. I have learned a great deal from him, particularly in improving my teaching skills. I also want to thank Dr. Eva Frühwald Hansson for being an exceptional and caring boss throughout my journey. Her support and provision of everything I needed for my career development have been invaluable. I am grateful for the opportunities she provided and the guidance she offered. I also would like to extend my gratitude to other colleagues at the Division of Structural Engineering, whose support and collaboration have played a significant role in shaping my research and personal development.

I am immensely grateful for the financial support provided by the Development Fund of the Swedish Construction Industry (SBUF) and the Masonry and Render

Construction Association (TMPB). Without their funding, this project would not have been feasible. I would also like to express my appreciation to all the reference group members, with special mention to Anders Planensten and Frej Josefsson. Their interest in my work, provision of materials, and sharing of knowledge and expertise in the field have been invaluable. I am sincerely thankful for their contributions to the project.

I also deeply appreciate the support Mr. Per-Olof Rosenkvist and Mr. Martin Gunder provided. Their cooperation was essential in facilitating the experimental part of the project. This research would not have been possible without their assistance in developing the test set-up and preparing the specimens. I am grateful to the Division of Building Materials for providing lab space essential to my research for this study.

Thanks to all my dearest friends/colleagues, including Iman, Amro, Oskar, Mohammad, Jie, Simone, Behshid, Hossein, Hassan, Amir, Shokoufeh, Shifteh, Kavan, Marziyeh, Amirhosein, Kourosh, and Alireza. Your kindness throughout my thesis journey and presence in the Fika room has been truly invaluable. Thank you, Jie, for your invaluable support during my Ph.D. I am particularly grateful for your encouragement to explore beyond the confines of my office and embrace the wonders of nature. I want to extend a special thank you to Oskar for our meaningful/hilarious conversations. Your suggestions, feedback on my work, and support in integrating with the new culture have been incredibly valuable to me.

To Amro and Iman, thank you for your presence and support during my intense period. Your friendship and support have made a significant difference. I am grateful to each and every one of you for being a part of my academic and personal growth. Thank you, Iman, for your support and friendship throughout my academic and non-academic endeavors. Thank you for being there for me, Iman.

I would like to extend special thanks to my non-academic friends within the Iranian community in Skåne, including Mojdeh, Reza, Shahrzad, Ghasem, Faezeh, Saeid, Pooneh, Hamid, Sedi, Majid, and Parnam. Your presence has made my five-year Ph.D. journey in Lund more exciting and pleasant. Your friendship, support, and shared experiences have brought joy to my life. Thank you all for being an integral part of my journey.

I would also like to extend my heartfelt thanks to my family, especially my parents. Their unconditional love, encouragement, and constant support have been instrumental in my academic pursuits. Thank you for always being there for me and for being my rock throughout this journey. To my beloved wife, Zeinab, words cannot express the depth of my gratitude for your support, boundless love, and constant presence by my side throughout my thesis journey and beyond. Her patience and encouragement throughout my study have been invaluable to me. I want to express my heartfelt thanks for the joy and happiness she brings into my life. Regardless of my ups and downs, she has remained my strongest source of support and unwavering backing.

Popular science summary

Clay brick masonry façades are widely used because of their extended durability and aesthetic appeal. They also offer good protection against wind-driven rain (WDR), one of the most common moisture sources in Northern Europe. In clay brick masonry, WDR is associated with elevated water content and the possibility of water penetration, which may negatively impact the hygrothermal performance of building envelopes. Maintenance measures are thus recommended to address elevated moisture content and water penetration associated with WDR, where repointing is a commonly used maintenance technique. Presently, in Sweden, repointing is typically scheduled every 40–50 years from the construction of the building, regardless of the condition of the façade. Given that repointing is a labor-intensive and expensive undertaking, there is a pressing need for a systematic approach to evaluating the necessity for repointing based on rational grounds.

Within this Ph.D. project, a new laboratory test setup is developed to study water absorption and penetration in clay brick masonry. The key feature is to enable uniform water spray exposure at considerably lower water spray rates than in existing test setups while continuously recording both the amount of absorbed and penetrated water. The developed test setup is used in four experimental campaigns to study the interaction of clay brick masonry exposed to water spray.

In the first two experimental campaigns, two series of clay brick masonry specimens without known cracks, built with two different types of bricks and three different mortar joint profiles, are exposed to water spraying. The obtained results indicate that in clay brick masonry without known cracks, water penetration starts when the masonry is nearly saturated (average moisture content above 90% saturation level). As there is a lack of consensus regarding the quantity of WDR penetration through clay brick masonry claddings and the appropriate methodology for incorporating penetration in hygrothermal analyses, a novel water penetration criterion in clay brick masonry is introduced.

As cracks provide low resistance pathways for water penetration, clay brick masonry specimens with different crack widths, created artificially, are exposed to water spray in the third campaign. Subsequently, in the fourth campaign, specimens tested in the third campaign were repointed and tested once again to study the effect of repointing on water absorption and penetration in clay brick masonry. The results indicate a reasonable correlation between the crack width and the average water

penetration rate. Further, a strong correlation is observed between the saturation level and the start of water penetration; the larger the crack width, the lower the saturation level at the start of water penetration. The obtained results suggest that repointing can effectively reduce water penetration in cracked clay brick masonry.

Finally, the experimental results are implemented in hygrothermal simulations, providing an understanding of scenarios where repointing may mitigate moisture risks in building envelopes. The results of the simulations suggest that repointing has the potential to notably decrease the mold risk of timber frame walls and reduce the moisture content of autoclaved aerated concrete (AAC) walls. The positive effects of repointing are particularly pronounced when the brick veneer exhibits signs of poor workmanship or visible cracks, especially when walls are exposed to high WDR loads.

Sammanfattning

Ytterväggar av tegelmurverk (tegelfasader) är ofta förknippade med långsiktig beständighet och estetiskt tilltalande åldrande. De erbjuder även högt motstånd mot slagregn, som är en av de vanligaste fuktkällorna i fasader i norra Europa. Slagregnsutsatta tegelfasader kännetecknas av periodvis förhöjda fuktnivåer och förhöjd risk för regngenomslag, tillstånd som kan medföra fuktrelaterade problem. För att hantera fuktrelaterade problem kopplade till slagregn, underhåll kan behöva utföras. En vanligt förekommande underhållsåtgärd är omfogning. Enligt svensk praxis omfogas tegelfasader vart fyrtio- till femtionde år, vanligtvis utan någon kartläggning av fasadens tillstånd. Med tanke på att omfogning är en arbetsintensiv och därmed dyr åtgärd, finns ett behov av ett mer rationellt angreppssätt för beslut om omfogning.

Inom doktorandprojektet har ett nytt försöksupplägg utvecklats för att i labbmiljö studera vattenupptagning i och vattenläckage genom tegelmurverk. En viktig aspekt i samband med den experimentella utvecklingen har varit möjligheten att bespruta murverket med en regnliknande droppsvärm av varierande intensitet, under kontinuerlig mätning av både vattenupptagning och läckage. Sammanlagt genomfördes fyra försöksserier.

I de två första försöksserierna tillverkades provkropparna av två olika sorters tegel, med tre olika fogtyper. Provkropparna innehöll inte några kända brister, såsom sprickor. Resultaten av vattenbesprutningsförsöken pekar mot att läckage inträffar först när murverket uppnår en fuktkvot motsvarande cirka 90 procent av vattenmättnad. Baserat på detta resultat, ett nytt kriterium för när vattenläckage kan äga rum i tegelmurverk har formulerats. Det nya kriteriet bör ses mot bakgrund av att det bland experter råder oenighet om hur regngenomslag bör hanteras i samband med fuktberäkningar.

Sprucket murverk har lägre motstånd mot regngenomslag. I den tredje respektive fjärde försöksserien vattenbesprutades provkroppar med konstgjorda sprickor med varierande vidd, före och efter omfogning. Resultaten visar att det finns en rimlig korrelation mellan sprickvidd och vattenläckagets intensitet samt att ökande sprickvidd medför att läckaget startar snabbare. Försöken visar också att omfogning har en tydlig positiv effekt när det gäller att begränsa läckage i vattenbesprutat tegelmurverk.

Slutligen, resultaten från försöken har använts i fuktberäkningar, med syfte att visa på fall då omfogning kan påverka risken för fuktproblem i byggnadsskalet. Beräkningarna visar att omfogning påtagligt kan minska risken för mögelangrepp i ytterväggar bestående av tegelskalmurar med bakomliggande träväggar eller fuktigheten i bakmurar av lättbetong. Omfogningens positiva effekter är särskilt tydliga när tegelskalmuren innehåller större sprickor eller uppvisar tecken på bristfälligt hantverk. De positiva effekterna är tydligast i väggar utsatta för stora mängder slagregn.

Nomenclature

Terminology

Bounce-off [-]	*is defined as the portion of WDR or water spray that bounces off or splashes back from the surface of masonry, rendering it inaccessible for absorption.*
Leakage [%]	*is defined as the ratio between the amount of water penetration [kg/m^2] and the amount of sprayed water [kg/m^2].*
Penetration rate [kg/(m^2.h)]	*is defined as the ratio between the average amount of water penetration [kg/m^2] and the difference between the total spraying time and the time at the start of water penetration.*
Water absorption [kg/m^2]	*is defined as the amount of absorbed water [kg] per unit area of the masonry specimen [m^2].*
Water penetration	*refers to the permeation of rainwater through brick masonry, measured as water reaching the backside of the brick wall and discharging into the cavity.*
Water penetration [kg/m^2]	*is defined as the amount of water [kg] that can be collected from the backside of a masonry specimen divided by its exposed area [m^2].*

Abbreviations

ACR	Air Change Rate
ASHRAE	American Society of Heating, Refrigeration and Air-Conditioning Engineers
ASTM	American Society for Testing and Materials
CoV	Coefficient of Variation
IRA	Initial Rate of Absorption

ISO	International Organization for Standardization
MRD	Mold Resistance Design
SF	Sharp Front
SMHI	Swedish Meteorological and Hydrological Institute
WDR	Wind-Driven Rain

Latin letters

A	Cross-sectional area	m^2
A_w	Water absorption coefficient	$kg/(m^2.s^{0.5})$
C_R	Terrain roughness coefficient	-
C_T	Topography coefficient	-
D	Length of crack /Width of opening	m
F_s	Surface tension force	N
G	Water quantity available to penetrate a horizontal crack	kg/h
g_{abs}	Absorption flux	$l/(m^2.s)$
g_r	Gravitational acceleration	m^2/s
g_s	Water spray rate	$l/(m^2.h)$ or $kg/(m^2.h)$
H	Height above the crack	m
h	height of the water column	m
h_B	Film thickness by Beijer [1]	mm
h_{Ex}	Film thickness from Experiment	mm
h_{tN}	Film thickness Predicted Numerically by Blocken & Carmeliet [2]	mm
I_A	Annual WDR index	l/m^2
K_R	Terrain factor	-
$K(\vartheta)$	Liquid conductivity	m/s
k	Permeability	m^2
m	Absorbed mass	kg
O	Obstruction factor	-

P_c	Capillary pressure	Pa
P_h	Hydrostatic pressure	Pa
P_s	Pressure due to surface tension	Pa
P_w	Wind pressure	Pa
p	Porosity	-
Q	Absorbed water	kg/m^2
Q_f	Volumetric flow rate	m^3/s
q_{runoff}	Runoff rate	l/(m.h)
R_h	Rainfall through the horizontal plane	mm/h
R_{WDR}	WDR intensity	mm/h or mm/s
r	radius	m
S	Sorptivity	$m/min^{1/2}$
t	Duration	s
t_f	Time to film formation	s
U & v	Wind velocity	m/s
U_{10}	Reference wind speed	m/s
$U_{terminal}$	Terminal velocity of the droplet	m/s
u	Flow rate	m/s
u(y)	Transverse water film velocity	m/s
w_0	Initial weight	kg
w_i	Weight at the time i	kg
W	Wall factor	-
x	Length	m
z	Height above ground	m
z_{min}	Minimum height	m
z_0	Roughness length	m
Δp	Pressure gradient	Pa

Greek letters

α	WDR coefficient	s/m
β	Wall inclination	°
γ	Surface tension	N/m
η	Factor varying between 0 and 1 [3]	-
θ	Angle	°
ϑ	Water content	-
μ	Dynamic viscosity	Pa.s
μ_c	Capillary resistance number	s/m^2
ν	Kinematic viscosity	m^2/s
ρ	Density	kg/m^3
ρ_{air}	Air density	kg/m^3
ρ_w	Water density	kg/m^3
$\nabla\varphi$	Gradient of the capillary potential	-

Publications

Appended papers

I. *Making decision on repointing of clay brick facades on the basis of moisture content and water absorption tests results – a review of assessment methods*
Kahangi Shahreza, S., Molnár, M., Niklewski, J., Björnsson, I. & Gustavsson, T. Proceedings of the 17th International Brick/Block Masonry Conference (17th IB2MaC 2020), July 5-8, 2020, Kraków, Poland.
doi: http://dx.doi.org/10.1201/9781003098508-86

II. *Experimental investigation of water absorption and penetration in clay brick masonry under simulated uniform water spray exposure*
Kahangi Shahreza, S., Niklewski, J. & Molnár, M., (2021)
Journal of Building Engineering. 43, p. 102583
doi: https://doi.org/10.1016/j.jobe.2021.102583

III. *Novel water penetration criterion for clay brick masonry cladding*
Kahangi Shahreza, S., Niklewski, J. & Molnár, M., (2022)
Construction and Building Materials. 353, 129109.
doi: https://doi.org/10.1016/j.conbuildmat.2022.129109

IV. *Impact of different water penetration criteria and cavity ventilation rates on the risk of mold growth in timber frame walls with brick veneer cladding*
Kahangi Shahreza, S. & Abdul Hamid, A.
Journal of Physics: Conference Series, Volume 2654, 13th Nordic Symposium on Building Physics (NSB-2023) June 12-14, 2023, Aalborg, Denmark.
doi: 10.1088/1742-6596/2654/1/012028

V. *Water penetration in cracked clay brick masonry before and after repointing*
Kahangi Shahreza, S., (2024)
Construction and Building Materials. 420, 135631.
doi: https://doi.org/10.1016/j.conbuildmat.2024.135631

VI. *Towards rational decision-making on repointing to mitigate moisture damage in building envelopes: a probabilistic study*
Kahangi Shahreza, S., Bayat Pour, M., & Abdul Hamid, A., (2024)

Developments in the Built Environment. 19, 100510.
doi: https://doi.org/10.1016/j.dibe.2024.100510

Author's contribution to appended papers

I. The author conducted the literature review and prepared the figures and tables. The author wrote the manuscript and revised it based on the feedback received from the co-authors.

II. The author developed the test setup and conducted experimental studies. The author analyzed the experimental results, while the second author did the image analysis part. Eventually, the author wrote the original draft, which the second and third authors then reviewed.

III. The author conceptualized the study, conducted experimental studies and numerical simulations, and investigated the results accordingly. The manuscript was written under the supervision of the second and third authors.

IV. The author ran numerical simulations and analyzed the results that were obtained. The manuscript was originally written by the author and then revised with the help of the second author.

V. The author did all of the work, including conceptualizing the framework of the study and conducting the experimental studies accordingly. The author did the analysis of the results, followed by writing the manuscript.

VI. The author conceptualized the framework of the study and analyzed the results. Numerical simulations were performed with the help of the second author. The author then wrote the manuscript and revised it according to the comments received from the co-authors.

Other related publications

Scientific contributions not included in the present thesis:

Journal papers

A. *Impact of extruded mortar joints on the hygrothermal performance of brick veneer walls: A probabilistic study*
Bayat Pour, M. & **Kahangi Shahreza, S.,** (2024)
Journal of Building Engineering. 94, p. 109936
doi: https://doi.org/10.1016/j.jobe.2024.109936

Conference papers

A. *Water absorption and penetration in clay brick masonry exposed to uniform water spray*
Kahangi Shahreza, S., Molnár, M., & Niklewski, J.
Proceedings of the 14th Canadian Masonry Symposium (14th CMS 2021), May 17-20, 2021, Montreal, Canada.

B. *Experimental investigation of water penetration in clay brick masonry with artificial cracks*
Kahangi Shahreza, S., Niklewski, J. & Molnár, M.
Proceedings of the 14th North American Masonry Conference (14th NAMC 2023), June 12-14, 2023, Omaha, NE, USA.

C. *Strategies for Enhanced Energy Efficiency and Moisture Management in Brick–AAC Cavity Walls*
Kahangi Shahreza, S., Bayat Pour, M., Abdul Hamid, A., & Molnár, M.
Proceedings of the 18th International Brick and Block Masonry Conference (18th IB^{2}MaC 2024), July 21-24, 2024, Birmingham, England.

D. *Effect of extruded mortar joints on mould growth in timber frame wall with brick veneer: Probabilistic and Machine Learning Modelling*
Bayat Pour, M., **Kahangi Shahreza, S.**, & Abdul Hamid, A.
Proceedings of the 9th International Building Physics Conference (9th IBPC 2024), July 25-27, 2024, Toronto, Canada.

Licentiate thesis

A. *Resistance of Clay Brick Masonry Façades to Wind-Driven Rain: Repointing of Eroded Mortar Joints*
Kahangi, M., 2021, Lund University. 63 p. ISBN 978-91-87993-20-6.

Popular science articles

A. *Omfogning av tegelfasader (Repointing of clay brick façades)*
Kahangi, M., Molnár, M., Gustavsson, T., Onno, J. & Planensten, A.
2020 Apr 2, Bygg & teknik, 2/20 3 p.

B. *Leder eroderade fogar till förhöjd vattenupptagning från slagregn? (Do eroded joints lead to increased water absorption from wind-driven rain?)*
Kahangi, M., Molnár, M., Niklewski, J., & Gustavsson, T.
2021 Mar 30, Bygg & teknik, 2/21 3 p.

C. *När behöver en tegelfasad fogas om? (When a clay brick façade needs to be repointed?)*
Kahangi, M., Molnár, M.
2023 Jun 7, Husbyggaren, 3/23 4 p.

1 Introduction

1.1 Background

Clay brick masonry has a history spanning thousands of years and is widely used for load-bearing walls and façades. Its extensive and enduring use highlights its exceptional durability and long-term performance. Despite the longevity and durability, exposure to particular climate conditions, particularly wind-driven rain (WDR), can gradually deteriorate brick masonry. This exposure poses significant moisture-related risks to building envelopes [4, 5]. WDR, specifically, stands as a prominent moisture source, contributing to premature building deterioration and raising concerns about increased water content and potential water penetration in masonry walls [6].

In Sweden, the use of solid masonry walls reached its peak during the late 19th and early 20th centuries. However, with the development of building codes, energy efficiency demands, and increased housing/building values, buildings have transitioned to taller structures with thinner walls, many built with brick masonry veneer walls. In order to mitigate potential moisture-related risks from WDR, solid masonry walls mainly utilize the so-called “mass or moisture storage” strategy. This involves absorbing and storing WDR that enters the exterior surface during rain events, followed by gradual release through diffusion and evaporation [7]. In contrast, clay brick veneers, which are much thinner, are more vulnerable to WDR penetration. The water penetration can, in turn, facilitate microbiological growth [8, 9], negatively impact the hygrothermal performance and durability of building envelopes [10, 11], as well as damage bio-based wall components [12].

Aside from rainwater, other sources of moisture in wall assemblies include condensation, rising dampness, snow melt, and the initial moisture content of the building materials used. While all the aforementioned moisture sources influence the hygrothermal performance and durability of building façades, water penetration is considered one of the most critical factors. The presented thesis thus focuses explicitly on water penetration in clay brick masonry and repointing as a possible measure to limit water penetration from WDR.

Repointing involves raking out the existing mortar up to around 25 mm depth and replacing it with a new mortar. In practice, this process is commonly part of the regular maintenance scheme for a building and is often carried out 40–50 years after

the building's erection. In other cases, repointing may be carried out when there are observations of eroded mortar joints, cracks in the mortar, gaps between the mortar and masonry unit, damp surfaces on the masonry, or water penetration [13, 14].

It has been claimed that repointing can effectively mitigate moisture/water penetration in brick masonry façades related to WDR [13-16]. However, there is a scarcity of studies investigating the actual impact of repointing on water penetration [17, 18]. On the other hand, repointing may also be adopted solely for aesthetic improvements. These situations can, however, be dealt with using alternative measures (e.g., cleaning) and may not be suitable due to the associated high costs and laborious procedures. Another relevant issue concerns the consequences of improper repointing practices. Improper repointing can, in fact, lead to premature deterioration of the mortar and masonry units, including erosion of the edges of soft masonry units and discoloration of the masonry units. Hence, it is essential to understand the effects of repointing better and be able to identify situations where its application is necessary. For instance, one of the main motivations for repointing in practice is eroded mortar joints. However, the decision on whether to repoint in these cases depends less on the mortar joint erosion itself and more on how this influences water absorption and penetration. In order to investigate this issue further, it is imperative to gain a comprehensive understanding of the basic interaction of clay brick masonry façades exposed to realistic WDR intensities.

Water penetration in masonry walls arises from a combination of factors, including the presence of water on a wall, openings that allow for its passage, and driving forces that draw or drive the water inward [19-22]. When wind and rain co-occur (i.e., WDR), the driving rain vector becomes oblique, and the water is transported through the wall in several different ways. While the brick-mortar interfacial zone is often cited as the primary path offering the least resistance [12, 23-25], other deficiencies like cracks and voids increase water penetration considerably [15, 22, 26, 27].

Water penetration arising from WDR depends on several factors such as climate conditions (WDR intensity and wind pressure) [28, 29], water flow pattern, the presence and size of openings or deficiencies [15], the type and quality of masonry units [12, 30, 31], the type of mortar and its consistency [12, 23], the compatibility of units and mortar [12, 32], joint thickness [32, 33], the profile of mortar joints [33, 34], and the workmanship [12, 23]. Owing to the complexity of the phenomenon, there is no general agreement on how to determine the amount of water that penetrates through brick masonry claddings nor how to consider this penetration in hygrothermal analyses [10, 11, 28, 29, 35].

Different standards and research studies have proposed various test setups to explore water penetration [12, 23, 36-41]. These setups often involve applying high water spray rates and differential air pressure representing extreme WDR conditions, yet initially developed with the aim of classifying façade components [12, 23, 36-40,

42-45]. However, for research purposes, several authors have pointed out the need to develop a simple test setup that can operate at considerably lower water application rates to understand better the interaction between masonry façade and frequently encountered WDR [12, 24, 29, 36, 46, 47]. Accordingly, several studies were carried out that applied alternative test conditions, including differential air pressure [23, 43, 48, 49] and water spray rate [24, 50, 51]. In order to better understand brick masonry resistance to WDR for existing buildings, the test parameters need to be adapted to be representative of the frequently encountered WDR events in the studied location.

1.2 Objectives and research questions

The present thesis aims to achieve two primary objectives. Firstly, it seeks to provide a better understanding of the response of clay brick masonry when exposed to more realistic and commonly encountered WDR events, with a focus on Swedish climate conditions. The knowledge gained is intended to enhance the assessment of moisture safety performance in building envelopes and contribute towards improved hygrothermal assessment of walls with brick masonry claddings. The second main objective is to explore how repointing mitigates moisture-related issues, specifically water penetration within building envelopes. The outcomes of this research are expected to yield scientifically grounded knowledge that can aid in assessing the need for repointing. Ultimately, this information will support the establishment of a framework to facilitate informed decision-making regarding repointing practices. The two main objectives can be broken into a number of explicit research questions, including the following:

Q1- What are the critical factors influencing the resistance of clay brick masonry to WDR?

Q2- How does WDR affect water absorption and penetration of clay brick masonry under different exposure conditions?

Q3- How does the presence of cracks or imperfections in clay brick veneers impact water penetration?

Q4- How does repointing influence brick masonry's response to WDR regarding water absorption and penetration?

Q5- In what scenarios can repointing of clay brick veneers be used as an effective measure to mitigate moisture-related risk in building envelopes?

Q6- How can knowledge gained from experimental studies on clay brick masonry response to WDR be utilized to improve the hygrothermal assessment of building envelopes and enhance risk-aware judgments regarding moisture safety?

1.3 Research methodology

The research questions presented above were addressed through a combination of experimental studies accompanied by numerical simulations. Initially, a comprehensive literature review was conducted on field and laboratory methodologies for assessing water content and water uptake caused by WDR. Subsequently, two experimental campaigns were carried out assessing the impact of various parameters, including brick absorption properties and mortar joint profiles, on water absorption and penetration in masonry when exposed to water spray. A third campaign was then designed and carried out to investigate how cracks influence water penetration in brick masonry. This was followed by a fourth campaign, which investigated the effects of repointing the cracked specimens. The aim was to study the effect of repointing on water absorption response and penetration of masonry exposed to water spray. Apart from the experimental work, two hygrothermal simulation studies were also conducted with the aim of exemplifying how the experimental outcomes could be implemented into hygrothermal simulations. The focus of the hygrothermal studies was on assessing the potential of repointing to mitigate moisture-related issues. Figure 1 illustrates the methodology framework (the related research questions are provided in parentheses; see Section 1.2).

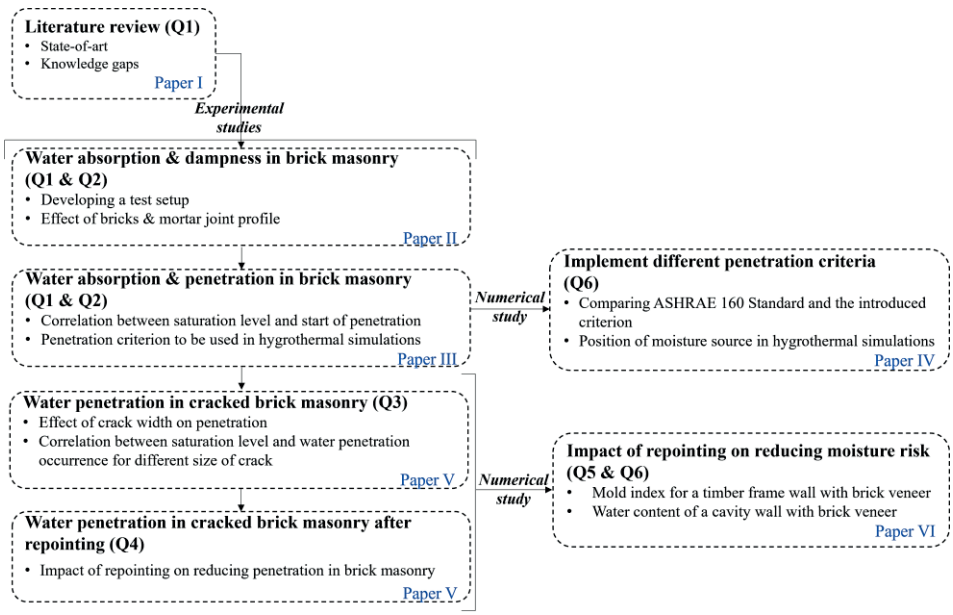

Figure 1. Research methodology framework

1.4 Limitations

The experimental investigations presented here are limited to studying the exposure of small-scale brick masonry specimens to uniform water spray, whereas a masonry façade includes windows, joints, and other connections that are expected to be more vulnerable to WDR exposure. While the study aims to quantify water penetration in brick masonry claddings, it is acknowledged that the prepared specimens may not fully represent real-world brick claddings, as they were built with only one head joint. Although this configuration probably reduced the likelihood of unintended disintegration of the specimens, it also meant that the percentage of head joints was lower than in existing real-world masonry – regardless of the bond type.

Apart from hydrostatic pressure due to runoff, air pressure differences due to wind can also contribute to driving water penetration. The experimental campaigns within this study were conducted without air pressure differential. Additionally, the experimental study on cracked masonry presented here is limited to 3-course masonry prisms containing an artificial through crack positioned in the bed joint. While this type of crack is examined, it is important to recognize that cracks can be formed in any size or location in masonry veneers, rendering the present study challenging to apply for the hygrothermal analysis of all crack types/sizes. Cracks that form in the head joints or hairline cracks, commonly found in masonry veneers, have the potential to alter the resistance of brick masonry to WDR.

The decision regarding repointing is motivated by the desire to preserve the integrity of the structure, enhance resistance to WDR, and improve its aesthetic appearance. However, this study solely evaluates the effect of repointing on mitigating moisture-related issues. It is worth noting that the study is limited to examining the short-term performance of repointed walls, as it only considers the effect of repointing after a one-time exposure to water spray. Due to time restrictions, the investigation lacks an examination of the long-term performance of repointed walls.

1.5 Outline of the thesis

The thesis is organized into nine chapters, which are outlined below. Following these chapters, the research papers that form the substance of this dissertation are included as appendices. The main findings extracted from the papers are included in these chapters; however, reading the papers themselves is suggested for a more thorough insight into the topic.

Chapter 2: Introduction to the durability of brick masonry and measures for maintenance with a focus on repointing

This chapter introduces the concept of brick masonry durability and explores various measures to maintain brick masonry claddings. The primary focus is on repointing, a common maintenance technique in Sweden.

Chapter 3: Interaction between brick masonry and wind-driven rain (WDR)
This chapter presents a widely used semi-empirical model to quantify WDR deposited on building façades. Then, it discusses the interaction between brick masonry and WDR, focusing on water penetration as a major source affecting the hygrothermal performance of building envelopes.

Chapter 4: Experimental campaigns on water penetration in clay brick masonry
A novel test setup (developed during this project) to study masonry exposed to water spraying is first described. Subsequently, the results of experimental campaigns regarding water absorption, water penetration, and damp patches in brick masonry are presented. Water penetration is investigated for brick masonry with and without known cracks, providing insights into the impact of cracks on water penetration.

Chapter 5: Introducing a novel criterion for water penetration and implementing it into hygrothermal simulations
Based on the results presented in Chapter 4, a novel criterion for water penetration in brick masonry is introduced. This criterion is then implemented into hygrothermal simulations, allowing for a more thorough analysis of moisture-related risks, including mold growth.

Chapter 6: Experimental study on water penetration in masonry after repointing
The findings of an experimental study conducted on water penetration in masonry after repointing are presented. The obtained results are then implemented in hygrothermal simulations, providing an understanding of scenarios where repointing may mitigate moisture risks in building envelopes.

Chapter 7: Conclusions
The chapter summarizes the main findings and discusses their implications. It reflects upon how the research successfully fulfilled its aims and addressed the research questions outlined earlier.

Chapter 8: Suggestions for future research
This chapter suggests areas for future research in the field of water penetration in brick masonry and repointing. It highlights potential directions for the advancement of the subject matter.
Chapter 9: Summary of appended papers
The final chapter of the thesis briefly summarizes the appended papers and their key findings. It serves as a concise overview of the research conducted throughout the Ph.D. project.

2 Clay brick masonry in the building envelope

This chapter begins by discussing the durability and long-term performance of brick masonry façades, with a specific focus on the impact of different climate agents, particularly wind-driven rain (WDR), as the primary moisture source in Nordic countries. The deterioration of brick masonry walls due to climate exposure necessitates regular maintenance. Accordingly, some maintenance measures, including repointing, are discussed. The process of repointing to deal with moisture-related problems is further presented. The motivations behind making informed decisions on repointing are discussed in detail.

2.1 Background

Brick masonry has a rich history as a construction material, frequently used in building enclosure walls that separate interior and exterior spaces. Until the mid-twentieth century, clay bricks were typically used in single-leaf walls in European countries. These walls played a crucial structural role in maintaining building stability. However, the advent of alternative structural solutions, like reinforced concrete, led to a shift in the role of masonry walls from structural to non-loadbearing elements [52].

Further, enclosure walls were commonly built as masonry cavity walls, composed of two leaves separated by an air cavity. This cavity was often filled, at least partially, with insulation material to enhance thermal or acoustic performance [53]. Nonetheless, the need to address moisture issues and concerns about thermal performance prompted the development of brick veneer walls [53]. Brick veneer walls act as the outermost layer of the building envelope, consisting of exterior masonry cladding separated from the structural backing by an air cavity. The structural backing system varies depending on the construction technology and can include concrete, timber, or light steel stud walls in Sweden, the United States, and Australia [52]. Further, reinforced concrete masonry infilled frames are commonly used as the structural backing in Europe.

2.2 Durability and performance

Clay brick masonry façades have long been favored for their durability and architectural appeal, making them valuable both from economic and cultural points of view. These buildings, often found in central locations and public spaces, can exhibit remarkable durability and long-term performance, with a service life that extends well beyond a century. The durability of brick masonry is reflected by its ability to withstand various environmental, physical, and chemical factors over time without significant deterioration, degradation, or loss of structural integrity while remaining serviceable without intensive maintenance [54-56]. It should be mentioned that the durability of bricks is closely tied to the quality of their firing process. When adequately fired, bricks exhibit a lifespan that exceeds that of the mortar joints.

However, clay brick façades still deteriorate over time due to climate exposure, such as WDR, freezing-thawing, wetting-drying cycles, and salt crystallization. Maintenance becomes necessary to ensure the prolonged durability of a clay brick façade due to the inevitable deterioration caused by climate factors. In Western and Northern Europe, WDR is a major moisture source that has the potential to deteriorate both the masonry itself and other components in the building envelope [57]. Additionally, in Nordic countries, freeze-thaw cycles contribute to issues such as spalling, delamination, cracking, and erosion of mortar joints, further worsening the effects of WDR.

Maintenance offers numerous economic, cultural, and climate advantages, prompting prioritization over new construction. Economically, maintaining masonry façades protects and prolongs the service life of valuable assets. Historical public buildings and centrally located dwellings, often constructed with clay brick masonry, hold cultural significance and contribute to the overall aesthetic appeal of urban environments. Their longevity and architectural excellence highlight their value as sound investments, making maintenance a practical economic choice. Culturally, clay brick masonry reflects the architectural heritage and the history of communities. Preserving these buildings through maintenance upholds craftsmanship and design principles of the past, fostering cultural continuity. In addition to historic and old dwellings, it is important to acknowledge that cultural and architectural aspects extend beyond traditional boundaries. There is a contemporary understanding that cultural heritage encompasses not only historic buildings but also modern ones from recent decades. It is noteworthy to emphasize that the restoration of older buildings, particularly those built with massive walls or old brick types, would not be replicated in the same manner if they were demolished. Maintenance thus emerges as the sole possibility for preserving these building types.

From a sustainability perspective, prioritizing maintenance aligns with climate action goals. Opting for new constructions often involves significant use of

resources, leading to a substantial carbon footprint. In contrast, maintaining existing masonry structures reduces the need for new building activities, conserving resources and minimizing environmental impact. Furthermore, the carbon footprint associated with construction materials, such as cement used in mortar, can be substantial. On the other hand, older solid masonry envelopes often have low energy performance [58].

Eventually, it needs to be acknowledged that while maintenance is a sustainable choice compared to extensive reconstruction, some measures, such as repointing as a common maintenance practice, contribute to emissions. Maintaining rather than rebuilding is a wise choice, but it is important not to invest resources in maintenance when it is unnecessary.

Before initiating maintenance work, conducting a preliminary assessment, including a visual inspection and review of existing documentation, is highly recommended. Non-destructive or destructive tests can provide valuable information for a thorough evaluation of the façade's condition. Informed decisions regarding the most appropriate maintenance strategies can be made through a cost-benefit analysis based on the gathered information. Paper I provides a review of tools and techniques for assessing the condition of clay brick façades and implementing relevant maintenance measures.

2.3 Maintenance measures related to moisture problems

In order to make informed decisions regarding maintenance measures, it is crucial to identify and address the root cause of moisture-related issues. Conducting thorough inspections can provide valuable information about the source of the moisture problem, ensuring that maintenance actions effectively solve the issue. Moisture-related issues typically arise from a combination of causes rather than stemming from a single factor alone. Specific water-tightness issues can be addressed with relatively straightforward solutions, while others may require more extensive and comprehensive measures. Examples of simpler remedies include improvements to the design aspects of openings, such as windows, enhanced ventilation strategies, and the repair of cracks. On the other hand, some cases may require more elaborate interventions to ensure an effective solution to water-tightness challenges.

An effective maintenance action that can help postpone more extensive repairs is cleaning, which can also unveil hidden defects during the inspection [7, 59]. Cleaning methods fall into three categories: abrasive, chemical, and water cleaning. Proper cleaning might be an adequate measure, providing an advantageous appearance, and it can potentially delay the need for costly measures. It is essential

to use appropriate cleaning techniques to avoid any damage to the masonry surface, especially in the case of historic façades.

Surface grouting can be a viable repair method for superficial hairline cracks in mortar joints. The selection of a matching texture, color, and properties of the existing mortar is critical for a seamless repair. In the case of larger cracks, the filling by injection grouts may be a viable solution, although it requires careful examination and material selection to achieve successful results [15].

Surface treatments, such as cement plaster and cement-lime plaster, can effectively reduce water penetration and damp surface areas in brick veneers. In an experimental study conducted by Ghanate et al. [31], it was found that among different surface treatments, the treatment with cement plaster was the most effective solution for improving the resistance of water penetration inside the building envelope. Another study by Anand et al. [43] highlights that surface treatment with cement plaster reduces water penetration in masonry walls. While the use of cement plaster offers high efficiency, its application on historical and existing façades normally is limited due to potential distortion of aesthetics and cultural aspects.

The use of reinforcement made from unprotected carbon steel or galvanized carbon steel was grounded in the belief that lime-cement mortars could provide long-lasting protection against corrosion. However, brick façades constructed prior to 1975 frequently display corrosion-induced cracking [60, 61], which may raise concerns about elevated moisture levels in the external walls and the associated issues. In order to mitigate further damage caused by corrosion, the corroded bed joint reinforcement should be removed and, when necessary, replaced with stainless steel reinforcement. The extent of retrofitting varies between partial to total removal of the reinforcement from cracked bed joints or from the entire façade. However, in some cases, only repointing of cracked bed joints is carried out without the removal of any reinforcement. If the corroding reinforcement is not removed, the new bed joints will crack in a few years, thus making such a measure inefficient [60].

Excessive water content, combined with repeated freeze-thaw cycles, can result in frost damage to bricks, commonly known as 'spalling.' Spalling is caused by various factors, including unsuitable brick selection for exposure, insufficient protection against saturation, or the use of subpar units in the wall [7, 62]. When encountering damaged bricks, they should be replaced with new bricks because there is no other treatment to render bricks frost-resistant. However, it is essential, if possible, to identify the root cause of excessive water content to prevent long-term damage.

The application of a water-repellent coating might significantly reduce the water penetration rate for treated clay bricks. Brown [63] observed a notable decrease in penetration rate upon the application of a clear water-repellent coating, resulting in a 64% reduction for clay bricks. In an experimental study conducted by Ghanate et al. [31], two water-repellent types were tested on brick masonry: water-based and

cream-based. The water-based treatment achieved a remarkable 74% reduction in water penetration, while this value was 60% in the case of cream-based water repellent. Aktas et al. [64] found that waterproofing can reduce water absorption in brick masonry by 35–96%, with silane/siloxane blend cream being the most effective.

In spite of the potential benefits of water-repellent coatings, there is an ongoing debate about their long-term effectiveness, as some studies suggest a potential increase in water penetration over time and the need for reapplication at specific intervals [65]. In a study conducted by Slapø et al. [23], hydrophobic impregnation effectively decreased water penetration in all four tested water repellents during the initial minutes. However, subsequent to this period, no significant further enhancement was evident, which can be attributed to the severe conditions of the testing procedure. Further, the application of water repellents might result in an unexpected worsening of water-tightness problems. This outcome can be attributed to several factors [15, 66]: a) ingress of water under high wind conditions, as water can penetrate through the water-repellent layer [23], and b) formation of micro-cracks after the application of the repellent, allowing rainwater to be absorbed through capillary action [66]. Research conducted by Groot and Gunneweg [15] revealed that in situations where water ingress occurs unexpectedly, the drying process of the masonry is substantially delayed when a water repellent is employed. This is in agreement with a study done by Hammett [7], which proposed that while water repellents can enhance the ability of a wall to shed water, they do not address cracks.

2.4 Repointing

A critical element in clay brick masonry with regard to durability and proper maintenance is the mortar used in the joints. While the longevity of clay brick units exceeds typically at least a century, the durability of mortars exposed to WDR usually is less than this desired lifetime; regular maintenance of mortar joints is thus essential over the service lifetime of clay brick façades.

One common maintenance technique for clay brick masonry façades is repointing, involving the process of raking out existing mortar joints to a certain depth, usually 25 mm, and then replacing them with new mortar. Figure 2 illustrates a clay brick masonry façade before, during, and after repointing. Today, the predominant approach to the maintenance of clay brick façades in Sweden is to follow recommendations in standardized checklists, according to which repointing shall be carried out every 40–50 years. In addition to the elapsed time since construction, eroded mortar joints are a key factor influencing decisions about repointing – also in cases when limited parts of the façade are affected [14]. Further, decisions on

repointing can often be based on damp walls or visible cracks. Although there is a tendency in practice to follow standardized schemes as a basis for decisions, this approach lacks a systematic evaluation based on objective condition indicators, leading to potential unnecessary costs and adverse environmental effects.

When considering the maintenance of façades with eroded mortar joints and cracks, the expected benefit of repointing includes a reduction of moisture-related risks stemming from penetration of WDR, as well as improvements in aesthetics, stimulating the façade for a fresher and restored appearance [18, 30]. Concerning the first aspect, factual evidence has been scarce. Concerning the second, the views are divergent since repointing carried out without awareness of building-historical aspects might distort a valuable part of the building stock [16, 67, 68].

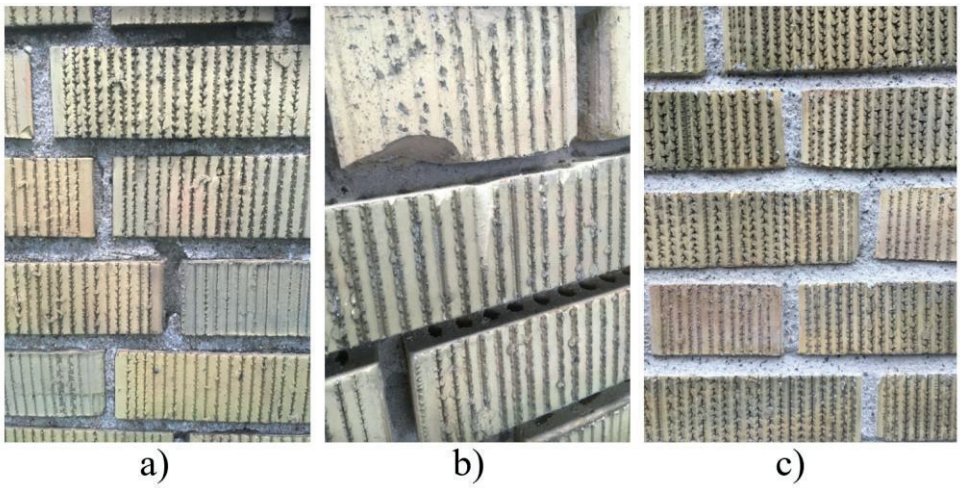

Figure 2. A clay brick masonry façade, before and after repointing, a) the initial state with eroded mortar joints; b) mortar joints raked out up to the depth of 25 mm; c) newly pointed mortar joints

Although repointing may improve the aesthetic of masonry and decrease water penetration into the façade, permanent damage to older masonry walls and premature failure of repointing can result from improper selection and application of repointing mortars [69, 70]. Specific problems include using incompatible materials between new mortar and existing mortar [68] or between new mortar and units (e.g., weak bond between new mortar and bricks) [71, 72], as well as poor workmanship. Compatibility in this context refers to the ability of mortar to be adapted to its surroundings in terms of moisture transport, bonding with bricks, and other physical characteristics. In some cases, the choice of pointing material and application techniques may not be suitable, leading to a higher risk of damage to the façade in the form of frost damage, spalling, and negative impacts on the appearance of the façade [15, 73]. For example, the use of cement-rich mortar is not recommended because of the tendency to shrink, resulting in a weak bond to the

bricks. This can lead to cracks at the brick/mortar interface, facilitating water penetration and higher saturation levels in nearby bricks. Instead, mortars consisting of a blend of cement, lime, and sand are recommended as they exhibit good bonding and low shrinkage characteristics, making them suitable for repointing [7, 74]. Figure 3 exemplifies some of the adverse effects of selecting improper mortar and poor workmanship during repointing.

Figure 3. An example of the adverse effects of selecting unsuitable mortar and shoddy workmanship during the replacement of bricks due to frost damage

Several researchers have proposed qualitative and quantitative criteria to analyze the need for repointing, e.g. [57, 75-78], recommending repointing when:

a) the surface of the mortar joints contains hairline cracks.

b) eroded mortar joints to a certain depth - a quarter of an inch, i.e., 6.4 mm - have been observed.

c) crack widths larger than 2 mm have been measured.

d) the rate of water absorption is more than 4.5 $l/m^2/h$.

e) the presence of voids is detected.

According to the proposed criteria, the extent to which high moisture content and water absorption/penetration are related to the outer part of the mortar joints and whether repointing can reduce water absorption/penetration should be investigated [69, 71]. It should be noted that only 2.5 times the mortar joint thickness, or 25 mm of the outer part of the cracked/eroded mortar joints, is normally raked out and replaced with a new mortar during repointing. In this context, the relation between the depth of erosion of the mortar joints and the possible increase in water absorption and penetration from WDR should be examined. In conclusion, a well-informed approach to repointing is vital to maintain the durability and aesthetics of clay brick

masonry façades. Recommended steps to reach a rational decision on repointing are further discussed in Paper I.

3 Theoretical frameworks

Since wind-driven rain (WDR) is one of the major moisture sources, this chapter first discusses various methods for quantifying WDR deposition on building façades, with a particular focus on the widely recognized ISO Standard. The model is then used to investigate WDR deposition for various locations in Sweden, providing a better understanding of realistic WDR ranges that occur in Sweden. Next, the response of brick masonry façades exposed to WDR is discussed, focusing on bounce-off, water absorption, runoff, and water penetration.

3.1 Wind-driven rain (WDR)

A significant portion of WDR research is dedicated to quantifying WDR deposition rates on building façades, providing useful information about their level of exposure, which is a fundamental input to hygrothermal analysis and an important factor in building façade design with respect to deterioration prevention and maintenance [79]. Further, information concerning WDR deposition enables researchers to establish relevant test parameters and conditions to study the water tightness of masonry walls in experimental studies [80].

3.1.1 Measurements and calculations

The WDR intensity on a building façade depends on several factors: rain intensity, raindrop size, wind speed and direction, building geometry, and topography [81]. Methods to quantify WDR deposition rate on building façades can be categorized as experimental, semi-empirical, and numerical. In experimental methods, WDR deposition on building façades is measured using wall-mounted WDR gauges [82-84], essential for developing and validating semi-empirical and numerical methods [81, 85]. Since there are no standards for the design of WDR gauges, experimental measurements exhibit a significant difference. While experimental methods to quantify WDR deposition rates on building façades provide useful information, they are time-consuming and costly.

Models within the semi-empirical category have been established to estimate WDR deposition on building façades based on common weather data, including wind

speed, wind direction, and rainfall through the horizontal plane. Assuming that the horizontal velocity of raindrops is equal to the wind speed and that the terminal velocity governs the vertical velocity, the equation for WDR intensity, R_{WDR} [mm/h], can be expressed as follows (Eq. (1)):

$$R_{WDR} = {}^{U}/_{U_{terminal}} \times R_h \times \cos\theta \qquad (1)$$

where U [m/s] is the wind velocity, $U_{terminal}$ [m/s] is the terminal velocity of the droplet, R_h [mm/h] is the rainfall through the horizontal plane, and θ is the angle between the wind direction and the normal to the façade.

Using factors such as building geometry, local topography, the presence of obstruction, and building exposure can improve the accuracy of semi-empirical models. The most advanced and frequently used semi-empirical models include the ISO Standard [86], the Straube and Burnett (SB) model [87], and the ASHRAE Standard 160–2021 [88]. Although models offer a fast and simple approach to WDR quantification, they are generally reliable only for stand-alone buildings in simple configurations [81]. In situations where complex flow patterns around buildings are affected by nearby structures, these models may not yield precise outcomes.

Given the limitations observed in quantifying WDR using experimental and semi-empirical methods, alternative approaches involving numerical models based on computational fluid dynamics have emerged. These models offer the advantage of incorporating building geometry by simulating wind-flow patterns and raindrop trajectories. Nonetheless, these models are complex and demands substantial computational resources [89, 90].

3.1.2 WDR intensity according to the ISO model

Initially, the BS 8104 standard [91] was developed based on a long series of WDR measurements on different buildings and locations in the UK. The more general ISO model [86], based on the BS 8104 standard, was later established to serve as a broader framework for quantifying WDR deposition rates on building façades. According to the ISO model, the WDR intensity, R_{WDR} [mm/h], on a building façade is calculated according to Eq. (2).

$$R_{WDR} = \alpha \times U_{10} \times {R_h}^{0.88} \times \cos\theta \qquad (2)$$

where α [s/m] is the WDR coefficient, which is equal to 2/9 for free-field conditions (i.e., free driving rain), U_{10} [m/s] is the reference wind speed (unobstructed streamwise wind speed at 10 m height), R_h [mm/h] is the rainfall through the horizontal plane, and θ is the angle between the wind direction and the normal to the façade. It should be noted that the model primarily applies to climate conditions

similar to those in the UK. Further, for locations with at least 10 years of hourly values of wind speed, wind direction, and rain intensity, an annual WDR index I_A [l/m^2] can be calculated according to Eq. (3):

$$I_A = \frac{\sum R_{WDR}}{N} \quad (3)$$

where N is the period considered (years), and R_{WDR} is the accumulated WDR over the same period.

In the ISO model, four main parameters are used to convert the amount of rain that would be collected by a free-standing rain gauge in a flat open field into the amount of rain that would impact a façade. Thus, the WDR coefficient, α, is calculated as follows:

$$\alpha = \frac{2}{9} \times C_R \times C_T \times O \times W \quad (4)$$

where C_R is the terrain roughness coefficient, C_T is the topography coefficient, O is the obstruction factor, and W is the wall factor.

The roughness coefficient, C_R, takes into account the variability of mean wind velocity at the site based on the height above the ground and the roughness of the terrain. The ISO model defines four different terrain categories (as presented in Table 1) and their relevant parameters to determine the roughness coefficient C_R, which is calculated as follows:

$$\mathrm{C_R(z)} = \mathrm{K_R}.\ln\left(\frac{\mathrm{z}}{\mathrm{z_0}}\right) \text{ for } z \geq z_{min} \quad (5)$$

$$\mathrm{C_R(z)} = \mathrm{C_R}\ (\mathrm{z_{min}}) \text{ for } z < z_{min} \quad (6)$$

where z is the height above ground [m]; K_R is the terrain factor [-]; z_0 is the roughness length [m], and z_{min} is the minimum height [m].

Table 1. Terrain categories and related parameters, as provided by the ISO Standard [86]

Terrain category	Description	K_R	z_0	z_{min}
I	Rough open sea; flat country without obstacles	0.17	0.01	2
II	Farmland with occasional small farm structures, houses, or trees	0.19	0.05	4
III	Suburban or industrial areas and permanent forests	0.22	0.3	8
IV	Urban areas in which at least 15 % of the surface is covered with buildings of average height exceeding 15 m	0.24	1	16

The topography coefficient, C_T, depends on the upwind slope and accounts for the increase in mean wind speed over hills and escarpments. For upstream slopes with less than 5% inclination, C_T is equal to 1, whereas, for buildings located at the crest of steep cliffs or escarpments, C_T can be considered 1.36.

The obstruction factor, O, accounts for the horizontal distance between the exposed wall and the nearest obstacle, which is at least as high as the wall. The obstruction factor is calculated based on information provided in Table 2. In this table, the "distance of the obstruction from the wall" represents the horizontal distance between the wall and the closest obstacle of similar dimensions to the wall along the line of sight from the wall. Thus, depending on the distance to the nearest obstacle, the obstruction factor varies in the range of 0.2 and 1.0.

Table 2. Obstruction factor as a function of the distance of the obstruction from the wall, as provided by the ISO Standard [86]

Distance of obstruction from wall (m)	Obstruction factor O
4–8	0.2
8–15	0.3
15–25	0.4
25–40	0.5
40–60	0.6
60–80	0.7
80–100	0.8
100–120	0.9
>120	1.0

The wall factor, W, considers wall types, overhangs, and the orientation of bricks affecting the amount of rain incident on a wall. The wall factor is between 0.2 and 0.5, increasing with increasing wall height. Despite many WDR measurements indicating that the WDR intensity increases from the middle of the façade to the sides [89], the ISO Standard assumes the same wall factor across the width of the wall.

It should be noted that the ISO model [86] is not applicable in the following situations: a) in mountainous regions with steep cliffs or deep gorges, b) in areas where over 25% of the annual rainfall is attributed to severe convective storms, and c) in areas and during time periods when a substantial portion of the precipitation consists of snow. Further, the model has several limitations [81]: i) the wall factor only provides limited information about the spatial variation across the façade, ii) the coefficient α, representing the WDR coefficient, is assumed to remain constant for a fixed position on the building, meaning it does not vary with time [81], and iii) it can only be used for the specific building configurations primarily focused on low-rise buildings. This focus is likely because the Standard Draft was initially developed with masonry walls in consideration.

3.1.3 Characterization of WDR events in Sweden

In this section, the ISO model is used to provide general information about WDR intensities in Sweden that can be used to determine reasonable parameters for water penetration testing. For this purpose, two locations, namely Gothenburg and Uppsala, located in two different regions of Sweden, are studied to analyze WDR

intensities on a building façade. The analysis is based on hourly rain intensities and wind velocities measured by the Swedish Meteorological Hydrological Institute (SMHI) [92] over a period of about 25 years (1995–2020).

Figure 4 shows that the average annual WDR index, I_A, varies between around 100 and 430 l/m^2 across the studied locations and highly depends on the wall orientation. In Gothenburg, located near the Swedish West Coast, walls facing south and west receive the largest amount of WDR.

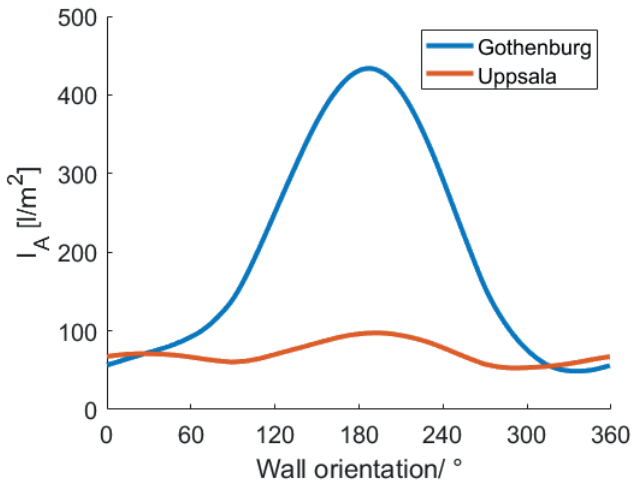

Figure 4. Average annual WDR index, I_A, at two Swedish sites for different wall orientations (0° north, 90° east) between 1995 and 2020

Figure 5 depicts the duration of each WDR event with at least 0.1 mm/h intensity for each location, indicating that the majority of WDR events lasted less than 5 hours. Similarly, a series of long-term WDR measurements in Europe show that 80% of WDR events last less than 6 hours [93, 94].

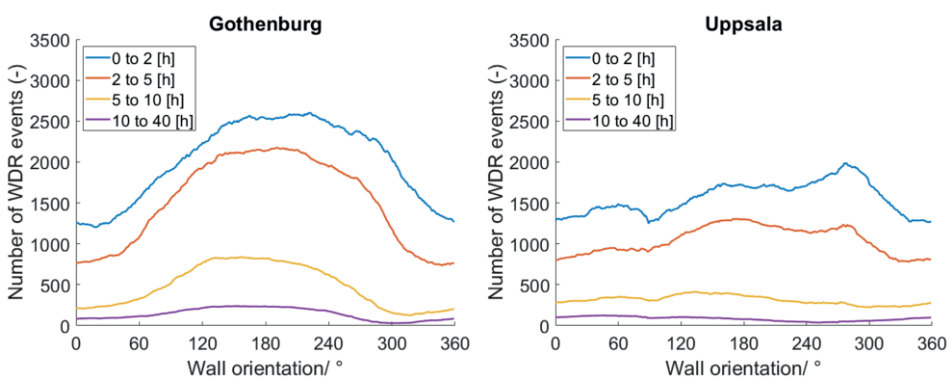

Figure 5. The number of WDR events of different lengths for two Swedish sites for different wall orientations (0° north, 90° east) between 1995 and 2020

In the following paragraphs, to better estimate WDR intensities that impacted a building façade in the previously mentioned locations, a building with a 15-m height is considered. The wind direction is assumed to be perpendicular to the façade (θ = 0°), and the building is adjacent to farmlands, thus belonging to terrain category II, according to the ISO model. Values of K_R, z_0, and z_{min} as a function of the terrain category are given in the ISO model, in which $K_R = 0.19$, $z_0 = 0.05$ m, and $z_{min} = 4$ m for terrain category II. Thus, the roughness coefficient C_R is equal to 1.084. Additionally, the building is considered to be located in flat terrain without any obstruction in its surroundings. Hence, the topography coefficient, CT, and obstruction factor, O, are equal to one. The wall factor, W, for a multi-story building without any overhang and protection, is equal to 0.5 for the upper part of the façade. Therefore, for the considered building, the WDR coefficient, α, is calculated according to Eqs. (4) – (6), is equal to 0.12 s/m.

Figure 6 illustrates the cumulative time-frequency distribution of WDR intensities for the particular building located in Gothenburg and Uppsala for the time period between 1995 and 2020. As can be seen, the majority of WDR events occurred with an intensity of less than 1 mm/h. Depending on location, the extreme WDR intensity varied between 8.5 and 36 mm/h for the studied locations from 1995 to 2020.

Findings from field-based WDR measurements are in line with the estimations delivered by the ISO model. Sandin [82] conducted a field measurement study in Gothenburg lasting 26 months, recording a maximum WDR deposition rate of 6 l/m^2/h. In Europe, WDR measurements show that WDR rates of more than 4 l/m^2/h occur in less than 10% of events [94]. Moreover, the literature review and preliminary field measurements done by Straube and Burnett suggest that WDR deposition rates of more than 5 l/m^2/h are rarely encountered, even on tall buildings [95, 96].

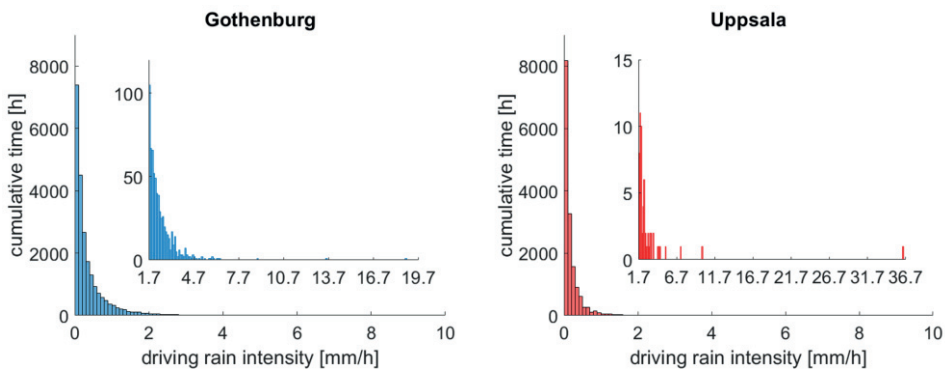

Figure 6. Driving rain intensities from 1995 to 2020 for the building considered in this section are a) Gothenburg and b) Uppsala – Calculations according to the ISO Standard [86]

Figure 7 shows the duration of each WDR event with an intensity of at least 0.1 mm/h for the considered building in each location, indicating that most of the

WDR events lasted for less than 5 hours of consecutive rain. The longest WDR event from 1995 – 2020 at the studied locations lasted 30 hours (Gothenburg).

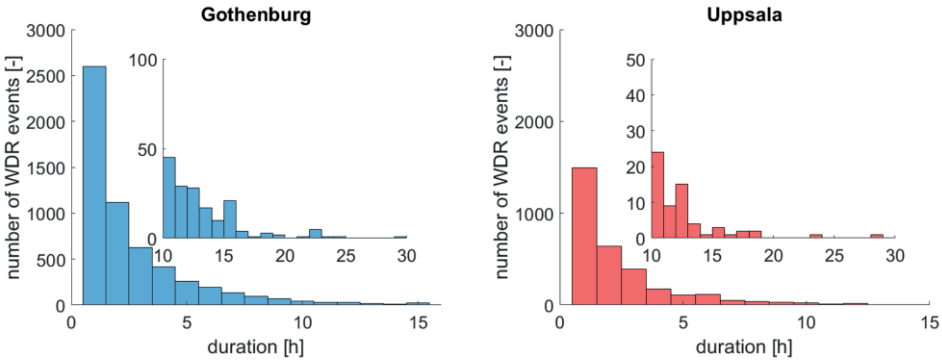

Figure 7. Number and duration of WDR events from 1995 to 2020 for the considered building located in a) Gothenburg and b) Uppsala – Calculations according to the ISO Standard [86]

For the same locations and time period, the average hourly wind speed at 10 m above ground during WDR spells with an intensity of at least 0.1 mm/h was between 2.7 m/s and 4.2 m/s. Hence, the mentioned wind speeds impose a pressure difference of less than 10 Pa across the building envelope. During the period of 1995 to 2020, the maximum registered wind speed during rainfall events for the studied building varied between 9.2 m/s and 18.5 m/s, corresponding to an air pressure difference of around 55 Pa – 220 Pa.

3.2 Interaction with wind-driven rain (WDR)

While one category of WDR studies attempts to quantify WDR deposition rates on building façades, the second category investigates the interaction between building façades and WDR, with a focus on phenomena such as bounce-off, absorption, runoff, and penetration. Figure 8 visually depicts the response of brick masonry when exposed to WDR.

- Some rainwater may bounce off upon impact, influenced by factors such as drop characteristics (size, velocity, and angle), the type of masonry material, and the surface roughness.
- The remaining water will adhere to the wall surface and be absorbed by brick and mortar until the surface is saturated by water.
- When the surface becomes saturated, the remaining water will instead form a water film, resulting in runoff along the masonry façade. Simultaneously, water is still absorbed until full saturation.

- Finally, a portion of WDR may penetrate through the brick masonry, which constitutes the primary focus of the presented thesis.

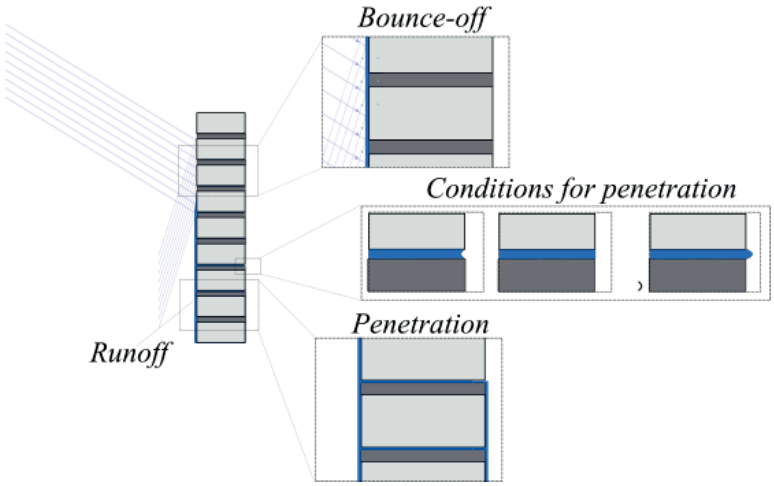

Figure 8. Schematic response of brick masonry to WDR

3.2.1 Bounce-off

During a rain event, not all raindrops adhere to the wall surface, and thus, not all of them serve as a source of moisture for the wall; instead, a portion of the raindrops may bounce off upon impact. Abuku et al. [97, 98], Erkal et al. [99], Couper [100], Mason and Andrews [101], and Mutchler and Hansen [102] have studied raindrops' bounce-off and spreading when hitting masonry façades.

An experimental study by Abuku et al. [98] revealed that large raindrops with high impact speeds and low impact angles tend to bounce off the surface. Further, the study [98] pointed out that the impact of WDR varies with the location of interest on a façade. Raindrops hitting lower locations may have a small impact angle, increasing the likelihood of bouncing off. Erkal et al. [99] found that rougher surfaces were more likely to result in bounce-off, and larger water drops tended to produce more pronounced bounce-off. In field tests, increased rain intensities led to higher percentages of bounce-off [100]. These findings align with earlier studies that examined the impact of raindrops on horizontal surfaces. Mason and Andrews [101] noted that having a thin water film on the surface raised the bounce-off percentage, and Mutchler and Hansen [102] reported an increase in bounce-off percentage with greater water film depth.

Understanding the phenomenon of bounce-off is essential when it comes to hygrothermal modeling, as it serves as an important input. A study conducted by Künzel [103] found that about 70% of rainfall adheres to vertical wall surfaces, whereas the remaining part takes the form of bounce-off, rendering it inaccessible

for absorption. This, in turn, became the default value of many hygrothermal simulation tools [104-106] due to the lack of standard protocols. Accordingly, in hygrothermal modeling, 30% of the rain is usually assumed to bounce off the wall and is therefore unavailable for capillary suction. The remaining part is considered to be available for absorption through liquid conductivity (capillary suction).

3.2.2 Water absorption and runoff

As already mentioned, considering the bounce-off of raindrops upon the impact, only a portion of water is available for absorption. At the same time, the amount of water that can be absorbed is influenced by the pore structure. Porous materials absorb water through capillary absorption. This process continues until saturation, given a sufficient supply of water and time. The dynamic of the process is mainly influenced by A_w [kg/(m^2.s$^{0.5}$)], the water absorption coefficient of the material, and WDR intensity [107-109].

The absorption flux, g_{abs}, prior to surface saturation, is equal to the supplied flux, meaning that prior to the surface saturation, all of the deposited water on a masonry wall is absorbed. The supplied flux, R_{WDR}, represents the water available for capillary absorption, subtracting the bounce-off from WDR. The time until a water film is formed depends on the rate of supplied water and the water absorption coefficient. Using the sharp front theory (SF), the time to surface saturation, t_f, can be calculated as follows (Eq. (7)).

$$t_f = \frac{A_w^2}{2 \cdot R^2{}_{WDR}} \tag{7}$$

It takes more time to attain surface saturation in masonry bricks with a higher water absorption coefficient, indicating that a higher absorption coefficient allows rapid moisture transport and postpones saturation of the exposed masonry surface layer [29]. For example, a masonry brick wall surface with a water absorption coefficient of 0.026 kg/(m^2.s$^{0.5}$) and a spray rate of 3 l/m^2/h reaches saturation after 8 minutes. In contrast, for a wall with a water absorption coefficient of 0.26 kg/(m^2.s$^{0.5}$) and the same spray rate, surface saturation occurs after around 13 hours.

After surface saturation, when a water film is formed on the surface, the boundary condition switches to a capillary saturation boundary condition, and the absorption flux, g_{abs} [l/(m^2.s)], can be calculated by Eq. (8) [107]:

$$g_{abs} = \frac{A_w}{2\sqrt{(t - \frac{t_f}{2})}} \tag{8}$$

where t_f [s] is the time to form the water film (surface saturation) according to Eq. (7), and t [s] is the total time of the WDR event. It should be noted that the

supplied intensity is not included in the equation, as the presence of a water film implies that the supply flux exceeds the absorption flux.

The proportion of water absorbed gradually decreases over time. The excess portion accumulates on the outer surface, forming a film that flows down due to gravitational forces.

Several investigations have been conducted through field and laboratory experiments to study rainwater runoff, including its velocity and thickness [1, 110, 111], where semi-empirical rainwater runoff models have been proposed. Regarding film thickness, Beijer [1] proposed a semi-empirical equation, Eq. (9), to calculate the water runoff film thickness on concrete walls subjected to WDR:

$$h_B = 0.04\sqrt{q_{runoff}} \tag{9}$$

where h_B [mm] is the water film thickness and q [l/(m.h)] is the runoff rate.

A simplified numerical model to quantify runoff rate and film thickness has been developed by Blocken and Carmeliet [2]. Within this model, the variation in runoff film thickness is governed by a first-order hyperbolic partial differential equation. This equation is derived by incorporating the continuity equation and introducing WDR intensity and the capillary absorption flux by the wall as source/sink terms. Additionally, it is based on the assumption of a parabolic velocity profile following the Nusselt solution, simplifying the representation of thin film flow. The Nusselt solution is exclusively applicable to describe the behavior of a thin film flow of an isothermal Newtonian liquid that maintains a constant density (ρ_w) and kinematic viscosity (ν). The action of gravity primarily influences the flow. The film flow rate, Eq. (10), and average velocity, Eq. (11), given by the Nusselt solution:

$$q = \int_0^{h_{tN}} u(y)dy = \frac{g_r \cdot {h_{tN}}^3}{3 \cdot \nu} \cdot \sin\beta \tag{10}$$

$$u = \frac{q}{h_{tN}} = \frac{g_r \cdot {h_{tN}}^2}{3 \cdot \nu} \cdot \sin\beta \tag{11}$$

where u(y) [m/s] is the transverse water film velocity (average velocity), g_r [m^2/s] is the gravitational acceleration, ν [m^2/s] is the kinematic viscosity, h_{tN} [m] is the film thickness, and β [degree] is the wall inclination.

In contrast to the conditions considered by Nusselt, it is important to note that the film thickness is not necessarily constant along the height of the wall, and the flow is not essentially steady. The solution by Nusselt was further developed by Blocken and Carmeliet [2] who added a source term. This source term represents the difference between the WDR intensity, R_{WDR} [mm/s], and capillary absorption, g_{abs} [l/(m^2.s)], with the latter added as a sink term for film flow. Accordingly, the

water film thickness, h, at different positions along the height of the façade at different times is expressed as:

$$\frac{\partial h}{\partial t} + \frac{g_r \cdot h^2}{3 \cdot \nu} \frac{\partial h}{\partial x} = \frac{R_{WDR} - g_{abs}}{\rho_w} \tag{12}$$

where R_{WDR} [mm/s] is the WDR intensity or WDR flux, g_{abs} [l/(m^2.s)] is the absorption flux, and ρ_w [kg/m^3] is the water density.

As already mentioned, the absorption flux, g_{abs}, prior to surface saturation, is equal to the supplied flux, R_{WDR}. Once water film is formed on the surface, presented in Eq. (7), depending on the WDR intensity, R_{WDR}, and water absorption coefficient, A_w, the boundary condition switches to a capillary saturation boundary condition, and the absorption flux is given by Eq. (8) [107].

Eq. (12) can be numerically solved using an explicit approach. The discretization technique, presented in Eq. (13), involves forward differencing in time and backward differencing in space.

$$\frac{h_j^{n+1} - h_j^n}{\Delta t^{n+1}} + \frac{g_r}{3 \cdot \nu} \left(\frac{\left(h_j^n\right)^3 - \left(h_{j-1}^n\right)^3}{\Delta x_{j-1}} \right) = \frac{(R_{WDR} - g_{abs})_j^{n+1}}{\rho} \tag{13}$$

where n is the time step number, and j is a number indicating the position on the wall.

3.2.2.1 Moisture transport

A porous material will exchange moisture with the air, and the moisture content will tend towards the equilibrium given by the sorption isotherm. Further, when exposed to WDR, water will be absorbed, and it is therefore important to understand moisture transport mechanisms in both vapor and liquid phases. Since this study focuses on the resistance of masonry to driving rain, a great emphasis is placed on understanding moisture transport within the liquid phase.

Different phases of water are subjected to different mechanisms for transport through the material. Water vapor transport is governed by diffusion, whereas liquid transport can be divided into unsaturated (capillary absorption) and saturated flow (permeation). Moisture transport in brick masonry is influenced by water saturation and microstructure. For instance, when the relative humidity ranges from approximately 5 to 95 %, effective moisture transfer is controlled by water vapor diffusion and capillary suction. Under saturated or nearly saturated conditions, the dominant mechanism is laminar flow, as outlined by Darcy's law. However, detailing these transport processes as a function of relative humidity is challenging. This challenge stems from the fact that pores of varying sizes can host different transport phenomena concurrently.

- Diffusion

Diffusion occurs as a mechanism driven by varying concentrations or partial pressure gradients of gases. The term diffusion encompasses diverse partial diffusion processes, such as water vapor diffusion or surface diffusion, each with distinct driving forces. Diffusion refers to the migration of molecules driven by concentration gradients, leading particles to move from regions of higher concentration to those of lower concentration or from higher vapor pressure to lower.

- Unsaturated flow

The capillary pressure mainly controls capillary absorption within capillary pores, where the difference in the water content between the wetter and drier locations is the driving force for capillary transport. It can be analyzed by the so-called extended Darcy equation, which can be written as follows:

$$\mathrm{u} = -K(\vartheta) \times \nabla\varphi \qquad (14)$$

Where u [m/s] is the flow rate within the porous medium and $K(\vartheta)$ [m/s] is the liquid conductivity, also known as unsaturated permeability, which depends on the water content, ϑ. Conductivity is a property of porous material measuring how easily water flows through the pore network. The driving force, $\nabla\varphi$ [-], is the gradient of capillary potential.

Capillary absorption can now be explored as a form of unsaturated flow, effectively described by the extended Darcy equation. Instead of considering the extended Darcy equation, which can only be used in a small number of cases in the analysis of capillary absorption, a simpler analysis method known as the Sharp Front (SF) theory is introduced [107]. The Sharp Front theory simplifies real smooth moisture fronts by assuming sharp separations between the wet and dry material zones [112]. The Sharp Front (SF) model simplifies capillary absorption by representing the wetted region with a rectangular profile. This approach is useful in understanding unsaturated flows and offers a straightforward means to approximate solutions for important capillary phenomena in construction, such as absorption into composite materials.

A crucial addition to this exploration is the introduction of the concept of sorptivity. Sorptivity is expressed as the tendency of a material to absorb and transmit water via capillary suction [94]. The sorptivity is calculated as the ratio between the water absorption coefficient, A_w [kg/(m^2.s$^{0.5}$)], and water density, ρ_w [kg/m^3]. This property holds significant importance in comprehending unsaturated flows across various contexts and characterizing porous construction materials. When water is absorbed in a dry porous medium, every point along the advancing waterfront shifts according to the square root of time, represented by $t^{1/2}$. Furthermore, the absorbed

mass of water exhibits proportionality to the square root of time and is expressed by Eq. (15):

$$m = \rho_w \, S \, A \, t^{1/2} \tag{15}$$

where m [kg] is the absorbed mass, ρ_w [kg/m^3] is the density of water, S [m/s$^{1/2}$] is the sorptivity, and A [m^2] is the cross-sectional area. The sorptivity serves as an intrinsic property characterizing the material's capability to absorb and convey water through capillarity. Following Eq. (15), it is possible to determine how far the capillary front reaches as a function of time. The time, t [s], for the capillary front to reach a certain distance, x [m], in a porous medium may be calculated as follows:

$$t = \mu_c \, x^2 \text{ where } \mu_c = (\frac{p}{S})^2 \tag{16}$$

where μ_c [s/m^2] is the capillary resistance number, and p [-] is the porosity. With this understanding, it is possible to explore the extent to which the capillary front advances over time.

While Equation (16) portrays the evolution of a moisture front within a homogenous material, it is essential to note that moisture transfer in masonry, being a multi-layered material encompassing brick and mortar, is not as straightforward as in single porous material. Real-world conditions often introduce imperfections in the interface between brick and mortar. Imperfections can be on a microscopic scale, leading to reduced hydraulic contact and reduced transfer of water from mortar to brick and vice versa. An imperfect hydraulic contact interface can result from variations in surface roughness, irregularities, or even the presence of voids.

More importantly, larger deficiencies in brick-mortar interfacial zones, including gaps, voids, and cracks, can create pathways that allow free water to penetrate farther into the wall. In such cases, the resistance at the brick-mortar interface becomes a critical factor influencing the overall moisture distribution [107, 113]. The phenomenon of water flow across interfaces has been extensively studied, and it is understood that imperfect hydraulic contact can be viewed as contact resistance [107, 113, 114]. Conversely, a limited number of studies focus on water transport parallel to the interface [115]. In such cases, deficiencies between the two materials can create a high conductivity pathway [107], potentially leading to water penetration (see Figure 9).

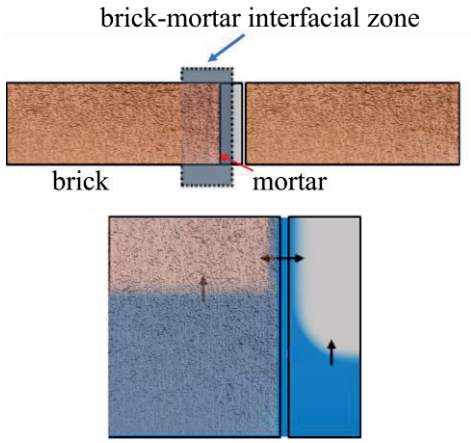

Figure 9. Moisture transport through a brick-mortar interfacial zone; high conductivity pathway - water transport parallel to the interface

- Saturated flow (permeation)

The mathematical description for the permeation of liquids through porous materials is based on Darcy's law, which can be written as follows [116, 117]:

$$Q_f = \frac{k \times A \times \Delta p}{\mu \times \Delta x} \quad (17)$$

Where Q_f [m^3/s] is the volumetric flow rate, k [m^2] is the permeability, A [m^2] is the cross-sectional area, Δp [Pa] is the pressure gradient, i.e., the pressure difference across the studied length, μ [Pa.s] is the dynamic viscosity, and Δx [m] is the length (Figure 10).

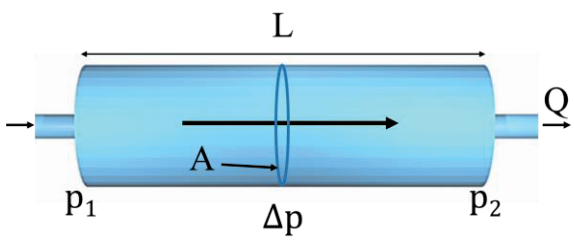

Figure 10. Simple Darcy flow through a liquid-saturated homogeneous medium (a saturated pore) under the action of a pressure gradient

By considering the hydraulic gradient applied between two points, Darcy's law is commonly written in terms of the flow rate or Darcy velocity, u [m/s], [116]:

$$u = \frac{Q}{A} = \frac{k \cdot \Delta p}{\mu \cdot \Delta x} \, [m/s] \quad (18)$$

A study by Mengel et al. [118] highlights that in cases where cracks larger than 0.1 mm are present, liquid transport is primarily controlled by permeation as the transport volume is several orders of magnitude higher compared to diffusion or capillary suction.

3.2.3 Water penetration

3.2.3.1 Mechanism

In the context of this thesis, water penetration refers to the permeation of rainwater through brick masonry, measured as the portion of WDR reaching the backside of the brick wall and leaking into the cavity. During WDR events, a thin water film may form on the exposed surface of the façades depending on the water absorption properties of masonry and WDR intensity. A portion of the film may penetrate through brick masonry walls if two conditions are met: a) the presence of pathways to permit its passage and b) forces to drive water through the interconnected pathways.

The deposited water on a masonry façade is transported through the wall in several different ways; the brick-mortar interfacial zone, particularly at the head joints, is often cited as the primary path offering the least resistance [12, 23, 35]. Likewise, many existing masonry façades contain cracks stemming from moisture and temperature movement combined with frequent freeze-thaw cycles or dynamic loading, facilitating water penetration in the building envelope [11, 15, 26, 27, 119].

3.2.3.2 Current studies on water penetration

Reviews of experimental studies attempting to quantify water penetration in brick masonry were conducted by Ritchie and Davison [32], Ritchie and Plewes [34], Van Den Bossche et al. [29], and Van Linden and Van Den Bossche [28]. Despite a large number of studies on water penetration, there is no agreement on how much water would penetrate through brick masonry [11]. The lack of consensus is related to the dependency of water penetration on several parameters, including brick and mortar material properties, the thickness of brick masonry, mortar water content during bricklaying, mortar joint profile and its thickness, workmanship, water spray rate, and pressure difference. The workmanship in this context pertains to brick-laying techniques and the execution of tasks, specifically focusing on how well mortar joints are filled and the overall compaction.

Brick and mortar absorption properties, particularly the initial rate of absorption (IRA) of bricks, are of great interest in studies investigating water penetration in brick masonry. Fishburn [120] investigated water penetration in masonry walls using 22 different types of bricks and found a consistent increase in water penetration with an increase in the value of the brick's IRA. Groot and Gunneweg [12] found that water penetration in brick masonry constructed with high IRA bricks

can be two to six times higher, depending on the masonry thickness, compared to the same masonry prepared using low IRA bricks.

The thickness of masonry is another parameter affecting water penetration. Groot and Gunneweg [12] investigated water penetration through clay brick masonry walls with various thicknesses, including half, one, and two brick lengths. The results revealed that the measured water penetration in the one-brick-thick wall was more than 50% lower compared to the wall with a half-brick thickness. This finding confirms the Darcy law, Eq. (17). In the study conducted by Ghanate et al. [31], they observed a reduction of approximately 21% in water penetration when the IRA value of the brick was decreased by about 31%, and the wall thickness was increased from 75 mm to 90 mm.

Calle [121] measured a significant decrease in the penetration rate for triple-wythe masonries compared to single-wythe and double-wythe masonries. The penetration rate for triple-wythe masonries was 1.30% of the spray rate, whereas single and double-wythe masonries showed penetration rates in the order of 21% of the spray rate. This can be related to the fact that in single and double wythe masonries, a continuous pathway like the brick-mortar interface exists connecting the inside and outside of the wall. However, in triple-wythe masonries (one and a half stone), the absence of continuous pathways results in a significantly lower constant penetration rate.

The effect of mortar joint thickness and profile was studied by Hines and Mehta [33], where it was found that depending on the joint profile, increasing joint thickness from 10 mm to 20 mm increases the amount of penetration by two times. Furthermore, the study revealed that the concave joint profile exhibited the least penetration amount, while the raked joint profile demonstrated the least resistance to water penetration. Tooling is thus identified as a factor affecting water penetration [122]. Further, tooling at an appropriate time can effectively reduce water penetration and influence overall wall appearance [123].

Another influential parameter on water penetration is workmanship, as mentioned by Fishburn et al. [17], Groot and Gunneweg [12], and Calle et al. [11]. A comparison of 14 different kinds of workmanship investigated by Fishburn [120] revealed that workmanship was the most significant factor influencing water penetration in masonry walls. Specifically, masonry walls with completely filled head joints exhibited markedly less water penetration compared to other workmanship methods. A study by Slapø et al. [23] revealed that the "buttering technique" used in constructing a brick masonry wall led to an impressive 80% reduction in water penetration compared to the "pushing the head joints" method for the same type of wall. Further, it was found that mortar water content during bricklaying significantly impacts the water penetration rate. In a study conducted by Calle et al. [11], it was observed that a mortared brick specimen with cracks and

poor workmanship exhibited a substantial 94% higher penetration rate compared to a specimen with ordinary workmanship.

Rathbone [50] observed that the penetration rate increased as the water spray rate increased. However, above a certain limit, further increasing the spray rate does not result in increasing the water penetration rate. This phenomenon can be explained by the fact that, at higher spray rates, a uniform water film forms on the exposed surface of brick masonry. Due to the increase in the water spray rate, the relative amount of waterdrops bouncing off the exterior surface also increases, resulting in a relatively lower amount of water available to penetrate [100]. Further, at a specific spray rate, the maximum amount of water able to penetrate through the existing pathways might be reached; further increase in spray rate might thus result in the increased runoff but no increase in penetration rate.

Eventually, the impact of air pressure difference on water penetration was explored in the study by Straube and Burnett [96]. They found that as the pressure difference increased from 0 Pa to 125 Pa, the water penetration rate doubled. This consistent trend of increasing water penetration with higher pressure differences was also observed in experimental studies conducted by Rathbone [50] and Calle et al. [11].

3.2.3.3 Test standards and setups concerning water penetration (Penetration by wind pressure)

The literature reveals that the ASTM E514 [38] standard is commonly utilized in studies investigating water penetration through masonry walls. Further, various test setups for exploring water penetration in masonry have been proposed in different standards and research studies, yet the applied water spray and air pressure rates represent rather extreme WDR conditions. For instance, a water application rate of 72–138 l/m^2/h is used in combination with a differential air pressure level of 400–1000 Pa [12, 23, 37, 40, 42]. As analyzed by Fishburn et al. [17] and Cornick and Lacasse [124], the test conditions outlined in these studies and standards represent extreme driving rain conditions that are infrequent and limited to specific locations. In light of this, Ribar [36] proposes the need for revisions in current test standards to incorporate a more realistic approach to exposure conditions. Further, from the analyses presented in Section 3.1.3, it can be concluded that experimental evaluation of the response of façades exposed to WDR in climate conditions similar to those prevailing in the studied locations in Sweden should be based on water spray intensities and differential pressure levels that are significantly lower than those used in many established testing standards.

To address the mentioned problem, some researchers have developed test setups with lower water application rates or air pressure differences. Rathbone [50] and Hens et al. [51] conducted experimental studies using water spray rates between 2.0 and 6.4 l/m^2/h, reducing the rates by 95% compared to the ASTM E514 standard [38]. Forghani et al. [48] adjusted the differential air pressure in the

ASTM E514 [38] from 500 Pa to 45 Pa. Other studies conducted by Slapø et al. [23], Anand et al. [43], and Lacasse et al. [49] carried out tests with differential air pressure ranging from 0 to 750 Pa.

In most existing studies, water penetration in brick masonry is commonly investigated using already saturated masonry, potentially leading to an inadequate understanding of how water penetrates under WDR conditions. This oversight implies that the buffering capacity of non-saturated masonry is ignored. Hence, conducting studies that simultaneously measure water content and penetration can offer a more accurate picture of the water penetration process through masonry walls during WDR exposure, ultimately enhancing the precision of hygrothermal analyses. Considering that water penetration in initially non-saturated clay brick masonry without large cracks takes time to develop [20, 24, 96, 125], measuring water content before penetration can be a valuable approach to establishing a meaningful correlation between water content and water penetration in masonry.

In summary, the available test standards and other studies have some limitations, such as conducting tests in a saturated state and using extreme test conditions concerning water spray rate and air differential pressure. It is worth mentioning that the leakage levels reported in the literature are obtained after several hours of testing at extremely high water spray rates and air pressure differences. Accordingly, to address the mentioned shortcomings, the author of this thesis has developed a new test setup, which will be further described in Section 4.1.

3.2.3.4 Penetration without wind pressure (balance of forces)

The conventional assumption that wind-induced pressure differences act as the primary driving force for water penetration in wall assemblies faces challenges when dealing with masonry walls. Several experimental studies have shown significant water penetration rates even without the application of any difference in air pressure [11, 21, 30, 126]. Water runoff from the exterior surface of the façade can be drawn into small cracks and pathways through capillary suction. In addition to capillary action, which involves moisture transport through porous materials via capillary pores, moisture can also be transported as free water by hydrostatic pressure alone through cracks and other larger voids [127]. This mode of transport poses a more problematic scenario for moisture safety compared to capillary moisture transport, primarily because the velocity of free water transport is considerably higher than that of capillary water transport. In this mode of water transport, hydrostatic pressure (the pressure exerted by a fluid at rest at a specific point within the fluid, resulting from the force of gravity) might act as the dominating driving force, although there is no consensus on the forces driving water out, resulting in water penetration [21, 22, 128, 129].

The existing literature predominantly focuses on water penetration through regular openings, varying in size between 1 and 8 mm, where a thin layer of polycarbonate

board or steel sheets has been used. Van Den Bossche [22] introduces three forces to analyze water penetration through gaps, namely surface tension (P_s), capillary pressure (P_c), and hydrostatic pressure (P_h). Capillary forces, P_c, play a role in directing water toward an opening, while the hydrostatic pressure, P_h, from a water column inside the opening promotes penetration. At the same time, surface tension, P_s, introduces a meniscus acting as a barrier that counteracts penetration. For penetration to occur, the meniscus formed on the backside of the opening due to surface tension must be breached, meaning that $P_c + P_h$ should be larger than P_s.

- Surface tension (P_s)

On the backside of an opening, the surface tension of water creates a meniscus that is formed due to the greater cohesive forces of water molecules near the surface compared to those away from it. Accordingly, the meniscus adopts a concave shape (Figure 11.a), which needs to be breached by an external force to transition the meniscus from concave to convex (Figure 11.b & 11.c). For a circular tube, the force, F_s [N], and pressure, P_s [Pa], resulting from the surface tension can be calculated using the following equations:

$$F_s = 2 \cdot \pi \cdot r \cdot \gamma \tag{19}$$

$$P_s = \frac{F_s}{A} = \frac{2 \cdot \gamma}{r} \tag{20}$$

where r [m] is the radius of the circular tube or pore, γ [N/m] is the surface tension of the water, depending on the temperature, and A [m^2] is the area of the circular tube.

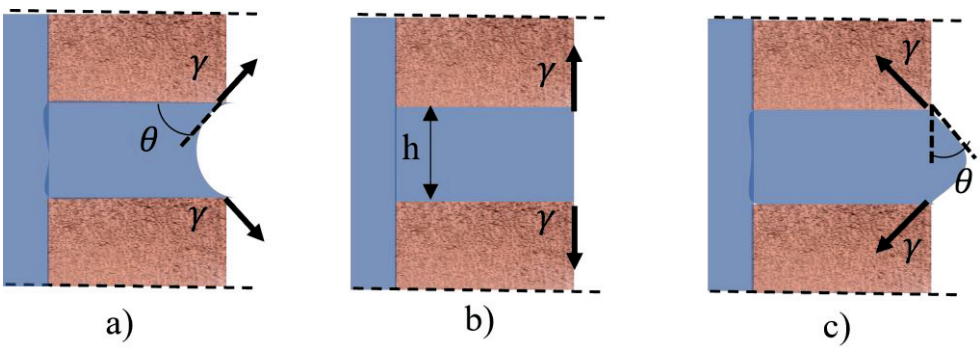

Figure 11. (a) Initially, water is drawn into the opening as a result of capillary action, (b) On the backside side of the opening, the meniscus takes on a flat shape with the surface tension preventing water penetration, and (c) The hydrostatic pressure increases, causing the contact angle of the meniscus to rise. This increase in the contact angle is countered by surface tension, as adapted from [21]

- Capillary pressure (P_c)

In the case of hydrophobic materials, characterized by a contact angle greater than 90°, capillary action results in a negative pressure on the water at the opening. In contrast, capillary pressure in hydrophilic materials, with a contact angle of less than 90°, draws water into the opening due to the forces between water and the inner surfaces of the opening. In this scenario, the opening functions like a capillary tube. Capillary flow ends at the backside of the opening (Figure 11.a). The capillary pressure, P_c [Pa], can be calculated using the Young-Laplace equation, Eq. (21):

$$P_c = \frac{2 \cdot \gamma \cdot \cos\theta}{r} \tag{21}$$

where θ [degree] is the contact angle between water and substrate.

- Hydrostatic pressure (P_h)

Hydrostatic pressure, P_h [Pa], is the pressure caused by a water column (the height of the water column in an opening) due to gravity. When an opening is filled with water, the highest hydrostatic pressure thus occurs at the bottom of the opening. In brick masonry, hydrostatic pressure can be built up in the joints that often contain gaps, voids, and sometimes cracks. Also, the brick might contain larger cracks originating from the drying and firing of the clay. The hydrostatic pressure can be determined as follows:

$$P_h = \rho_w \cdot g_r \cdot h \tag{22}$$

where P_h [Pa] is the hydrostatic pressure, ρ [kg/m^3] is the water density, g_r [m/s^2] is the gravitational acceleration, and h [m] is the height of the water column.

In the case of brick masonry, pores with dimensions less than 0.1 mm have such high capillary suction that they rarely contribute to rain penetration [127]. On the other hand, larger irregularities, such as cracks and unbonded interfaces, exhibit lower capillary suction but can hold a greater volume of water. These larger irregularities become important contributors to water penetration when an additional driving force is present. Since the surface tension of water is approximately 0.075 N/m, the capillary suction pressure for irregularities in the range of 0.1 mm to 1 mm wide will be in the order of 750 to 75 Pa, considering a contact angle of 60°. Once the water reaches the protected side of the brick masonry, the surface tension creates a meniscus that must be breached for penetration to occur. The hydrostatic pressure from the water, which accumulates in the irregularities of the masonry, will act as a driving force that can breach the meniscus. For instance, a hydrostatic pressure of around 600 Pa may result from an interfacial crack between the brick and mortar over a typical brick with a height of 60 mm, sufficient to breach the meniscus in a 0.125 mm wide pathway (~ crack width of 0.125 mm) [21, 95, 126]. Nevertheless, to get the full hydrostatic effect, the gap at the brick-mortar

interface should be wide enough; otherwise, the water will be retained by capillary suction. The occurrence of water penetration in brick masonry specimens without any difference in applied air pressure is studied and discussed in Papers III and V.

A theory similar to Van Den Bossche's [22] has been presented by Hagentoft and Olsson [128] and Olsson [129]. According to Hagentoft and Olsson [128] and Olsson [129], capillary action is not considered a driving force for water penetration through an opening; it is active only when water is sucked into the opening (Figure 11.a). Only when an external pressure, such as hydrostatic pressure, applies to the opening does the meniscus protrude from the opening. In this scenario, surface tension acts to counteract water penetration. As the external pressure increases, the contact angle between the meniscus and the opening also increases (transit from concave to convex) up to the point where the meniscus breaches (see Figure 11). Thus, in contrast to the study by Van Den Bossche [22], only the horizontal component of the surface tension for a meniscus with contact angle θ counteracts penetration, while hydrostatic and wind pressure promote penetration.

Accordingly, the required hydrostatic pressure to breach the meniscus of water in a crack with a rectangular cross-section (see Figure 11.c) can be calculated as stated by Van Linden [21]:

$$P_h = \frac{\gamma \sin\theta (2D+2h)}{D \cdot h} \tag{23}$$

where D [m] is the length and h [m] is the height of the rectangular crack.

It should be noted that in addition to the hydrostatic pressure, pressure difference due to wind pressure, P_w, promotes penetration. In the calculation method utilized by Hagentoft and Olsson [128] and Olsson [129], the total pressure difference, P_{tot}, is thus obtained by considering three components, namely, surface tension (P_s), hydrostatic pressure from the water column (P_h), and wind pressure (P_w).

- Wind pressure (P_w)

In the case of a pressure-equalized or well-ventilated façade, the air pressure difference across the façade layer due to wind pressure is limited [128, 129]. However, façades with no or partial pressure equalization might exist where the wind can create a pressure difference. The wind pressure, P_w [Pa], across the façade layer can be calculated by the following equation:

$$P_w = \frac{\rho_{air} \cdot \mathrm{v}^2}{2} \tag{24}$$

where ρ_{air} [kg/m^3] is the air density, and v [m/s] is the wind velocity.

The results obtained by Olsson [129] indicate that for an absorbing material, the counteracting meniscus may not form at the backside of the opening, as described

above. Neglecting the counteracting force from the meniscus implies that penetration occurs even under small wind and hydrostatic pressures. There exist cases where no water penetration is registered, even in the presence of hydrostatic pressure or air pressure differences [17]. This is further discussed in Papers III and V. This observation can be related to the fact that the experiments conducted by Van Den Bossche [22], Olsson [129], and Van Linden [21] primarily focused on thin layers of non-absorbent material with varying crack sizes.

Although brick masonry shares similarities with the mentioned studies, water transport through brick masonry can differ significantly due to its thickness, porosity, and the presence of cracks or voids. Accordingly, no measured water penetration despite hydrostatic pressure can be attributed to insufficient hydrostatic pressure forming in the head joint because of good workmanship or good contact between brick and mortar to counteract pressure loss resulting from flow resistance [128] and friction in the interconnected pathways.

4 Experimental investigation of brick masonry exposed to water spraying

This chapter starts with presenting the development of a test setup designed to address the limitations of previous studies, with the primary objective of investigating the resistance of brick masonry to water spraying. The chapter proceeds to present the outcomes of two experimental campaigns carried out using this setup to study the response of brick masonry without known cracks exposed to water spraying. Subsequently, the results of a third experimental campaign conducted on cracked masonry are presented. The results are discussed in three subsections: water absorption, water penetration, and damp patches. The results are presented and discussed in detail in Papers II, III, and V, while this section provides a summary and discussion of all results combined.

4.1 Development of a new test setup

Several test setups are presented in the literature [46, 130, 131], aiming to study water penetration in masonry walls qualitatively or quantitatively. A comparative study reviewing the features of existing water penetration and leakage tests conducted by Driscoll and Gates [46] identifies a need for test methods to complement existing ones since little attention has been given to the correlation between tests and the factors contributing to water penetration.

Accordingly, a new test setup was developed in this project to study more realistic scenarios of masonry exposure to wind-driven rain (WDR) events. The test setup is able to produce a uniform water spray covering the exposed surface of small masonry specimens. A uniform and well-distributed water spraying pattern was achieved using a low-flow full-cone nozzle and pressure regulators. Applying a wide range of water spray rates is possible, simulating different driving rain intensities. Additionally, two digital scales are employed to continuously measure water absorption and water penetration. A digital camera mounted on the protected side of the specimens traces the appearance of damp patches. Figure 12 shows the schematic of the test setup.

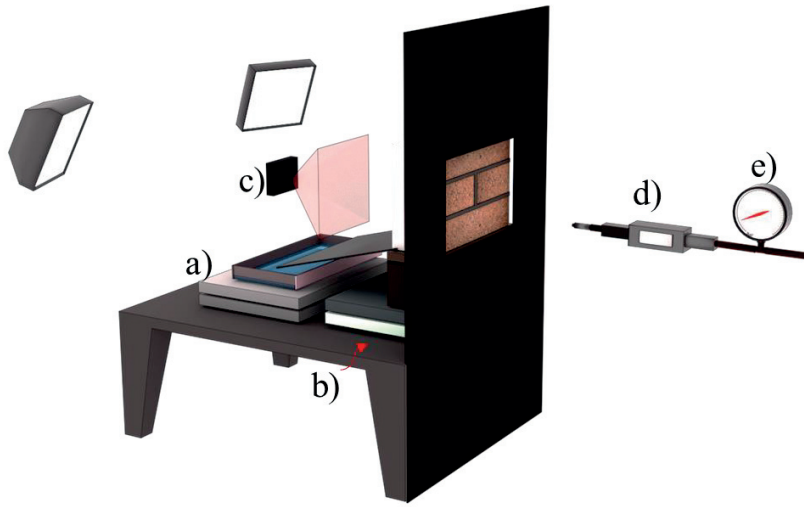

Figure 12. Schematic of the developed test setup: a) scale measuring water penetration, b) scale measuring water absorption, c) digital camera, d) water flow meter, and e) water pressure regulator

In the setup utilized for testing, a digital camera was positioned behind the specimens, facilitating the capture of the first visible dampness and the subsequent evolution of the damp area as time elapsed.

The presented test setup was developed with specific consideration to produce a varied range of spray rates and a uniform distribution of the spray droplets. Firstly, a low water flow nozzle with a full cone spray pattern was utilized, and the distance between the nozzle and specimens was adjusted to ensure uniform coverage of the exposed surface. A visual examination was conducted using a paper towel exposed to the water spray for 1–2 seconds (see Figure 13) to verify the quality and uniformity of water droplets. A more detailed description of the test setup is presented in Papers II and III.

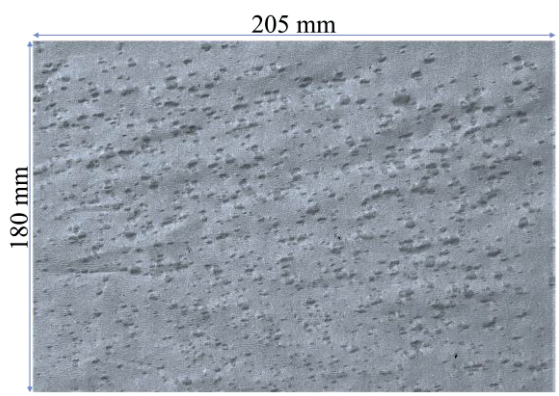

Figure 13. Wet dots on a paper sheet exposed to water spray for 1–2 seconds

Compared to existing test setups, two significant improvements are achieved. Firstly, the continuous measurement of water absorption (mass gain) offers valuable insights into the moisture content of masonry at the start of water penetration. While many research studies employ high water spray rates and differential air pressure to study the resistance of masonry in the saturated state, the developed test setup is capable of investigating an initially dry brick masonry. Secondly, the exposed surface of the specimens is uniformly covered with water drops, which differs from other methods where a thin water film is applied from a nozzle close to the upper part of the masonry to ensure the immediate formation of a water film upon exposure.

Test conditions

Two experimental campaigns were performed to study the response of brick masonry, without known cracks, exposed to water spray. During the first experimental campaign – campaign A (Paper II), tests were conducted at zero differential air pressure, and water spray rates were adjusted to fall within the range of 2.0 to 3.6 $l/m^2/h$. These rates represent WDR intensities commonly observed in Sweden and are approximately 95% lower than the rates specified in current standards [37, 38, 40]. Various combinations of water pressure and nozzle-to-specimen distances were explored to achieve the desired low water spray rates. Ultimately, a water pressure of 0.55 bar and a nozzle-to-specimen distance of 55 cm were chosen, although it was later recognized that selecting a water pressure of 0.55 bar was not optimal due to the nozzle's recommended operating range of 0.7–20 bars. The water flow became more sensitive to changes in water pressure in the city network.

In the second experimental campaign – campaign B (Paper III), efforts were made to minimize water flow variations and better control the water spray rate. The water pressure was adjusted to approximately 1.05 bar, and the nozzle-to-specimen distance was reduced to approximately 50 cm. Consequently, the tests in this campaign were performed with a water spray rate of 6.3 $l/m^2/h \pm 5\%$ and zero differential air pressure. Straube and Brunett [96] considered a water spray rate ranging from 5 to 10 $l/m^2/h$ to be representative of more realistic WDR events.

While the first two campaigns deal with brick masonry without known cracks, the third campaign (Paper V) was designed to investigate the resistance of cracked brick masonry exposed to water spray. In the third campaign, the specimens were exposed to an average water spray rate of around 7 $l/m^2/h$ without applying any differential air pressure.

For all experimental campaigns, the masonry specimens underwent testing for 23 hours, comprising six consecutive cycles. Each cycle consisted of 210 minutes of water spraying followed by a 20-minute pause. Notably, the tests were conducted at zero differential air pressure.

4.2 Tests on masonry without known cracks

4.2.1 Experimental details

4.2.1.1 Bricks and mortars

This study focused on two commonly used solid clay bricks available on the Swedish construction market, denoted as bricks type I and II. To characterize their water absorption properties, twenty bricks from each type were subjected to tests following the ASTM C67 standard [132]. The tests included the initial rate of absorption (IRA) and the 24-hour water absorption. The IRA quantifies the rate at which the surface of a brick absorbs water during the first minute of contact, while the 24-hour water absorption measures the amount of water a brick can absorb when fully immersed, expressed as a ratio relative to its initial weight. The average IRA values for bricks type I and II were found to be 1.95 kg/m^2 and 1.81 kg/m^2, respectively. Accordingly, bricks type I and II can be classified as medium suction bricks, denoted [I] and [II]. The 24-hour water absorption properties of bricks were 16.0% and 8.6%. The density, IRA, and 24-hour water absorption parameters of the bricks are summarized in Table 3.

Table 3. Material properties of bricks and mortars including density, IRA, 24-h water absorption, and water absorption coefficient (A_w)

Materials	Dimensions (mm × mm × mm)	Density ρ (kg/m^3)	Average IRA ($kg/m^2/min$)	CoV (%)	Average 24-h water absorption (%)	CoV (%)	Average A_w (kg/(m^2.s$^{0.5}$))	CoV (%)
Brick type I	250×120×62	1800	1.95	2.3	16.0	1.6	0.193	0.8
Brick type II	250×120×62	2050	1.81	5.1	8.6	14.5	0.133	16.1
Mortar M 2.5	100×100×100	1869	0.30	15.8	6.3	2.8	0.022	8.7
Mortar NHL 3.5	100×100×100	1715	0.80	20.4	-	-	0.159	9.2

Furthermore, the water absorption coefficient of bricks, denoted as A_w, was determined through tests conducted on ten bricks of each type in accordance with the ASTM C1403 – 15 standard [133]. The procedure involved immersing the bricks in water, allowing water to penetrate to a depth of 3-5 mm from the bed face. Subsequently, the weight of the bricks was measured at distinct time intervals. The measure of absorbed water per unit area of the brick (Q [kg/m²]) was calculated by dividing the difference between the increased weight (w_i [kg]) and the initial weight (w_0 [kg]) by the cross-sectional area of the brick (A [m²]) (as defined by Eq. (25)).

$$Q = \frac{w_i - w_0}{A} \quad [kg/m^2] \tag{25}$$

The test results are presented by plotting Q [kg/m^2] against the square root of time [s$^{1/2}$]. The water absorption coefficient, A_w [kg/(m^2.s$^{0.5}$)], is mathematically

defined as the slope of the initial linear segment of the Q – $t^{1/2}$ relationship (Figure 14). The average water absorption coefficient for each type of brick is provided in Table 3.

This study used two types of pre-mixed dry mortars to prepare masonry specimens: a cement-based mortar M 2.5 and a natural hydraulic lime (NHL) 3.5 mortar. Mortar M 2.5 is a pre-mixed dry mortar widely employed in brick masonry façades; conversely, NHL 3.5 is a ready-mixed hydraulic lime mortar recommended for repointing. Tests have been conducted to characterize these mortars in terms of their initial rate of absorption (IRA) and water absorption coefficient, following the ASTM C67 standard [132] and ASTM C1403–15 standards [133], respectively. Furthermore, the 24-hour water absorption capacity of mortar M 2.5 has been evaluated according to the ASTM C67 standard [132]. Table 3 summarizes the average IRA and water absorption coefficients of three different types of mortar, and Figure 14 shows the water absorption rate of the mortars over the square root of time.

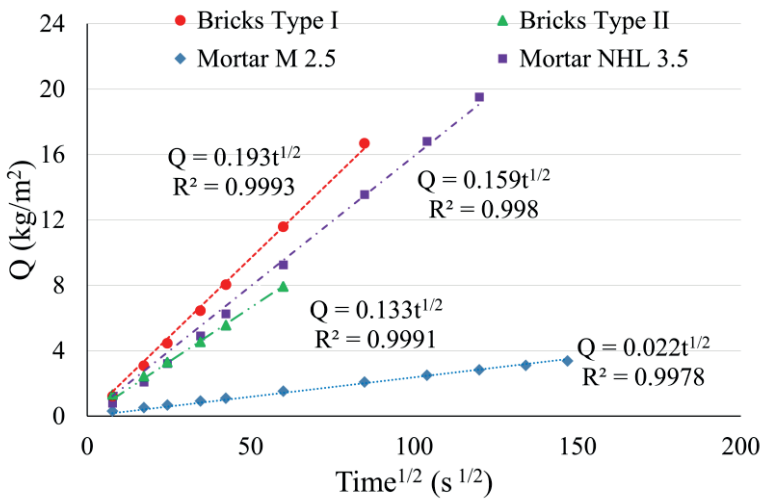

Figure 14. Average water absorption per unit area against the square root of time for bricks type I & II III and for mortar M 2.5 & NHL 3.5 during the initial stage of the test

4.2.1.2 Masonry specimens

Three-course masonry prisms were prepared with bricks of type I and II using mortar type M 2.5. The mortar joint profile was prepared with a flush and raked finish. The flush profiles were further divided into standard and after-pointed categories. The after-pointing technique involves removing the outer part of the joint before hardening and then completing it with repointing mortar type NHL 3.5 to have a flush finish. Raked specimens may simulate eroded mortar joints. By comparing water absorption and penetration in flush and raked specimens, insights

were gained into how mortar joint erosion might influence water absorption and penetration.

The specimens, mimicking a masonry veneer wall, measured 250 ± 5 mm in length, 218 ± 3 mm in height, and 120 ± 2 mm in depth. The size was chosen for ease of handling while maintaining integrity. As summarized in Table 4, Campaign A involved 39 3-course masonry prisms, while Campaign B included 24 specimens. All specimens in the two campaigns were prepared at the same time. The prepared masonry specimens are divided into two series depending on the brick type (Figure 15 and Table 4). Series I is made up of specimens built using medium suction bricks [I], while Series II comprises specimens built with medium suction bricks [II]. Within each Series, further divisions are made into three groups based on the joint profile finish. Group G1 encompasses specimens constructed with mortar M 2.5 featuring a tooled flush joint profile. Meanwhile, group G2 includes specimens built with mortar M 2.5, utilizing a raked joint profile. Group G3 also comprises specimens constructed with mortar M 2.5; however, compared to G1, the outer 6 mm of the mortar joint is pointed one day after bricklaying using mortar NHL 3.5, showcasing a tooled flush joint profile.

Table 4. Specimen designation and configurations

Experimental campaign	Series	Group	Brick	Mortar	Joint profile finish	Ave water spray rate ($l/m^2/h$)	No. of specimen
First campaign A	Series I	G1	Medium suction type [I]	M 2.5	Flush	3.6	5
		G2	Medium suction type [I]	M 2.5	Raked	3.6	5
		G3	Medium suction type [I]	M 2.5 / NHL 3.5	After-pointed	3.4	5
	Series II	G1-a	Medium suction type [II]	M 2.5	Flush	3.2	5
		G1-b	Medium suction type [II]	M 2.5	Flush	2.0	3
		G2	Medium suction type [II]	M 2.5	Raked	2.3	8
		G3	Medium suction type [II]	M 2.5 / NHL 3.5	After-pointed	2.0	8
Second campaign B	Series I	G1	Medium suction type [I]	M 2.5	Flush	6.3	4
		G2	Medium suction type [I]	M 2.5	Raked	6.3	4
		G3	Medium suction type [I]	M 2.5 / NHL 3.5	After-pointed	6.3	4
	Series II	G1	Medium suction type [II]	M 2.5	Flush	6.3	4
		G2	Medium suction type [II]	M 2.5	Raked	6.3	4
		G3	Medium suction type [II]	M 2.5 / NHL 3.5	After-pointed	6.3	4

The bricks were not pre-wetted prior to bricklaying to adhere to supplier recommendations. These recommendations align with those mentioned in [32], which states that pre-wetting bricks in the low to medium range of IRA is not required. To mitigate uncertainties tied to workmanship, a single craftsman undertook the preparation of all specimens. Particular attention was paid to ensuring consistent water addition to every batch of mortar mix, thereby minimizing the impact of mortar flow on water penetration. Specimens in group G1, employing

mortar M 2.5, were tooled with a wooden stick to attain a flush profile. For specimens showcasing the raked joint profile in group G2, a 5 mm screw was employed to remove excess mortar, achieving a 5 mm depth. Specimens employing the after-pointing technique had surplus mortar removed using a 6 mm screw, and the subsequent day, the 6 mm void was filled with NHL 3.5, then tooled to yield a flush joint profile (Figure 15).

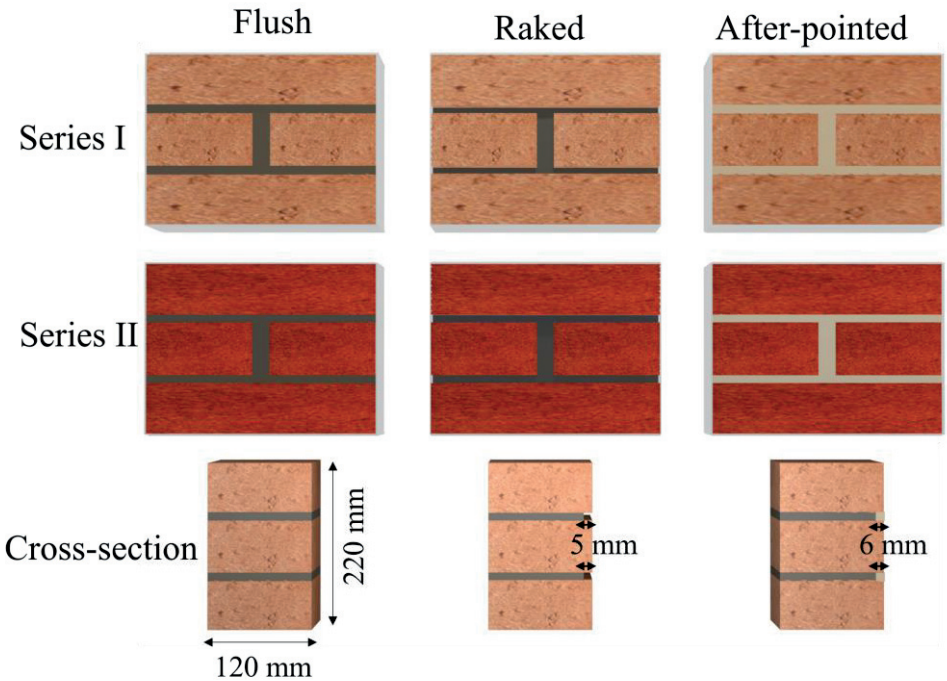

Figure 15. Representative specimens from each group and Series after sealing and Schematic of the mortar joint profile finishes (the bottommost row) [35]

Before conducting the testing, all sides of the specimens, except for the exposed surface and the backside, were sealed using a two-component sealant (ARDEX P2D and ARDEX S1-K). This process resulted in the application of a flexible waterproof coating. This sealing is aimed at preventing unintended water absorption on surfaces other than the exposed one.

In the first campaign (A), the specimens in groups G1, G2, and G3 of Series I were exposed to an average water spraying rate of 3.6, 3.6, and 3.4 $l/m^2/h$, respectively. Specimens of group G1 Series II are divided into two subgroups, G1-a and G1-b, based on the average water application rate. The average water spraying rate for groups G1-a, G1-b, G2, and G3 of Series II was 3.2, 2.0, 2.3, and 2.0 $l/m^2/h$, respectively (Table 4). In the second campaign (B), all specimens were exposed to a uniform and constant water spray rate of 6.3 $l/m^2/h \pm 5\%$ (Table 4).

4.2.2 Results and discussions

4.2.2.1 Water absorption

The water absorption was measured throughout the testing in campaigns A and B. The water absorption, Q [kg/m^2], herein is defined as the amount of absorbed water [kg] per unit area of the masonry specimen [m^2]. Figure 16 shows the water absorption behavior of each group tested in campaign A exposed to varying water spray rates. Series I and Group G1-a of Series II encountered a more intensive spray rate (3.2–3.6 l/m^2/h) compared to Series II groups G1-b, G2, and G3 (2.0–2.3 l/m^2/h). A linear absorption trend is observed in the initial cycle (3.5 hours), indicating substantial absorption of sprayed water into the specimens. The water spray rate and absorption coefficient of bricks particularly influenced this linear behavior during the first cycle before surface saturation. Similar trends in absorption were observed for Series I specimens and Series II Group G1-a, with distinct brick absorption properties. The absorption behavior of Series II Group G1-b, G2, and G3 exhibited similar patterns during the initial cycle (Figure 16). Slight absorption discrepancies post the first cycle were attributed to variations in water spray rates, brick absorption properties, and mortar joint profile. Bounce-off was estimated between 8% and 23% for the 1st cycle, accounting for the difference between sprayed and absorbed water.

As the tests progressed, nonlinearity in absorption behavior indicated surface saturation. As mentioned, the time taken to reach saturation was determined by the water spray rate and water absorption coefficient. Surface saturation was observed later for Series I than for Series II Group G1-a, reflecting a higher absorption coefficient facilitating rapid moisture transport. Surface saturation occurred after the third cycle for most Series I and II groups, except Group G1-a, where nonlinearity emerged in the second cycle. Subsequent saturation led to a water film forming on the exposed surface. The absorption continued until nearly the 6th cycle for Series I, indicating proximity to full saturation. Conversely, Series II groups G1-b, G2, and G3 experienced absorption until the end of testing due to relatively lower spray rates. Notably, Series II Group G1-a reached near saturation in the 5th cycle, with negligible water accumulation beyond this point. The results for individual specimens and additional discussions have been documented in Paper II.

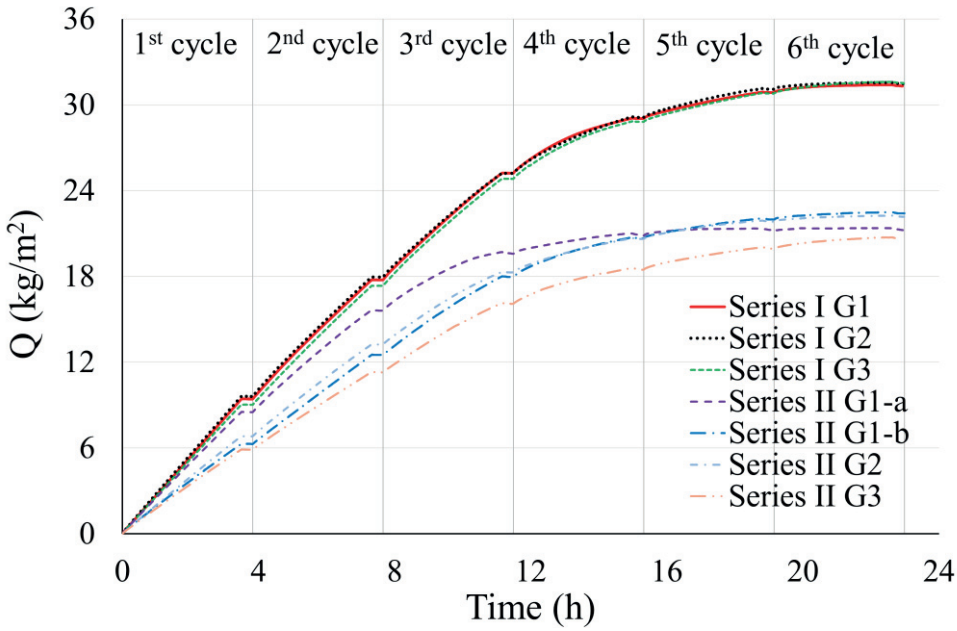

Figure 16. Average water absorption vs. time response of a) Series I and Series II group G1-a; b) Series II group G1-b, G2, and G3 in the first experimental campaign (A)

In campaign B, all specimens were exposed to a uniform and consistent water spray rate of 6.3 l/m^2/h ± 5%. Figure 17 shows the water absorption behavior observed over a 23-hour testing period. Similar to the specimens tested in campaign A, a comparable trend is observed: an initial linear response before surface saturation is followed by a nonlinear response, indicating surface saturation is reached depending on the spray rate and water absorption coefficient. In the initial 1 to 2 hours of testing, depending on the Series, a significant portion of the sprayed water was absorbed, showing that surface saturation had not yet been achieved. The bounce-off varied in the range of 7% to 14%. With the attainment of surface saturation, recognizable from the deviation from the linear slope in the absorption curve, the absorption response transited into a nonlinear behavior, accompanied by a diminishing slope that eventually approached zero. At the end of the 4th cycle, the absorption ends for Series I and II, encompassing medium suction bricks of types I and II. The outcomes underline the reliance of water absorption rate in masonry specimens on the water absorption coefficient of the bricks and the water spray rate, while the total water absorption predominantly aligns with the brick's absorption capacity.

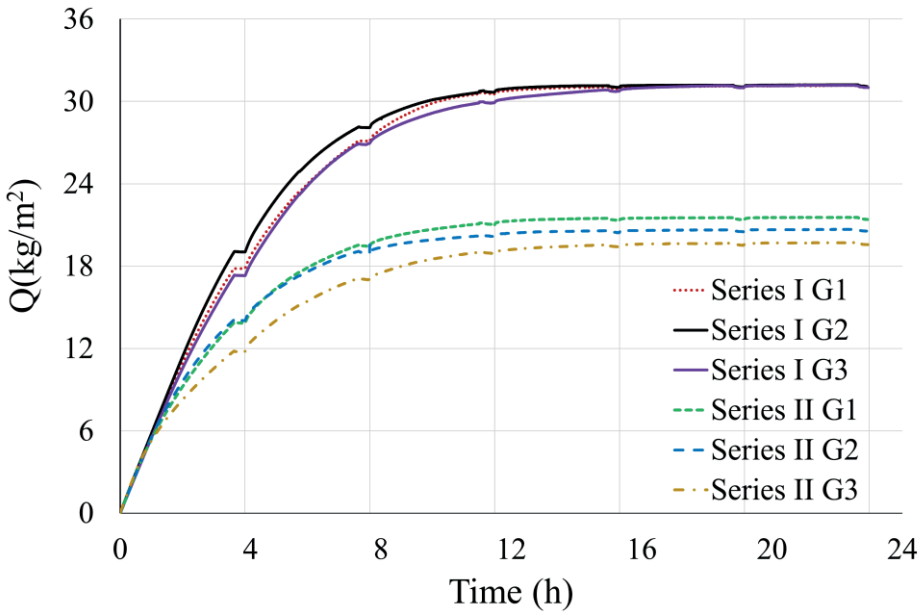

Figure 17. Average water absorption vs. time response of Series I, Series II, and Series III in the second experimental campaign (B), a) during 23 h of testing and b) during the first two hours after starting the test

The absorption response is plotted against time here, although it was previously mentioned that the absorbed mass of water demonstrates proportionality to the square root of time (Section 3.2.2.1). This is related to the fact that four conditions should be fulfilled for the cumulative absorption (Q) in a single-sided water absorption test to undergo an increase proportional to the square root of the elapsed time ($t^{1/2}$) [107]. These conditions are as follows: (1) the initial water content is uniform; (2) the flow inside the material is strictly one-dimensional, and water is freely available at the inflow face; (3) the material is homogeneous; and (4) the material is unchanged structurally and microstructurally by changes in water content. While efforts were directed towards satisfying conditions 1 and 4, it is important to highlight that the fulfillment of conditions 2 and 3 was impossible due to the water spray rate and masonry composition, consisting of brick and mortar.

Table 5 provides a summary of water absorption after the first water spraying cycle (210 min) and the total absorption in each group within each series. The amount of absorbed water during the first cycle in group G3, after-pointed joint profile, is lower than that of group G1 and G2 in all series of campaigns A and B. For instance, in campaign A Series II, the lowest average water absorption, amounting to 5.9 kg/m^2, is exhibited by group G3, which is exposed to the lowest average water spray rate of 2.0 l/m^2/h group G1-b. Similarly, in campaign B, group G3 in both Series I and II absorbed the least amount of water compared to groups G1 and G2. In addition to the variation in water spray rate and masonry absorption properties, the

lower absorption in group G3 can be related to the compaction achieved with the after-pointing technique.

The average total absorption in Series I specimens, tested in both experimental campaigns, A and B, was approximately 31.0 kg/m^2, highlighting negligible differences in average water absorption across groups G1, G2, and G3. On the other hand, the average water absorption for Series II groups G1, G2, and G3 ranged from 20.6 kg/m^2 to 22.4 kg/m^2 in Campaign A and 19.6 kg/m^2 to 21.4 kg/m^2 in Campaign B. These findings underline a strong correlation between the total absorption of masonry and brick absorption capacity, considering the high variability in the water absorption capacity of the bricks type II (CoV = 14.5 %).

Table 5. The average water absorption and time to the appearance of the first visible damp patch on the backside of each group within each Series in Campaigns A and B after the first and the sixth cycle

		Water spray rate (l/m^2/h)	1st cycle Absorption (kg/m^2)	Total Absorption (kg/m^2)	CoV %	Time to the 1st dampness (h)
Campaign A	Series I G1	3.6	9.4	31.3	0.6	7.9
	Series I G2	3.6	9.6	31.5	0.3	7.8
	Series I G3	3.4	9.0	31.5	0.2	8.0
	Series II G1-a	3.2	8.5	21.2	10.4	4.8
	Series II G1-b	2.0	6.3	22.4	6.3	6.3
	Series II G2	2.3	6.8	22.2	6.0	5.9
	Series II G3	2.0	5.9	20.6	5.6	6.4
Campaign B	Series I G1	6.3	17.8	30.9	0.9	2.7
	Series I G2	6.3	19.0	30.9	0.5	3.4
	Series I G3	6.3	17.3	31.0	0.7	2.7
	Series II G1	6.3	13.8	21.4	10.0	2.6
	Series II G2	6.3	14.0	20.5	10.4	2.3
	Series II G3	6.3	11.8	19.6	2.7	2.7

The obtained results indicate that joint profile finishes do not considerably influence water absorption, suggesting that eroded (recessed) mortar joints have a marginal impact on water absorption from WDR. Specimens prepared with raked and after-pointed joint profiles offer insightful guidance for decision-makers. While the former, symbolizing eroded mortar joints, indicates that the impact of such erosion on water absorption in masonry façades is unlikely to be significant, the latter highlights that the application of secondary compaction (adding new mortar) could potentially lead to a reduction in water absorption rates within masonry façades.

4.2.2.2 Water penetration

As no considerable amount of water could be collected from the backside of the specimens studied in Campaign A, this section only presents the results of water penetration in specimens tested in Campaign B.

Figure 18 and Table 6 present the average water penetration [kg/m^2] for each group within Series I and II during the 23-hour test period in Campaign B. Notably, water penetration commenced either towards the end of the second cycle or the beginning

of the third cycle, indicating that it started when the masonry specimens were close to saturation. This behavior is consistent with observations by Straube and Burnett [96] and Fishburn et al. [17]. Once water penetration starts, it continues approximately at a constant rate until the end of the test, except during the 20-minute long pause between each spraying cycle, during which no penetration is registered. Paper III contains the results for individual specimens as well as additional remarks.

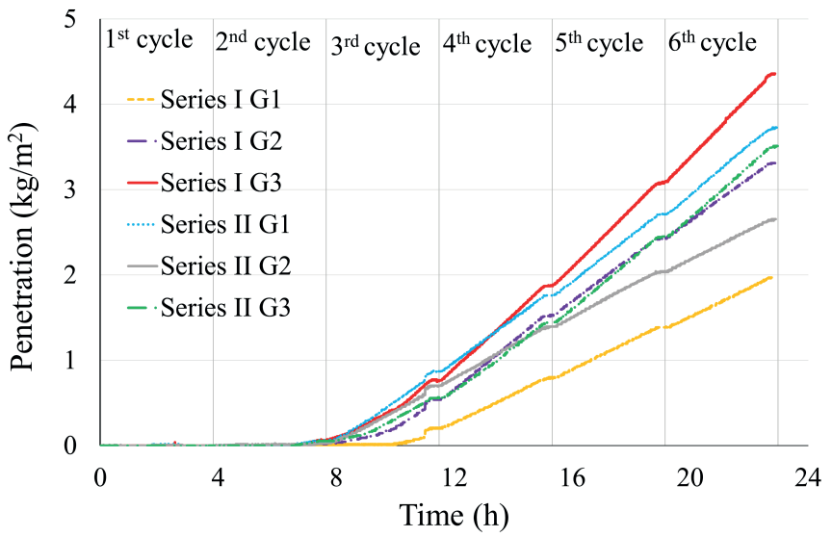

Figure 18. Average water penetration vs. time response of all Series in campaign B

The coefficient of variation (CoV), as presented in Table 6, highlights considerable variability in the results of water penetration among individual specimens within each group (4 specimens tested within each group). Several factors could contribute to this wide scatter in water penetration response of specimens of the same type/group: a) variations in workmanship quality might lead to incomplete joint filling, particularly the head joint, and b) adequate contact between brick and mortar might not be achieved in some specimens.

Table 6. Water penetration in terms of time to penetration, the corresponding saturation level, the amount of penetration, and leakage percentage for each group of Campaign B

		Time to penetration (h)	Saturation level (%)	Penetration (kg/m^2)	CoV (%)	Penetration rate ($kg/m^2/h$)	Leakage (%)	Avg (%)
Campaign B	Series I group G1	10.4	94.5	2.0	33	0.16	2.6	3.8
	Series I group G2	8.8	94.8	3.3	71	0.24	3.9	
	Series I group G3	8.2	87.6	4.4	78	0.31	4.9	
	Series II group G1	9.4	93.4	3.7	66	0.26	4.1	3.8
	Series II group G2	8.6	94.5	2.7	61	0.18	2.9	
	Series II group G3	9.0	93.0	3.5	23	0.25	4.2	

The results indicate that water penetration started when the saturation level of masonry was around 90%. The saturation level of masonry specimens at which the water penetration started is summarized in Table 6. Further, Figure 19 indicates that in both Series I and II, water penetration starts when the masonry is close to saturation, highlighting the benefit gained from the water absorption capacity of brick masonry to buffer and thus postpone water penetration [96].

In current standards and research studies, traditional test setups often employ high water spray rates and differential air pressure on an already saturated masonry specimen. These test setups may provide a phenomenologically misleading image of the evolution of water penetration induced by WDR by disregarding the water buffering capacity of non-saturated masonry. In contrast, campaign A, characterized by low water spray rates and no differential air pressure, resulted in minimal observable water penetration. This suggests that the specimens absorbed most of the sprayed water and got saturated close to the end of the test.

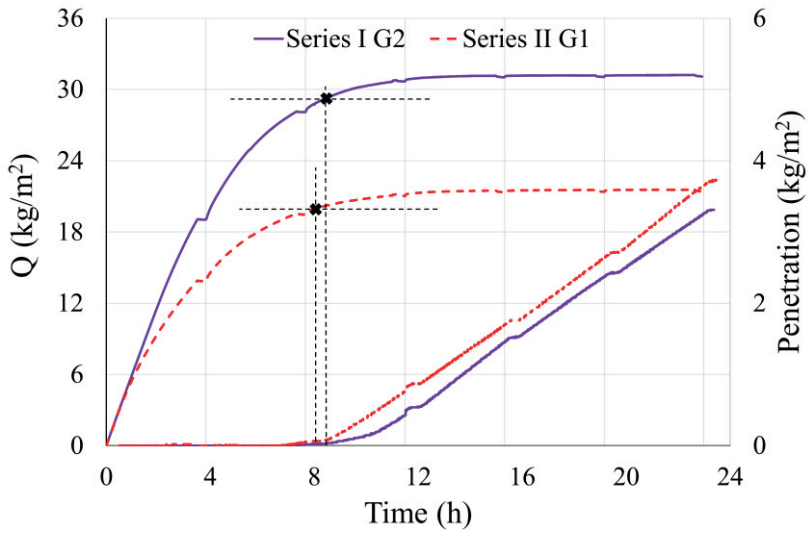

Figure 19. Water absorption and penetration of two representative groups of campaign B, indicating the correlation between the start of penetration and saturation level – the horizontal dashed lines indicate roughly 90 % saturation

The results in terms of leakage, defined as the ratio between the amount of penetrated water and the amount of sprayed water, are summarized in Table 6. In light of the present study, a water spray rate of 6.3 l/m^2/h applied during 21 h might lead to an average leakage of between 2.5–5 % of the sprayed water. It should be mentioned that the penetrated water mainly passed through the brick-mortar interface, indicating the importance of the interfacial zone on masonry's resistance to WDR. As no differential air pressure was applied in campaign B, the driving potential forcing water to penetrate might be the hydrostatic pressure due to runoff, as stated by Calle et al. [11] and Straube and Burnett [96].

The obtained results suggest that water penetration is highly dependent on the saturation level of masonry (predominantly occurring above 90% saturation) and the water spray rate. When comparing water penetration among the different groups within each Series, it becomes evident that the impact of mortar joint profiles on water penetration is minimal – the highest amount of leakage in Series I was recorded for group G3, whereas in Series II, specimens of group G1 had the greatest amount of water penetration. It should be noted that instances of penetration might occur in initially dry masonry after approximately 8 to 10 hours of exposure to WDR at an intensity of 6.3 $l/m^2/h$, depending on the masonry's water absorption coefficient and water absorption capacity. Notably, as discussed in Section 3.1, most WDR events in Sweden typically last around 1 to 4 hours with an intensity of less than 1 mm/h, implying a low likelihood of encountering a WDR event lasting 21 hours at an intensity of 6.3 $l/m^2/h$. Nonetheless, in some areas of Europe or North America, masonry walls might experience prolonged periods of nearly saturated or wetness, typically during weather conditions with limited solar radiation, elevated relative humidity levels, and frequent WDR events [29]. This question is further analyzed in Paper III.

Head joints have been identified as a common pathway for water penetration because of the challenges of filling and compacting compared to bed joints. The testing conducted in this study confirms that water penetration primarily took place through the brick-mortar interfacial zone, particularly at the head joints. This observation aligns with previous research where head joints were identified as vulnerable points in resisting WDR [12, 21, 23]. In order to validate the finding regarding the low resistance of head joints to water penetration, specimens were inspected by raking out the head joints to a depth of 25–30 mm. Interestingly, even under controlled laboratory conditions, numerous voids and cracks were visible in the head joints of many specimens, as shown in Figure 20.

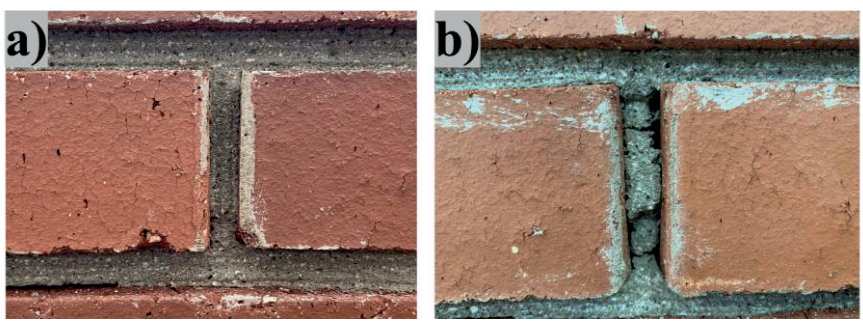

Figure 20. State of head joint of representative specimens after being raked out up to 25–30 mm: a) good/acceptable contact/bond and b) voids in the head joint

In this study, 3-course masonry prisms were built with only one head joint. While this likely reduced the risk of undesirable specimen breaking, it also meant that the

proportion of head joints was lower than what is typically found in real-world masonry, regardless of the bond type used. More head joints would likely lead to a higher water penetration rate per unit wall area. Moreover, increasing the mortar-to-brick ratio could potentially result in lower saturation levels at the start of penetration, given that the water absorption coefficient of mortar is lower than that of brick.

4.2.2.3 Damp patches

As shown in Figure 21, the location of the initial visible damp patch on the backside of the representative specimens subjected to testing in campaigns A and B is revealed. In most cases, the first damp patch was observed close to the brick-and-mortar interface, underlining the critical role of the interfacial zone, particularly at the head joint, as the primary path for water penetration.

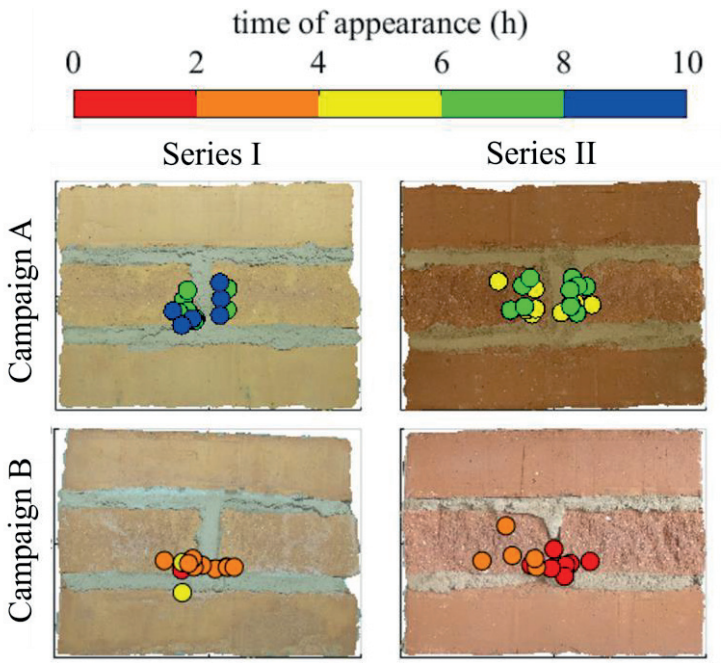

Figure 21. Location and time to the appearance of the first damp patch on the backside of specimens

Table 5 provides an overview of the average duration until the appearance of the first dampness on the backside of each group, encompassing both experimental campaigns. In campaign A, the average time for dampness to emerge for all Series I groups is approximately 8 hours, revealing the minor influence of joint profile finish. Within Series II, the first dampness of group G1-a specimens occurred after 4.8 hours at a water spray rate of 3.2 l/m^2/h. In contrast, group G1-b and G3 specimens, subjected to a water spray rate of 2.0 l/m^2/h, exhibited dampness after

nearly 6.4 hours. Additionally, a comparison between the time to the appearance of the first damp patch among all Series I groups and group G1-a within Series II, despite a similar water spray rate, emphasizes the influence of brick absorption capacity on the timing of initial dampness. In campaign B, the initial dampness typically appeared on the backside of the specimens during the first testing cycle.

While the time to the appearance of the first dampness varied between the two campaigns, the obtained results highlight that a certain saturation level is required. Despite variations in the water spray rate within the 1.7 to 3.8 $l/m^2/h$ range in campaign A, the time elapsed until the initial dampness corresponded to 49–58%. This observation underscores the role of masonry's buffering capacity in delaying the onset of dampness on the protected side of the masonry. The same results were observed in campaign B, as the appearance of the initial dampness coincided with when the water content of the specimens reached approximately half of their saturation capacity. This is further discussed in Papers II and III.

The results reveal the low resistance of head joints to WDR, which might be related to the difficulty of the workmanship in filling the head joints and low compaction in comparison with bed joints [134], valid for all series within campaigns A and B. Further, the effect of joint profile finishes on the time and location of the first visible dampness is negligible, whereas water spray rate and water absorption properties of bricks may strongly influence the time to the appearance of the first damp patch.

In Campaign B, while the first damp patch often occurs during the first test cycle when the water content level in specimens is roughly half of their saturation capacity, water penetration starts when the water content is above 90% saturation capacity (Figure 22). Table 5 summarizes the time it takes for the first damp patch to appear on the backside of the specimens, while Table 6 presents the initiation time for water penetration. Importantly, there is no discernible correlation between these two phenomena, aligning with findings by Fishburn et al. [17] as well as Ritchie and Davison [32]. For example, dampness emerges after 2.6 hours and 2.7 hours, while water penetration occurs after 9.4 hours and 9.0 hours for groups G1 and G3 of Series II, respectively.

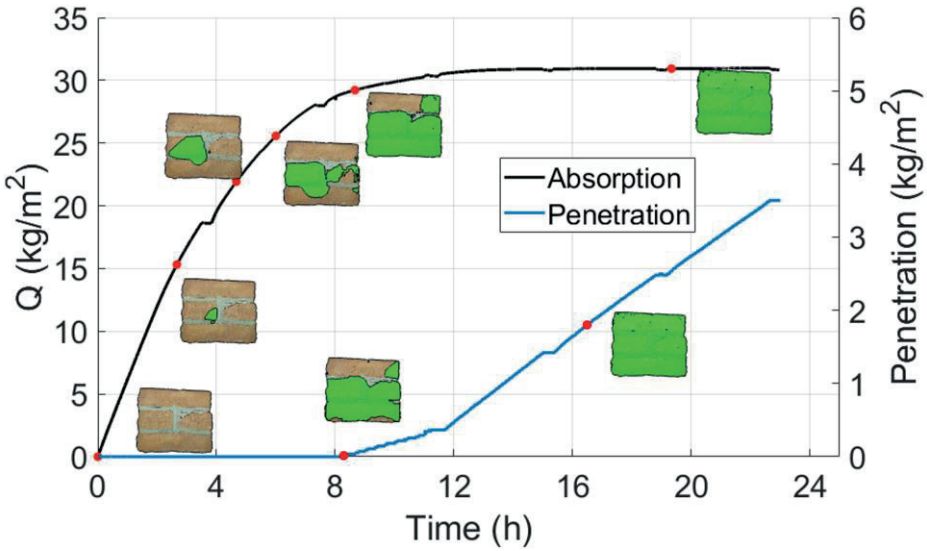

Figure 22. Appearance and growth of dampness (green marking) on the backside of a representative specimen at different times [35]

The difference between the time it takes for damp patches to appear and the initiation of water penetration lies in their respective transport mechanisms. Damp patches are primarily a result of capillary transport from the exposed side to the backside, while water penetration is likely related to laminar flow through larger pores and cracks driven by hydrostatic pressure due to runoff. Moisture transport in porous materials is generally dominated by capillary suction or laminar flow [118], depending on the water saturation level.

As already mentioned, dampness typically emerges on the backside of specimens when the water content is approximately half of the saturation capacity, indicating capillary suction as the controlling factor. Conversely, water penetration mainly occurs when masonry specimens are nearly saturated (above 90% of saturation capacity), suggesting that laminar flow governs the moisture transport. In the absence of significant air pressure differences, water penetration is attributed to the gravitational effect of runoff and hydrostatic pressure, aligning with findings from experiments conducted by Calle et al. [11] and Straube and Brunett [96].

4.3 Cracked masonry

Aside from the brick-mortar interfacial zone, which has been identified as a pathway facilitating both unsaturated and saturated water transport, the presence of cracks

could potentially create additional pathways for water transport. While much of the research on water penetration in masonry has focused on masonry without known cracks, water penetration in masonry with cracks is of great practical relevance since numerous brick masonry claddings have imperfections such as cracks resulting from factors like temperature and moisture gradients, settling, and applied loads.

4.3.1 Masonry specimens

While the specimens tested in campaigns A and B were prepared without any known cracks, the aim of the third campaign, campaign C, was to investigate the effect of artificial cracks on facilitating water penetration in brick masonry.

4.3.1.1 Preparation of specimens

Solid clay bricks from the Swedish construction market were used to build 3-course masonry prisms. Tests were conducted to determine the water absorption properties of brick, including the initial rate of absorption (IRA), 24-hour absorption capacity, and absorption coefficient for both the stretcher and bed faces. Mortar M 2.5, a cement-based type, was used to prepare the specimens. The IRA of brick was equal to 1.51 kg/m^2 for the stretcher face and 1.64 kg/m^2 for the bed face, alongside a 24-hour absorption capacity of 8.6%. The water absorption coefficients for bricks were measured as 0.160 kg/(m^2.s$^{0.5}$) for the stretcher face and 0.155 kg/(m^2.s$^{0.5}$) for the bed face. The mortar exhibited an A_w of 0.062 kg/(m^2.s$^{0.5}$) and a 24-hour absorption capacity of 10.9%.

The same professional bricklayer as in campings A and B built a total of 62 3-course masonry prisms; forty-nine specimens were created with a crack length of 50 mm and a width ranging from 0.3 mm to 0.9 mm, while thirteen specimens were kept as a reference for comparison. Since the bricks used are classified as medium suction, they were employed without prior wetting, following the manufacturer's recommendations.

Figure 23 illustrates the stepwise process of preparing 3-course masonry prisms with varying crack widths. Plastic strips, 50 mm wide and with nominal thicknesses of 0.3 mm, 0.5 mm, 0.7 mm, and 0.9 mm, were positioned on the lowermost brick before mortar M 2.5 was applied to the bed joint. Two brick halves were then placed on the first layer, followed by filling of the head joint from the top and front. Subsequently, the mortar was applied to the bed joint, and the third brick course was placed on the top. Finally, the mortar joints were tooled to a flush profile using a wooden stick. The optimal time for strip removal was determined through trials on dummy specimens. This timing prevents the mortar from being too hard or too loose during strip removal, thus preventing mortar loosening or crack closure. Still, no perfect control of the crack width was achieved.

Specimens were grouped into G0, G03, G05, G07, and G09 based on crack width. G0 comprised specimens without known cracks, and G03 and G05 had crack widths between 0.25–0.35 mm (average 0.3 mm) and 0.45–0.55 mm (average 0.5 mm), respectively. Groups G07 and G09 represent specimens with crack widths of 0.65–0.75 mm (average 0.7 mm) and 0.85–0.95 mm (average 0.9 mm).

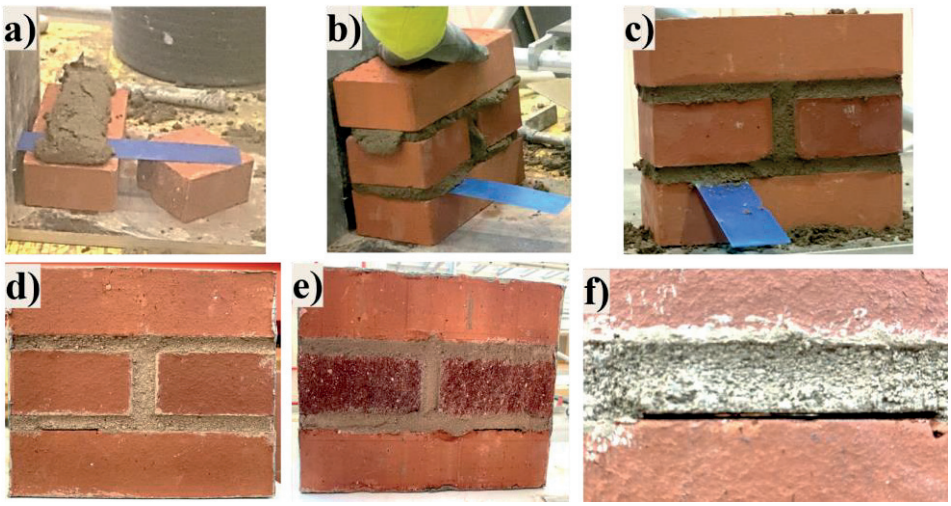

Figure 23. Preparation of specimens with an artificial crack: a) laying the first brick course and placing a plastic strip to create the crack, b) placing the third brick course, c) a 3-course masonry prism prior to removing the plastic strip, d & e) front view and backside, and f) close view of the artificial crack [135]

The same test setup used in campaigns A and B, as illustrated in Figure 12, was operated in campaign C, while the specimens were subjected to an average water spray rate of roughly 7 l/m^2/h with no differential air pressure applied. Each test consisted of six consecutive cycles totaling 23 hours; each cycle lasted 210 minutes of water spraying followed by 20 minutes of pausing.

4.3.2 Results and discussions

4.3.2.1 Water absorption

Figure 24 shows the response of cracked specimens in terms of water absorption, Q (kg/m^2), during the 23-hour testing period. It is evident that the behavior of the cracked specimens closely resembles that of the reference specimens, specimens without known cracks. The initial linear absorption persisted until the point of surface saturation. Once saturation was achieved, the response transitioned into a nonlinear phase and continued until full saturation of the specimens. This pattern parallels the trend observed in specimens tested in campaigns A and B. Notably, a slight variation in the amount of absorption after the first cycle can be observed

between group G0 and groups G03–G09. This difference suggests that cracks create a pathway of low resistance, facilitating water absorption. The results are further discussed in Paper V.

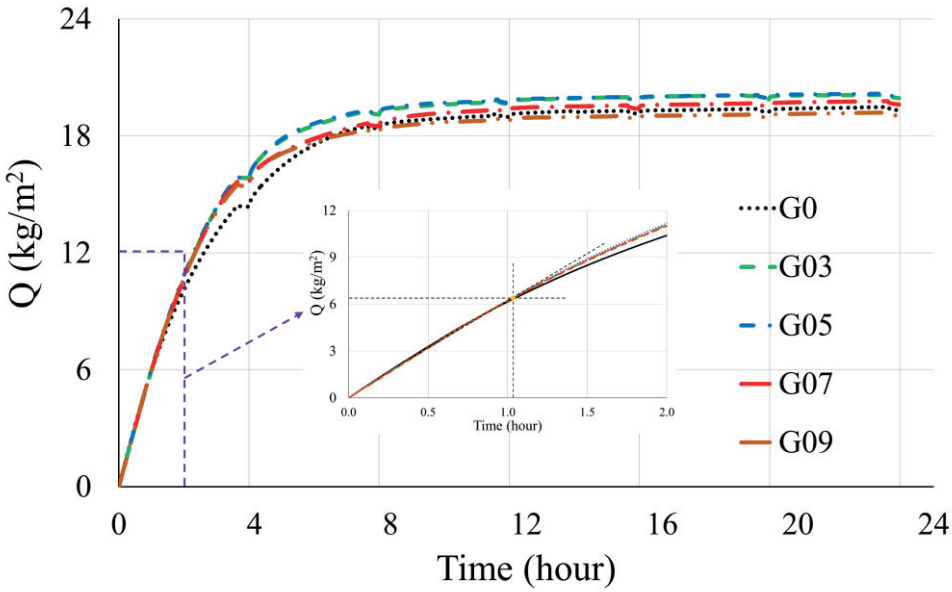

Figure 24. Average water absorption, Q, vs. time during 23 h of testing for all groups of Campaign C

4.3.2.2 Water penetration

Figure 25 shows the average water penetration within each group over the 23-hour exposure period, while Table 7 provides the results regarding the time to initiation of water penetration and water penetration rate. Notably, there exists a delay between test initiation and the onset of water penetration, even in cracked specimens, highlighting the moisture buffering capacity of brick masonry as a beneficial attribute in retarding water penetration. Once penetration commences, it continues at a consistent rate, except during the 20-minute pauses between spray cycles. It is evident that, on average, the penetration rate increases with increasing crack width. It should be noted that penetration was also observed in group G0, which consisted of reference specimens with no artificial crack. The penetration rate varied between 0.20 kg/m^2/h and 1.05 kg/m^2/h. The average time to the start of penetration was between 3.1 and 7.4 hours, with the shortest time observed in the specimens of group G09 and the longest in the reference specimens (group G0).

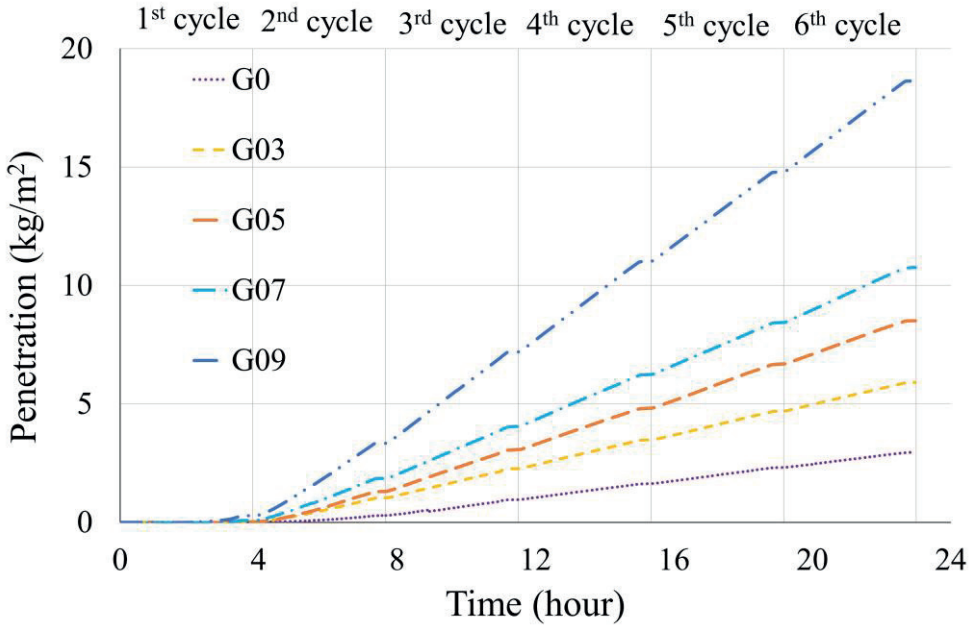

Figure 25. Average water penetration in each group during the 23 hours of testing

Although the results show a clear tendency to increase penetration rate with increasing crack width, high variability among individual specimens within the studied groups was observed (Table 7). Firstly, the quality of joint filling during bricklaying differed due to the challenge of completely filling head joints, as shown in Figure 20. This variance could create a pathway for water penetration. Secondly, uncertainty exists concerning the geometry of the created cracks in this study due to the tortuosity and roughness of the crack's surface. Upon removing the plastic strips used for crack creation, the mortar, which was not yet fully hardened, could have flowed into some parts of the cracks due to gravity. Thirdly, uncertainties might stem from tolerances in the nominal thickness of the plastic strips used for creating the cracks. Uneven deformation during strip removal could result in not having a straight crack path. This is further discussed in Paper V. It should be mentioned that the largest CoV can be seen in the reference specimens, group G0, while the lowest is in the specimens with the largest crack width, group G09, which is related to a large uncertainty when a specimen without flaws has to be created, compared to specimens with a large flaw.

The results in terms of the corresponding saturation level at the start of water penetration for each group are presented in Table 7. A certain saturation level is required for the start of water penetration. On average, for group G0, water penetration started when the saturation level was 93.6%, which is in agreement with the results of campaign B. Moreover, an average saturation level of 72–87% was

observed at the initiation of water penetration for groups G03–G09. These findings imply a potential correlation between crack width and saturation level at the onset of penetration: the larger the crack width, the lower the saturation level at the start of water penetration. The average leakage, defined as the ratio between the amount of penetrated water and the amount of sprayed water, was 2.2% for group G0, consisting of specimens without known cracks. Conversely, the average leakage for cracked specimens increased to 4.2%, 5.9%, 7.7%, and 13.3% for groups G03, G05, G07, and G09, respectively. These findings highlight the substantial influence of crack width on leakage.

Table 7. Water penetration in terms of time to penetration, corresponding saturation level, penetration rate, and leakage percentage for each group

		Time to penetration (h)	Saturation level (%)	Penetration (kg/m^2)	CoV (%)	Penetration rate (kg/m^2/h)	Leakage (%)
Campaign C	Group G0	7.4	93.6	3.0	89	0.204	2.2
	Group G03	4.6	87.2	5.9	65	0.348	4.2
	Group G05	4.3	84.1	8.3	68	0.488	5.9
	Group G07	3.8	80.7	10.8	62	0.619	7.7
	Group G09	3.1	72.3	18.6	33	1.045	13.3

4.3.2.3 Runoff measurements

The test setup developed in this study might provide an indication for measuring film thickness running down on the exposed surface of the specimens. The results indicate that 2g water loss was registered in the scale once the first cycle paused. This is consistent quite for all specimens exposed to a water spray rate of around 7 l/m^2/h. This is equivalent to a water film thickness of around 0.037 mm. However, it should be noted that as the tolerance of the scale is 2 g, the actual value of water loss could be between 1g and 3g. Accordingly, the film thickness formed on the exposed face can be around 0.019–0.056 mm.

In order to validate the measurements, the numerical model proposed by Blocken and Carmeliet [2] was used (Section 3.2.2 – Eq. (13)). Figure 26 shows the evolution of water film thickness during the first cycle of water spraying (total time of 210 minutes). The water spray rate was reduced by 20%, accounting for the bounce-off; thus, an R_{WDR} of 5.6 mm/h was considered with the water absorption coefficient of 0.155 kg/m^2.s$^{0.5}$. The spatial discretization interval Δx is taken at 0.005 m, and the required time step Δt to limit the instabilities at the downward moving film front is 0.01 s, satisfying the convergence conditions described in [2]. Accordingly, the maximum water film thickness after the first cycle is around 0.037 mm, which is the same as the measurement.

Further, the semi-empirical equation, Eq. (9), proposed by Beijer [1], was used to estimate the film thickness. Based on the numerical model, the runoff rate is equal to 1.486 l/(m.h); thus, the value of film thickness based on the equation provided by

Beijer (h_B) equals 0.049 mm, while the thickness (h_{tN}) predicted by the model is equal to 0.037 mm. Despite the challenging nature of runoff measurements, the level of agreement between the measurement in this thesis, the model by Beijer, and the result obtained from the numerical model (= Nusselt solution) [2] is considered very good (as summarized in Table 8).

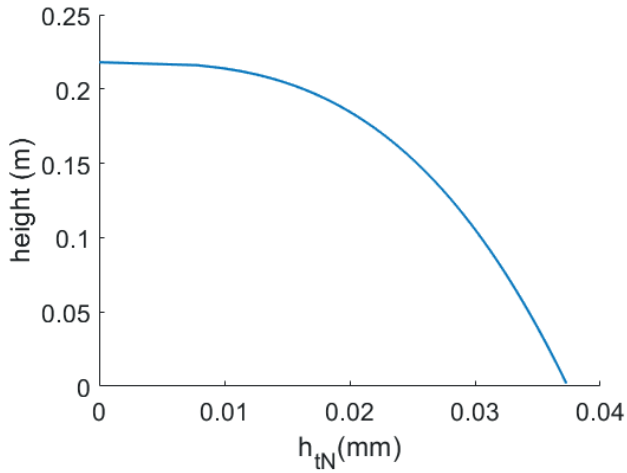

Figure 26. Water film thickness (h_{tN}) profile for the 3-course masonry prisms during 210 minutes of water spraying over the height of specimens (= 218 mm)

Table 8. Film thickness, h_{Ex} as obtained from the experimental results, h_N as predicted by the numerical model [2], and h_B as proposed by Beijer [1]

q_{runoff}	h_{Ex}	h_{tN}	h_B
l/(m.h)	mm	mm	mm
1.49	0.019 – 0.056	0.037	0.049

4.3.2.4 Balance of forces

The experimental results indicate that water penetration starts when the least resistance pathway is nearly saturated. Once the water reaches the backside of masonry specimens, since the path is filled with water and the meniscus becomes flat, the capillary action is no longer active. In this experimental campaign, as no air pressure difference is applied, hydrostatic pressure due to runoff should overcome the horizontal component of surface tension for the water penetration to occur. The surface tension of the water at 10°C is considered to be 0.074 N/m. The theoretically required pressure to breach the meniscus of water for different crack widths is summarized in Table 9. The values are obtained based on Eq. (23), considering the contact angles of 45°, 30°, and 15°.

Table 9. The required pressure to breach the surface tension for different crack widths and the corresponding penetration rate

crack width (mm)	P_{tot}* (Pa)	P_{tot}** (Pa)	P_{tot}*** (Pa)	Penetration rate – experiment**** (kg/m²/h)
0.3	352	249	129	0.144
0.5	212	150	78	0.284
0.7	152	107	56	0.415
0.9	119	84	43	0.841

* Considering the contact angle of 45°
** Considering the contact angle of 30°
*** Considering the contact angle of 15°
**** The average penetration rate of specimens without known cracks is considered a baseline for water penetration in masonry specimens; thus, it is deducted from the water penetration rate in different crack widths.

The water quantity that loads a penetration, G [kg/h], which is based on the area (catch area) above the crack, can be calculated as follows [3]:

$$G = \eta \cdot H \cdot D \cdot g_s \tag{26}$$

where η is a factor varying between 0 and 1, H [m] is the height above the crack, D [m] is the length of the crack, and g_s [kg/(m^2.h)] is the water spray rate. The factor η is dependent on different parameters, including the total pressure (the difference between the hydrostatic pressure and surface tension) and the catch area above the crack. Considering the height above the crack is 0.16 m, the crack length equals 0.05 m, and the spray rate is 7 kg/(m^2.h), the maximum amount of water available to penetrate is equal to 0.045 kg/h, considering the bounce off 20%. Since the surface of the masonry specimens was equal to 0.218 m × 0.250 m, the maximum penetration rate can be around 0.833 kg/m^2/h. This agrees well with the measured penetration rate for masonry specimens with a crack width of 0.9 mm (see Table 9). The higher breaching pressure results in a higher value of η, as proposed by Olsson and Hagentoft [3]. As can be seen, the breaching pressure in specimens with larger crack widths is larger than that of specimens with smaller widths; thus, a higher value of η and correspondingly higher penetration is expected for specimens with a crack width of 0.9 mm. As summarized in Table 9, there is a reasonable proportionality between the total pressure and the penetration rate for each crack width. It should be noted that pressure is not the only factor influencing water penetration rate in specimens with different crack widths. Additionally, the cross-section of the area that liquid can penetrate through is also important – Thus, specimens with larger crack widths are expected to have a greater penetration rate.

5 Implementation into hygrothermal analyses

This section commences with an overview of the available water penetration criteria applicable to hygrothermal simulations. Given the lack of consensus, this chapter introduces a novel penetration criterion that can be effectively integrated into hygrothermal analyses. Subsequently, the utilization of this criterion within simulation tools is demonstrated using a representative case, specifically a timber frame wall featuring brick veneer cladding. The application of the proposed criterion is then compared against the criterion in the well-established ASHRAE 160-2021 standard [88]. Ultimately, the risk of mold growth in timber frame walls with brick veneer cladding is analyzed, considering the influence of the two water penetration criteria.

5.1 Background

An investigation carried out in 2012 [136] identified 57 hygrothermal simulation software programs, all intended to investigate the hygrothermal response of building envelopes. WUFI [106], DELPHIN [105], and recently COMSOL Multiphysics [137] have gained widespread use as reliable options for analyzing hygrothermal performance [138-142]. Nevertheless, the question of water penetration presents a challenge in hygrothermal analyses, with a lack of consensus regarding a) the magnitude of water penetration, b) where penetrated water should be placed as a moisture source, and c) how the penetrated water should be distributed within the layer—whether as a point source or distributed evenly.

Several research studies [8, 11, 143] indicate that incorporating various water penetration criteria into hygrothermal simulations notably impacts the moisture response of external walls. Despite its significant consequences, only a limited number of studies have proposed methods for phenomenologically accounting for water penetration (leakage) resulting from wind-driven rain (WDR) in hygrothermal and moisture safety analyses [10, 11, 21].

The most widely used guideline in this regard is outlined by the North American Standard (ASHRAE 160-2021) [88]. For multi-layer external walls, this standard

recommends that, in the absence of full-scale test methods, 1% of the WDR deposited on a façade is considered to penetrate behind the façade cladding, which should be placed on the exterior surface of the water-resistive barrier, if provided. Although certain research attempts have sought to support this 1% value for WDR water penetration [96, 144], an examination of existing experimental studies reveals a range of 0–20% penetration through clay brick cladding [28, 29]. Accordingly, a study by Van Linden [21] indicates that using 1% of the WDR load as a moisture source could either overestimate or underestimate the penetration percentages.

In a study by Carbonez et al. [140], the impact of moisture source position on the wetting and drying behavior of sheathing was evaluated using 2D simulations, comparing point source to uniformly distributed moisture source. Accordingly, a point moisture source at the base of the wall was considered because a uniformly distributed moisture load does not take into account the possible accumulation of water due to gravity. Further, Calle et al. [11] studied eight different methods for incorporating a moisture source representative of water penetration into the hygrothermal analysis of a cavity wall. Among these methods, one approach involves disregarding any penetration, while the remaining methods, for instance, consider penetration to be simulated if the façade surface exhibited capillary saturation at a depth of 5 mm or if the intensity of WDR surpassed the absorption rate of the brick masonry. Further, the position of the moisture source was studied with a focus on mortar extrusion as a point moisture source, acting as a capillary bridge.

Van Linden [21] introduced a quantitative approach to assess rainwater penetration, offering data for hygrothermal simulations. This method considers the performance of individual wall component layers, such as exterior cladding, drainage cavity, and drainage barrier. The approach takes into account factors like moisture sensitivity of materials, rain exposure, building function, and the complexity of the building envelope.

According to the findings presented in this thesis, a distinct time lag exists between the start of WDR exposure and the start of water penetration, even under extreme testing conditions, as the commencement of water penetration into brick masonry necessitates a certain saturation level. These findings are consistent with previous work by Straube and Burnett [96], where clay brick masonry was exposed to a spray rate of 200 $l/m^2/h$ for 30 minutes before any penetration was observed. At water spray rates lower than 10 $l/m^2/h$, penetration occurred after 5–8 hours, which is attributed to the masonry's absorption capacity [30, 96]. This implies that penetration of WDR into masonry walls might not occur during periods when the walls have the potential to absorb and retain water.

Although different studies attempt to quantify water penetration, a notable shortcoming related to most of the proposed methods is neglecting the moisture storage capacity of brick masonry. In instances where initially non-saturated clay

brick masonry is involved, the initiation of water penetration takes time. Thus, considering a portion of all WDR leading to water penetration may not provide an accurate picture of water penetration in clay brick masonry.

5.2 A Novel water penetration criterion

The lack of agreement on water penetration between previous studies shows a need for an explicit implementation method to include water penetration in hygrothermal simulations to evaluate the impact on walls with masonry veneer cladding. Based on the experimental results presented in Section 4.2.2, this study proposes a novel water penetration criterion that can be implemented into hygrothermal simulations.

The proposed criterion states that a certain saturation level is required before the start of water penetration. Once this criterion is met, a portion of the WDR deposited on the wall will penetrate. The specific threshold, as well as the amount of water, depends on whether the masonry is cracked or not. For instance, in the case of masonry without known cracks, the findings point to a threshold of about 90%, at which point an average of 3.8% of the deposited water will penetrate through the cladding.

Paper III discusses the limitations and practical implementation of the proposed criterion in more detail. In real-world situations, the potential for penetration could be worsened due to inadequate bonding between bricks and mortar and the presence of cracks. However, as presented in Section 4.3.2 and shown in Paper V, masonry built with other brick types and good workmanship may have a lower penetration rate.

It should be noted that the averaged saturation level may not have a precise physical basis to explain the onset of water penetration in masonry. Water penetration will occur when a pathway from the exterior to the interior becomes saturated. Prior to saturation, all water will instead be absorbed before reaching the rear face. Empirically, it was observed that the conditions for penetration to occur were met at a consistent saturation level. Since the average saturation level can be obtained from hygrothermal one-dimensional simulations, this was deemed an appropriate and practical predictor of penetration. The limitations and additional aspects related to the proposed criterion are discussed in detail in Paper III.

5.3 Hygrothermal simulation of a timber frame wall

Hygrothermal analyses on a timber frame wall with brick veneer cladding were conducted to investigate the impact of two WDR penetration criteria, the proposed

criterion and the AHRAE 160-2016 standard, on the risk of mold growth. In addition to studying the impact of water penetration, other parameters, including the type of moisture source (uniformly distributed or point source) and its position in the wall assembly, air change rate (ACR) (representing different workmanship scenarios), WDR coefficient, and locations (Gothenburg and Rensjön, with different average annual rainfall and temperature), were considered. While Gothenburg, the most exposed city to WDR in Sweden, is located on the west coast, Rensjön, characterized by a cold climate, is located north of the Arctic Circle.

The simulations were done for a thirteen-year period with WUFI Pro and WUFI 2D, commercial software for hygrothermal analysis of multi-layer building components. For a comprehensive long-term moisture assessment, recent studies recommend simulations spanning at least ten years in order to assess the wall in a state of equilibrium with the surrounding climate and reduce the impact of the initial conditions [9]. While simplifying a brick veneer as a homogeneous layer has inherent limitations, this approach has demonstrated reasonable outcomes [145, 146]. Nevertheless, WUFI 2D was also utilized to study interactions between layers and dig deeper into heat and moisture distribution. In WUFI Pro (1D), the brick masonry cladding is modeled as a homogeneous layer, while WUFI 2D includes a more detailed representation with head joints and timber studs. Since 1-dimensional simulation can only implement a uniformly distributed moisture source, 2D modeling was conducted to investigate the effect of a point moisture source.

Historical weather data, including hourly rain intensity, wind velocity, and wind direction, was obtained from the Swedish Meteorological and Hydrological Institute (SMHI) [92]. WUFI proposes two methods for calculating the WDR coefficient: the first is based on the building height and location on the façade, while the second is based on the ASHRAE 160-2021 standard [88]. Based on the former, the WDR coefficient for the upper part of a building with a height of more than 20 m is 0.2 s/m. The most critical orientations for walls in Gothenburg and Rensjön in terms of WDR are south and north, respectively; thus, applied in the simulations. The material properties used for simulating the walls are obtained from experimental results presented in Section 4.2.1 and the software database. The description of the model and relevant climate input are presented in detail in Paper IV.

5.3.1 Method

Among several types of building envelopes in Sweden, timber frame walls with brick masonry veneer are one of the most commonly built wall assemblies. A vast majority of such walls are in need of maintenance since they are prone to high damage risk, especially those exposed to high amounts of WDR. The performance evaluation of such walls involves three primary types of moisture-related damage: mold growth, decay of timber components, and frost damage of the clay brick veneer. This study focused on assessing the risk of mold growth, particularly at the

surface of the timber studs, a highly sensitive component in this type of wall. Because mold growth causes health problems for building users, it is critical to detect mold and renovate the building accordingly.

Determining the presence and extent of mold growth damage necessitates destructive sampling. As a result, accurate hygrothermal modeling of the wall may result in a better understanding of the wall's status prior to performing any costly maintenance action. Furthermore, by providing knowledge about influential parameters on mold growth risk, a more rational action can be taken into account during the design/maintenance of such walls. A schematic of a timber frame wall with brick veneer modeled in this study is shown in Figure 27. It should be mentioned that this type of wall was commonly built during the 1960s–1970s, while the currently built timber frame walls are generally insulated with much thicker insulation.

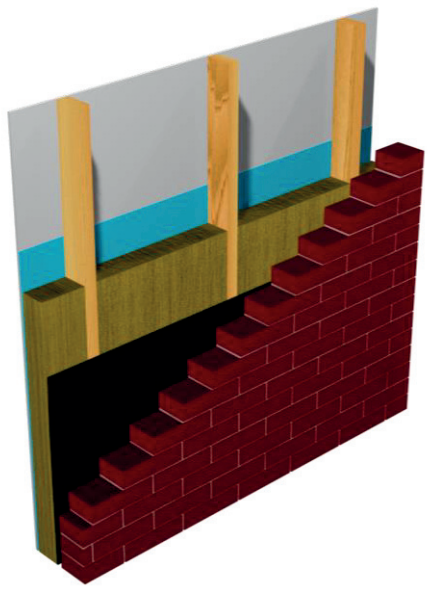

Figure 27. A schematic of a timber frame wall with brick veneer cladding; layers from the right (exterior) to the left (interior): brick masonry veneer (120 mm), air gap (20 mm), asphalt impregnated paper (1 mm), mineral wool insulation (95 mm), timber studs (95 mm × 45 mm) with a center to center distance of 600 mm, vapor retarder (1 mm), and gypsum board (12.5 mm)

Two common models are used to evaluate the risk of mold growth: Viitanen's (VTT) model [147] and the mold resistance design (MRD) model [148]. In this study, mold growth was calculated on the surface of the timber stud element by evaluating all simulation results using the updated Viitanen model implemented in WUFI. Viitanen's model calculates a mold index (M) based on the relative humidity and temperature data. A higher mold index indicates a higher risk of mold growth. The sensitivity class "sensitive" and decline class "relatively low decline" were assumed,

which is recommended for a planed timber and wood-based board. The differences in building materials' mold growth sensitivity are divided into four sensitivity classes (very sensitive, sensitive, medium resistant, and resistant) and four decline classes (strong decline, significant decline, relatively low decline, and almost no decline). The mold index classes used in Viitanen's model are summarized in Table 10.

Table 10. Mold index for experiments and modeling [147]

Index M	Growth rate	Description
0	No mold growth	Spores not activated
1	Small amounts of mold on surface (microscope)	Initial stages of growth
2	<10% coverage of mold on surface (microscope)	
3	10%–30% coverage of mold on surface (visual)	New spores produced
4	30%–70% coverage of mold on surface (visual)	Moderate growth
5	>70% coverage of mold on surface (visual)	Plenty of growth
6	Tight and dense mold growth covers nearly 100% of surface	Coverage around 100%

5.3.2 Implementing the new criterion

As already mentioned, two criteria for water penetration implementation are compared: a) a widely accepted reference model, ASHRAE 160-2021 standard [88], in which one percent of all WDR deposited on the façade penetrates the clay brick cladding, and b) a new criterion in which 3.8% of WDR penetrates when the water content of the brick veneer cladding is greater than 90% of its saturation capacity.

Incorporating the ASHRAE criterion into the model involves defining a moisture source at a specified location, typically recommended on the water-resistive barrier. This source is assigned 1% of the WDR deposited on the façade.

In order to incorporate the proposed criterion into the hygrothermal simulation, the simulation has to be carried out in two steps. The model was first run to capture the water content fluctuations in the brick cladding. Once the water content was acquired, a specific threshold was established and implemented accordingly in the second step. This threshold denotes the necessary saturation level for initiating water penetration. Accordingly, in periods when the water content is below the threshold, no water penetration occurs. Conversely, during periods when the masonry cladding's water content exceeds 90% saturation, approximately 3.8% of WDR is considered a moisture source.

Figure 28.a shows the water content trends within the simulated masonry veneer located in Gothenburg. During the majority of winter periods, the wall reaches capillary saturation. This outcome strongly suggests a high probability of WDR penetration during winter, as the water content consistently exceeds 90% of the saturation capacity – a condition proposed for water penetration in this thesis. Figure 28.b shows the amount of penetrated water based on the ASHRAE Standard 160 and the proposed criterion. There is a clear difference between the cumulative water

penetration obtained from the proposed criterion compared to the ASHRAE Standard 160. The proposed criterion yields a more nuanced moisture load influenced by seasonal variations in the saturation level.

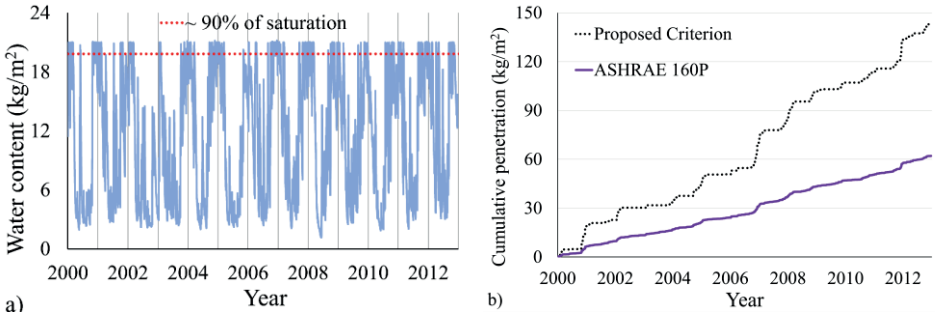

Figure 28. a) water content of the brick masonry cladding located in Gothenburg during 2000 – 2012 and b) cumulative water penetration according to ASHRAE 160 standard [88] and the criterion proposed in this study

Figure 29.a shows the water content of the masonry cladding located in Rensjön. In contrast to the Gothenburg wall (Figure 28.a), the water content in this scenario did not frequently approach 90% saturation, implying a low likelihood of water penetration over the studied period. Under the proposed criterion, cumulative water penetration was around 10–15% lower than that of the ASHRAE Standard 160 (Figure 29.b).

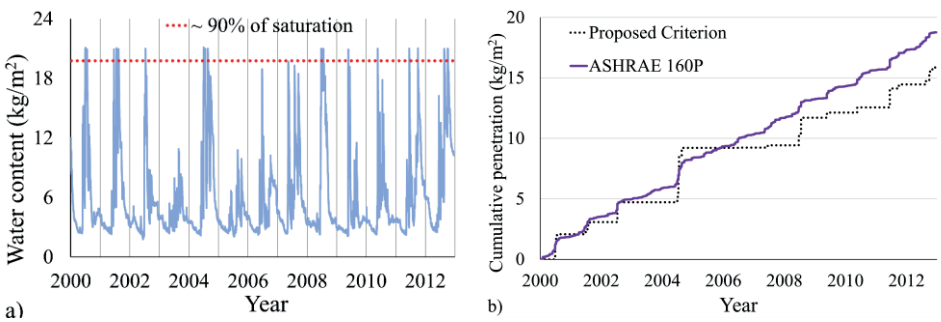

Figure 29. a) water content of the brick masonry cladding during 2000 – 2012 located in Rensjön and b) cumulative water penetration according to ASHRAE 160 standard [88] and the criterion proposed in this study

5.3.3 Results and discussions

As already mentioned, different parameters, including location, WDR coefficient, water penetration criterion, type of moisture source (uniformly distributed or point source) and its position in the wall assembly, and air change rate (ACR) (representing different workmanship scenarios), were considered to assess the risk of mold growth in a timber frame wall with brick veneer cladding. Different scenarios assessing the impact of different parameters are summarized in Table 11.

Table 11. Overview of simulation methods and results in terms of mold growth index (M)

Scenarios	Location	Model	WDR Coeff (s/m)	Moisture source	Penetration criterion	ACR (h^{-1})	Time at max M (years)	Max M (-)
A	Gothenburg	1D	0.2	-	0	10	12.82	3.36
B				U1	ASHRAE		8.21	5.28
C					KS*	0	8.90	5.30
D						10	8.90	5.30
E						40	8.22	5.30
F				U2	ASHRAE	10	12.89	3.75
G					KS		12.89	3.62
H				U3	ASHRAE		12.82	3.37
I					KS		12.82	3.36
J			0.12	U1	ASHRAE		7.06	5.01
K			0.3				8.21	5.30
L	Rensjön		0.2	-	0		1.73	1.06
M				U1	ASHRAE		4.77	2.30
N					KS		1.73	1.09
O	Gothenburg	2D	0.2	-	0	10	12.82	3.17
P				U1	ASHRAE		7.07	5.28
Q					KS		8.21	5.30
R				PS1	ASHRAE		7.06	5.13
S					KS		8.20	5.30
T				PS2	KS		7.06	5.30
U				PS2***		0	7.06	5.30
V	Rensjön			PS1	ASHRAE	10	4.77	2.03
W					KS		1.74	2.72

U1: Uniformly distributed on the exterior surface of the timber stud – cut-off at max water content (3 mm)
U2: Uniformly distributed on the asphalt layer – no cut-off (1 mm)
U3: Uniformly distributed behind (on the interior of) the cladding – no cut-off (3 mm)
PS1: Point source on timber stud close to the contact zone with the insulation (10 * 3 mm2)
PS2: Point source on timber stud in the same level as the extruded mortar joint (25 * 3 mm2)
KS*: the criterion proposed in this thesis
0**: air gap partially filled with mortar to represent poor workmanship

The results of the maximum mold index (M) and its corresponding time for each simulation are summarized in Table 11. The findings feature a pronounced risk of mold growth in timber frame walls with brick masonry veneer, particularly in situations with substantial exposure to WDR. The mold index for walls in Renjsön is lower compared to Gothenburg, highlighting exposure to WDR as the most influential parameter.

The position of the moisture source significantly influences the mold growth risk. Placing the moisture source on the exterior of the timber stud results in a higher mold index, whereas placing it on the asphalt layer, a water-resistive barrier, yields a lower value.

The results indicate a minimal difference in the maximum mold index between the ASHRAE 160 standard [88] and the proposed criterion in this study for walls in Gothenburg. However, for walls in Rensjön, the difference was more pronounced, which could be attributed to the ASHRAE standard producing a more continuous pattern of cumulative penetration, whereas the proposed criterion produces a more differentiated moisture load pattern.

Comparing simulation results between WUFI Pro and WUFI 2D shows minor differences in Gothenburg but more substantial divergence for low WDR loads, Rensjön. Placing a uniformly distributed moisture source is similar to modeling a point moisture source, though the risk of mold growth is slightly lower with a point moisture source. The presence of extruded mortar as a capillary bridge significantly affects the wall's hygrothermal performance. Mold growth develops earlier in walls with extruded mortar in contact with the asphalt layer than in walls without extruded mortar.

This study emphasizes the significance of influential parameters on the hygrothermal performance of timber frame walls with brick veneer cladding. It underlines the high mold growth risk in such walls, particularly in regions with high WDR exposure. Regardless of the penetration criterion, simulation tool, or input parameters, careful consideration is essential when designing or constructing such walls in climates similar to Gothenburg. The study highlights effective measures for designing/maintaining timber frame walls with brick masonry veneer. These involve limiting water penetration, particularly shielding sensitive elements like timber studs and removing extruded mortar that can hinder cavity air ventilation due to poor workmanship. Rain penetration is one of the most impactful parameters affecting the risk of mold growth. The results and impact of the considered parameters, including air change rate (ACR), WDR coefficient, and locations, are further discussed in Paper IV.

6 Repointing

This chapter first presents the results of a fourth experimental campaign, Campaign D, conducted on 3-course masonry prisms to investigate the effect of repointing on water penetration. It is followed by a section where the obtained results are implemented in hygrothermal studies of different wall types with brick veneer cladding. Eventually, recommendations and further aspects to be considered for repointing are discussed, aiming to facilitate rational decision-making.

6.1 Experimental study

Specimens with artificial cracks tested in the third experimental campaign, Campaign C, were repointed and once again exposed to water spray to study the effect of repointing on water penetration. The test setup detailed in Chapter 4 was utilized, with identical test conditions as in Campaign C – a water spray rate of 7 $l/m^2/h$ without air pressure difference.

6.1.1 Masonry specimens

6.1.1.1 Specimens preparation

The repointing procedure began by raking out the mortar joints to a depth of roughly 25–30 mm. Bed and head joints were raked out using a mortar rake blade and a raking bit, respectively, as shown in Figure 30. Subsequently, the specimens were cleaned of dust and gently washed with water. The following day, mortar type M 1, characterized by an absorption coefficient, A_w, of 0.179 $kg/(m^2.s^{0.5})$, was employed to repoint the specimens. Mortar M 1 is widely used for repointing brick masonry in Sweden. An experienced craftsman manually filled the joints and used a wooden stick to compact them, as shown in Figure 30. Subsequently, the repointed specimens were cured for 28 days in the laboratory before undergoing a second round of exposure to water spraying.

The repointed specimens are labeled with an "R," distinguishing them from the cracked specimens. For instance, G03 includes cracked specimens with a crack width of 0.3 mm, while the same group is represented as G03 - R after repointing.

Figure 30. Different steps of repointing a specimen: a) raking out joints, b) applying new mortar, and c) compaction of the mortar [135]

6.1.2 Results and discussions

6.1.2.1 Water absorption

The results in terms of water absorption follow a pattern similar to that of the cracked specimens but with a lower absorption rate. As shown in Figure 31, the response is linear until the attainment of surface saturation. Once the specimens attain surface saturation, the absorption behavior becomes nonlinear. The absorption continues until the specimens become nearly saturated. Although the average total water absorption remained consistent before and after repointing across all groups, indicating that bricks dominated the water absorption capacity of masonry, repointing did lead to a decrease in the absorption rate.

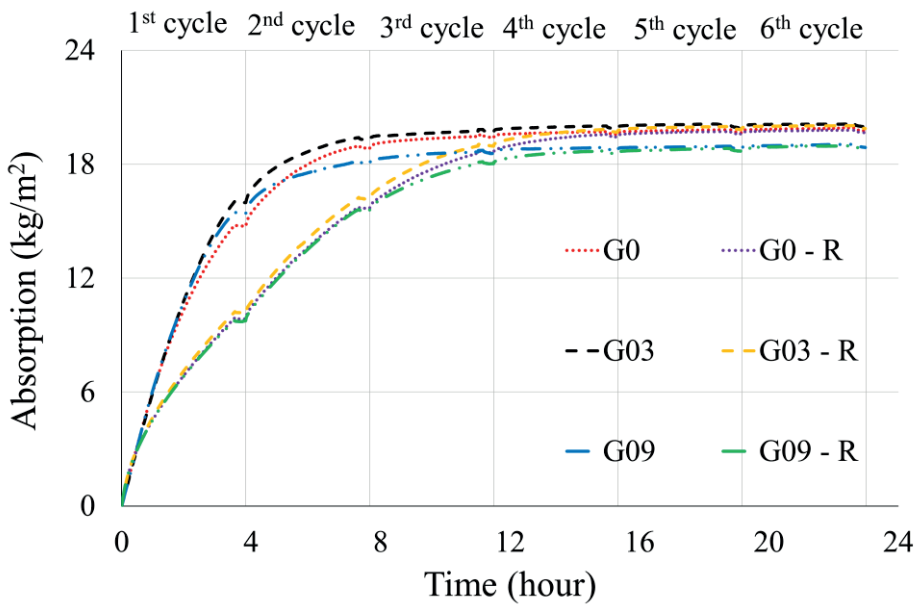

Figure 31. Average water absorption vs. time response during 23 h of testing for groups G0, G03, and G09 before and after repointing

The reduction in the absorption rate of the specimens is notable because the mortar used for repointing (M 1) had a higher water absorption coefficient compared to M 2.5. The reduction in absorption rate can be attributed to the compaction of the applied mortar, M 1, which effectively might have tightened the pathways for water uptake. Before repointing, water could easily penetrate the brick-mortar interface, but the compaction of the new mortar created a sealing effect, directing water absorption primarily through the exposed brick face. Further, while raking out the mortar joints and subsequent washing, some of the pores in bricks might be filled with sawdust (clogged pores), which in turn results in lower absorption through bricks. Therefore, these findings suggest that incorporating repointing into a maintenance plan can effectively reduce absorption in masonry exposed to wind-driven rain (WDR). Similar outcomes were reported in a study by Fusade et al. [18], which demonstrated a reduction in water ingress depth in lime-mortar joints after repointing.

6.1.2.2 Water penetration

Figure 32 shows water penetration in each group after repointing during 23 hours of testing. Similar to the previous campaigns, there is a time lag between the start of the test and the onset of water penetration. This time lag highlights the moisture buffering capacity of brick masonry, a valuable attribute delaying water penetration. Once water penetration starts, it maintains a consistent rate, except for the initiation phase, when the penetration rate goes from zero to constant. Further, no penetration is recorded during the 20-minute pause between each spray cycle.

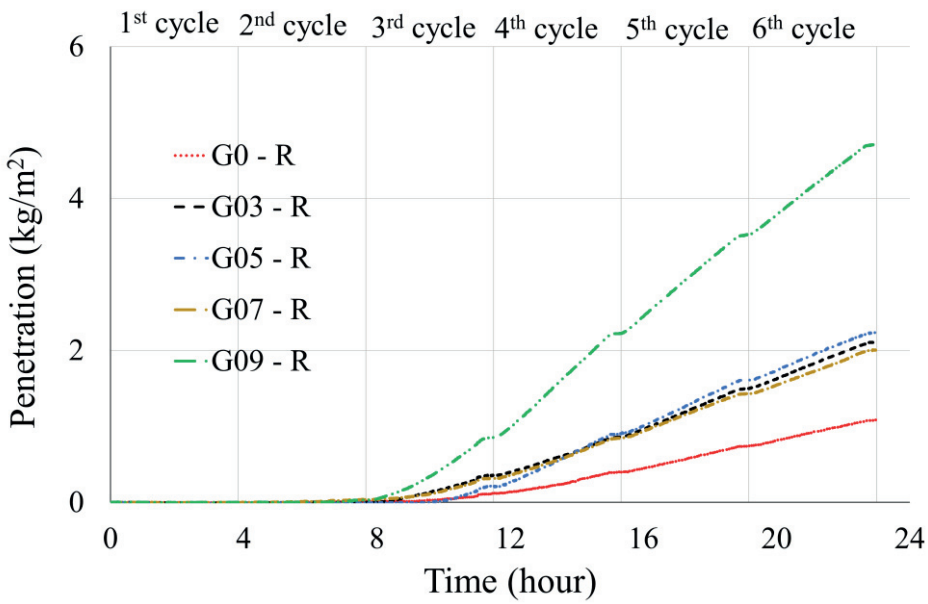

Figure 32. Average water penetration during the 23h of testing after repointing [135]

The results in terms of time to the initiation of penetration and corresponding saturation levels are summarized in Table 12. Groups G0-R to G09-R experienced an average delay in the onset of water penetration, ranging from approximately 9.5 to 11.5 hours. There was a significant increase in the average time it took for water to penetrate in all these groups, compared to groups G0–G09 (as presented in Table 7). In the case of group G0, repointing resulted in a delay of approximately 3.5 hours in the initiation of water penetration, shifting from 7.4 hours to 10.8 hours. As for cracked specimens, the findings suggest that repointing delayed the initiation of water penetration by nearly 6.5 hours, the impact being more pronounced for specimens with wider cracks.

At the start of penetration, the corresponding saturation level was around 90–95 %, indicating a negligible difference between group G0-R (reference specimens after repointing) and groups G03-R to G09-R (cracked specimens after repointing). The results of repointing indicate that mortar compaction is effective in increasing the resistance in the artificial crack and other low-resistance pathways of the masonry, as opposed to the cracked specimens prior to repointing, where penetration starts at a lower saturation level. Paper V contains the results for individual specimens as well as additional remarks.

Table 12. Water penetration in terms of time to penetration, corresponding saturation level, penetration rate, and leakage percentage for each group after repointing

		Time to penetration (h)	Saturation level (%)	Penetration (kg/m^2)	CoV (%)	Penetration rate ($kg/m^2/h$)	Leakage (%)
After repointing	Group G0 - R	10.8	90.7	1.1	106	0.094	0.8
	Group G03 - R	10.5	90.0	2.1	88	0.186	1.5
	Group G05 - R	11.6	95.0	2.2	96	0.194	1.6
	Group G07 - R	10.3	90.0	2.0	77	0.161	1.4
	Group G09 - R	9.5	91.0	4.7	92	0.351	3.4

The average leakage, defined as the ratio between the amount of penetrated water and the amount of sprayed water, was 0.8% for group G0-R, consisting of specimens without known cracks. Conversely, the average leakage for cracked specimens after repointing (G03-R – G09-R) varied between 1.4% and 3.4%. Compared to before repointing, leakage is relatively reduced by around 60% – 80%, where the largest reduction was measured for group G07, from 7.7% to 1.4%.

After repointing, the average water penetration rate decreases by more than 50%. The most significant reduction was observed in group G07, which consisted of specimens with a crack width of 0.7 mm. In this group, the average penetration rate decreased by 74%, going from 0.619 $kg/m^2/h$ to 0.161 $kg/m^2/h$. A similar pattern was observed in the case of the reference specimens in group G0, where the average penetration rate decreased by 54%, declining from 0.204 $kg/m^2/h$ to 0.094 $kg/m^2/h$. In all groups, the scatter in penetration rate after repointing was larger than before

repointing, indicating that the least resistance pathway for water penetration turns from cracks (large flaws) to indefinite/small pathways after repointing.

There are several factors that could explain the significant differences in the average water penetration for each group before and after repointing: 1) repointing of the cracked specimens involved filling the cracks (the least resistance path for water to penetrate) to a depth of around 25–30 mm. Furthermore, if there were inadequately filled head joints (Figure 20.b), these were addressed during the repointing process. Both cracks and head joints with gaps or voids can serve as pathways for water penetration, so filling these openings during repointing can enhance the resistance of masonry, thereby reducing the rate of water penetration. 2) Repointing offers the opportunity to compact mortar joints, which can significantly improve the ability of masonry to resist water ingress. A study by Fishburn et al. [17] confirms the significant reduction in water penetration after the repointing.

However, it should be noted that repointing may not consistently lead to a decrease in the water penetration rate when comparing individual specimens before and after repointing, a feature further discussed in Paper V. The observed differences in the outcomes of repointing can be attributed to several factors: 1) The compaction, filling, and resistance of the mortar joints, including both the head joint and bed joints, in some specimens were already optimal even before repointing. This is evident from their initially limited water penetration rate, suggesting that repointing may not have significantly enhanced the resistance of these specimens to water penetration. 2) During the raking process, some specimens might have been unintentionally damaged, resulting in defects that could lead to increased penetration. The results are further discussed in Paper V.

6.1.2.3 Damp patches

The location of the first damp patch that appeared on the backside of individual specimens within each group is shown in Figure 33. Before repointing, the first dampness appeared close to the head joint for reference specimens, group G0. These findings align with previous campaign results, indicating the relatively low resistance of head joints, which serve as a primary pathway for water penetration in masonry without known cracks. Before repointing, in approximately 35% of the cracked specimens, the initial dampness was observed in the vicinity of the crack. In contrast, after repointing, none of the specimens displayed the first visible damp patch in the vicinity of the crack.

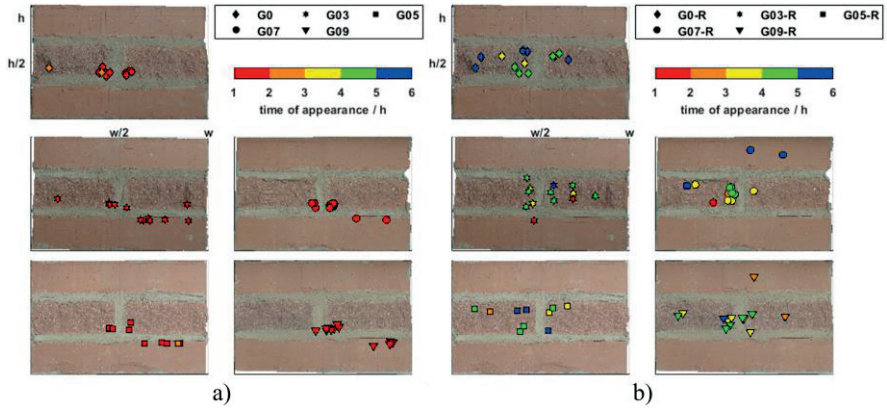

Figure 33. The location and time of the first damp patch that appeared on the backside of individual specimens a) before repointing and b) after repointing

Table 13 summarizes the average time it took for the first appearance of dampness. Across all groups before repointing, the average time for the initial dampness to appear was in the range of 1.1–1.5 hours. While the presence of cracks can facilitate the start of water penetration, there is no significant difference in the time it takes for the first dampness to appear between the reference specimens (group G0) and the specimens with artificial cracks (groups G03-G09). Following repointing, there was an average delay of around 4.0 hours to 4.5 hours before the first damp patch was recorded on the backside of specimens, with no noticeable difference between the reference specimens and those with artificial cracks.

As already discussed in Section 4.2.2, comparing the time to the start of the penetration and the time to the appearance of the first visible damp patch for individual specimens indicates no significant correlation. These observations suggest the involvement of two different water transport mechanisms: capillary suction and laminar flow. The appearance of dampness can be attributed to unsaturated flow, where the difference in the water content between the wetter and drier locations is the driving force for capillary suction. Conversely, water penetration occurs under saturated or nearly saturated conditions, where the water transport is likely governed by laminar flow.

Table 13. The average time to the appearance of the first damp patch on the backside of specimens in each group before and after repointing

	Before repointing		After repointing	
	Time until the first dampness (h)	CoV (%)	Time until the first dampness (h)	CoV (%)
Group G0	1.5	42.1	4.5	17.0
Group G03	1.4	27.1	4.0	28.4
Group G05	1.5	29.1	4.4	24.4
Group G07	1.4	23.9	4.0	32.6
Group G09	1.1	31.8	4.0	16.7

These results highlight the significance of repointing in delaying the appearance of the first visible dampness, a benefit likely linked to filling deficiencies/voids within the head joints and the additional compaction achieved through repointing.

6.2 Numerical study

While the obtained experimental results indicate that repointing may decrease water penetration in brick masonry in many cases, research concerning whether repointing can improve the performance of a wall assembly is scarce. Prior to making any decision concerning repointing, there is a need to analyze the possible benefits of repointing in reducing the damage caused by rainwater penetration. Additionally, once the decision to repoint is made, it is typically applied to the entire building, even when only one façade a) is exposed to more significant WDR loads or b) has cracks or eroded mortar joints. In such cases, repointing may not be fully justifiable for all orientations.

A probabilistic hygrothermal model was developed to investigate the impact of repointing on reducing the risk of mold growth and moisture content. Two wall types were considered: a) timber frame cavity walls with brick veneer and b) masonry cavity walls with autoclaved aerated concrete (AAC) as the inner leaf and brick masonry as the outer leaf. The analysis encompasses various parameters, including wall condition, location, and façade orientation. It incorporates data on water penetration obtained from experimental research conducted on masonry before and after repointing, presented in Section 4.3 and Paper V. The study aims to provide a better understanding of the need for repointing through probabilistic hygrothermal analyses, including 96 simulation cases (100 scenarios for each simulation case) with over 9600 simulations.

6.2.1 Wall assemblies

While timber frame cavity walls featuring brick masonry veneer are usually built in Sweden, the use of masonry cavity walls with an inner leaf constructed from AAC is not as widespread. Timber frame cavity walls, in particular, may require maintenance due to their susceptibility to mold growth risk, especially in areas exposed to heavy driving rain. On the other hand, moisture-related damage cases have been reported in masonry cavity walls, primarily attributed to the elevated moisture content in the AAC element, particularly in regions with high WDR loads. Apart from moisture-related damages, the high moisture content has a negative impact on the thermal properties of the AAC, as the thermal and hygric behaviors of porous building materials are closely interconnected [149]. Figure 34 and Figure 35 provide a schematic illustration of the timber frame cavity wall with a brick

veneer and the masonry cavity wall with an internal leaf of AAC, as modeled in this study.

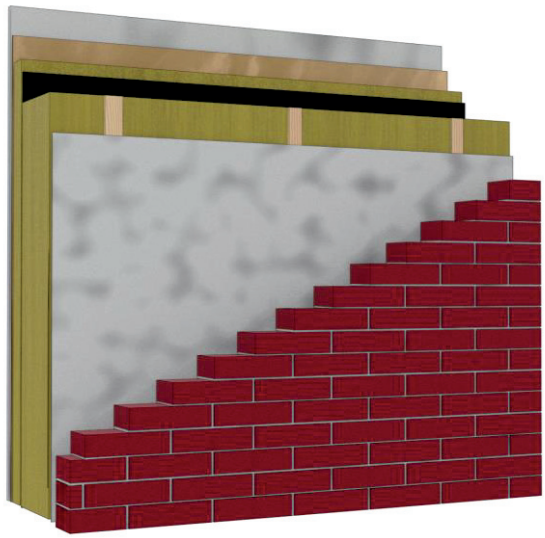

Figure 34. Schematic of a timber frame wall with brick veneer (total thickness of ~ 415 mm). Layers from the right side (exterior): brick masonry veneer (120 mm), air gap (30 mm), gypsum board (16 mm), wood fiber insulation (170 mm), vapor retarder, wood fiber insulation (50 mm), oriented strand board – OSB (12 mm), and gypsum board (16 mm) [150]

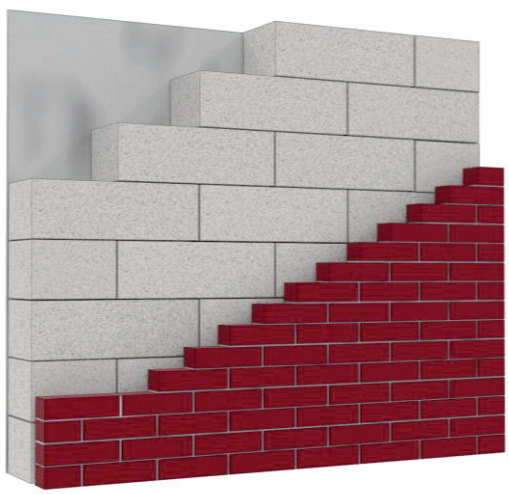

Figure 35. Schematic of a masonry cavity wall with brick veneer as the outer leaf and autoclaved aerated concrete (AAC) as the inner leaf (total thickness of ~ 345 mm). Layers from the right side (exterior): brick masonry veneer (120 mm), air gap (10 mm), AAC (200 mm), and gypsum board (16 mm) [150]

The hygrothermal performance of the wall is investigated using Delphin 6.1 [105], a commercial software program capable of simulating heat, air, and moisture transport in porous building materials and building envelopes. It is important to note that this study concentrates on a typical cross-section of the wall without considering specific construction details such as corners or embedded wooden beam ends. While representing a brick veneer as a homogeneous layer comes with certain limitations, previous research has shown that this simplification can yield satisfactory results when the wall is exposed to real-world climatic conditions. The study specifically focuses on three locations in Sweden: Gothenburg, Rensjön, and Uppsala, each representing different climate conditions with large differences in the amount of WDR and temperature. Hygrothermal analyses were carried out with a simulation period of over five years, spanning from 2018 to 2023. The climate data used in this study and material properties modeled in the simulation are presented in Paper VI.

6.2.2 Penetration criteria

The results of the third and fourth experimental campaigns were applied in probabilistic hygrothermal analyses, enabling analyses of wall conditions before and after repointing. While the specimens in the experimental campaign were divided into five groups depending on the crack width, in this numerical study, the brick masonry was divided into two groups: a) cracked masonry, including results of specimens with crack widths ranging from 0.3 mm to 0.9 mm and b) masonry without known cracks, including the results of reference specimens. This choice is motivated by the fact that while visual inspections are instrumental in assessing wall conditions, accurately identifying poorly executed workmanship, often accompanied by voids and cracks, can be quite challenging. Additionally, measuring the width and length of cracks presents its own challenges, given their diverse forms – from hairline cracks to the wide cracks deep in the wall, each characterized by unique uncertainties in terms of shape and tortuosity.

To address these challenges, this study attempts to simplify the categorization of brick masonry cladding conditions into two easily distinguishable groups through visual inspection, labeled G (representing good standard façades) and D (representing deficient façades). The former denotes walls exhibiting good workmanship, minimal erosion, and a lack of significant cracks, while the latter encompasses walls with many visible cracks, eroded mortar joints, and relatively poor workmanship. Consequently, the experimental results obtained from the cracked specimens represent poor workmanship conditions, whereas results from water penetration in brick masonry without known cracks represent scenarios reflecting good wall conditions.

6.2.3 Results and discussion

The mold index decreases after repointing, regardless of whether the brick veneer in timber frame walls is at a good standard or in deficient condition. Similarly, the average water content reduction for masonry cavity walls is noticeable after repointing. The obtained results further indicate that repointing could be more effective in reducing mold index and water content in walls categorized as deficient, regardless of the wall's location and orientation. In contrast, the improvements due to repointing are more limited for walls classified as good standards. This indicates that investing resources to improve brick veneer in good technical condition might be questionable. This is further discussed in Paper VI.

The findings underline that repointing can effectively reduce risks associated with water penetration due to WDR, depending on the wall's condition and location. Walls categorized as deficient are expected to experience higher water penetration compared to walls in good condition, making repointing an effective strategy for lowering the risks associated with water penetration due to WDR. Repointing might give larger positive effects at locations with high WDR loads. Accordingly, the positive effect of repointing might be greater in Gothenburg than in Rensjön and Uppsala, locations with lower amounts of WDR.

Nevertheless, when considering wall orientation, the interplay between solar radiation and exposure to WDR complicates the establishment of a clear link between orientation and improvements in wall performance post-repointing, particularly in regions with low WDR loads. The results are further discussed in detail in Paper VI.

7 Conclusions

The aim of this thesis was to study water penetration induced by wind-driven rain (WDR) in brick masonry and how repointing could affect water penetration. Accordingly, the response of clay brick masonry exposed to a uniform water spray was studied by employing a newly developed test setup. Four experimental campaigns were performed, and different parameters were considered, including water spray rate, water absorption properties of bricks, mortar joint profile, and crack width. This is followed by implementing the experimental results in hygrothermal simulations of walls built with brick masonry veneer. Based on the obtained results, the following conclusions can be drawn (the related research questions are provided in parentheses):

Research questions:

Q1- What are the critical factors influencing the resistance of clay brick masonry to WDR?

Q2- How does WDR affect water absorption and penetration of clay brick masonry under different exposure conditions?

Q3- How does the presence of cracks or imperfections in clay brick veneers impact water penetration?

Q4- How does repointing influence brick masonry's response to WDR regarding water absorption and penetration?

Q5- In what scenarios can repointing of clay brick veneers be used as an effective measure to mitigate moisture-related risk in building envelopes?

Q6- How can knowledge gained from experimental studies on clay brick masonry response to WDR be utilized to improve the hygrothermal assessment of building envelopes and enhance risk-aware judgments regarding moisture safety?

The drawn conclusions:

1) Water absorption in brick masonry is dependent mainly on the water spray rate and water absorption coefficient of bricks (Q1 & Q2). While the effect of cracks on water absorption was not considerable (Q3), repointing could significantly reduce the water absorption rate in brick masonry (Q4).

2) In masonry without known cracks, the first dampness appeared close to the brick-mortar interface in the vicinity of the head joint, indicating the lower resistance of head joints to WDR (Q1). The effect of the mortar joint profile on water absorption and penetration was not considerable (Q1).

3) Crack width had a limited effect on the time to the emergence of the first dampness (Q3). However, repointing was shown to be an effective measure to postpone the emergence of the first dampness in brick masonry (Q4).

4) Water penetration in masonry without known cracks started when the specimens were close to full saturation, highlighting the benefit gained from the moisture buffering capacity of masonry to postpone the occurrence of water penetration (Q1 & Q2). In brick masonry without any known crack, water penetration consistently started at a moisture content corresponding to about 90% saturation (Q6).

5) Cracks significantly affect the time to the start of penetration as well as the water penetration rate; the greater the crack width, the less time needed for penetration initiation and the higher the penetration rate (Q3). Furthermore, it was observed that larger cracks were associated with lower saturation levels at the start of water penetration (Q3).

6) In addition to the cracks providing the least resistance pathway for water penetration, it is essential to acknowledge the potential of the brick-mortar interfacial zone to facilitate such penetration (Q1). There is a need to highlight the importance of workmanship in filling the joints, particularly the head joints, which are probably the weakest part of clay brick masonry concerning water penetration.

7) Repointing could considerably postpone the start of water penetration and reduce the water penetration rate with at least a 50% reduction in cracked specimens and specimens without known cracks (Q4).

8) Repointing can be considered as a maintenance technique to reduce moisture-related risk in building envelopes with clay brick veneers, particularly those in deficient condition and located in areas with high exposure to WDR (Q5).

Given the fact that repointing is a costly and laborious measure, this study recommends considering partial repointing, addressing only those wall orientations where the performance improvement resulting from repointing is evident, as opposed to repointing all façade sections and wall orientations (Q5 and Q6). It is important to note that these recommendations primarily address the technical aspects, and other factors like aesthetic considerations should also be weighed. Ultimately, the decision on whether to opt for full, partial, or no repointing requires a comprehensive evaluation of various aspects, with this study highlighting a couple of aspects for consideration.

8 Future research

The primary objective of this Ph.D. project was to investigate the resistance of brick masonry veneer walls to wind-driven rain (WDR) and its implications for decisions on repointing as a mitigating measure. The following is a list of potential future studies aimed at enhancing methodological and experimental aspects, with a focus on more accurately representing the 'real-world masonry façade' and its complexities, incorporating considerations for 'real-world maintenance' and its associated factors, and improving the accuracy of hygrothermal simulations.

Methodological and experimental aspects

Although the obtained results highlight that the main driving force for water to penetrate is hydrostatic pressure due to runoff, the impact of air pressure difference was not considered. Thus, an important point for future research is to investigate masonry exposure to WDR under varying levels of differential air pressure.

The current Ph.D. project focused primarily on investigating the response of brick masonry to WDR, including water absorption and penetration. Although elevated moisture content and water penetration due to WDR adversely affect the hygrothermal response of a building envelope, it is also essential that moisture leaves the masonry by evaporation to help it dry once it has entered. Thus, it is equally crucial to evaluate the drying characteristics of brick masonry veneers.

Real-world masonry façades

In this research, masonry specimens were built with only one head joint, a configuration to minimize undesired disintegration. However, it is important to note that this design choice resulted in a lower percentage of head joints compared to typical real-world masonry structures, regardless of the bond type. Future studies should thus consider masonry specimens with more head joints to gain more practical insights, as the water penetration rate per unit wall area would likely increase in such cases.

The masonry specimens in the present study were prepared with solid bricks. However, many clay brick masonry façades have been constructed with perforated bricks. Therefore, studying water absorption and penetration in masonry with perforated bricks could yield valuable knowledge.

The limitations regarding the applicability of this project's findings in assessing the hygrothermal performance of cracked masonry should be carefully considered. The experimental studies were conducted on 3-course masonry prisms with a through crack in the bed joint, which may not fully represent the wide variety of cracks that can occur in masonry veneers. Cracks can differ in size and location, and various types of cracks, such as those in head joints or hairline cracks, necessitate a more comprehensive examination. Furthermore, other imperfections, e.g., caused by workmanship, can also create pathways for water penetration. As the present study highlights the importance of workmanship in filling head joints, it prompts further investigation into the effect of different workmanship methods on the resistance of masonry to WDR.

Real-world maintenance

During repointing, it is common practice to rake out joints to a depth of around 25 mm or 2.5 times the thickness of the mortar joint. However, considering that head joints typically provide the least resistance pathway for water to penetrate, it is worth exploring the possibility of increasing the raking depth, specifically in head joints. This raises the question of how much the reduction in water penetration could be correlated with the increased raking depth.

Further, there is a need to study the effect of repointing on the long-term performance of masonry walls. In this study, repointing showed an improvement in reducing water penetration after a one-time exposure to water spray (short-term performance), yet there is a need to investigate the performance of repointed walls after several times of exposure to WDR (long-term behavior). While repointing can enhance the resistance of brick masonry cladding to WDR, in order to have an accurate hygrothermal analysis of brick masonry after repointing, there is a need to study the impact of repointing on the drying response of masonry walls.

In practice, techniques that are used to apply new mortar during repointing may affect water absorption and penetration into clay brick masonry. Compared to the traditional method of filling the raked joints with a trowel by hand, machine-driven equipment to apply new mortar has recently been used. The mortar used for machinery equipment usually has higher water content, resulting in difficulties in compacting the mortar. Consequently, filling mortar joints with machine-driven equipment may result in air voids and poor contact between bricks and mortar. Thus, the effects of different methods to fill the raked joints should be investigated.

Numerical aspects

The simulations done in this study were based on historical climate data obtained from weather stations provided by the Swedish Meteorological and Hydrological Institute (SMHI). The Climate variables used in the hygrothermal simulations may have two main uncertainties, particularly regarding rain intensity, wind velocity, and wind direction. Firstly, the hourly data of rain and wind is used where many

rain events occur over a shorter time, necessitating the implementation of weather data with a smaller temporal resolution, such as 5–10 min.

The second uncertainty concerns spatial variability, i.e., whether the location of the measurements is representative of the studied location. In large geographic areas, a single weather station might not represent the ranges of rain and wind that may occur in the area of interest. Thus, there is a need to quantify the WDR intensity at a smaller scale.

9 Summary of the appended papers

Paper I

Repointing is a maintenance technique that has the potential to address problems caused by eroded mortar joints due to wind-driven rain (WDR). However, there is a lack of well-established criteria for making informed decisions on when repointing is necessary. While various criteria exist to guide this decision, some existing criteria may be questioned. This paper presents the findings of a state-of-the-art study on field and laboratory methods for assessing water content and water uptake caused by WDR. The use of the obtained information to assess whether repointing could improve the technical condition of clay brick façades affected by WDR is discussed in more detail. It is recommended that visual inspection, if inconclusive, be complemented by one of the discussed test methods to assess the façade's condition and make a more informed decision on repointing. Additionally, alternative maintenance techniques that could postpone more costly repairs and identify potential defects or issues are presented.

Paper II

This study aims to investigate the resistance of brick masonry to water spraying to replicate the response of masonry claddings exposed to WDR. While existing standards and research studies typically address extreme WDR events and focus on water penetration in saturated masonry, developing a test setup to assess masonry's response to WDR in an unsaturated state is relevant since clay brick masonry has a considerable water buffering capacity. The experimental study employs a novel test setup to study water absorption and penetration in 3-course masonry prisms exposed to water spray. A mounted digital camera is used to record damp patches on the backside of the specimens. Several parameters are considered, including brick absorption properties and mortar joint profiles. Three types of bricks and two types of joint profile finishes (flush and raked) are utilized, with the raked joints representing eroded mortar joints. The specimens are exposed to a uniform water spray rate ranging between 1.7 and 3.8 $l/m^2/h$. The results reveal that water absorption primarily depends on the water absorption coefficient and capacity of the bricks, while the impact of mortar joint profiles on water absorption is insignificant. The presence of damp patches in the vicinity of the head joints indicates that the brick-mortar interfacial zone is a primary path for water to transport, primarily due to inadequate compaction and challenges in achieving complete joint filling.

Paper III

An experimental campaign is conducted to investigate water absorption and penetration in 3-course masonry prisms when subjected to a uniform water spray. The specimens are subjected to a water spray rate of approximately 6.5 $l/m^2/h$. The experimental setup incorporates two digital scales that allow for continuous measuring of water absorption and penetration over a 23-hour testing duration. The findings highlight the significant influence of brick absorption properties on water absorption. Conversely, the impact of joint profile on water absorption and penetration is found insignificant. Water penetration primarily occurs through the brick-mortar interfacial zone, mainly through the head joint, which is attributed to challenges in achieving complete filling of the head joints during construction and lower compaction compared to the bed joints. Moreover, a novel criterion is introduced for implementing water penetration into hygrothermal analyses, whereby no water penetration occurs unless the water content of the specimens is above 90% of their saturation capacity. The saturation level at which penetration initiates remains consistent across all joint profiles and brick types. The utility and implications of the proposed criterion are briefly demonstrated by evaluating water content and water penetration in a clay brick masonry façade. The study compares the resulting water penetration with the outcomes obtained using a commonly accepted reference model, which assumes that only one percent of WDR deposited on the façade penetrates the clay brick cladding.

Paper IV

The paper investigates the implementation of two water penetration criteria for the risk of damage in a common type of building envelope in Nordic countries, timber frame walls with brick masonry veneer. The walls are evaluated based on mold growth risk as a damage criterion. Given the lack of consensus regarding the position and distribution of moisture sources in hygrothermal models, the study considers several parameters, including the water penetration criterion, type and position of the moisture source within the wall assembly, air change rate (ACR), WDR coefficient, and different locations with varying average annual rainfall and temperature. The study compares two different criteria for implementing water penetration: a) a commonly accepted reference model that assumes one percent of all WDR deposited on the façade penetrates the clay brick cladding, and b) a new criterion proposed in Paper III suggesting that 3.8% of WDR penetrates when the water content of the brick veneer cladding exceeds 90% of its saturation capacity. The results in this study suggest that an effective measure for the design/maintenance of such walls should incorporate: a) limiting the amount of water penetrating through the cladding, particularly stopping water from reaching the sensitive elements, i.e., timber studs, b) removing extruded mortar stemming from poor workmanship, if any, which may act as a capillary bridge.

Paper V

Water penetration, a major source of moisture, significantly affects the performance of building envelopes. Despite the detrimental role of cracks in facilitating water penetration in masonry cladding, limited research exists on the resistance of cracked masonry to WDR. In this study, 3-course masonry prisms with artificial cracks of varying widths (ranging from 0.3 mm to 0.9 mm) are subjected to a uniform water spray, while reference specimens without known cracks are also studied for comparison. The findings demonstrate a reasonable correlation between crack width and the average water penetration rate. Additionally, a strong correlation is observed between the saturation level and the initiation of water penetration. In the reference specimens, water penetration starts when the water content exceeds 90% of the saturation capacity. Water penetration commences at saturation levels ranging from 72% to 87% for the cracked specimens, depending on the crack width. The specimens are repointed and once again exposed to water spray. On average, the water penetration rate decreases by approximately 54% in the reference specimens and between 47% and 74% in the specimens with cracks. Since the process of repointing involves raking the mortar joints, voids and gaps are discovered, especially in the head joints. This finding confirms that head joints are likely the weakest part of clay brick masonry in terms of water penetration.

Paper VI

While the effectiveness of repointing as a maintenance technique is often claimed, there remains a scarcity of concrete evidence regarding the impact of repointing on enhancing building envelope performance. This study seeks to bridge this gap by investigating the effect of repointing to reduce the risk of damage to building envelopes by employing a probabilistic hygrothermal assessment. Several factors, including wall type (timber frame and autoclaved aerated concrete (AAC) cavity walls with brick veneer cladding), wall location, and façade orientation, are taken into account in the analyses. The findings indicate that repointing may significantly reduce the mold index of timber frame walls and the moisture content of AAC, particularly in cases where the brick veneer exhibits poor workmanship, visible cracks, and apparent deficiencies. This reduction is most pronounced for walls exposed to high WDR loads. Conversely, the difference in performance before and after repointing is limited for brick veneers without substantial defects, cracks, or erosion. These outcomes highlight the critical importance of visually inspecting the wall's condition, especially for signs of more comprehensive cracking, before committing to repointing as a maintenance strategy. Furthermore, the study suggests that instead of routinely repointing all façade orientations, a more targeted approach should be adopted based on the wall location/orientation and its specific condition.

References

[1] O. Beijer, "Concrete walls and weathering," in *Proceedings of the RILEM/ASTM/CIB Symposium on Evaluation of the Performance of External Vertical Surfaces of Buildings, Espoo, Finland, 23–31 August & 1-2 September*, 1977, pp. 66-76.

[2] B. Blocken and J. Carmeliet, "A simplified numerical model for rainwater runoff on building facades: Possibilities and limitations," *Building and Environment,* vol. 53, pp. 59-73, 2012.

[3] L. Olsson and C.-E. Hagentoft, "New algorithm for water leakages flow through rain screen deficiencies," in *Proceedings of the 7th International Building Physics Conference*, Syracuse, NY, USA, 2018.

[4] M. Abuku, H. Janssen, and S. Roels, "Impact of wind-driven rain on historic brick wall buildings in a moderately cold and humid climate: Numerical analyses of mould growth risk, indoor climate and energy consumption," *Energy and Buildings,* vol. 41, no. 1, pp. 101-110, 2009/01/01/ 2009.

[5] G. B. Coelho and F. M. Henriques, "Influence of driving rain on the hygrothermal behavior of solid brick walls," *Journal of Building Engineering,* vol. 7, pp. 121-132, 2016.

[6] P. Johansson *et al.*, "Interior insulation retrofit of a historical brick wall using vacuum insulation panels: Hygrothermal numerical simulations and laboratory investigations," *Building and Environment,* vol. 79, pp. 31-45, 2014.

[7] M. Hammett, "The repair and maintenance of brickwork," *Structural Survey,* vol. 9, no. 2, pp. 153-160, 1991.

[8] K. Calle and N. Van Den Bossche, "Sensitivity analysis of the hygrothermal behaviour of homogeneous masonry constructions: Interior insulation, rainwater infiltration and hydrophobic treatment," *Journal of Building Physics,* vol. 44, no. 6, pp. 510-538, 2021.

[9] S. Nath, M. Dewsbury, H. Künzel, and P. Watson, "Mould Growth Risks for a Clay Masonry Veneer External Wall System in a Temperate Climate," *Atmosphere,* vol. 13, no. 11, p. 1755, 2022.

[10] H. Künzel and D. Zirkelbach, "Influence of rain water leakage on the hygrothermal performance of exterior insulation systems," in *Proceedings of the 8th Nordic symposium on building physics in the Nordic countries*, 2008, pp. 253-260.

[11] K. Calle, C. Coupillie, A. Janssens, and N. Van Den Bossche, "Implementation of rainwater infiltration measurements in hygrothermal modelling of non-insulated brick cavity walls," *Journal of Building Physics,* vol. 43, no. 6, pp. 477-502, 2020.
[12] C. Groot and J. Gunneweg, "The influence of materials characteristics and workmanship on rain penetration in historic fired clay brick masonry," *Heron, 55 (2),* 2010.
[13] R. C. Mack and J. S. Askins, "An Introduction to Repointing," *Bulletin of the Association for Preservation Technology,* vol. 11, no. 3, pp. 44-60, 1979.
[14] S. M. Tindall, "Repointing Masonry—Why Repoint," *Old-House Journal,* pp. 24-31, 1987.
[15] C. Groot and J. Gunneweg, "Water permeance problems in single wythe masonry walls: the case of wind mills," *Construction and Building Materials,* vol. 18, no. 5, pp. 325-329, 2004/06/01/ 2004.
[16] A. Maurenbrecher, K. Trischuk, M. Rousseau, and M. Subercaseaux, "Repointing mortars for older masonry buildings–design considerations," *Construction Technology. Update,* no. 67, pp. 1206-1220, 2008.
[17] C. C. Fishburn, D. Watstein, and D. E. Parsons, *Water permeability of masonry walls*. US Department of Commerce, National Bureau of Standards, 1938.
[18] L. Fusade, S. A. Orr, C. Wood, M. O'Dowd, and H. Viles, "Drying response of lime-mortar joints in granite masonry after an intense rainfall and after repointing," *Heritage Science,* vol. 7, no. 1, pp. 1-19, 2019.
[19] G. K. Garden, "Rain penetration and its control," in *Canadian building digest 1-100*, 1963, pp. 4-4.
[20] J. F. Straube, "Moisture control and enclosure wall systems," Doctor of Philosophy in Civil Engineering, University of Waterloo, 1998.
[21] S. Van Linden, "Fourth Generation Watertightness: A Performance-Based Strategy to Control Rainwater Infiltration in Façade Systems," Ghent University, 2022.
[22] N. Van Den Bossche, "Watertightness of building components: principles, testing and design guidelines," Ghent University, 2013.
[23] F. Slapø, T. Kvande, N. Bakken, M. Haugen, and J. Lohne, "Masonry's Resistance to Driving Rain: Mortar Water Content and Impregnation," *Buildings,* vol. 7, no. 3, p. 70, 2017.
[24] S. Kahangi Shahreza, J. Niklewski, and M. Molnár, "Experimental investigation of water absorption and penetration in clay brick masonry under simulated uniform water spray exposure," *Journal of Building Engineering,* vol. 43, p. 102583, 2021/11/01/ 2021.
[25] S. Kahangi Shahreza, M. Molnár, and J. Niklewski, "Water absorption and penetration in clay brick masonry exposed to uniform water spray," in *14th Canadian Masonry Symposium*, Montreal, Canada, 2021.

[26] S. Selvarajah and A. Johnston, "Water permeation through cracked single skin masonry," *Building and Environment,* vol. 30, no. 1, pp. 19-28, 1995.
[27] K. Calle and N. Van Den Bossche, "Towards understanding rain infiltration in historic brickwork," *Energy Procedia,* vol. 132, pp. 676-681, 2017.
[28] S. Van Linden and N. Van Den Bossche, "Review of rainwater infiltration rates in wall assemblies," *Building and Environment,* vol. 219, p. 109213, 2022/07/01/ 2022.
[29] N. Van Den Bossche, M. Lacasse, and A. Janssens, "Watertightness of masonry walls: an overview," in *12th International conference on Durability of Building Materials and Components (XII DBMC-2011)*, 2011, vol. 1, pp. 49-56: FEUP Edições.
[30] M. Kahangi, *Resistance of Clay Brick Masonry Façades to Wind-Driven Rain: Repointing of Eroded Mortar Joints* (no. 1055). Lund University, 2021.
[31] K. Ghanate, M. Khanverdi, and S. Das, "Wind-driven rainwater penetration through brick veneer with and without surface treatments," *Journal of Building Engineering,* vol. 62, p. 105347, 2022/12/15/ 2022.
[32] T. Ritchie and J. I. Davison, "Factors affecting bond strength and resistance to moisture penetration of brick masonry," (in eng), *ASTM Special Technical Publication,* no. 320, pp. 16-30, 1963.
[33] T. Hines and M. Mehta, "The Effect of Mortar Joints on the Permeance of Masonry Walls," in *in proceedings of the 9th International Brick/Block Masonry Conference*, Berlin, Germany, 1991, pp. pp. 1227-1234.
[34] T. Ritchie and W. G. Plewes, "A review of literature on rain penetration of unit masonry," (in eng), *Technical Paper (National Research Council of Canada. Division of Building Research),* 1957/05 1957, Art. no. iii, 72 p.
[35] S. Kahangi Shahreza, J. Niklewski, and M. Molnár, "Novel water penetration criterion for clay brick masonry claddings," *Construction and Building Materials,* vol. 353, p. 129109, 2022/10/24/ 2022.
[36] J. Ribar, "Water permeance of masonry: a laboratory study," in *Masonry: Materials, Properties, and Performance*: ASTM International, 1982.
[37] *NBI 29/1983 Mørtler. Tetthet mot slagregn (Mortars. Resistance to driving rain)*, 1983.
[38] A. International, "ASTM E514 / E514M-14a, Standard Test Method for Water Penetration and Leakage Through Masonry," ed. West Conshohocken, PA: ASTM International, 2014.
[39] R. Cacciotti, "Brick masonry response to wind driven rain," *Engineering Structures,* vol. 204, p. 110080, 2020.
[40] *NEN 2778:2015 nl. Vochtwering in gebouwen (Moisture control in buildings)*, 2015.
[41] R. R. Vilató, "WATER PENETRATION TEST ON CONCRETE BLOCK MASONRY," in *the 15th International Brick and Block Masonry Conference*, Florianópolis – Brazil, 2012.

[42] J. C. Z. Piaia, M. Cheriaf, J. C. Rocha, and N. L. Mustelier, "Measurements of water penetration and leakage in masonry wall: Experimental results and numerical simulation," *Building and Environment,* vol. 61, pp. 18-26, 2013.

[43] K. B. Anand, V. Vasudevan, and K. Ramamurthy, "Water permeability assessment of alternative masonry systems," *Building and Environment,* vol. 38, no. 7, pp. 947-957, 2003/07/01/ 2003.

[44] T. Ritchie, "Small-panel method for investigating moisture penetration of brick masonry," in "Internal Report (National Research Council of Canada. Division of Building Research); no. DBR-IR-160," National Research Council of Canada1958/09/01 1958.

[45] S. Van Goethem, N. Van Den Bossche, and A. Janssens, "Watertightness Assessment of Blown-in Retrofit Cavity Wall Insulation," *Energy Procedia,* vol. 78, pp. 883-888, 2015/11/01/ 2015.

[46] M. E. Driscoll and R. E. Gates, "A Comparative Review of Various Test Meteods for Evaluating the Water Penetration Resistance of Concrete Masonry Wall Units," in *Masonry: Design and Construction, Problems and Repair*: ASTM International, 1993.

[47] L. R. Baker and F. W. Heintjes, "Water leakage through masonry walls," *Architectural Science Review,* Article vol. 33, no. 1, pp. 17-23, 1990.

[48] R. Forghani, Y. Totoev, S. Kanjanabootra, and A. Davison, "Experimental investigation of water penetration through semi-interlocking masonry walls," *Journal of Architectural Engineering,* vol. 23, no. 1, p. 04016017, 2017.

[49] M. Lacasse, T. O'Connor, S. Nunes, and P. Beaulieu, "Report from Task 6 of MEWS project: Experimental assessment of water penetration and entry into wood-frame wall specimens-final report," *Institute for Research in Construction, RR-133, Feb,* 2003.

[50] A. Rathbone, *Rain and air penetration performance of concrete blockwork*. Cement and Concrete Association, 1982.

[51] H. Hens, S. Roels, and W. Desadeleer, "Rain leakage through veneer walls, built with concrete blocks," in *CIB W40 meeting in Glasgow*, 2004.

[52] A. Martins, G. Vasconcelos, and A. C. Costa, "Brick masonry veneer walls: An overview," *Journal of Building Engineering,* vol. 9, pp. 29-41, 2017.

[53] S. Pompeu dos Santos, "Enclosure masonry walls systems worldwide, CIB Publication," ed: Taylor and Francis, 2007.

[54] B. S. Institution, *Guide to durability of buildings and building elements, products and components*. British Standards Institution, 2003.

[55] M. Coronado, T. Blanco, N. Quijorna, R. Alonso-Santurde, and A. Andrés, "7 - Types of waste, properties and durability of toxic waste-based fired masonry bricks," in *Eco-Efficient Masonry Bricks and Blocks*, F. Pacheco-Torgal, P. B. Lourenço, J. A. Labrincha, S. Kumar, and P. Chindaprasirt, Eds. Oxford: Woodhead Publishing, 2015, pp. 129-188.

[56] A. Hendry and F. Khalaf, "Masonry Wall Construction. London and New York," ed: Taylor & Francis Group, Spon Press, 2001.
[57] I. M. Griffin, "Deterioration mechanisms of historic cement renders and concrete," Doctoral dissertation, University of Edinburgh, 2013.
[58] J. I. Knarud, T. Kvande, and S. Geving, "Hygrothermal Simulation of Interior Insulated Brick Wall—Perspectives on Uncertainty and Sensitivity," *Buildings,* vol. 13, no. 7, p. 1701, 2023.
[59] R. C. Mack and A. E. Grimmer, *Assessing cleaning and water-repellent treatments for historic masonry buildings*. Government Printing Office, 2000.
[60] M. Molnár and O. L. Ivanov, "Clay brick masonry facades with cracks caused by corroding bed joint reinforcement–Findings from field survey and laboratory study," *Construction and Building Materials,* vol. 125, pp. 775-783, 2016.
[61] T. Kvande and K. R. Lisø, "Climate adapted design of masonry structures," *Building and environment,* vol. 44, no. 12, pp. 2442-2450, 2009.
[62] K. Balksten and P. Strandberg-de Bruijn, "Understanding deterioration due to salt and ice crystallization in scandinavian massive brick masonry," *Heritage,* vol. 4, no. 1, pp. 349-370, 2021.
[63] R. Brown, *Initial effects of clear coatings on water permeance of masonry*. ASTM International, 1982.
[64] Y. D. Aktas, H. Zhu, D. D'Ayala, and C. Weeks, "Impact of surface waterproofing on the performance of brick masonry through the moisture exposure life-cycle," *Building and Environment,* vol. 197, p. 107844, 2021.
[65] D. Chiovitti, M. Gonçalves, and A. Renzullo, "Performance evaluation of water repellents for above grade masonry," *Journal of Thermal Envelope and Building Science,* vol. 22, no. 2, pp. 156-168, 1998.
[66] B. Lubelli and R. van Hees, "Evaluation of the effect of nano-coatings with water repellent properties on the absorption and drying behaviour of brick," in *6th International Conference on Water Repellent Treatment of Building Materials; Aedificatio Publishers: Freiburg, Germany*, 2011, pp. 125-136.
[67] S. Johnson, "The neglected craft of repointing–an architect's view," ed: Crown copyright NSW Heritage Office & the author, 2000.
[68] R. Veiga and F. Carvalho, "Some performance characteristics of lime mortars for rendering and repointing ancient buildings," in *Proc. Br. Masonry Soc. No. 8*, 1998, pp. 353-356.
[69] A. H. P. Maurenbrecher, K. Trischuk, M. Z. Rousseau, and M. I. Subercaseaux, "Repointing mortars for older masonry buildings: design considerations," (in eng), *Construction Technology Update; no. 67,* 2008/03/01 2008, Art. no. 6 p.
[70] P. M. C. L. Paul Jeffs, "Repointing Masonry Walls – Matching the Techniques for Success or Failure," ed. Technical Workshop Restoration, Reconstruction and Maintenance of Masonry Structures, Dalhousie

University Continuing Technical Education: Conservation of Heritage Structures & Older Buildings.
[71] D. Young, "Repointing mortar joints: some important points," in *Australia ICOMOS Conference*, Adelaide Australia, 2015.
[72] C. W. Westermann, Heinrich and Schulz, Jens-Uwe, "Increased Durability of Repointing In Historical Masonry – Engineering Model and Sensitivity Analysis," presented at the 13th Canadian Masonry Symposium, Halifax, Canada, 4-7 June, 2017.
[73] A. Maurenbrecher, K. Trischuk, M. Rousseau, and M. Subercaseaux, "Key Considerations for Repointing Mortars for the Conservation of Older Masonry (IRC-RR-225)," *Canada: Institute for Research in Construction, National Research Council of Canada, Ottawa,* 2007.
[74] P. Maurenbrecher and J. E. Lindqvist, "RILEM TC 203-RHM: Repair mortars for historic masonry : Requirements for repointing mortars for historic masonry," (in eng), *Materials and Structures,* article vol. 45, no. 9, pp. 1303-1309, 2012 2012.
[75] S. M. Tindall, "Repointing Masonry—Why Repoint?," *Old-House Journal,* pp. 24-31, January/February 1987.
[76] M. Holland, *Practical Guide to Diagnosing Structural Movement in Buildings*. John Wiley & Sons, 2012.
[77] B. Brief, "Repointing (Tuckpointing) Brick Masonry," *Brick Industry Association,* July 2005.
[78] J. G. Stockbridge, "Repointing masonry walls," *APT bulletin,* vol. 21, no. 1, pp. 10-12, 1989.
[79] C. Giarma and D. Aravantinos, "Estimation of building components' exposure to moisture in Greece based on wind, rainfall and other climatic data," *Journal of Wind Engineering and Industrial Aerodynamics,* vol. 99, no. 2, pp. 91-102, 2011/02/01/ 2011.
[80] N. Van Den Bossche, M. A. Lacasse, and A. Janssens, "A uniform methodology to establish test parameters for watertightness testing: Part I: A critical review," *Building and Environment,* vol. 63, pp. 145-156, 2013/05/01/ 2013.
[81] B. Blocken and J. Carmeliet, "A review of wind-driven rain research in building science," *Journal of Wind Engineering and Industrial Aerodynamics,* vol. 92, no. 13, pp. 1079-1130, 2004/11/01/ 2004.
[82] K. Sandin, "The moisture conditions in aerated lightweight concrete walls," *situ measurements of the effect of the driving rain and the surface coating. Rapport TVBM–3026. Division of Building Materials, Lund Institute of Technology, Sweden,* 1987.
[83] H. Ge, U. D. Nath, and V. Chiu, "Field measurements of wind-driven rain on mid-and high-rise buildings in three Canadian regions," *Building and Environment,* vol. 116, pp. 228-245, 2017.

[84] E. Cho, C. Yoo, M. Kang, S.-u. Song, and S. Kim, "Experiment of wind-driven-rain measurement on building walls and its in-situ validation," *Building and Environment,* vol. 185, p. 107269, 2020/11/01/ 2020.

[85] B. Blocken and J. Carmeliet, "On the accuracy of wind-driven rain measurements on buildings," *Building and Environment,* vol. 41, no. 12, pp. 1798-1810, 2006/12/01/ 2006.

[86] "EN ISO 15927-3, Hygrothermal performance of buildings-Calculation and presentation of climatic data. Part 3: calculation of a driving rain index for vertical surfaces from hourly wind and rain data," ed: European Committee for Standardization, 2009.

[87] J. Straube and E. Burnett, "Simplified prediction of driving rain on buildings," in *Proceedings of the international building physics conference*, 2000, pp. 375-382: Eindhoven University of Technology Eindhoven, the Netherlands.

[88] A. Standard, "Standard 160-2021: Criteria for Moisture Control Design Analysis in Buildings," *American Society of Heating, Refrigerating and Air-Conditioning Engineers, Atlanta,* 2021.

[89] B. Blocken and J. Carmeliet, "Overview of three state-of-the-art wind-driven rain assessment models and comparison based on model theory," *Building and Environment,* vol. 45, no. 3, pp. 691-703, 2010/03/01/ 2010.

[90] C. Chen, H. Zhang, C. Feng, Y. Xuan, T. Qian, and J. Xie, "Analysis of wind-driven rain characteristics acting on building surfaces in Shanghai based on long-term measurements," *Journal of Building Engineering,* vol. 45, p. 103572, 2022/01/01/ 2022.

[91] B. S. Institution, *Code of Practice for Assessing Exposure of Walls to Wind-driven Rain*. British Standards Institution, 1992.

[92] (accessed September 2023). https://www.smhi.se/data.

[93] R. E. Lacy, "Driving rain maps and the onslaught of rain on buildings," in *Proc. of CIB/RILEM Symposium on Moisture Problems in Buildings, Helsinki, 1965*, 1965.

[94] H. Künzel, "Wärme-und Feuchteschutz von zweischaligem Mauerwerk mit Kerndämmung," *Bauphysik,* vol. 13, no. 1, pp. 3-11, 1991.

[95] J. F. Straube and E. F. Burnett, "Driving rain and masonry veneer," in *Water leakage through building facades*: ASTM International, 1998.

[96] J. Straube and E. Burnett, "Rain control and screened wall systems," in *Proc. 7th Conf. on Building Science and Technology. Durability of Buildings. Design, Maintenance, Codes and Practices. Toronto*, 1997, pp. 20-21.

[97] M. Abuku, B. Blocken, J. Poesen, and S. Roels, "Spreading, splashing and bouncing of wind-driven raindrops on building facades," in *11th Americas Conf. on Wind Engineering, Univ. of Washington, Seattle*, 2009, pp. 22-26.

[98] M. Abuku, H. Janssen, J. Poesen, and S. Roels, "Impact, absorption and evaporation of raindrops on building facades," *Building and Environment,* vol. 44, no. 1, pp. 113-124, 2009/01/01/ 2009.
[99] A. Erkal, D. D'Ayala, and L. Sequeira, "Assessment of wind-driven rain impact, related surface erosion and surface strength reduction of historic building materials," *Building and Environment,* vol. 57, pp. 336-348, 2012.
[100] R. Couper, "Factors affecting the production of surface runoff from wind-driven rain," in *Proceedings of the second international symposium on moisture problems in buildings, paper*, 1974, vol. 1, no. 1.
[101] B. J. Mason and J. Andrews, "Drop-size distributions from various types of rain," *Quarterly Journal of the Royal Meteorological Society,* vol. 86, no. 369, pp. 346-353, 1960.
[102] C. K. Mutchler and L. M. Hansen, "Splash of a waterdrop at terminal velocity," *Science,* vol. 169, no. 3952, pp. 1311-1312, 1970.
[103] H. M. Künzel, "Simultaneous heat and moisture transport in building components: One-and two-dimensional calculation using simple parameters," PhD-thesis, IRB-Verlag Stuttgart, Fraunhofer Institute for Building Physics, 1995.
[104] A. D. Trindade, G. B. Coelho, and F. M. Henriques, "Influence of the climatic conditions on the hygrothermal performance of autoclaved aerated concrete masonry walls," *Journal of Building Engineering,* vol. 33, p. 101578, 2021.
[105] Delphin, "https://bauklimatik-dresden.de/delphin/index.php?aLa=en," Accessed August 2023.
[106] WUFI, "https://wufi.de/en/," (Accessed 26th August 2023).
[107] C. Hall and W. D. Hoff, *Water transport in brick, stone and concrete*. CRC Press, 2021.
[108] C. Hall and A. Kalimeris, "Water movement in porous building materials—V. Absorption and shedding of rain by building surfaces," *Building and Environment,* vol. 17, no. 4, pp. 257-262, 1982.
[109] C. Hall, "Water movement in porous building materials—IV. The initial surface absorption and the sorptivity," *Building and Environment,* vol. 16, no. 3, pp. 201-207, 1981.
[110] M. El-Shimi, R. White, and P. Fazio, "Influence of facade geometry on weathering," *Canadian journal of civil engineering,* vol. 7, no. 4, pp. 597-613, 1980.
[111] O. Beijer and A. Johansson, "Driving rain against external walls of concrete," 1976.
[112] H. Janssen, H. Derluyn, and J. Carmeliet, "Moisture transfer through mortar joints: a sharp-front analysis," *Cement and Concrete Research,* vol. 42, no. 8, pp. 1105-1112, 2012.
[113] H. J. P. Brocken, "Moisture transport in brick masonry-the grey area between bricks," TU Delft, Delft University of Technology, 1998.

[114] H. Derluyn, P. Moonen, and J. Carmeliet, "Moisture transfer across the interface between brick and mortar joint," in *Proceedings of the Nordic Symposium on Building Physics 2008*, 2008, vol. 2, pp. 865-872.
[115] J. Knarud, S. Geving, and T. Kvande, "Experimental Investigation of Capillary Absorption Along Mortar-Brick Interface Plane," in *Proceedings of the Central European Symposium on Building Physics, Dresden, Germany*, 2016, vol. 16.
[116] C. Hall and W. D. Hoff, *Water transport in brick, stone and concrete*, 2nd Edition ed. CRC Press, 2011.
[117] P. K. Mehta and P. J. Monteiro, *Concrete: microstructure, properties, and materials*. McGraw-Hill Education, 2014.
[118] L. Mengel, H.-W. Krauss, and D. Lowke, "Water transport through cracks in plain and reinforced concrete–Influencing factors and open questions," *Construction and Building Materials,* vol. 254, p. 118990, 2020.
[119] C. T. Grimm, "Masonry cracks: a review of the literature," *Masonry: materials, design, construction, and maintenance,* 1988.
[120] C. C. Fishburn, *Water permeability of walls built of masonry units*. US Department of Commerce, National Bureau of Standards, 1942.
[121] K. Calle, "Renovatie van historische gevels: redding of doodsteek," Doctoral Thesis, Ghent University, 2020.
[122] D. Sauve, K. Sroka, and C. Nmai, "A new concept in preventing water leakage through single-wythe concrete masonry walls," in *Water Problems in Building Exterior Walls: Evaluation, Prevention, and Repair*: ASTM International, 1999.
[123] S. L. Roller, *Effects of pressure on water penetration in brick masonry*. University of Wyoming, 1994.
[124] S. Cornick and M. Lacasse, "An Investigation of Climate Loads on Building Façades for Selected Locations in the United States," *Journal of ASTM International,* vol. 6, no. 2, pp. 1-22, 2009.
[125] T. Ritchie and W. G. Plewes, "Moisture penetration of brick masonry panels," (in eng), *ASTM Bulletin,* no. 249, pp. 39-43, 1961.
[126] J. F. Straube, "The Performance of Wall Systems Screened with Brick Veneer," University of Waterloo, 1994.
[127] C. J. Groot and J. Gunneweg, "Two views on dealing with rain penetration problems in historic fired clay brick masonry," in *Historic Mortars: Characterisation, Assessment and Repair*: Springer, 2012, pp. 257-266.
[128] C.-E. Hagentoft and L. Olsson, "Stochastic simulation of rain intrusion through small defects due to water rivulet overpressure. Introducing a driving rain leakage potential," in *Journal of Physics: Conference Series*, 2021, vol. 2069, no. 1, p. 012052: IOP Publishing.
[129] L. Olsson, *Driving rain tightness, intrusion rates and phenomenology of leakages in defects of façades: A new calculation algorithm*. Chalmers Tekniska Hogskola (Sweden), 2018.

[130] C. T. Grimm, "Water permeance of masonry walls: a review of the literature," in *Masonry: Materials, Properties, and Performance*: ASTM International, 1982.
[131] M. Y. L. Chew, "A modified on-site water chamber tester for masonry walls," *Construction and Building Materials,* vol. 15, no. 7, pp. 329-337, 2001/10/01/ 2001.
[132] A. International, "ASTM C67 / C67M-20, Standard Test Methods for Sampling and Testing Brick and Structural Clay Tile," ed. West Conshohocken, PA: ASTM International, 2020.
[133] A. International, "ASTM C1403 - 15, Standard Test Method for Rate of Water Absorption of Masonry Mortars," ed. West Conshohocken, PA: ASTM International, 2015.
[134] P. Jonell and T. Moller, "Moisture Penetration of Solid Facing Brick Walls," in "Technical Translation (National Research Council of Canada); no. NRC-TT-618," National Research Council of Canada0077-5606, 1956 1956.
[135] S. Kahangi Shahreza, "Water penetration in cracked clay brick masonry before and after repointing," *Construction and Building Materials,* vol. 420, p. 135631, 2024/03/22/ 2024.
[136] J. M. Delgado, E. Barreira, N. M. Ramos, and V. P. De Freitas, "Hygrothermal numerical simulation tools applied to building physics," 2012.
[137] C. Multiphysics, "https://www.comsol.com/," Accessed 26th August 2023.
[138] J. I. Knarud and S. Geving, "Comparative study of hygrothermal simulations of a masonry wall," *Energy Procedia,* vol. 132, pp. 771-776, 2017.
[139] J. I. Knarud and S. Geving, "Implementation and benchmarking of a 3D hygrothermal model in the COMSOL Multiphysics software," *Energy Procedia,* vol. 78, pp. 3440-3445, 2015.
[140] K. Carbonez, N. Van Den Bossche, H. Ge, and A. Janssens, "Comparison between uniform rain loads and point sources to simulate rainwater leakage with commercial HAM-models," in *International Symposium on Building Pathology (ISBP 2015)*, 2015: FEUP Edições.
[141] S. Mundt Petersen, *Moisture Safety in Wood Frame Buildings-Blind evaluation of the hygrothermal calculation tool WUFI using field measurements and determination of factors affecting the moisture safety*. Lund University, 2015.
[142] B. Hejazi, N. Sakiyama, J. Frick, and H. Garrecht, "Hygrothermal simulations comparative study: assessment of different materials using WUFI and DELPHIN software," in *Proceedings of the 16th IBPSA International Conference, Rome, Italy*, 2019, pp. 2-4.
[143] H. Künzel and D. Zirkelbach, "Hygrothermal consequences of rainwater leaks investigated for different wall structures with exterior insulation," in

1st Central European Symposium on Building Physics (CESBP), Cracow - Lodz, Poland, 2010.

[144] H. Saber, M. Lacasse, T. Moore, and M. Nicholls, "Mid-rise wood constructions: investigation of water penetration through cladding and deficiencies," *Report to Research Consortium for wood and wood-hybrid mid-rise buildings,* 2014.

[145] E. Vereecken and S. Roels, "Hygric performance of a massive masonry wall: How do the mortar joints influence the moisture flux?," *Construction and Building Materials,* vol. 41, pp. 697-707, 2013.

[146] V. M. Nik, S. O. Mundt-Petersen, A. S. Kalagasidis, and P. De Wilde, "Future moisture loads for building facades in Sweden: Climate change and wind-driven rain," *Building and Environment,* vol. 93, pp. 362-375, 2015/11/01/ 2015.

[147] H. Viitanen and T. Ojanen, "Improved model to predict mold growth in building materials," *Thermal Performance of the Exterior Envelopes of Whole Buildings X–Proceedings CD,* pp. 2-7, 2007.

[148] S. Thelandersson and T. Isaksson, "Mould resistance design (MRD) model for evaluation of risk for microbial growth under varying climate conditions," *Building and Environment,* vol. 65, pp. 18-25, 2013/07/01/ 2013.

[149] C.-M. Capener and K. Sandin, "Performance of a Retrofitted 1950's Multi-Unit Residential Building: Measurements and Calculated Transient Hygrothermal Behaviour," in *Thermal Performance of the Exterior Envelopes of Whole Buildings XII International Conference*, 2013.

[150] S. K. Shahreza, M. B. Pour, and A. A. Hamid, "Towards Rational Decision-Making on Repointing to Mitigate Moisture Damage in Building Envelopes: A Probabilistic Study," *Developments in the Built Environment,* p. 100510, 2024.

Paper I

Brick and Block Masonry - From Historical to Sustainable Masonry – Kubica, Kwiecień & Bednarz (eds)

Making decision on repointing of clay brick facades on the basis of moisture content and water absorption tests results – a review of assessment methods

S.K. Shahreza, M. Molnár, J. Niklewski & I. Björnsson
Department of Building and Environmental Technology, Division of Structural Engineering, Lund University, Lund, Sweden

T. Gustavsson
Tomas Gustavsson konstruktioner AB, Lund, Sweden

ABSTRACT: Use of clay brick masonry in façades is often motivated by its aesthetic values and durability. Yet, mortar joints exposed to climate agents erode over time, expected to cause elevated moisture content and water absorption. Thus, it is often recommended that 40- to 50-year-old facades should be repointed – a measure which is intrusive and costly. Decision is in many cases taken without a clear evidence that repointing will diminish water absorption and moisture content in the renovated walls. This paper presents the results of a state-of-the-art study on field and laboratory methods to measure moisture content and water absorption in clay brick masonry. For common buildings, use of low cost and time efficient measurement methods is feasible. However, prior to measurements, analysis of technical and climate data combined with a visual inspection might give a rational basis for decision on repointing or other alternative maintenance measures.

1 INTRODUCTION

Clay brick masonry is one of the most common building materials in the facades of residential buildings in the Nordic countries. The ubiquitous use of clay brick masonry as façade material is due to its aesthetic values, good durability and low maintenance needs. Although the expected technical life time of a clay brick façade is more than hundred years, maintenance can still be needed due to inevitable deterioration caused by climate and ambiance actions. Important climate actions in a Nordic climate include wind-driven rain (WDR) and freeze-thaw-cycles – actions that individually or in conjunction can cause spalling, delamination or cracking of bricks and erosion and cracking of mortar joints.

The focus in this paper is on the repointing of mortar joints, since it is an intrusive and costly maintenance measure. A common argument for repointing is that the erosion of mortar joints facilitates water up-take in facades exposed to WDR (Fried et al., 2014). Further, erosion of mortar joints is, at least in the Nordic countries, regarded as detrimental from an aesthetic point of view, since it creates, seen superficially, the impression of poor technical condition of the building. Understanding that aging of clay brick facades can be perceived as an aesthetic value, e.g. through exposure of fossil shells in the surface of the mortar joints, is generally poor (Tägil et al., 2011).

According to the present practice in the Nordic countries, repointing shall be carried out as part of a regular maintenance scheme, after 40-50 years from erection or when limited façade parties with more or less eroded mortar joints are observed (Tindall, 1987, Brief, 2017). No further investigations, e.g. concerning factual water up-take, are usually carried out. Nor are alternative measures, such as partial repointing of eroded façade parties, considered - full repointing is regularly carried out without a more in-depth analysis of the possible technical, economic or aesthetic implications of this measure. In the light of the presented practices it can be objected that decision concerning repointing of clay brick facades usually is not based on rational grounds.

In the present paper the results of a state-of-the-art study concerning field and laboratory methods to assess water content and water up-take caused by WDR are presented. Using information on water content and water up-take to rationally analyse whether repointing can improve the technical condition of clay brick facades in relation to WDR action is discussed and research and development needs are identified.

2 RESEARCH APPROACH

A literature review concerning repointing of clay brick façades has been carried out with keywords

including repointing, masonry, clay brick façade, masonry façade, brick masonry, mortar joints, mortar, environmental factors, wind-driven rain, impingement, water up-take, water penetration, moisture content, durability, erosion and deterioration. Other search terms include destructive and non-destructive tests, study of WDR, field, laboratory, etc. Main literature sources and databases include Lund University Library, National Library of Sweden including the libraries of all Swedish universities, ASCE Library, Engineering Village (Elsevier), Wiley Online Library. In addition to library searches, meetings with Swedish and German researchers and industry representatives provided additional sources of information.

3 RESULTS

3.1 *Tests measuring moisture content*

A number of non-destructive and destructive experimental procedures for assessing moisture conditions of brick facades have been reviewed based on previous research studies (Emerisda, 2014, Bison et al., 2011, Litti et al., 2015, Hola, 2017, Larsen, 2012). Experimental procedures can be categorized into three groups based on their destructiveness and their type of output. The groups are described as follows: *group A* - destructive tests (DT) measuring moisture content quantitatively; *group B* non-destructive tests (NDT) measuring moisture content quantitatively; and *group C* - NDT indicating moisture content qualitatively. The potential for making on-site measurements using each experimental procedure is also assessed.

Tests belonging to *group A* include, among others, gravimetric tests, the calcium carbide test and the chemical method (Karl Fisher). Although destructive tests are generally seldom carried out on historical buildings, there is no consensus whether or not they are appropriate for residential buildings.

Gravimetric testing involves sampling by core drilling, after which the samples are dried in an oven at a specified temperature. Finally, the actual moisture content (MC) is generally derived from the difference in weight of the sample before and after drying (Camuffo and Bertolin, 2012, EN, 1993). Gravimetric testing is considered being a precise and reliable method to measure moisture content in masonry walls; however, sampling by core drilling is perceived as a drawback.

The calcium carbide test involves grinding a sample from the masonry wall and mixing the powder with a certain amount of calcium carbide (Blystone et al., 1962, ASTM, 2011, Camuffo and Bertolin, 2012). Subsequently, the moisture content can be derived from the pressure of the gas released during the reaction between calcium carbide and water, by the use of a calibration curve (Binda et al., 1996). While the test is appropriate for on-site measurements, it is less reliable than the gravimetric test.

The chemical method, invented by Karl Fisher, is based on the reaction between iodine and water, producing a non-conductive chemical substance. It is possible to carry out titration on site to determine trace amounts of water in a sample. The capabilities of this test are measuring accurately small amounts of moisture and determining the water content level from low values till saturation (Schöffski, 2006, Bruttel and Schlink, 2003). However, it is stated that the chemical method would be helpful for small samples and not reliable for masonry walls (Hola et al., 2012).

Among tests belonging to *group B*, nuclear magnetic resonance (NMR) and neutron radiography are of special interest. *Nuclear magnetic resonance* (NMR) is a non-contacting, fast, accurate, and reliable technology to measure the water content in masonry walls and to evaluate the distribution of moisture content along the wall surface (Pel et al., 1996, Wolter and Krus, 2005, Litti et al., 2015). *Neutron radiography* records the radiation passing through an object by a position sensitive detector. Although both methods quantitatively and non-destructively measure the water content in walls, their high cost and limited availability (Hola, 2017) make their applicability to common buildings rather limited. They could, however, be employed under certain circumstances, such as for buildings with great cultural or economic values.

Tests in *group C* include, among others, the paper indicator method, infrared thermography (IRT), holographic radar and the dielectric and microwave methods. The *paper indicator* method is a simple and inexpensive method to qualitatively evaluate the moisture content in a masonry wall. In this test, contact between chemical papers and the moist surface of a facade provides indications of the moisture content based on the subsequent change in colour of the paper; similar to the litmus paper test for evaluating acidity (Hola, 2017).

IRT uses thermal imagery to map the location of damp areas and the existence of voids (Griffin, 2013), yet without the possibility of quantitative evaluation of the moisture content. This non-destructive test is carried out in-situ with at a relatively low cost. The time when the test can be performed is critical and limits its use, since it is strongly affected by environmental conditions [high relative humidity and low temperature] (Emerisda, 2014, Bison et al., 2011).

Holographic radar has the capability to detect moisture in the range of 50 to 200 mm beneath the surface as a function of continuous wave frequency (Litti et al., 2015, Bison et al., 2011). Also, detection of voids is possible. In contrast with IRT, the holographic radar technique is not influenced by relative humidity or air temperature (Litti et al., 2015).

The *dielectric* method works on the principle of variation of the dielectric constant of a material in the presence of water. The dielectric constant increases with increasing moisture content, making differences in moisture content detectable. This test is commonly employed by surveyors to determine the moisture distribution along the height of masonry walls. The method is, however, limited to depths of 50 to 100 mm (Hola, 2017). The *microwave* method is another non-destructive method which works on the principle of reduction of the radiation intensity as microwaves pass through a damp material (Hola, 2017). Thus, the more water the specimen contains, the bigger the energy loss. This method is procedurally similar to the dielectric one, however the microwave method can be used to depths up to 300 mm (Hola, 2017). The advantages of these two techniques are low cost of the equipment and ease of use (Emerisda, 2014, Hola, 2017).

The main features of the test methods described in this section are, together with methods to be described in section 3.2, summarized in Table 1.

3.2 *Tests measuring water absorption*

There are several quantitative methods available for measuring the amount of water being absorbed through a brick masonry wall. They are divided into two groups - *group D* comprising low-intrusive methods, while group E including NDT methods. Again, the potential for making on-site measurements using each experimental procedure is also assessed.

A newly developed, *group D* technique to measure water absorption is named Wasseraufnahme Messgerät – WAM (*Instrument for measurement of water up-take* – the author's translation), which measures water absorption in the absence of wind pressure (Möller and Stelzmann, 2013, Stelzmann et al., 2015). The apparatus includes a scale, a storage tank and a pipe with nozzles. The apparatus is attached to a section of the wall with the edges and sealed in order to create a closed system (Figure 1a). The apparatus then projects a water film on the entire section. Run-off water that is not absorbed is collected. The rate of absorption can be calculated and monitored in real time by continuously weighing the amount of moisture in the closed system. The apparatus is portable and can easily be used in-situ. If attached to the lower end of a wall, the apparatus can rest on the ground or alternatively on a small support. In order to test the upper parts of a wall, the apparatus needs to be attached by 8 screws, making it semi-intrusive (*group D*).

Among NDT methods (*group E*), the RILEM tube test, the Franke plate and the Stockbridge method are reviewed here. The *RILEM tube test* is widely used to quantify water absorption during a specified period of time through an up-take tube, with possible application in laboratory and on site (RILEM, 1978, Crissinger, 2005). The uptake tube is first sealed to the substrate with a putty and then filled with water. The amount of absorbed water is recorded during specified time intervals. This simple NDT test is helpful for assessing the water absorption rate before and after repointing. However, it only provides results for a small area of masonry wall and results are not precise when the tube is applied on mortar joints. In order to speed up the procedure, it is suggested to use several tubes in different locations (Figure 1.b).

The Franke-Platte method consists of a plate (25 cm × 8.1 cm absorption area) and a tube like the RILEM tube (Figure 1.c). The procedure is similar to the RILEM tube test with the exception that rather than attaching a tube to a small area, a plate is attached to an area including bricks and mortar

Table 1. Summary of test method features.

Test	Group	Destructiveness[1]	Output[2]	Application	On site
Gravimetric	A	De	QN	moisture content and its distribution	-
Calcium carbide	A	De	QN	moisture content	✓
Chemical method (Karl Fisher)	A	De	QN	moisture content indirectly	✓
Nuclear magnetic resonance (NMR)	B	N	QN	surface (flat) moisture content	✓
Neutron radiography	B	N	QN	moisture content	✓
Paper indicator method	C	N	QL	moisture content level	✓
Infrared thermography (IRT)	C	N	QL	surface moisture content	✓
Holographic radar	C	N	QL	moisture content (flat surface)	✓
Dielectric method	C	N	QL	moisture content	✓
Microwave method	C	N	QL	moisture content	✓
Wasseraufnahme Messgerät (WAM)	D	L	QN	water penetration	✓
RILEM tube test	E	N	QN	water penetration	✓
Franke-Platte	E	N	QN	water penetration	✓
Stockbridge (Stockbridge, 1989)	E	N	QN	water penetration	✓

1. De – destructive, N – non-destructive, and L – low intrusive
2. QL – qualitative and QN – quantitative

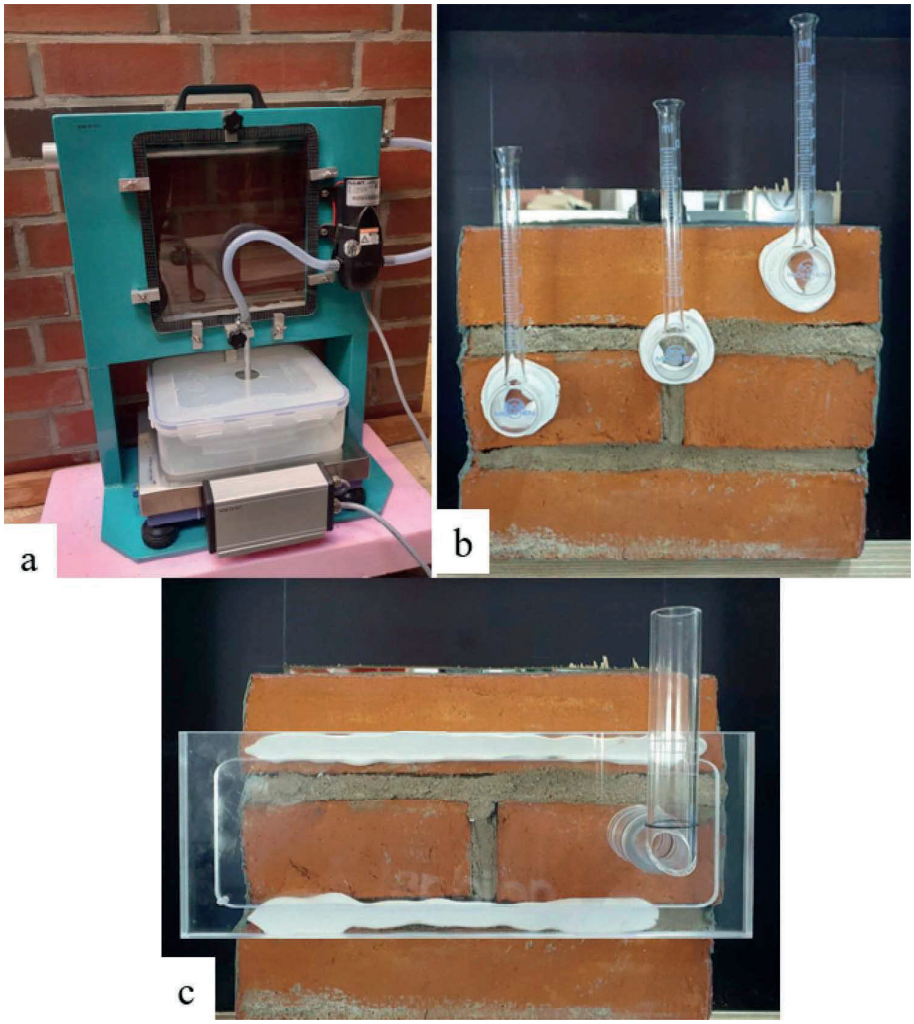

Figure 1. Apparatus and set-up of test methods measuring water absorption; (a) WAM Device, (b) RILEM tube test, (c) Franke Platte.

joints (Franke and Bentrup, 1991, Neumann et al., 2014, Stelzmann et al., 2015).

Stockbridge developed a watertight frame (91 × 122 cm area of the wall) to be attached to a masonry façade while measuring the water absorption (Stockbridge, 1989, ASTM, 2014), without refilling the absorbed water. It is recommended that if the rate of absorption is less than one litre per hour, no repointing is needed. Further, it is stated that if the absorption rate is larger than five litres per hour, repointing will result in a substantial decrease in water absorption. Unfortunately, it is not shown how these criteria have been established.

4 DISCUSSION AND STRATEGIES

The results presented in the previous section show that there are a couple of methods to assess moisture content and water absorption in clay brick facades. Each method is associated with costs related to investment in equipment and operation. Qualitative or quantitative information possible to obtain must be valued in relation to its usefulness. In the following sections a brief analysis and discussion are presented concerning circumstances when decision on repointing can be more rational by using information obtained by the presented methods.

4.1 *Preliminary investigations*

Prior to carrying out potentially costly and time-consuming experimental studies, either in laboratory or on-site, gathering basic information concerning the building, local climate and weather history can provide useful information such as:

- Age of the building; previous façade maintenance measures; type and/or brand of the bricks and of the mortar;
- Occupants' or building owners' reports on problems with dampness of external walls; dampness or discoloration of facades;
- Local climate data indicating temperature, precipitation, wind intensity and direction; current, reliable weather records.

Based on the above information, previous experience and knowledge of the performance of similar facades, a competent inspector might conclude whether increased dampness of facades and external walls depends on moisture and water absorption characteristics of the bricks and mortar, seasonal increase in WDR or recent heavy driving rain events. Further investigations might not be needed nor repointing.

A visual inspection can further shed light on the general condition of the façade, including moisture and moisture related aspects, by registering incidence of:

- Eroded mortar joints with respect to erosion depth and cracks;
- Damaged bricks with respect to spalling and cracks;
- Efflorescence, discoloration and microbiolo-gical growth.

Presence of eroded mortar joints indicate that climate actions have a tangible impact on the facade, a hypothesis that can be further underpinned if the incidence and degree of erosion is correlated with the exposure of the façade to WDR. Efflorescence, discolorations and microbiological growth concentrated to façade parties with eroded mortar joints might indicate that the erosion of the mortar joints constitute the root cause of these phenomena, making repointing, especially of the eroded parties, justifiable. Yet, there is a lack of knowledge concerning to what extent water absorption from WDR can be diminished by repointing.

4.2 *On-site and laboratory testing*

When preliminary examinations are considered inconclusive, on-site and laboratory testing of moisture content and water absorption might be justifiable. By taking into consideration benefits and drawbacks, one or more suitable test methods among those presented in *section 3* might be chosen.

Despite their high accuracy, the usability of Group A tests is somewhat limited, since they damage the examined buildings. Similarly, although the nuclear magnetic resonance (NMR) method can provide accurate results concerning moisture content, its high cost will limit its usage when it comes to common residential buildings. Thus, in most residential projects, NDT methods determining moisture content qualitatively (Group C) are recommended, though their accuracy is lower than that of other methods'.

Although high moisture content is not necessarily an indicator that repointing is needed, alteration of moisture content over time might indicate erosion of both mortar joints and of bricks. Thus, recurring measurements or continuous monitoring over time of moisture content of brick facades of high cultural or economic value might, in spite of high costs, be justifiable.

Methods measuring water absorption, named group D and E in this paper, can indicate the degree of erosion of different façade parties, since both larger, protrusive cracks and surfaces with micro-cracks are expected to absorb more water. Clay brick facades with eroded and recessed joints are further believed to absorb more water, yet, to the knowledge of the authors, no quantitative models have been established.

4.3 *Criteria for decision on repointing*

Qualitative and quantitative criteria concerning the need for repointing have been proposed by e.g. (Griffin, 2013, Tindall, 1987, Holland, 2012, Brief, 2005, Stockbridge, 1989), recommending repointing when a) the surface of the mortar joints contain hairline cracks, b) eroded mortar joints to a certain depth [a quarter of an inch, i.e. 6.4 mm] have been observed, c) high suction/retention mortar has been used, d) crack widths larger than 2 mm have been measured, e) the rate of water absorption is more than 4.5 litre/hour/m^2, or f) presence of voids has been detected, e.g. by means of the IRT test.

Considering the suitability of the mentioned criteria and that during repointing joints are generally raked out to approximately 25 mm or 2.5 times of the mortar joint thickness (Maurenbrecher et al., 2008, Young, 2015), it should be investigated to what extent high moisture content and water absorption are related to the condition of the outer part of the mortar joints and whether a repointing can make a difference. In this context, the relation between the depth of erosion of the mortar joints and the possible increase in water absorption from WDR should be quantified.

Furthermore, the rationality of some of the proposed criteria can be questioned, e.g. concerning acceptable crack width, since it has been shown that water ingress in cementitious materials increases exponentially when the crack width exceeds 0.2 mm (Wang et al., 1997, Aldea et al., 1999).

Eventually, possible benefits and drawbacks of other maintenance techniques rather than repointing

to restore the appearance and technical condition of a facade should be considered as well.

4.4 *Alternative maintenance techniques*

Cleaning and plant removal techniques can be used to postpone the need of costlier maintenance actions. Furthermore, their implementation may uncover potential hidden defects or problems.

Cleaning techniques can be categorized into three different groups: abrasive cleaning, chemical cleaning and water cleaning. Cleaning dirt, soil, stains and paints is not only a way to restore aesthetics of a facade; it is also a method to maintain the structure and postpone repointing (Mack and Grimmer, 2000). However, if inappropriate cleaning techniques are adopted, damage to the masonry facade may result. Generally, washing gently with low pressure water is a lenient cleaning technique. Application of mechanical or chemical cleaning is not recommended, particularly not in the case of historic façades, since it might damage the masonry surface.

Plant removal can even be considered as an alternative technique to repointing. The presence of biological growths like ivy, lichens, and mosses affect water penetration, water evaporation and drying process. As such, removing these growths will result in a reduced moisture content and potentially eliminate the need for repointing.

Superficial hairline cracks in mortar joints can be repaired by surface grouting. Texture, colour, and properties of the repair grout must be chosen to match the existing mortar. Bricks with larger cracks can be replaced.

High water content in combination with freeze-thaw cycles over the service life of the facade may cause spalling (with the brick face flaking and crumbling) due to the volume increase of water when it is freezing. Damaged bricks should be with new units with similar properties. However, to limit future damages, the root cause of high-water content has to be identified and dealt with appropriately, if possible.

Water-repellent (WR) coating has been considered as a technique to reduce water penetration (Brown, 1982, Coney and Stockbridge, 1988), although there is a debate about its efficiency. In some cases it has been argued that applying water repellents cannot protect the brick-mortar interfacial zone from water ingress (Slapø and AL, 2017).

5 CONCLUSIONS

To reach a rational decision concerning repointing, different methods to measure moisture content and water absorption in clay brick façades were discussed. A systematic review of the available techniques, as presented in this paper, might contribute to improve current recommendations with respect to maintenance of clay brick masonry facades. To sum up, a rational strategy including following steps can reveal the real need for repointing:

- Preliminary studies prior to conducting costly and time-consuming measurements might clarify whether repointing is needed.
- Measurements of moisture content and water absorption can deliver data for deeper analyses. In selecting the most appropriate measuring technique, the stakeholder should consider the purpose of the measurements and the value of the data.
- Non-destructive, qualitative and inexpensive measurement techniques such as the RILEM tube or the dielectric method may therefore be favourable over more complex ones.
- Criteria available in the literature, can be used, with due engineering judgement, to reach a rational decision on repointing.
- Other maintenance techniques such as removal of microbiological growth or cleaning by water, have the potential to reduce moisture content and water absorption into brick façades, and thus to postpone the need of more fundamental maintenance measures such as repointing.

ACKNOWLEDGMENTS

The authors gratefully acknowledge financial support from SBUF - The Development Fond of the Swedish Construction Trade (grant 13576) and TMPB - The Masonry and Render Construction Association.

REFERENCES

Aldea, C.-M., Shah, S. P. & Karr, A. 1999. Permeability of cracked concrete. *Materials and structures*, 32, 370–376.

ASTM 2011. Standard Test Method for Field Determination of Water (Moisture) Content of Soil by the Calcium Carbide Gas Pressure Tester, D4944-18. West Conshohocken, Pennsylvania: American Society for Testing and Materials.

ASTM 2014. Standard test method for field determination of water penetration of masonry wall surfaces, C1601-14a. West Conshohocken, PA: ASTM International.

Binda, L., Squarcina, T. & Van Hees, R. 1996. Determination of moisture content in masonry materials. Calibration of some direct methods.

Bison, P., Cadelano, G., Capineri, L., Capitani, D., Casellato, U., Faroldi, P., Grinzato, E., Ludwig, N., Olmi, R., Priori, S., Proietti, N., Rosina, E., Ruggeri, R., Sansonetti, A., Soroldoni, L. & Valentini, M. 2011. Limits and Advantages of Different Techniques for Testing Moisture Content in Masonry. *Materials Evaluation*, 69, 111–116.

Blystone, J., Pelzner, A. & Steffens, G. 1962. Moisture content determination by the calcium carbide gas pressure method. *Highway Research Board Bulletin*.

Brief, B. 2005. Repointing (Tuckpointing) Brick Masonry. *Brick Industry Association*.

Brief, B. 2017. Maintenance of Brick Masonry. *Brick Industry Association, Technical Notes on Brick Construction*, 46, 1–11.

Brown, R. H. 1982. Initial effects of clear coatings on water permeance of masonry. *Masonry*: *Materials*, *Properties, and Performance*. ASTM International.

Bruttel, P. & Schlink, R. 2003. Water determination by Karl Fischer titration. *Metrohm monograph*, 8, 50003.

Camuffo, D. & Bertolin, C. 2012. Towards standardisation of moisture content measurement in cultural heritage materials. *E-Preserv. Sci*, 9, 23–35.

Coney, W. B. & Stockbridge, J. G. 1988. The effectiveness of waterproofing coatings, surface grouting, and tuckpointing on a specific project. *Masonry*: *Materials, Design*, *Construction, and Maintenance*. ASTM International.

Crissinger, J. 2005. Measuring moisture resistance to wind-driven rain using a RILEM tube. Tech. Rep.

EMERISDA 2014. Summary report on existing techniques, procedures and criteria for assessment of effectiveness of interventions. TU Delft: Emerisda.

EN 1993. Wood-based panels – Determination of moisture content, 322. Brussels: European Committee for Standardisation (CEN TC 346).

Franke, L. & Bentrup, H. 1991. Einfluss von Rissen auf die Schlagregensicherheit von hydrophobiertem Mauerwerk und Prüfung der Hydrophobierbarkeit, Teil 2. *Bautenschutz Bausanierung*, 14, (117–121).

Fried, A., Tovey, A. & Roberts, J. 2014. *Concrete masonry designer's handbook*, CRC Press.

Griffin, I. M. 2013. *Deterioration mechanisms of historic cement renders and concrete*. Doctoral dissertation, University of Edinburgh.

Hola, A. Measuring of the moisture content in brick walls of historical buildings–the overview of methods. IOP Conference Series: Materials Science and Engineering, 2017. IOP Publishing, 012067.

Hola, J., Matkowski, Z., Schabowicz, K., Sikora, J., Nita, K. & Wójtowicz, S. 2012. Identification of moisture content in brick walls by means of impedance tomography. *COMPEL: Int J for Computation and Maths. in Electrical and Electronic Eng*., 31.

Holland, M. 2012. *Practical Guide to Diagnosing Structural Movement in Buildings*, John Wiley & Sons.

Larsen, P. K. 2012. Determination of Water Content in Brick Masonry Walls using a Dielectric Probe. *Journal of Architectural Conservation*, 18, 47–62.

Litti, G., Khoshdel, S., Audenaert, A. & Braet, J. 2015. Hygrothermal performance evaluation of traditional brick masonry in historic buildings. *Energy and Buildings*, 105, 393–411.

Mack, R. C. & Grimmer, A. E. 2000. Assessing cleaning and water-repellent treatments for historic masonry buildings. *Preservation briefs*.

Maurenbrecher, A. H. P., Trischuk, K., Rousseau, M. Z. & Subercaseaux, M. I. 2008. Repointing mortars for older masonry buildings: design considerations. *Construction Technology Update; no. 67*.

Möller, U. & Stelzmann, M. 2013. Neue Messmethode zur Bewertung der kapillaren Wasseraufnahme von Fassaden. *wksb*, 69, 62–65.

Neumann, H.-H., Niermann, M. & Steiger, M. 2014. *Methodenentwicklung zur zerstörungsfreien Prüfung des Wassertransportes für die Planung und zum Bautenschutz in historischem Ziegelmauerwerk bei dem Einsatz von Innenraumdämmungen: Abschlussbericht zu dem DBU-geförderten Vorhaben, Förderkennzeichen: 28751-45*, Universität Hamburg, Fachbereich Chemie, Anorganische und Angewandte Chemie.

Pel, L., Kopinga, K. & Brocken, H. 1996. Moisture transport in porous building materials. *Heron*, 41, 95–105.

RILEM, D. Protection of Stone Monuments. Experimental Methods. Test No. II. 4. Water absorption under low pressure (pipe method). International Symposium UNESCO-RILEM Paris, 1978.

Schöffski, K. S., D. 2006. Karl Fischer Moisture Determination. *Encyclopedia of Analytical Chemistry*.

Slapø, F. & Al, E. 2017. Masonry's Resistance to Driving Rain: Mortar Water Content and Impregnation. *Buildings*, 7, 70.

Stelzmann, M., Möller, U. & Plagge, R. 2015. Waterabsorption-measurement instrument for masonry façades. *ETNDT6, Emerging Technologies in Non-Destructive Testing*, 6, 27–29.

Stockbridge, J. G. 1989. Repointing masonry walls. *APT bulletin*, 21, 10–12.

Tägil, T., Gustavsson, T., Bergkvist, K. & Staaf, B. M. 2011. *Modernismens tegelfasader (The clay brick facades of the Modernism) in Swedish*, Arkus Publication.

Tindall, S. M. 1987. Repointing Masonry—Why Repoint? *Old-House Journal*, 24–31.

Wang, K., Jansen, D. C., Shah, S. P. & Karr, A. F. 1997. Permeability study of cracked concrete. *Cement and concrete research*, 27, 381–393.

Wolter, B. & Krus, M. 2005. Moisture Measuring with Nuclear Magnetic Resonance (NMR). *In:* KUPFER, K. (ed.) *Electromagnetic Aquametry: Electromagnetic Wave Interaction with Water and Moist Substances*. Berlin, Heidelberg: Springer Berlin Heidelberg.

Young, D. Repointing mortar joints: some important points. Australia ICOMOS Conference, 5-8 November 2015 Adelaide Australia.

Paper II

Journal of Building Engineering 43 (2021) 102583

Contents lists available at ScienceDirect

Journal of Building Engineering

journal homepage: www.elsevier.com/locate/jobe

Experimental investigation of water absorption and penetration in clay brick masonry under simulated uniform water spray exposure

Seyedmohammad Kahangi Shahreza *, Jonas Niklewski, Miklós Molnár

Division of Structural Engineering, Department of Building and Environmental Technology, Lund University, John Ericssons Väg 1, SE-223 63, Lund, Sweden

ARTICLE INFO

Keywords:
Clay brick masonry
Wind-driven rain
Water absorption
Dampness
Water penetration
Mortar joint profile

ABSTRACT

In this study, we performed an experimental investigation of water absorption and penetration in clay brick masonry exposed to cyclic water spraying by employing a newly developed test setup. Several parameters, including brick absorption properties and different mortar joint profiles, were investigated. The specimens were exposed to a uniform water spray rate ranging between 1.7 and 3.8 l/m^2/h, and water absorption and dampness patches on the non-exposed backside (the protected side) of the specimens monitored continuously. The results indicate that the amount of absorbed water is highly dependent on the water absorption coefficient and absorption capacity of the bricks, whereas the mortar joint profiles do not influence water absorption. The first dampness patches on the specimens' backside appeared in the vicinity of the head joint, and the time until the first patch appeared correlated well with water content levels. Accordingly, the first visible dampness patches appeared on the specimens' backside at water content levels corresponding to 50%–60% of full saturation level. Additionally, the specimens' backside reached 90% dampness at water content levels corresponding to 95% of full saturation level. As a feature attributed to the absence of known defects and zero differential air pressure, no measurable amounts of penetrated water could be collected at the specimens' backside. The newly developed test setup might facilitate verification of moisture simulations and provide a basis for rational decision-making concerning clay brick masonry design and maintenance.

1. Introduction

Clay brick masonry façades are widely used in Nordic countries because of their durability and a lowered need for costly maintenance. Nevertheless, exposure to wind-driven rain (WDR) may cause moisture accumulation and water penetration [1–3], that is, conditions that have the potential to deteriorate both the masonry itself and other wall components in exterior walls [4–6]. WDR might further cause erosion of the joints in clay brick masonry [7,8], thus impairing the aesthetics of façades. Currently, there is a widespread perception among practitioners that eroded mortar joints cause increased water uptake from WDR, a perception that is used as motivation for repointing. Yet, there is a divergence in experts' views on this question [9,10]. Accordingly, studying water absorption and water penetration in clay brick masonry with mortar joint profiles resembling eroded mortar joints might create rational decision support concerning repointing.

Generally, WDR studies can be divided into two categories: i) quantification of WDR deposition on façades, with rain intensity, raindrop size, wind speed, building geometry, and the topography of the surrounding terrain as important parameters [11–14]; and ii) the response of façades to WDR impingement in relation to, for example, splashing, bouncing, runoff, differential air pressure, material properties, and presence of cracks and voids [15,16].

During WDR events, the outer surface of masonry façades absorbs parts of the incident rainwater, dependent on the capillary absorption properties of units and mortar, until capillary saturation is attained. Once the exposed surface is saturated, a water film is formed on the exposed surface. When cracks and voids are present, large amounts of water may penetrate through the masonry [17–19]; in such instances, wind pressure is a significant agent that promotes water penetration.

Formation of a water film on the façade surface and subsequent water penetration due to wind pressure is the basis for many established test setups used in experimental studies of WDR penetration in walls [17,20–22]. In the test setups of the earliest studies on water penetration in brick masonry [17,20,22–24], which then became the basis of many of the current testing standards, water was sprayed with the aid of a pipe placed near the upper edge of specimens and the surface of specimens kept covered with a water film. Although various test setups for

* Corresponding author.
E-mail addresses: mohammad.kahangi@kstr.lth.se (S. Kahangi Shahreza), jonas.niklewski@kstr.lth.se (J. Niklewski), miklos.molnar@kstr.lth.se (M. Molnár).

https://doi.org/10.1016/j.jobe.2021.102583
Received 10 December 2020; Received in revised form 14 April 2021; Accepted 17 April 2021
Available online 24 April 2021

exploring water penetration in masonry have been proposed in different standards and research studies, the applied water spray and air pressure rates represent rather extreme WDR conditions [20,25–34]. For instance, water application rates of 72–138 l/m^2/h [25–27,29,31–33,35–37] in combination with differential air pressure levels of 400–1000 Pa [25–27,31,35,38] represent extreme driving rain conditions [22,23], most probably relevant for tall buildings. Hence, several authors have pointed out the need to develop a simple test setup able to operate at considerably lower water application rates [25,28,39–41].

Accordingly, Forghani et al. [37] adjusted the differential air pressure of 500 Pa in the ASTM E514 [31] to 45 Pa. Further, tests with differential air pressure in the range of 0–750 Pa were carried out in studies conducted by Slapø et al. [26], Anand et al. [29], and Lacasse et al. [42]. In experimental studies carried out by Rathbone [43] and Hens et al. [44], clay brick masonry walls were subjected to water spray rates between 2.0 and 6.4 l/m^2/h. Although Rathbone [43] and Hens et al. [44] reduced the water spray rates by 95% in comparison with the ASTM E514 standard [31], still the method to spray water was similar to the one applied in ASTM E514 [31], i.e. concentrated to a line close to the specimens' top aiming to create a water film on the exposed surface.

To overcome shortcomings highlighted with water penetration methods used in ASTM E514 [31], we have developed a new test method for producing a uniform water spray exposure in this study. The test setup is adapted to simulate exposure to a wide range of WDR intensities. The mass gain—that is, the amount of absorbed water by the test specimens—is measured continuously throughout the test, and water penetration through clay brick masonry specimens is studied by employing a digital camera to record when and where visible dampness patches appear and how they spread on specimens' backside. Thus, the present study diverges from existing studies investigating water penetration and dampness on the backside, the protected side, of masonry walls, exposed to extreme conditions [9,25,26,31], facilitating acquisition of information about the moisture conditions and water accumulation in masonry.

The experimental campaign included two series of clay brick masonry specimens, prepared with two different types of bricks and two different mortar joint profiles, namely raked and flush. Raked specimens were used to gain knowledge on how WDR related water absorption and penetration might be affected in eroded mortar joints. Flush profiles were subdivided into standard and after-pointed. After-pointing is a common technique in Nordic countries in which the joints are filled with mortar; then, prior to hardening of the mortar, the outer part is removed; and the day after bricklaying, the remained part is finally filled with mortar and tooled. The tests were conducted at zero differential air pressure, at water spray rates varying between 1.7 and 3.8 l/m^2/h, approximately 95% lower than the water application rate specified in current standards and many studies [25,27,29,31,35,37].

2. Materials and methods

2.1. Test setup

In this study, a test setup was designed to expose brick masonry specimens to water spraying, simulating WDR. A uniform and well-distributed water spraying pattern was achieved using a low flow, full cone BETE WL nozzle (WL – 1/4, Full Cone, and 90° Spray Angle), creating a conical spray pattern with droplets, which was placed 55 cm away from the specimens' surface. The schematic of the test setup is shown in Fig. 1. Moreover, two pressure regulators were mounted in series to minimize fluctuations stemming from pressure variations in the urban water supply. An IFM SM4000 electronic magnetic-inductive water flow meter was also used to continuously monitor the output flow for further corrections. The tests were performed with zero differential air pressure between the specimens' exposed side (the front side) and protected side (the backside) with a water application rate varying between 1.7 and 3.8 l/m^2/h, representing WDR intensities frequently encountered in Sweden, see Fig. A.1. Significant efforts have been made to reduce the water application rate to the mentioned interval, which indicates that using larger water application rates poses no difficulties.

The tests were carried out with zero differential air pressure because high wind speeds usually occur only for a small percentage of rain duration, whereas in this study, the specimens were subjected to water spraying for 21 h.

Each test lasted 23 h, divided into six cycles, with each cycle consisting of 210 min of watering and 20 min of pausing. The specimens' front face, the exposed side, was carefully centered within the test apparatus to be uniformly covered by water droplets. To this end, first, a sealing tape was applied on the scale plate to avoid any undesired water accumulation under the specimens, and the specimens were then placed on the sealing tape. A DINI ARGEO digital scale 30 kg/2 g was used for continuous logging of the weight of the specimens. Although the weighing of specimens is usually done before and after the test in other studies [26], the possibility to measure it continuously during the test was considered in the modified test setup. Additionally, a digital camera was placed behind the specimens to take photos every 2 min, resulting in time-lapse videos. Hence, the time and location of the first visible dampness patch appearing on the backside of specimens were recorded as well as the spatial distribution and spread of subsequent patches.

2.1.1. Image processing

A GoPro HERO8 Black digital camera with a 12-megapixel sensor recorded the backside of the specimens every 2 min; its position was fixed, and a ColorChecker was placed next to the masonry specimen. The first recorded image was used as a reference image, and each subsequent image was compared with it to detect dampness patches. The image analysis was performed in MATLAB (R2019a) using the following procedure. As slight changes in illumination occurred, the ColorChecker was used for color correction. Any displacement between the two images—owing to, for example, vibrations causing unintended camera

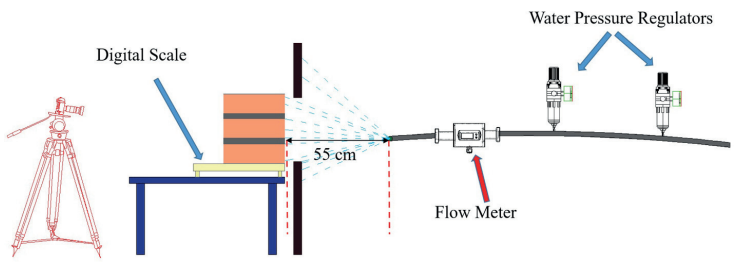

Fig. 1. Schematic of the test setup.

movement—was corrected using image cross-correlation. The difference between each image and the reference image was then calculated as the squared sum of the difference in each color channel (R, G, and B). The resulting image, representing the change in color from the initial state, was then thresholded with a fixed value. Finally, the resulting binary image was subjected to a morphological filter to reduce any residual noise. The relative damp area could then be calculated in each time step as the sum of white pixels divided by the sum of pixels within the area confined by the specimen edges. The algorithm used for the analysis was designed to ignore any patches originating from the specimen boundary, which occurred in some instances.

2.2. Materials

Units and mortars selected in this study are representative of that used in typical Swedish brick masonry façades. Two types of bricks, based on their absorption properties, and two different types of mortars, namely M 2.5 and natural hydraulic lime (NHL) 3.5 mortar, were used in the experimental campaign. The bricks, type Röd Slät and Röd Marktegel, are Haga red solid clay bricks from Wienerberger AB. Mortar M 2.5 is a cement-based mortar typically used for bricklaying in Northern Europe, whereas NHL 3.5 mortar is recommended for repointing clay brick façades with high and medium suction bricks. Ready-mixed mortars M 2.5 and NHL 3.5 were supplied from Weber Saint-Gobain AB and Målarkalk, respectively.

In the following sections, the water absorption properties of both bricks and mortars are presented.

2.2.1. Bricks

In total, 40 bricks (20 bricks of each kind) were used to determine their initial rate of absorption (IRA) and 24-h water absorption properties. Tests to determine the IRA and water absorption properties of bricks were performed as described in the ASTM C67 standard [45].

The average IRA of type I bricks, amounting to 1.95 kg/m^2, is 7.7% higher than the average IRA of type II bricks, which amounts to 1.81 kg/m^2. Therefore, both types of bricks can be classified as medium suction bricks. Nevertheless, the average 24-h water absorption of type I bricks is 86% larger than that of type II bricks (Table 1). The IRA represents the surface absorption rate when the brick just contacts water, whereas the 24-h water absorption represents the amount of water that a brick can absorb when fully immersed in water, here expressed as the ratio between the absorbed water and the initial weight.

Moreover, to determine the water absorption coefficient A_w, 10 bricks from each type were studied. In this regard, the bricks were immersed in water at a depth of 3–5 mm for a specific period of time, as described in the ASTM C1403 – 15 standard [46]. The increase in mass as a result of water absorption was registered after 1, 5, 10, 20, 30, 60, 120, 180, 240, 300, 360, 1440, and 4320 min. The amount of absorbed water per unit area of the brick Q [kg/m^2] is defined as the ratio between the difference of increased weight (w_i [kg]) and initial weight (w_0 [kg]) and the cross-sectional area of the brick A [m^2] (Eq. (1)).

$$Q = \frac{w_i - w_0}{A} \; [kg / m^2] \tag{1}$$

To present the results of the tests, Q [kg/m^2] is plotted against the square root of time [s$^{1/2}$] (Fig. 2.a). Eventually, the water absorption coefficient A_w [kg/(m^2.s$^{0.5}$)] is mathematically defined as the tangent to the initial, linear branch of the Q – t$^{1/2}$ function (Fig. 2.b).

The IRA, 24-h cold-water absorption, and water absorption coefficient of bricks type I and II are summarized in Table 1. For simplicity and according to the IRA test values, in the following sections, brick types I and II are considered medium suction brick [I] and [II], respectively. Although both types of bricks were classified as medium suction bricks according to their IRA value, the difference in the 24-h absorption and water absorption coefficient results is notable.

2.2.2. Mortars

A total of 15, 100 mm-side cubic mortar specimens, 12 M 2.5, and 3 NHL 3.5, were cast to determine the water absorption coefficient of the respective mortar types. The same preconditioning and test method used

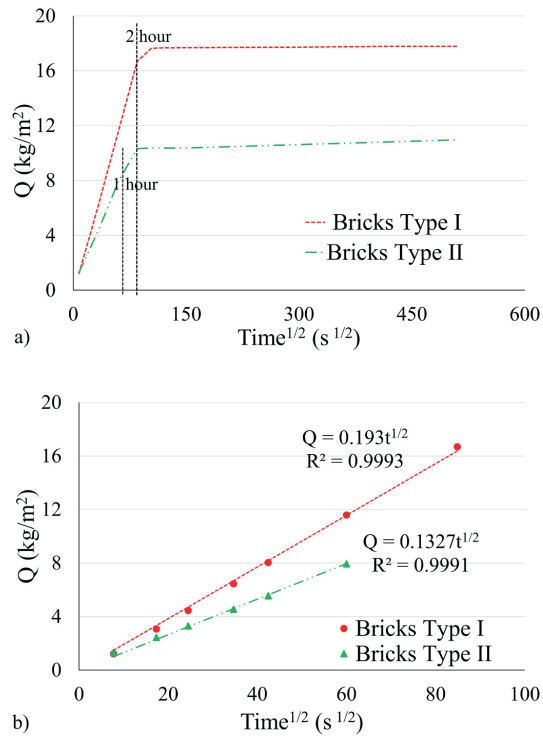

Fig. 2. Plot of water absorption per unit area against the square root of time for 10 masonry brick units from each type (bricks type I & II): a) up to 72 h; and b) during the initial stage of the test.

Table 1
Density and average water absorption properties, including initial rate of absorption, 24-h absorption, and water absorption coefficient of bricks and mortars.

	Dimensions (mm × mm × mm)	Density ρ (kg/m^3)	Average IRA (kg/m^2/min)	CoV (%)	Average 24-h water absorption (%)	CoV (%)	Average water absorption coefficient A_w (kg/(m^2.s$^{0.5}$))	CoV (%)
Bricks I	252 × 120 × 62	1800	1.95	2.3	16.0	1.6	0.193	0.8
Bricks II	252 × 120 × 62	1990	1.81	5.1	8.6	14.5	0.133	16.1
M 2.5	100 × 100 × 100	1869	0.30	19.7	–	–	0.022	19.7
NHL 3.5	100 × 100 × 100	1715	0.80	20.4	–	–	0.159	20.4

to determine the water absorption coefficient of the bricks was performed for the cubic mortar specimens, as described in the ASTM C1403 – 15 standard [46]. Fig. 3 shows the water absorption rate of the mortars over the square root of time, and Table 1 summarizes the average results of the IRA and water absorption coefficient properties of two different types of mortar.

2.3. Masonry specimens

This experimental work focused on studying water absorption and penetration in brick masonry specimens as a function of (i) the brick type (medium suction [I], medium suction [II]), and (ii) the mortar joint profile finish (flush, raked, after-pointed). A total of 39 triplet masonry specimens were built from the same batch of brick. The specimens were intended to be representative of a masonry veneer wall. The sample size is limited to three bricks in order to facilitate manual handling without damaging either the specimens or the operator. A similar choice was made by Ritchie [20], who studied water penetration in brick masonry by using specimens consisting of five bricks yet without any head joints. As shown in Fig. 4, the masonry specimens consisted of three courses of brick, with the length of one brick and the depth of half brick. The thickness of the bed joints varied between 13 and 18 mm to achieve a fixed height of 215 ± 3 mm for all specimens. The length and depth of the specimens were 250 ± 5 mm and 120 ± 2 mm, respectively.

The specimens are divided into two series based on the brick types (Table 2). Series I, which included 15 specimens, was built with bricks type I (medium suction bricks [I]), whereas Series II comprised 24 specimens built with bricks type II (medium suction bricks [II]).

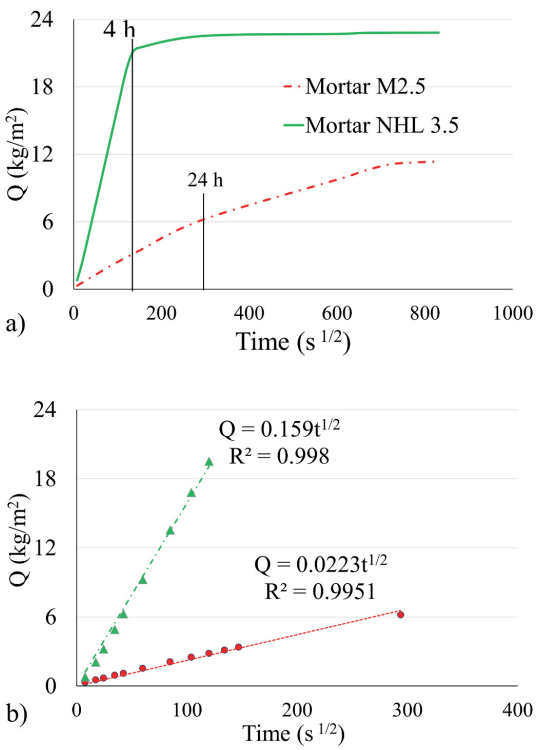

Fig. 3. Average absorption of mortar M 2.5 and NHL 3.5: a) up to 8 days; and b) during the initial stage of the test.

Additionally, specimens within each series were divided into three groups, namely G1, G2, and G3, according to the mortar joint finish (Table 2). Group G1 comprises specimens pointed with mortar M 2.5 and tooled to have a flush joint profile. Specimens with a 5 mm raked joint pointing with mortar M 2.5 belong to group G2. Group G3 is also made up of specimens with mortar M 2.5, but compared with G1, the outer 6 mm of the mortar joint was pointed one day after bricklaying with mortar NHL 3.5 and tooled to flush joint profile. A schematic of the prepared specimens and joint profile finishes is shown in Fig. 4.

The specimens are named according to the notation X-Y-Z, where X, Y, and Z correspond to the brick type (I = medium suction [I], II = medium suction [II]), mortar joint profile finishes (F = flush, R = raked, and AF = after-pointed), and specimen number, respectively. For example, specimen I-R-2 belongs to Series I, was built with medium suction bricks [I], with a 5 mm raked joint, and it is the second specimen of group G2.

Before bricklaying, all bricks were stored for three weeks in a laboratory with a controlled indoor climate (18–20 °C and 30–35% RH). To follow the recommendations of the brick manufacturer, the specimens were prepared without pre-wetting of the bricks before bricklaying. Each mortar mix was prepared with the same amount of water. Specimens of group G1, with mortar M 2.5, were tooled professionally to have a flush profile. For specimens with the raked joint profile, group G2, the specimens were pointed with mortar M 2.5, and then a 5 mm screw was used to remove extra mortar to reach the depth of 5 mm. For specimens prepared with the after-pointing technique, the excess mortar was removed using a 6 mm screw, and the following day, the 6 mm gap was filled with NHL 3.5 and tooled to have a flush joint profile. Finally, all specimens were cured for 28 days by daily wetting and storage under plastic sheets.

Testing took place three months after the bricklaying. Prior to testing, the specimens were stored in a climate room for two months at a temperature of 20 °C and relative humidity of 60%. All sides of the specimens, except front and back sides, were sealed to avoid any undesirable water absorption/evaporation through the top, bottom, and lateral sides. A two-component sealant composed of a base component and activator component, typically used for waterproofing applications, was employed.

2.4. Testing regime

As shown in Table 2, specimens in groups G1, G2, and G3 of Series I were exposed to an average water spraying rate of 3.6, 3.6, and 3.4 l/m^2/h, respectively. Specimens of group G1 of Series II are divided into two groups, G1-a and G1-b, based on the average water application rate. In this regard, the average water spraying rate for groups G1-a, G1-b, G2, and G3 of Series II was 3.2, 2.0, 2.3, and 2.0 l/m^2/h, respectively.

3. Results

3.1. Water absorption time response

The average amount of absorbed water Q (kg/m^2) for all groups in Series I and II during 23 h of testing is presented in Fig. 5a and Fig. 5b. In order to better compare the water spraying tests and the water absorption tests for bricks and mortars (Figs. 2 and 3), Q is plotted against the square root of time ($t^{1/2}$). It should further be kept in mind that the specimens in Series I and Series II Group G1-a were exposed to a more intensive spray rate (3.0–3.8 l/m^2/h) than the specimens in Series II Group G1-b, G2, and G3 (1.7–2.6 l/m^2/h).

As shown in Fig. 5a, the absorption behavior of Series II group G1-a is similar to those of Series I during the first cycle, indicating that most of the sprayed water was absorbed, no matter what the absorption properties of bricks were. Similarly, the absorption behavior of group G1-b, G2, G3 during the first cycle is similar to each other (Fig. 5.b), indicating that in this case, the water spray rate is the governing agent influencing

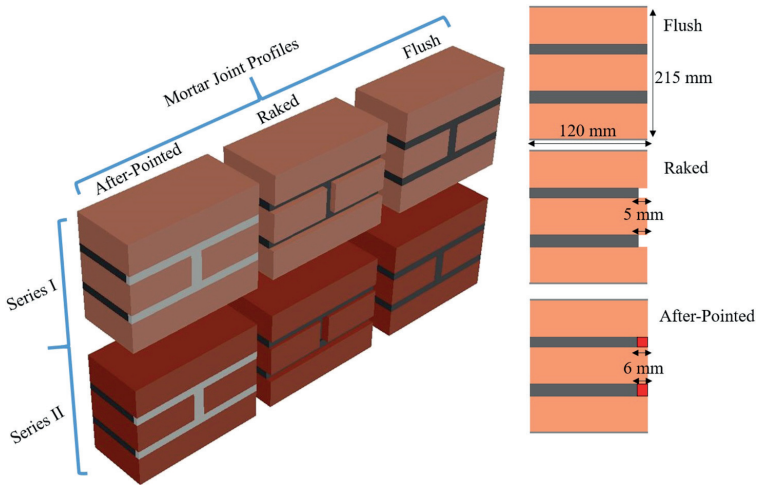

Fig. 4. Schematic of the specimens and mortar joint profile finishes.

Table 2
Specimen designation and configurations.

	Group	Brick	Mortar	Joint profile finishes	No. of specimens	Water spray rate (l/m^2/h)
Series I (250 mm × 215 mm × 120 mm)	G1 G2 G3	Medium Suction Type (I)	M 2.5 M 2.5 M 2.5/ NHL 3.5	Flush Raked After-pointed	5 5 5	3.6 3.6 3.4
Series II (250 mm × 215 mm × 120 mm)	G1-a G1-b G2 G3	Medium Suction Type (II)	M 2.5 M 2.5 M 2.5 M 2.5/ NHL 3.5	Flush Flush Raked After-pointed	5 3 8 8	3.2 2.0 2.3 2.0

the amount of absorbed water. Accordingly, the slight difference in the amount of absorption after the 1st cycle is due to the difference in the water spray rate; Series II group G2 was exposed to a higher water spray rate in comparison with group G1-b and G3.

After performing the 1st cycle, the absorption response versus the square root of time became linear. The linearity of the Q – $t^{1/2}$ relationship indicates that the capacity of the specimens to absorb water was in balance with the water supplied to the surface. Subsequently, once surface saturation occurred, the absorption behavior against the square root of time became nonlinear. Surface saturation was attained at the end of the 3rd cycle for all groups of Series I and II, except Series II group G1-a in which the absorption curve became nonlinear at the end of the 2nd cycle. It can be seen that surface saturation was attained more quickly in group G1-a of Series II, exposed to a water spray rate close to those of all groups within Series I, indicating that a higher water absorption coefficient allows rapid moisture transport and postpones saturation of the exposed masonry surface layer, as stated by Van Den Bossche et al. [41].

Moreover, it can be seen that for the specimens in Series I, absorption continues until the middle of the sixth cycle. From the middle of the sixth cycle (21 h after starting the test), roughly no water is absorbed in

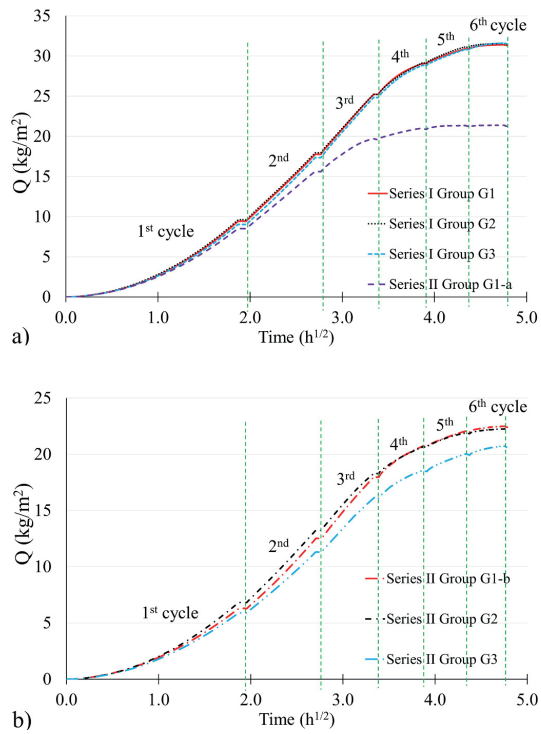

Fig. 5. Average water absorption vs. square root of time response of a) Series I and Series II group G1-a; b) Series II group G1-b, G2, and G3.

the specimens, indicating that they are close to full saturation. At the same time, for specimens of group G1-a in Series II, saturation took place at the beginning of the fifth cycle, indicated by the slope of the Q – $t^{1/2}$ curve becoming close to zero (i.e., nearly no water accumulation in the

specimens) during the remainder of the test. In contrast, for specimens of groups G1-b, G2, and G3 of Series II, the absorption did not end, indicating that the specimens did not attain full saturation, a fact mainly attributed to the relatively low water spray rate. Since saturation of the mortar used in the joint takes more than 23 h, see Fig. 3.a, it seems reasonable that neither Series I nor Series II achieve full saturation during the 23 h long water spraying tests.

For each specimen, the water application rate and water absorption after the first and the sixth cycle are summarized in Table 3. Results indicate that the water absorption in the first cycle is dependent on the water spray rate. For instance, in Series II, the lowest average water absorption, amounting to 5.9 kg/m^2, is exhibited by group G3, exposed to the lowest average water application rate of 2.0 l/m^2/h. Similarly, group G1-a, which was exposed to the highest average water application rate of 3.2 l/m^2/h, has the highest average water absorption of 8.5 kg/m^2 in Series II. Fig. 6 shows the water absorption in each specimen after the first cycle as a function of the corresponding water application rate V_0 (l/m^2/h). As surface saturation was not attained in the first cycle and the specimens absorbed most of the sprayed water, there is a nearly linear relationship between water application rate and water absorption. Furthermore, from Fig. 6 it can be observed that the rate of water absorption decreases with increasing water application rate, which indicates that bounce off increases with increasing water application rates, as already noted by Van Den Bossche et al. [41] and Abuku et al. [47].

Eventually, as the test progressed and the surface of the specimens became saturated, the results indicate that the water absorption was decreasingly influenced by the water application rate. Consequently, the amount of absorbed water at the end of the test is mostly correlated to the absorption capacity of the masonry. Accordingly, for Series I, it can be observed that after the sixth cycle, there is a negligible difference in the average water absorption between groups G1, G2, and G3, as the average water absorption for all three groups is approximately equal to 31.5 kg/m^2. In contrast, in Series II, the average water absorption varies between 20.6 and 22.4 kg/m^2, mainly attributed to a higher variability in the water absorption capacity of these bricks, 14.5%, versus 1.6% for Series I bricks.

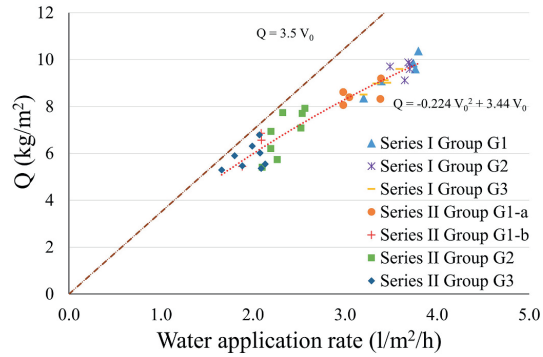

Fig. 6. Water absorption in the first cycle vs. water application rate, V_0.

Fig. 7 shows the average amount of absorbed water after each cycle

Table 3
Water absorption of tested specimens after the first and sixth cycle.

	Specimens	Initial Weight (g)	Water spray rate (l/m^2/h)	Average (l/m^2/h)	First cycle Absorp. (kg/m^2)	Average (kg/m^2)	Total Absorp. (kg/m^2)	Average (kg/m^2)	CoV (%)
Series I Group G1	I–F-1	11700	3.8	3.6	10.4	9.4	31.6	31.3	0.6
	I–F-2	11722	3.8		9.6		31.1		
	I–F-3	11434	3.7		9.8		31.2		
	I–F-4	11656	3.2		8.4		31.4		
	I–F-5	11694	3.4		9.1		31.3		
Series I Group G2	I-R-1	11672	3.7	3.6	9.6	9.6	31.4	31.5	0.3
	I-R-2	11586	3.7		9.8		31.5		
	I-R-3	11622	3.6		9.1		31.3		
	I-R-4	11588	3.5		9.7		31.7		
	I-R-5	11668	3.7		9.9		31.4		
Series I Group G3	I-AF-1	11756	3.6	3.4	9.6	9.0	31.6	31.5	0.2
	I-AF-2	11598	3.4		9.1		31.6		
	I-AF-3	11552	3.5		9.0		31.4		
	I-AF-4	11634	3.3		9.0		31.5		
	I-AF-5	11738	3.2		8.5		31.5		
Series II Group G1-a	II-F-1	12664	3.4	3.2	9.2	8.5	21.5	21.2	10.4
	II-F-2	12623	3.4		8.3		18.3		
	II-F-3	12591	3.0		8.4		23.2		
	II-F-4	12684	3.0		8.6		24.0		
	II-F-5	12468	3.0		8.1		19.2		
Series II Group G1-b	II-F-6	12684	1.9	2.0	5.4	6.3	21.3	22.4	6.3
	II-F-7	12637	2.1		6.9		24.4		
	II-F-8	12669	2.1		6.6		21.5		
Series II Group G2	II-R-1	12762	2.1	2.3	5.4	6.8	24.0	22.2	6.0
	II-R-2	12575	2.5		7.1		20.1		
	II-R-3	12628	2.5		7.7		22.3		
	II-R-4	12762	2.6		7.9		21.3		
	II-R-5	12624	2.3		7.7		24.0		
	II-R-6	12649	2.2		6.9		22.6		
	II-R-7	12609	2.2		6.2		20.9		
	II-R-8	12665	2.3		5.7		22.3		
Series II Group G3	II-AF-1	12598	1.9	2.0	5.5	5.9	20.6	20.6	5.6
	II-AF-2	12995	2.1		5.5		20.4		
	II-AF-3	12697	2.1		6.0		19.6		
	II-AF-4	12669	2.1		6.8		21.1		
	II-AF-5	12712	2.0		6.3		20.4		
	II-AF-6	12599	2.1		5.4		19.7		
	II-AF-7	12745	1.8		5.9		23.4		
	II-AF-8	12669	1.7		5.3		19.6		

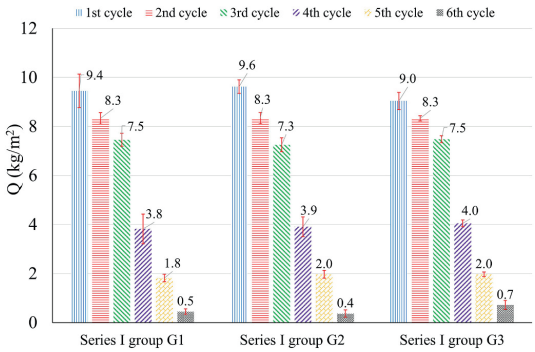

Fig. 7. Effects of the joint finishes (G1, G2, and G3) on the average water absorption in Series I.

for each group of Series I. The average water absorption after each cycle is of similar magnitude, irrespectively, of the mortar profile finish, as shown in Fig. 7. This indicates that mortar joint profile finishes have a negligible effect on water absorption.

3.2. Dampness patches

Since no water runoff that could be collected from the backside of the specimens was observed during the tests, only dampness on the backside of the specimens is reported. As mentioned in Section 2.1.1, a digital camera taking photos every second minute was employed to monitor the specimens' backside. The images were post-processed to identify the time and location of the first dampness patch and used to trace the spread of dampness until the end of the test. Fig. 8 shows the relative location of the first dampness patch in the x and y directions projected on the image of a single specimen to visualize the geometry. The exact geometry and location of the head joint were subject to some variation between specimens, which explains the scatter in the x-direction.

The high concentration of points around the head joint (position w/2) shows that the first visible dampness patch consistently appeared on the bricks in the second course, close to the head joint.

The appearance of the first visible dampness patch in the vicinity of the head joint could be related to the poor compaction of the head joint, difficulty in filling the head joint adequately [17], and open brick-mortar interfaces [25].

The first dampness patch appeared on the bricks in the second course, close to the brick-mortar interface zone, and then typically spread on the entire second course, including the head joint, see Fig. 9. Appearance of the first dampness patches in the vicinity of the head joint indicates that besides capillary transport through the pore system of the bricks, moisture might have also been transported by a system of gaps at the brick–head joint interface [25]. Subsequently, the bottommost course became damp. The dampness eventually spread to the uppermost course until the entire protected side of the specimen became damp.

The time to appearance of the first visible dampness patch on the backside of specimens is summarized in Table 4. The first dampness patch appeared after 7.8–8.0 h in Series I and 4.8–6.4 h in Series II. The time to the appearance of the first visible dampness patch on the backside of the specimens and the corresponding water application rate is shown in Fig. 10.

As shown in Fig. 10, a higher water application rate corresponds to a shorter time to the appearance of the first visible dampness patch on the protected side of the specimens. Furthermore, time to the appearance of the first visible dampness patch is not only dependent on the water application rate but also is influenced by the specimens' water absorption properties. Accordingly, when specimens are exposed to similar water spray rates, the time to the appearance of the first visible dampness patch is longer for specimens with high water absorption capacity (Series I, made of bricks with an average absorption capacity of 16%) than for specimens with medium water absorption capacity (Series II, group G1-a, made of bricks with an average water absorption capacity of 8.6%). Higher water absorption capacity seems to delay the time to appearance of dampness patches on the protected side.

The time to achieving 90% of the specimens' backside covered with dampness patches is reported in Table 4. The average time to reach 90% dampness coverage on the backside of specimens was 16.0, 16.3, and 16.8 h for groups G1, G2, and G3 of Series I, respectively. For groups G1-a, G1-b, G2, and G3 of Series II, it took 12.5, 16.5, 15.3, and 17.2 h, respectively. Thus, the water application rate affected not only the time to the appearance of the first visible dampness patch but also the time to reach 90% of dampness on the specimens' backside.

Besides the water application rate, the appearance of dampness patches is also influenced by the water content in the specimens. As shown in Fig. 11.a, the first dampness patch appeared at a water

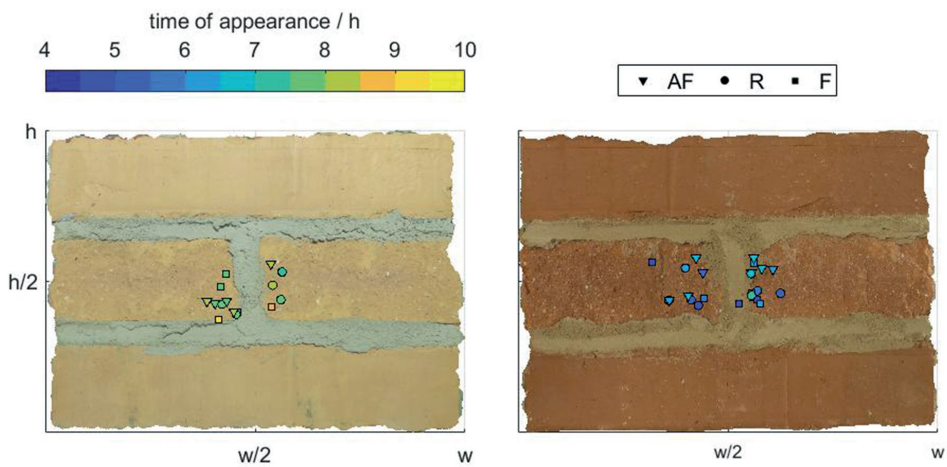

Fig. 8. Location of the first visible dampness patch on the backside of the specimens: a) Series I; and b) Series II.

Fig. 9. Dampness appearance and growth on the backside of specimen II-F-6 at different time intervals.

Table 4
Time to the first dampness patch and to 90% of dampness on the backside of specimens and their corresponding water absorption.

	Specimen	time to the 1st (h)	Average (h)	Absorption (kg/m^2)	Average (kg/m^2)	time to reach 90% (h)	Average (h)	Absorption (kg/m^2)	Average (kg/m^2)
Series I Group G1	I–F-1	7.6	7.9	18.6	18.6	15.9	16.0	29.9	29.6
	I–F-2	7.1		17.7		16.5		29.7	
	I–F-3	7.5		18.1		15.7		29.4	
	I–F-4	9.1		20.0		15.5		29.6	
	I–F-5	8.4		18.3		16.5		29.6	
Series I Group G2	I-R-1	7.6	7.8	18.1	18.3	15.8	16.3	29.8	29.9
	I-R-2	7.8		18.4		16.5		30.0	
	I-R-3	7.5		17.6		15.9		29.7	
	I-R-4	8.2		19.0		16.4		30.0	
	I-R-5	7.9		18.3		16.7		29.8	
Series I Group G3	I-AF-1	7.9	8.0	18.7	18.3	15.9	16.9	29.8	30.0
	I-AF-2	8.1		18.4		17.1		30.0	
	I-AF-3	7.9		17.9		16.8		29.9	
	I-AF-4	8.1		18.5		17.1		30.1	
	I-AF-5	8.2		18.2		17.4		30.0	
Series II Group G1-a	II-F-1	4.3	4.8	10.4	10.7	12.4	12.5	20.6	20.2
	II-F-2	4.6		9.9		11.7		17.5	
	II-F-3	4.8		10.6		12.9		21.8	
	II-F-4	5.6		12.7		13.6		22.7	
	II-F-5	4.7		9.8		12.1		18.6	
Series II Group G1-b	II-F-6	6.4	6.3	9.7	10.8	18.4	16.5	20.6	21.1
	II-F-7	6.1		11.3		15.5		22.4	
	II-F-8	6.5		11.3		15.6		20.3	
Series II Group G2	II-R-1	6.7	5.9	10.9	10.7	16.3	15.3	22.6	20.8
	II-R-2	4.5		8.5		14.2		19.0	
	II-R-3	5.4		11.3		14.0		21.2	
	II-R-4	5.5		11.4		14.0		20.0	
	II-R-5	5.7		11.5		15.0		22.1	
	II-R-6	5.5		10.2		14.9		20.8	
	II-R-7	6.3		10.3		16.7		19.5	
	II-R-8	7.2		11.8		17.6		21.0	
Series II Group G3	II-AF-1	6.8	6.4	10.3	10.3	16.5	17.2	19.5	19.8
	II-AF-2	6.7		10.4		17.7		19.2	
	II-AF-3	6.9		11.1		16.4		19.0	
	II-AF-4	5.4		9.7		16.2		20.1	
	II-AF-5	6.6		10.9		17.8		18.8	
	II-AF-6	6.1		9.0		18.9		22.8	
	II-AF-7	6.2		10.7		16.9		19.1	
	II-AF-8	6.7		10.2		17.1		19.6	

absorption of 18.3–18.6 kg/m^2 and 10.3–10.8 kg/m^2 in the specimens of Series I and II, respectively. The difference in the amount of absorbed water within the same Series is rather limited, indicating that the mortar joint finish has a limited effect on the time to the apparition of the first dampness patch.

The registered water absorption levels correspond to 58% and 49%

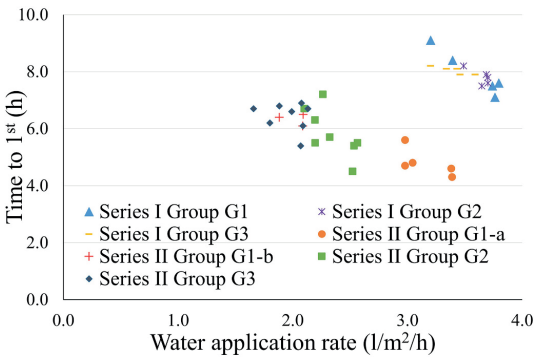

Fig. 10. Water application rate vs. time to the appearance of the first dampness patch.

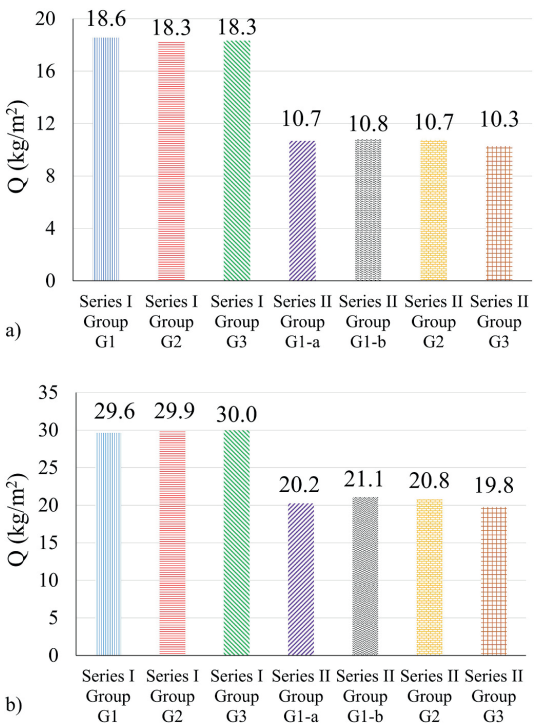

Fig. 11. Corresponding average water absorption: a) when the first dampness appeared on the backside of specimens; and b) when the specimens' backside became 90% damp.

of the final water content of Series I and II, respectively. The registered difference might be related to a more permeable contact zone in the head joints of the specimens prepared with bricks with lower water absorption coefficient and lower water absorption capacity. Similar to the appearance of the first visible dampness patch, the time to reach 90% dampness area on the backside of the specimens was roughly the same within each Series. Accordingly, the corresponding average water absorption was approximately 29.6–30.0 kg/m^2 for Series I and varied between 19.8 kg/m^2 and 21.1 kg/m^2 for Series II, as shown in Fig. 11.b.

4. Discussion

4.1. Influence of test parameters

4.1.1. Water absorption

Experimental results indicate that a large proportion of the water applied on the surface of the specimens during the first cycle, namely 76%–92%, was absorbed by the specimens. As shown in Fig. 6, in the first cycle, there is a nearly linear relationship between the water application rate and absorption. The remainder of the applied water spray, namely 8%–23%, is considered to have bounced off from the specimens' surface.

This conclusion is supported by visual observations carried out during the test, indicating the absence of runoff during the first test cycles. The plausibility of this conclusion is also underpinned by the fact that the amount of bounce off increased with increasing spraying rate, which can be observed by comparing group G1-a and G1-b of Series II, where the specimens have the same material and mortar joint finish characteristics. The specimens in group G1-a, exposed to a water spray rate of 3.2 l/m^2/h, accumulated 8.5 kg/m^2 water during the first cycle, corresponding to a bounce off of around 24%, see Table 3. In comparison, the specimens in group G1-b, exposed to a water spray rate of 2.0 l/m^2/h, accumulated 6.3 kg/m^2 water during the same cycle, corresponding to a bounce off of nearly 10%. These findings indicate, that increasing WDR intensities increase the percentage of bounce off, a phenomenon described by Van Den Bossche et al. [41] and Abuku et al. [47].

As mentioned in Section 3.1, the linear relationship between the amount of absorbed water and the square root of time during the 2nd and the 3rd cycle indicated that the amount of absorption is in good agreement with the absorption behavior of the bricks. For instance, the slope of the Q – $t^{1/2}$ curve in the 2nd and the 3rd cycle for specimens of Series I is approximately equal to 0.192 kg/(m^2.s$^{0.5}$), showing the influence of the water absorption coefficient of the bricks. The mortar joint finish does not seem to have a discernible effect on the absorption behavior of the masonry specimens.

Moreover, based on the available results, first, the impact of joint profile finishes on water absorption of masonry is negligible, particularly after long exposure to driving rain. Second, when surface saturation is attained, the water application rate is less significant.

4.1.2. Dampness patches

As mentioned in Section 3.2, the first visible dampness appeared on the bricks in the second course, in the vicinity of the head joint. This indicates that the primary path for water to penetrate a brick masonry wall is passing through the brick-mortar interfacial zone [25,48]. The location of the first dampness patch in the vicinity of the head joints might be explained by deficient contact between mortar and bricks or the presence of voids, often attributed to practical difficulties during bricklaying. In the present study, the specimens were built by pushing the head joint, while the recommended technique is to butter the end of bricks prior to laying to ensure optimal filling of the head joints [19,26]. Jonell and Moller [17] suggest that it is practically difficult to get the vertical joint completely filled with pushing technique; thus, unfilled joints are the primary path for water penetration in brick walls. Slapø et al. [26] found that buttering the bricks can significantly improve the masonry quality. This highlights the importance of good workmanship to control water penetration in masonry walls [9,17,19,26].

According to Table 4, the first visible dampness patch in the Series I specimens appeared at the end of the second and the beginning of the third exposure cycle. In contrast, for specimens of Series II, group G1-b to G3, the first dampness patch was already observed during the second exposure cycle, that is, approximately 90 min earlier than in the specimens of Series I.

For all groups, except group G1-a of Series II, the dampness area reached 90% on the specimens' backside during the fifth cycle. For group G1 of Series II, 90% of dampness was observed on the specimens' backside during the fourth cycle.

Based on the available results, the impact of joint profile finishes on the appearance of the first dampness patch on the specimens' backside is negligible, particularly after long exposure to driving rain. Hence, the present findings do not support the results presented by Hines and Mehta [9], namely that joint profile finishes substantially influence water penetration in masonry walls. This difference in results might be explained by the fact that, in their study [9], a considerably higher water exposure rate was used in combination with high differential air pressure.

4.2. Time to attain surface saturation

The time to reach surface saturation for a masonry façade when exposed to driving rain is dependent on both the sorptivity of the masonry and the WDR intensity, as shown by Hall and Kalimeris [49]. According to the Sharp Front (SF) model [50], the time to attain surface saturation, t_s [h], is given by Eq. (2)

$$t_s = 0.5\,\frac{60 \times S^2}{{V_0}^2} \tag{2}$$

where S is the sorptivity [mm/min$^{0.5}$], and V_0 is the driving rain intensity [mm/h]. The sorptivity is calculated as the ratio between the water absorption coefficient, A_w [kg/(m^2.s$^{0.5}$)], and the density [kg/m^3] of water.

In the present study, the average time to reach surface saturation, t_s, for both bricks and mortars are summarized in Table 5. It should be noted that for Series I and Series II group G1-a, around 23% of the applied water is considered to have been bounced off. The corresponding bounced off for Series II, except group G1-a, is considered to be around 11%. It can be seen that the theoretical time to attain surface saturation of bricks, t_s, varied between 8.7 h–9.8 h for Series I, whereas, for Series II, it ranged from 5.2 h to 10.0 h. It must be observed that the average water spray rate varied between 2.0 and 3.6 mm/h. While the time to surface saturation of the bricks generally varies between 5 and 10 h, the time to attain surface saturation for mortar M 2.5 is only around 0.1 h and 0.3 h. In the case of mortar NHL 3.5, the time to surface saturation varies between 6.6 and 14.4 h, though this calculation is valid only if the joint was fully filled with mortar NHL 3.5, while it is not the case in the specimens of group G3, which were filled with 114 mm of mortar M 2.5 and 6 mm of mortar NHL 3.5. As the surface of the joints manufactured with mortar M 2.5 became saturated earlier, the water running off from the joints was probably absorbed by the bricks. Consequently, the actual time to attain surface saturation for bricks during testing might have happened earlier than indicated by t_s.

Fig. 12 shows the average water absorption versus time response for all groups in Series I and II during 23 h of testing. The linear branch in the first cycles shows that the specimens absorbed a large part of the sprayed water. As the test progressed, the water absorption curve became nonlinear, indicating runoff due to saturation of the exposed surface. Therefore, according to Fig. 12, the time when the absorption curve became nonlinear can be considered as the time to surface saturation. This time is denoted t_{exp} as summarized in Table 5. It can be seen that the absorption behavior became nonlinear roughly at the end of the 3rd cycle for all groups within Series I and II except group G1-a in Series II. For group G1-a in Series II, the absorption curve against time became

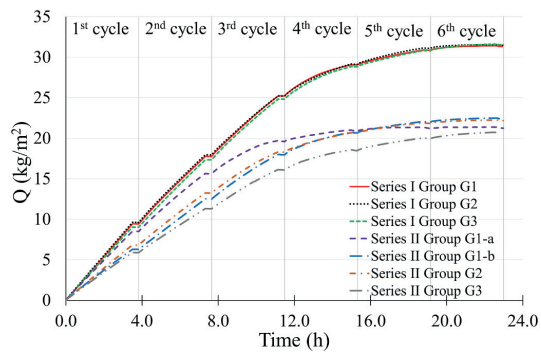

Fig. 12. Average water absorption time response.

Table 5
Average time to attain surface saturation and the corresponding amount of absorbed water. t_s – time calculated with Eq. (2); t_{exp} – time estimated using Fig. 12.

		Sorptivity (mm/min$^{0.5}$)	Water spray rate (mm/h)	Time to surface saturation t_s (h)	Q_t at the time of surface saturation (kg/m^2)	Q_{exp} at the time of surface saturation t_s (kg/m^2)	Time to surface saturation t_{exp} (h)
Series I Group G1	Brick type I	1.49	3.6	8.7	24.2	21.7	10.0
	Mortar M 2.5	0.17		0.1	0.3		
Series I Group G2	Brick type I	1.49	3.6	8.7	24.2	21.8	10.0
	Mortar M 2.5	0.17		0.1	0.3		
Series I Group G3	Brick type I	1.49	3.4	9.8	25.6	23.5	10.0
	Mortar NHL 3.5	1.23		6.6	–		
Series II Group G1-a	Brick type II	1.03	3.2	5.2	12.9	12.4	6.5
	Mortar M 2.5	0.17		0.1	0.4		
Series II Group G1-b	Brick type II	1.03	2.0	10.0	17.8	17.4	10.0
	Mortar M 2.5	0.17		0.3	0.5		
Series II Group G2	Brick type II	1.03	2.3	7.6	15.5	14.3	8.5
	Mortar M 2.5	0.17		0.2	0.4		
Series II Group G3	Brick type II	1.03	2.0	10.0	17.8	15.7	10.0
	Mortar NHL 3.5	1.23		14.4	–		

nonlinear at the end of the 2nd cycle.

The amount of absorbed water Q_t (kg/m^2) at the time when the surface saturation was attained is summarized in Table 5. Q_t is defined as the product of the water spray rate and the time to reach surface saturation of the bricks, t_s, taking into account the already mentioned percentage of the bounce off. Q_{exp} represents the amount of absorbed water at t_s taken from Fig. 12. It should be noted that the 20 min pausing between each cycle was deducted and not considered in the calculations of Q_t and Q_{exp}. Comparing Q_t and Q_{exp} (Table 5), corresponding to theoretical and experimental water absorption at the time of attaining surface saturation, respectively, a reasonable accordance can be seen. The differences between theoretically and experimentally determined data might be related to a) bricks might have different sorptivity properties in different directions, mentioned as anisotropy in sorptivity [50, 51]; and b) Q_t has been calculated based on the sorptivity of the bricks, whereas the experimentally determined Q_{exp} represents the amount of water absorbed by the masonry.

4.3. Test setup

In this study, three main criteria were considered to develop the test setup: 1) the sprayed water on the specimens' surface should be distributed uniformly on the exposed surface; 2) the sprayed water should consist of water drops, a representative for rainfall, and not mist or drizzle; and 3) the water application rate should be lowered in comparison with the test conditions of ASTM E514 [31] to be more representative of a wide range of WDR events. To achieve a uniform spray pattern covering the whole area of the exposed face, a full cone nozzle was used. Furthermore, many trials were done to find a suitable water pressure level and distance between the nozzle and the specimen, finally arriving at the test parameters presented in Fig. 1. It must be mentioned that the chosen combination of test parameters is only one out of many possible combinations.

The capability of different nozzle types to produce a water spray consisting of droplets was examined visually and by exposing sheets of paper with high absorption capacity for the water spray during approximately 1–2 s. The result of such a test is shown in Fig. 13, where the wet dots are attributed to water droplets.

To meet the third criterion, different low-flow nozzles have been tested. The largest difficulty consisted in combining low flow levels with a water spray consisting of droplets since this, in many cases, required operation of the nozzles below the pressure range specified by the supplier. When choosing water spray rates to be used in the tests, weather data and WDR intensities for three different locations in Sweden, a region with moderate WDR events, were analyzed; the details are provided in Appendix A.

Notably, continuous water absorption measurement provides valuable information about moisture conditions in the specimens. As during short-duration rainfalls or initial phases of rainfall events similar to the first and second cycles of the performed tests in this study, dampness patches usually do not appear on the backside of masonry walls, monitoring water absorption is a suitable measure to characterize the response of masonry exposed to WDR. Furthermore, results from water absorption measurements, combined with data on water penetration and appearance of dampness areas on the backside of masonry, can be beneficial for subsequent modeling of moisture conditions in masonry.

Fig. 13. Wet dots on a paper sheet exposed to water spray for 1–2 s.

Nevertheless, the results suggest that for a more realistic investigation of masonry façade's response to WDR exposure, the conditions in the newly developed test setup need to be revised as no water penetration that could be collected from the backside of specimens was observed, in spite of 21 h of exposure of water spraying.

Notably, this study has addressed the question of the effects of mortar joint profile finishes on water absorption and water penetration in masonry exposed to water spraying, yet without any differential air pressure. As the specimens were prepared without known defects, the results of this study cannot be taken as representative of the response of masonry façades with cracks and voids, especially when these are exposed to WDR with high wind pressure. Thus, it is anticipated that the test setup can be developed to encompass studies of the WDR response of specimens with defects exposed to significant differential air pressure.

5. Conclusions

In this study, we investigated the response of clay brick masonry exposed to uniform water spray with application rates of 1.7–3.8 l/m^2/h at zero differential air pressure on triplet specimens, with dimensions 250 mm (length) × 215 mm (height) × 120 mm (depth), in laboratory conditions. The mass gain in the specimens was continuously measured, and the specimens' backside was photographed every second minute to trace dampness areas. Based on these results, the following conclusions can be drawn:

1. The amount of absorbed water is highly dependent on not only the water absorption coefficient and absorption capacity of the bricks but also the water spray rate, whereas the mortar joint profile finish had limited influence on the amount of absorbed water.
2. The first dampness patches on the specimens' backside appear in the vicinity of the head joint, at water content levels corresponding to 50%–60% of full saturation level. This corresponds to 5–8 h of exposure at the actual water spray rates.
3. The specimens' backside reached 90% dampness at water content levels corresponding to 95% of full saturation level.
4. As a feature attributed to the actual, relatively low, water application rates, absence of known defects and zero differential air pressure, no measurable amounts of penetrated water could be collected at the specimens' backside.
5. The newly developed test setup might facilitate the verification of moisture simulations as it enables continuous water absorption measurement combined with tracing of dampness areas on the backside of masonry specimens.
6. Time-lapse image analysis could provide useful information in the context of masonry characterization under conditions with indiscernible WDR penetration.

Further improvement of the test setup by application of a differential air pressure in conjunction with water spraying will create conditions that can more realistically reproduce wind-driven rain. Further studies with specimens containing known defects, e.g., cracks or incompletely filled joints, might produce more conclusive results that could support decision-making in practical situations.

Author statement

Seyedmohammad Kahangi Shahreza: Methodology, Validation, Visualization, Writing – Original Draft, Data Curation, Formal Analysis, Investigation **Jonas Niklewski:** Validation, Visualization, Writing – Review and Editing, Supervision, Investigation **Miklós Molnár:** Conceptualization, Supervision, Writing – Review and Editing, Project Administration, Funding acquisition.

Declaration of competing interest

The authors declare that they have no known competing financial interests or personal relationships that could have appeared to influence the work reported in this paper.

Acknowledgments

The authors gratefully acknowledge financial support from SBUF - The Development Fund of the Swedish Construction Trade (grant 13576) and TMPB - The Masonry and Render Construction Association.

Appendix A

A.1. WDR events characteristic for Swedish conditions

As one of the aims of this study is to expose masonry specimens to water spray that reflects realistic WDR events in Sweden, in this section, we calculated WDR intensities for a multi-story building located in three different geographical locations in Sweden. Notably, Sweden can be a good representative of regions with moderate WDR events. Among available semi-empirical WDR deposition models [52–54], the advanced and widely used ISO model [52] is considered. The climate data is taken from the Swedish Meteorological Hydrological Institute (SMHI) [55]. First, the WDR relationship and ISO model are briefly presented. Second, the hourly rain intensities and wind velocities in Malmö, Gothenburg, and Uppsala for the period 1995–2020 are used to calculate driving rain intensities for the considered building.

A.1.1. WDR calculations

The general equation to calculate WDR intensity, R_{wdr} [mm/h] on a building façade in semi-empirical models can be written as follows:

$$R_{wdr} = \alpha \times U_{10} \times R_h^{0.88} \times \cos\theta \tag{A.1}$$

where α is WDR coefficient [s/m] to be elaborated in the next paragraph; U_{10} is the reference wind speed (unobstructed streamwise wind speed at 10 m height) [m/s]; R_h is the unobstructed horizontal rainfall intensity (i.e., the intensity of rainfall falling through a horizontal plane, as measured by a standard rain gauge with a horizontal orifice) [mm/h]; and θ is the angle between the wind direction and the normal to the façade [°].

As in free-field conditions, WDR intensity can differ from WDR intensity on a building façade [56], the two factors, α and cos θ, were introduced in Eq. (A.1).

The WDR coefficient α in the ISO model [52] is given in Eq. (A.2):

$$\alpha = \frac{2}{9} \times C_T \times O \times W \times C_R \tag{A.2}$$

where C_T is the topography coefficient [−]; O is the obstruction factor [−]; W is the wall factor [−]; and C_R is the roughness coefficient [−].

Although the ISO model provides the average annual amount of WDR, it can nevertheless be used to determine WDR intensity for any period during a year [56]. In this regard, based on the ISO model, Blocken and Carmeliet [56] presented Eq. (A.3) to calculate WDR intensity on a building façade by inserting Eq. (A.2) to Eq. (A.1):

$$R_{wdr} = \frac{2}{9} \times C_T \times O \times W \times C_R \times U_{10} \times R_h^{0.88} \times \cos(\theta) \tag{A.3}$$

A.1.2. WDR for multi-story building

WDR intensities R_{wdr} are calculated for a 15-m high multi-story building with a flat roof. The wind direction is perpendicular to the façade ($\theta = 0°$). Regarding the topography coefficient C_T and obstruction factor O, it is considered that the building is located in a terrain that is flat and free of obstructions. Therefore, C_T and O are equal to one. The wall factor, W, for a multi-story building with a flat roof is 0.5 for the top 2.5 m and 0.2 for the remainder of the exposed façade. In this case, the top part of the façade is considered; thus, W is equal to 0.5. The equation to calculate the roughness coefficient (C_R), dependent on the terrain category, as provided in the ISO model, is as follows:

$$C_R(z) = K_R.\ln\left(\frac{z}{z_0}\right) \quad for\ z \geq z_{min} \tag{A.4}$$

$$C_R(z) = C_R\ (z_{min})\ for\ z < z_{min} \tag{A.5}$$

where z is the height above ground [m]; K_R is the terrain factor [−]; z_0 is the roughness length [m]; and z_{min} is the minimum height [m].

It is further assumed that the 15-m high building is neighboring to farmlands, thus belonging to terrain category II, according to the ISO model [52]. Values of K_R, z_0, and z_{min} as a function of the terrain category are given in the ISO model [52], in which $K_R = 0.19$, $z_0 = 0.05$ m, and $z_{min} = 4$ m. Hence, C_R is equal to 1.084, and the WDR coefficient α, for the given building façade is then equal to 0.12.

To calculate the WDR intensity R_{wdr}, the same building with the same terrain and building geometry was considered to be located in Malmö,

Gothenburg, and Uppsala.

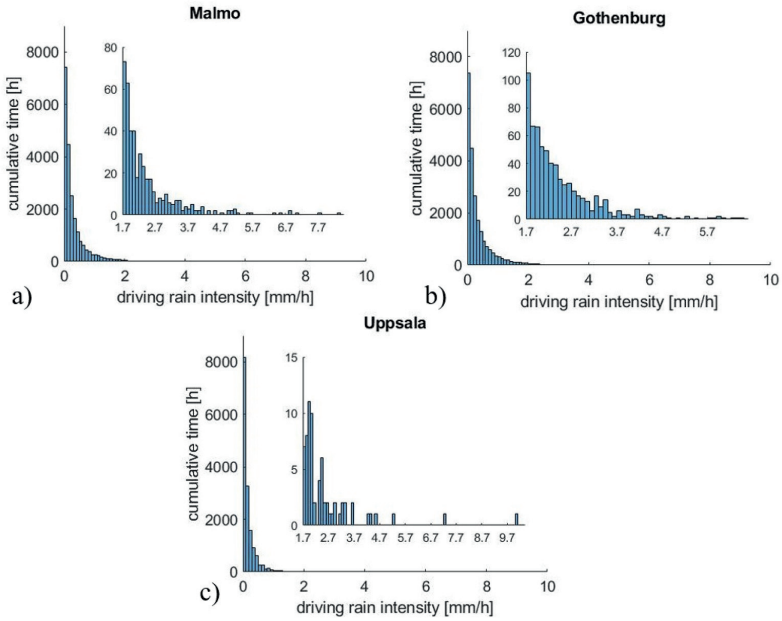

Fig. A.1. Driving rain intensities from 1995 until 2020 for a) Malmö, b) Gothenburg, and c) Uppsala; Small diagrams show highest driving rain intensities.

Fig. A.1 shows that the highest WDR intensity for Malmö, Gothenburg, and Uppsala is equal to 8.4, 6.5, and 10.1 mm/h, respectively. As shown in the figure, the range of the water application rate used in this study, varying between 1.7 and 3.8 $l/m^2/h$, falls within the range of realistic WDR intensities in Sweden, although a clear majority (>99%) of the WDR events has intensities below 1 mm/h. Thus, the test setup should be further developed to reproduce even lower water application rates.

References

[1] J. Carmeliet, B. Blocken, Driving Rain, Rain Absorption and Rainwater Runoff for Evaluating Water Leakage Risks in Building Envelopes, 2004, 9th International Conference on Performance of Exterior Envelopes of Whole Buildings (Buildings IX).

[2] A. Day, R. Lacy, J. Skeen, Rain Penetration through Walls, A Summary of the Investigations Made at the UK Building Research Station from 1925 to 1955, Building Research Station Note, 1955.

[3] M. Pountney, R. Maxwell, A. Butler, Rain penetration of cavity walls: report of a survey of properties in England and Wales, Building Research Establishment Information Paper 2, 1988.

[4] J.M. Pérez-Bella, J. Domínguez-Hernández, B. Rodríguez-Soria, J.J. del Coz-Díaz, E. Cano-Suñén, Combined use of wind-driven rain and wind pressure to define water penetration risk into building façades: the Spanish case, Build. Environ. 64 (2013) 46–56.

[5] A.S. Kaslegard, Climate Change and Cultural Heritage in the Nordic Countries, Nordic Council of Ministers2011.

[6] S. Shahreza, M. Molnár, J. Niklewski, I. Björnsson, T. Gustavsson, Making Decision on Repointing of Clay Brick Facades on the Basis of Moisture Content and Water Absorption Tests Results–A Review of Assessment Methods, Brick and Block Masonry-From Historical to Sustainable Masonry, CRC Press2020, pp. 617-623.

[7] W. Tang, C.I. Davidson, S. Finger, K. Vance, Erosion of limestone building surfaces caused by wind-driven rain: 1. Field measurements, Atmos. Environ. 38 (33) (2004) 5589–5599.

[8] M.E. Young, Dampness penetration problems in granite buildings in Aberdeen, UK: causes and remedies, Construct. Build. Mater. 21 (9) (2007) 1846–1859.

[9] T. Hines, M. Mehta, The effect of mortar joints on the permeance of masonry walls, in: Proceedings of the 9th International Brick/Block Masonry Conference, 1991, pp. 1227–1234. Berlin, Germany.

[10] C.T. Grimm, Water Permeance of Masonry Walls: a Review of the Literature, Masonry: Materials, Properties, and Performance, ASTM International1982.

[11] B. Blocken, J. Carmeliet, A review of wind-driven rain research in building science, J. Wind Eng. Ind. Aerod. 92 (13) (2004) 1079–1130.

[12] B. Blocken, D. Derome, J. Carmeliet, Rainwater runoff from building facades: a review, Build. Environ. 60 (2013) 339–361.

[13] H. Ge, Influence of time resolution and averaging techniques of meteorological data on the estimation of wind-driven rain load on building facades for Canadian climates, J. Wind Eng. Ind. Aerod. 143 (2015) 50–61.

[14] B. Blocken, G. Dezsö, J. van Beeck, J. Carmeliet, Comparison of calculation models for wind-driven rain deposition on building facades, Atmos. Environ. 44 (14) (2010) 1714–1725.

[15] A. Erkal, D. D'Ayala, L. Sequeira, Assessment of wind-driven rain impact, related surface erosion and surface strength reduction of historic building materials, Build. Environ. 57 (2012) 336–348.

[16] M. Abuku, H. Janssen, J. Poesen, S. Roels, Impact, absorption and evaporation of raindrops on building facades, Build. Environ. 44 (1) (2009) 113–124.

[17] P. Jonell, T. Moller, Moisture Penetration of Solid Facing Brick Walls, National Research Council of Canada, 1956. Technical Translation (National Research Council of Canada); no. NRC-TT-618.

[18] T. Ritchie, Rain Penetration of Walls of Unit Masonry, Canadian Building Digest; No, CBD-6, 1960.

[19] T. Ritchie, W.G. Plewes, A Review of Literature on Rain Penetration of Unit Masonry, National Research Council of Canada. Division of Building Research, 1957. Technical Paper.

[20] T. Ritchie, Small-panel Method for Investigating Moisture Penetration of Brick Masonry, Internal Report (National Research Council of Canada. Division of Building Research); No. DBR-IR-160, National Research Council of Canada, 1958.

[21] T. Ritchie, Influence of Silicone Treatment of Bricks on Moisture Penetration and Bond Strength of Brickwork, Internal Report (National Research Council of Canada. Division of Building Research); No. DBR-IR-207, National Research Council of Canada, 1960.

[22] T. Ritchie, W.G. Plewes, Moisture penetration of brick masonry panels, ASTM Bull. 249 (1961) 39–43.

[23] C.C. Fishburn, D. Watstein, D.E. Parsons, Water Permeability of Masonry Walls, US Department of Commerce, National Bureau of Standards, 1938.

[24] C.C. Fishburn, Water Permeability of Walls Built of Masonry Units, US Department of Commerce, National Bureau of Standards1942.

[25] C. Groot, J. Gunneweg, The influence of materials characteristics and workmanship on rain penetration in historic fired clay brick masonry, Heron 55 (2) (2010) 2010.

[26] F. Slapø, T. Kvande, N. Bakken, M. Haugen, J. Lohne, Masonry's resistance to driving rain: mortar water content and impregnation, Buildings 7 (3) (2017) 70.
[27] J.C.Z. Piaia, M. Cheriaf, J.C. Rocha, N.L. Mustelier, Measurements of water penetration and leakage in masonry wall: experimental results and numerical simulation, Build. Environ. 61 (2013) 18–26.
[28] J. Ribar, Water Permeance of Masonry: a Laboratory Study, Masonry: Materials, Properties, and Performance, ASTM International1982.
[29] K.B. Anand, V. Vasudevan, K. Ramamurthy, Water permeability assessment of alternative masonry systems, Build. Environ. 38 (7) (2003) 947–957.
[30] R. Cacciotti, Brick masonry response to wind driven rain, Eng. Struct. 204 (2020) 110080.
[31] A. International, ASTM E514/E514M-14a, Standard Test Method for Water Penetration and Leakage through Masonry, ASTM International, West Conshohocken, PA, 2014.
[32] NEN 2778, 2015 Nl. Vochtwering in Gebouwen (Moisture Control in Buildings), 2015. Nederlands.
[33] NBI 29/1983 Mørtler, Tetthet Mot Slagregn (Mortars. Resistance to Driving Rain), Norges byggforskningsinstitutt, Oslo, Norway, 1983, pp. 75–76.
[34] S. Van Goethem, N. Van Den Bossche, A. Janssens, Watertightness assessment of blown-in retrofit cavity wall insulation, Energy Procedia 78 (2015) 883–888.
[35] R.R. Vilatò, WATER PENETRATION TEST on CONCRETE BLOCK MASONRY, the 15th International Brick and Block Masonry Conference, Florianópolis – Brazil, 2012.
[36] D. Chiovitti, M. Gonçalves, A. Renzullo, Performance evaluation of water repellents for above grade masonry, J. Therm. Envelope Build. Sci. 22 (2) (1998) 156–168.
[37] R. Forghani, Y. Totoev, S. Kanjanabootra, A. Davison, Experimental investigation of water penetration through semi-interlocking masonry walls, J. Architect. Eng. 23 (1) (2017), 04016017.
[38] S.K. Ghosh, J.M. Melander, Air Content of Mortar and Water Penetration of Masonry Walls, Portland Cement Association Skokie, IL, 1991.
[39] M.E. Driscoll, R.E. Gates, A Comparative Review of Various Test Meteods for Evaluating the Water Penetration Resistance of Concrete Masonry Wall Units, Masonry: Design and Construction, Problems and Repair, ASTM International, 1993.
[40] L.R. Baker, F.W. Heintjes, Water leakage through masonry walls, Architect. Sci. Rev. 33 (1) (1990) 17–23.
[41] N. Van Den Bossche, M. Lacasse, A. Janssens, Watertightness of Masonry Walls: an Overview, 12th International Conference on Durability of Building Materials and Components (XII DBMC-2011), FEUP Edições, 2011, pp. 49–56.
[42] M. Lacasse, T. O'Connor, S. Nunes, P. Beaulieu, Report from Task 6 of MEWS project: experimental assessment of water penetration and entry into wood-frame wall specimens-final report, Inst. Res. Constr. RR-133 (2003) Feb.
[43] A.J. Rathbone, Rain and Air Penetration Performance of Concrete Block Work, Technical report 553, 5th Ed., Cement and Concrete Association, 1982. ISBN: 978-0-7210-1261-2.
[44] H. Hens, S. Roels, W. Desadeleer, Rain Leakage through Veneer Walls, Built with Concrete Blocks, CIB W40 meeting, Glasgow, 2004.
[45] A. International, ASTM C67/C67M-20, Standard Test Methods for Sampling and Testing Brick and Structural Clay Tile, ASTM International, West Conshohocken, PA, 2020.
[46] A. International, ASTM C1403 - 15, Standard Test Method for Rate of Water Absorption of Masonry Mortars, ASTM International, West Conshohocken, PA, 2015.
[47] M. Abuku, B. Blocken, J. Poesen, S. Roels, Spreading, Splashing and Bouncing of Wind-Driven Raindrops on Building Facades, 11th Americas Conf. On Wind Engineering, Univ. of Washington, Seattle, 2009, pp. 22–26.
[48] T. Ritchie, J.I. Davison, Factors Affecting Bond Strength and Resistance to Moisture Penetration of Brick Masonry, vol. 320, ASTM Special Technical Publication, 1963, pp. 16–30.
[49] C. Hall, A. Kalimeris, Water movement in porous building materials—V. Absorption and shedding of rain by building surfaces, Build, Environ. Times 17 (4) (1982) 257–262.
[50] C. Hall, W.D. Hoff, Water Transport in Brick, Stone and Concrete, second ed. ed., CRC Press2011.
[51] K.J. Krakowiak, P.B. Lourenço, F.J. Ulm, Multitechnique investigation of extruded clay brick microstructure, J. Am. Ceram. Soc. 94 (9) (2011) 3012–3022.
[52] EN ISO 15927-3, Hygrothermal Performance of Buildings-Calculation and Presentation of Climatic Data. Part 3: Calculation of a Driving Rain Index for Vertical Surfaces from Hourly Wind and Rain Data, European Committee for Standardization, 2009.
[53] ASHRAE, Standard 160-2016. Criteria for Moisture-Control Design Analysis in Buildings, ASHRAE, Atlanta, GA, 2016.
[54] J. Straube, E. Burnett, Simplified Prediction of Driving Rain on Buildings, Proceedings of the International Building Physics Conference, Eindhoven University of Technology Eindhoven, the Netherlands, 2000, pp. 375–382.
[55] https://www.smhi.se/data. (Accessed September 2020).
[56] B. Blocken, J. Carmeliet, Overview of three state-of-the-art wind-driven rain assessment models and comparison based on model theory, Build. Environ. 45 (3) (2010) 691–703.

Paper III

Construction and Building Materials 353 (2022) 129109

Contents lists available at ScienceDirect

Construction and Building Materials

journal homepage: www.elsevier.com/locate/conbuildmat

Novel water penetration criterion for clay brick masonry claddings

Seyedmohammad Kahangi Shahreza *, Jonas Niklewski, Miklós Molnár

Division of Structural Engineering, Department of Building and Environmental Technology, Lund University, John Ericssons väg 1 SE, 223 63 Lund, Sweden

ARTICLE INFO

Keywords:
Clay brick masonry
Water penetration
Water absorption
Brick absorption properties
Mortar joint profile
Damp patches

ABSTRACT

Despite the impact of water penetration on the performance of building envelopes, no general agreement is available on implementing water penetration due to wind-driven rain (WDR) in hygrothermal and moisture safety analyses. This study proposes a novel criterion for water penetration in clay brick masonry that depends on the water content level of masonry. An experimental campaign investigating water penetration in clay brick masonry exposed to uniform water spray is conducted on masonry triplets prepared from bricks with different water absorption properties and three mortar joint profiles. During each test, water absorption and water penetration are registered continuously. The results show that no water penetration occurs unless the water content of the specimens is above 90% of their saturation capacity. The saturation level at which penetration starts is consistent across all joint profiles and brick types. Accordingly, exposure to driving rain at levels below the threshold may not lead to water penetration. The utility and implications of the proposed criterion are briefly demonstrated by analyzing water content and water penetration in a clay brick masonry façade. The resulting water penetration is compared with the results obtained using a commonly accepted reference model that assumes one percent of all wind-driven rain deposited on the façade to penetrate the clay brick cladding. By linking water penetration in clay brick masonry to the water content, the proposed criterion is an attempt to logically explain a phenomenon of high scientific and practical relevance for moisture analyses of a frequently used type of building envelope.

1. Introduction

Residential buildings with clay brick masonry façades are commonly built in Nordic countries because of their architectural qualities and long service life; moreover, they efficiently shield against wind-driven rain (WDR), which is a significant source of moisture in Nordic countries. WDR is associated with elevated water content and the risk of water penetration in masonry walls [1]. Such water penetration can facilitate microbiological growth [2,3], negatively impacting the hygrothermal performance and durability of building envelopes [1–6], as well as damage bio-based wall components, if present [7].

Incorporating different values of water penetration in hygrothermal simulations significantly affects the average water content of external walls [3,8–10], indicating that it may dominate the hygrothermal behavior and durability of wall assemblies. Despite the impact of water penetration on building envelope performance, only a few available studies propose methods for accurately considering water penetration (leakage) due to WDR in hygrothermal and moisture safety analyses [3,9–11]. Further, there is no general agreement on the amount of water that penetrates through brick masonry claddings and how penetration should be implemented in hygrothermal analyses [3,10,11,13]. Currently, in the absence of fully verified models, 1 % of WDR deposited on a façade is considered to penetrate behind the cladding, in accordance with the North American Standard (ASHRAE 160–2016) [14]. Several research studies have attempted to justify the water penetration value of 1 % for the WDR [15,16], but a review of existing experimental studies shows that between 0 and 20 % of the WDR may penetrate a clay brick cladding [10,12,13,17,18]. In addition, a distinct period exists between the start of exposure to WDR and the first recorded penetration even under extreme test conditions [16,19,20] because the initiation of water penetration in brick masonry without deficiencies requires a certain level of saturation [17,21]. For example, in a study conducted by Straube and Burnett [16], clay brick masonry was exposed to a water spray rate of 200 $l/m^2/h$, but more than 30 min elapsed until water penetration was registered in an initially dry masonry. For water spray rates of less than 10 $l/m^2/h$, water penetration was registered after 5–8 h, which was attributed to the absorption capacity of the masonry [16,17,22]. These results suggest that penetration of WDR in masonry

* Corresponding author.
E-mail addresses: mohammad.kahangi@kstr.lth.se (S. Kahangi Shahreza), jonas.niklewski@kstr.lth.se (J. Niklewski), miklos.molnar@kstr.lth.se (M. Molnár).

https://doi.org/10.1016/j.conbuildmat.2022.129109
Received 27 May 2022; Received in revised form 20 August 2022; Accepted 7 September 2022
Available online 16 September 2022

walls may not take place during periods in which the walls can potentially absorb and store water.

In most existing studies, water penetration in brick masonry is investigated by applying a high water spray rate on one face of an already saturated masonry specimen while measuring the mass of water collected on the other side. The mass of the absorbed water, which defines the saturation level of the masonry itself, is rarely measured [10,23–27]. These test setups may give a phenomenologically misleading picture of the evolution of water penetration caused by WDR by ignoring the water buffering capacity of non-saturated masonry [22]. Therefore, studies that measure the water content and water penetration simultaneously can better illustrate water penetration through masonry walls on exposure to WDR, a feature that may improve the precision of hygrothermal analyses. Since the initiation of water penetration in initially non-saturated clay brick masonry takes time [16,17,28,29], measurement of water content prior to water penetration may prove useful in finding a reasonable correlation between the water content and water penetration of masonry.

In clay brick masonry, water absorption (water content) and water penetration depend on parameters such as material properties (absorption properties of brick and mortar), mortar water content at bricklaying, joint thickness, presence of cracks in the brick itself, brick–mortar interface, and wall thickness [1,7,18,23,30,31]. In addition, masonry walls with the same prescribed characteristics may differ widely in performance due to workmanship during bricklaying [10,18–20,23]. There are several hygrothermal analysis tools to simulate temporal moisture content variations in masonry claddings. Modeling water transport in masonry is a complex process involving two different materials (brick/mortar) with imperfect hydraulic contact stemming from a lack of adhesion or bonding. Water flow across the interface has been studied extensively and imperfect hydraulic contact can be considered a contact resistance [32–34]. In contrast, there are few studies available on water transport parallel to the interface [35], where poor contact between the two materials will instead create a high conductivity pathway for water absorption [33] and possibly penetration.

Nevertheless, hygrothermal modeling of masonry walls is predominately performed with one-dimensional models, considering masonry as a homogenous material. Further, the complex nature of water penetration and its many dependencies render it accurately modeling difficult despite numerous studies on water penetration in masonry [10–13,17,18]. Taking into consideration that correct estimation of water penetration in clay brick masonry may require that several parameters that are difficult to control shall be considered. A simple criterion for the initiation of water penetration might be a step forward from both a scientific and practical perspective.

Therefore, the present study focuses on a) providing information about how water penetration in clay brick masonry might be related to water content; b) how the information can be used in hygrothermal analyses. In doing so, this paper presents the results of an experimental campaign on water penetration in clay brick masonry exposed to a controlled water spray. The aim is to explore the adequacy of a criterion for the initiation of water penetration depending on the water content of masonry. Accordingly, masonry triplets are exposed to a uniform water spray at a rate of around 6.3 $l/m^2/h$ and zero differential air pressure. The test parameters include bricks with different water absorption properties as well as mortar joint profiles, namely, flush, raked, and after-pointed. Water absorption and water penetration are measured continuously during the tests. Based on the results, a criterion for the start of water penetration in relation to the water content of masonry is proposed. Additionally, the water content of brick masonry walls located in Gothenburg (the west coast of Sweden) during a ten-year interval is studied numerically. The proposed novel criterion is then applied to simulated walls, and the determined water penetration is compared with that obtained by using the water penetration criterion of the ASHRAE 160 standard [14].

2. Materials and methods

2.1. Characterization of materials

2.1.1. Bricks

In this study, two types of commonly used solid clay bricks in the Swedish construction market are considered. Tests are performed to characterize the water absorption properties of these bricks, including the initial rate of absorption (IRA), 24-h water absorption capacity (defined as the ratio between the amount of absorbed water and dry weight), and water absorption coefficient (A_w). Moreover, tests are conducted to determine the IRA and 24-h water absorption capacity according to the ASTM C67 standard [36], and the water absorption coefficient is determined as described in the ASTM C1403 standard [37] (Table 1). Since the IRA of brick types I and II range between 1 and 3 $kg/m^2/min$, they can be categorized as medium suction bricks [I] and [II], respectively. The 24-h water absorption capacity of the bricks is calculated as the ratio between the weight of the absorbed water and the initial dry weight of the bricks. The 24-h water absorption capacity of bricks type [I] is roughly twice larger than that of bricks type [II], 16.0 % and 8.6 %, respectively.

2.1.2. Mortars

In this study, two types of mortar, namely, cement-based mortar M 2.5 supplied from Weber Saint-Gobain Sweden AB [38] and natural hydraulic lime (NHL) 3.5 mortar supplied from Målarkalk Sweden AB [39], are used to prepare masonry specimens. Mortar M 2.5 is a factory-mixed dry mortar commonly used for brick masonry façades. The binder is composed of around 65 % cement and 35 % lime [34]. NHL 3.5 is a ready-mixed hydraulic lime mortar recommended for repointing and does not contain any additives. During production, it is mixed with dried well-graded natural sand [35]. Tests are conducted to characterize the IRA and water absorption coefficient of the mortars according to the ASTM C67 standard [36] and ASTM C1403–15 standard [37], respectively. Additionally, the 24-h water absorption capacity of mortar M 2.5 has been determined according to the ASTM C67 standard [36]. Table 1 summarizes the determined water absorption properties of the mortars.

2.2. Masonry specimens

The design of the specimens was intended to represent a masonry veneer wall. Twenty-four masonry triplets with the length, height, and depth of 250 ± 2 mm, 218 ± 2 mm, and 120 ± 2 mm, were prepared in laboratory conditions without prewetting the bricks. The thickness of the bed joints and head joints varied between 15 and 20 mm to achieve a fixed height and length of 218 ± 2 mm and 250 ± 2 mm for all specimens to fit in the test setup. During bricklaying, a consistent water-to-mortar ratio was used to minimize the effect of any variation on the results. The specimens herein were built by the so-called pushing (slushing) technique, i.e., by throwing mortar into the joint with the edge of a trowel [23,40,41].

The prepared masonry specimens are divided into two series depending on the brick type (Fig. 1 and Table 2). Series I and II included specimens built with medium suction bricks [I] and [II], respectively. Within each Series, the specimens are divided into three types, namely, F, R, and AF, according to their joint profile (Fig. 1). Masonry specimens in type F were built with mortar M 2.5 and a tooled flush joint profile; moreover, in type R, they were built with mortar M 2.5 and a raked joint profile. Finally, type AF included masonry specimens built with mortar M 2.5 and after-pointed with NHL 3.5 mortar to a flush joint profile.

For type F, a wooden stick was used to compact the mortar joint. For type R, a 5 mm screw was used to remove the mortar from the outer layer of the joint. The specimens in type AF were prepared such that a 6 mm screw was used to remove the mortar. On the day after bricklaying, the outer part of the joint (approximately 6 mm) was pointed with NHL mortar. NHL 3.5 was used for pointing the specimens, following the

Table 1
Material properties of bricks and mortars.

Materials	Dimensions (mm × mm × mm)	Density ρ (kg/m^3)	IRA ($kg/m^2/min$)	CoV* (%)	24-h water absorption (%)	CoV* (%)	A_w ($kg/m^2.s^{0.5}$)	CoV (%)
Brick type I	250 × 120 × 62	1800	1.95	2.3	16.0	1.6	0.193	0.8
Brick type II	250 × 120 × 62	2050	1.81	5.1	8.6	14.5	0.133	16.1
Mortar M 2.5	100 × 100 × 100	1869	0.30	15.8	6.3	2.8	0.022	8.7
Mortar NHL 3.5	100 × 100 × 100	1715	0.80	20.4	–	–	0.159	9.2

* CoV: Coefficient of variation.

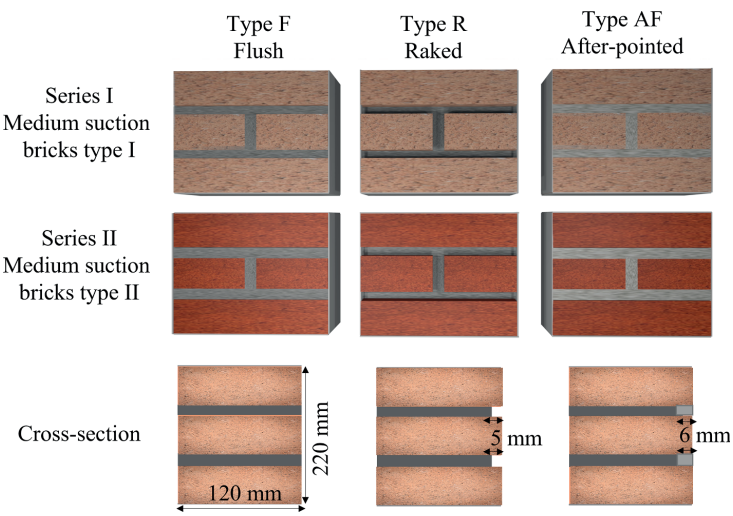

Fig. 1. Schematic of the prepared masonry specimens; cross-section (the bottommost row).

Table 2
Designations and configurations of specimens.

Series	Type	Brick	Mortar	Joint profile	Avg. water spray rate ($l/m^2/h$)	No. of specimens
Series I	F	Medium suction type [I]	M 2.5	Flush	6.3 ± 5 %	4
	R		M 2.5	Raked		4
	AF		M 2.5 / NHL 3.5	After-pointed		4
Series II	F	Medium suction type [II]	M 2.5	Flush		4
	R		M 2.5	Raked		4
	AF		M 2.5 / NHL 3.5	After-pointed		4

recommendations of the mortar manufacturer. Finally, all specimens were gently cleaned with a brush to remove excess mortar.

The specimens are named following the designation X-*T*-C, where X represents the Series (I and II), T corresponds to the mortar joint profile (F, R, and AF for flush, raked, and after-pointed, respectively), and C refers to the specimen number. For example, specimen II-F-2 is one of the specimens belonging to Series II, built with medium suction bricks [II], with a flush joint profile, and the second specimen of type F.

2.3. Test setup

The employed test setup is equipped with a low flow, full cone BETE WL nozzle, IFM SM4000 electronic magnetic-inductive water flow meter, two water pressure regulators, two DINI ARGEO digital scales 30 kg/2 g, and GoPro HERO8 Black digital camera with a 12-megapixel sensor to study the interaction of clay brick masonry and water spray [17,22] (Fig. 2). The test setup achieves a uniform water spray pattern while keeping the water application rate in a range that does not exceed extreme WDR events in Sweden [22]. All specimens are exposed to a uniform and constant water spray rate of 6.3 $l/m^2/h$ ± 5 % without applying any air differential pressure (Table 2). The distance between the exposed surface of the specimens and the nozzle is set to approximately 50 cm. A 2 cm gap between the wooden panel and the exposed surface of the specimens is provided to prevent runoff from the panel above.

The prepared masonry specimens were placed on a digital scale to continuously measure the specimens' weight during the tests. Water penetrating through the backside of the specimens was led by a collector to the second scale. The two scales were connected to a laptop, where data was measured every 10 s. Data logging was then done by installing WEIMONITOR software, making it possible to monitor and record in real-time all the weighing. The appearance and spread of damp patches on the protected side of the specimens are tracked by a digital camera mounted behind the specimens. The camera was mounted in a fixed position behind the specimens, and a ColorChecker was used for further color correction. Every 2 min, an image was recorded by the camera, where the first image was used as a reference image. The following images were then compared with the reference image to detect damp patches and monitor their spread. All images were analyzed by MATLAB (2019b), where the difference between each image and the reference image was calculated as the squared sum of the difference in each color channel (R, G, and B). The resulting binary image, representing the change in color from the initial state, was then thresholded with a fixed

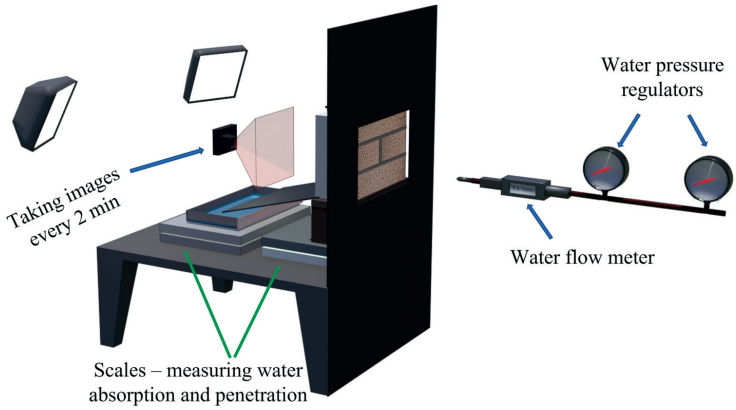

Fig. 2. Schematic of the test setup.

value. The relative damp area could then be calculated in each time step as the sum of white pixels divided by the sum of pixels within the area confined by the specimen edges. A more detailed description of how damp patches were detected and monitored throughout the test by means of image analysis is available in [22]. Each test lasted 23 h, including six consecutive cycles; each cycle consisted of 210 min of water spraying and 20 min of pausing. An in-detail description of the test setup and achieving a uniform water spray is available in [22].

Prior to testing, all sides except the exposed surface and backside of the specimens were sealed using a two-component sealant (ARDEX P2D and ARDEX S1-K), producing a highly elastic waterproof coating. The sealing was implemented to avoid undesirable water absorption on any other side except the exposed surface.

3. Experimental results

3.1. Water absorption and water penetration

This section first presents the response of masonry specimens in terms of water absorption during 23 h of cyclic spraying. In this study, water absorption Q [kg/m^2] is defined as the ratio between the amount of absorbed water (i.e., the difference between the increased weight w_i [kg] and initial weight w_0 [kg]) and the exposed surface area A [m^2].

$$Q = \frac{w_i - w_0}{A} \tag{1}$$

Fig. 3a shows the average water absorption of all types within each Series during the 23 h of testing. When masonry is in direct contact with liquid water and the specimen face is maintained saturated, the absorption rate is normally proportional to the square root of time, implying that the rate of absorption decreases over time. In contrast, the first 1–2 h of the test, depending on the specimen type, indicates a constant absorption rate because the exposed face is not yet saturated, and the absorption is thus limited by the water supply rate. The bounce-off varies between 7 % and 14 %. Before surface saturation is attained, the absorption can be described as a linear function of time with a slope strongly dependent on the spray rate (see "reference line" in Fig. 3b). When the surface becomes saturated, and runoff begins, then the absorption will deviate from the reference line as only a fraction of the water is absorbed into the specimen. The surface saturation for Series I and II are attained after approximately-one and two hours, respectively, as shown in Fig. 3b.

The results indicate that with a constant water spray rate, the time to attain surface saturation is strongly correlated with the water absorption coefficients of the bricks. Moreover, surface saturation is attained during the first cycle for all types within each Series, but more time elapses for Series I, specimens prepared from bricks with an absorption coefficient of 0.193 kg/m^2.s$^{0.5}$, in comparison with Series II, specimens built from bricks with an absorption coefficient of 0.133 kg/m^2.s$^{0.5}$. Based on the obtained results (Fig. 3a), the slight difference in the amount of absorbed water after the first cycle for each type within each Series may be related to the: a) variability in brick absorption properties (Table 1); b) variation in the applied spray rate, estimated to approximately 5 %; and c) effect of the mortar joint profile.

After attaining surface saturation in the specimens, the absorption behavior becomes nonlinear, and the slope of the Q–t curve decreases

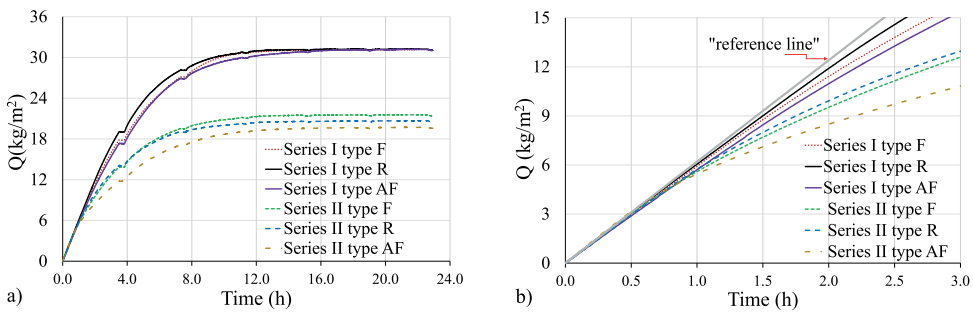

Fig. 3. Average water absorption vs time response: a) during 23 h of testing and b) during the first three hours of the test.

until it becomes close to zero, i.e., nearly no water accumulation in the specimens. Eventually, water absorption ends during the fourth cycle. The results show that the water absorption rate in masonry specimens mainly depends on the spray rate and water absorption coefficient of the bricks, but the amount of absorbed water is mainly correlated with the absorption capacity of masonry. The drop in the Q–t curve between each cycle is related to the 20 min of pausing followed by 210 min of water spraying in the test regime.

Table 3 summarizes the average absorption Q [kg/m^2] within each type after performing six cycles. Note that the average absorption in the specimens of Series I is approximately equal to 31.0 kg/m^2, highlighting a negligible difference in the average absorption between types F, R, and AF. Moreover, the specimens of Series I are prepared from brick type I with a coefficient of variation (CoV) of approximately 1.5 %. The average water absorption for types F, R, and AF of Series II varies between 19.6 kg/m^2 and 21.4 kg/m^2. According to the obtained results, the effect of joint profiles on the water absorption in masonry specimens is negligible.

It must be mentioned that the average absorption for both Series after six cycles of water spraying only differs by approximately 2 % from the saturation capacity of the masonry. The latter is calculated using the 24-h water absorption capacity of bricks and mortar (type M 2.5).

Since this study aims to propose a criterion for the initiation of water penetration considering the moisture content, the water content level of individual specimens when water penetration starts is summarized in Table 3. The water content level [%] is calculated as the ratio of the absorbed water at the start of water penetration and the saturation capacity of the masonry. Note that water penetration starts when the water content level of masonry specimens is above 90 % of the saturation capacity, highlighting the benefit gained from the water absorption capacity of brick masonry to buffer and thus postpone water penetration [16]. Thus, the obtained results indicate that water penetration may start when masonry specimens absorb water corresponding to more than 90 % of their saturation capacity.

The average amount of water penetration [kg/m^2] for each type within each Series during the 23 h of testing is shown in Fig. 4. Herein, water penetration is defined as the amount of water that can be collected

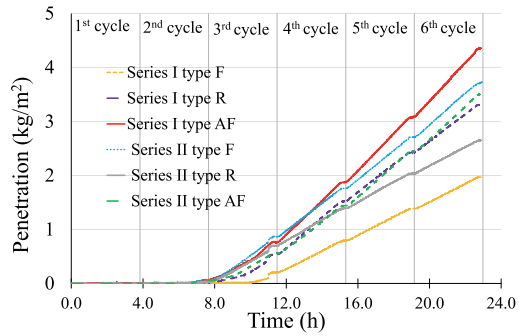

Fig. 4. Average water penetration vs time response.

from the backside of a specimen divided by its exposed area. Note that the water penetration in all types within Series I and II starts at the end of the second cycle or at the beginning of the third cycle, indicating that it starts when the prepared masonry specimens are close to saturation.

The average amount of penetrated water of types F, R, and AF of Series I and II is 2.0–4.4 kg/m^2. Once water penetration starts, it continues approximately linearly until the end of the test, except during the 20 min of long pause between each spraying cycle during which no penetration is registered. Additionally, water mainly penetrates through the brick–mortar interface, indicating the importance of the interfacial zone for the resistance of masonry against WDR.

Table 4 summarizes the amount of water penetration for each specimen. The amount of penetrated water varies between 0–8 kg/m^2 and 0.3–6.3 kg/m^2 in Series I and II, respectively. Interestingly, the largest and smallest amounts of water penetration, 8.2 and 0 kg/m^2, respectively, are registered in the same type of specimens, type AF in Series I. Fig. 5 shows the significant variability in the water penetration between the individual specimens of Series I type R.

Table 3
Average water absorption after the sixth cycle, the time elapsed till the appearance of the first visible damp patch, and water content level at the initiation of water penetration for each type within each Series.

	Specimens	Average absorption (g)	Average absorption (kg/m^2)	Avg. (kg/m^2) / CoV (%)	Time till the first dampness (h)	Avg. (h)	Time till leakage (h)	Avg. (h)	water content level (%)	Avg. (%)
Series I	I-F-1	1693	30.9	30.9	2.0	2.7	11.0	10.4	96.8	94.5
	I-F-2	1678	30.6	(0.9)	3.3		9.9		90.8	
type F	I-F-3	1722	31.4		1.7		10.1		94.4	
	I-F-4	1691	30.8		3.9		10.4		96.0	
Series I	I-R-1	1688	30.8	30.9	4.0	3.4	8.4	8.8	93.3	94.8
	I-R-2	1692	30.9	(0.5)	4.2		6.9		89.9	
type R	I-R-3	1692	30.9		3.2		9.4		98.5	
	I-R-4	1710	31.2		2.3		10.4		97.6	
Series I	I-AF-1	1717	31.3	31.0	2.0	2.7	8.5	8.2	92.2	87.6
	I-AF-2	1684	30.7	(0.7)	2.8		9.4		89.8	
type	I-AF-3	1700	31.0		3.0		6.6		80.8	
AF	I-AF-4	1696	30.9		3.1		–		–	
Series II	II-F-1	1154	21.0	21.4	3.5	2.6	8.1	9.4	90.1	93.4
	II-F-2	996	18.2	(10.0)	3.2		15.0		97.1	
type F	II-F-3	1226	22.4		1.7		7.3		95.2	
	II-F-4	1316	24.0		1.8		8.0		91.2	
Series II	II-R-1	1286	23.5	20.5	2.6	2.3	7.8	8.6	96.0	94.5
	II-R-2	1076	19.6	(10.4)	1.8		8.2		91.8	
type R	II-R-3	1170	21.3		3.3		11.0		96.7	
	II-R-4	970	17.7		1.6		7.5		93.5	
Series II	II-AF-1	1068	19.5	19.6	1.6	2.7	11.1	9.0	92.7	93.0
	II-AF-2	1074	19.6	(2.7)	2.8		6.6		89.9	
type	II-AF-3	1116	20.4		3.2		9.0		96.0	
AF	II-AF-4	1036	18.9		3.1		9.1		93.2	

Table 4
Water penetration in terms of time elapsed till leakage, amount of penetration, rate of penetration, and leakage (ratio between the penetrated and applied water) percentage.

	Specimens	Time till leakage (h)	Avg. (h)	Penetration (kg/m^2)	Avg. (kg/m^2)	Penetration rate (kg/m^2/h)	Avg. (kg/m^2/h)	Leakage after penetration start (%)	Avg. (%)
Series I	I-F-1	11.0	10.4	1.1	2.0	0.10	0.16	1.5	2.6
	I-F-2	9.9		2.2		0.18		2.8	
type F	I-F-3	10.1		2.7		0.22		3.5	
	I-F-4	10.4		1.9		0.16		2.5	
Series I	I-R-1	8.4	8.8	3.5	3.3	0.25	0.24	3.9	3.9
	I-R-2	6.9		2.8		0.19		3.0	
type R	I-R-3	9.4		6.3		0.49		7.8	
	I-R-4	10.4		0.6		0.05		0.8	
Series I	I-AF-1	8.5	8.2	3.5	4.4	0.26	0.31	4.1	4.9
	I-AF-2	9.4		5.9		0.45		7.2	
type AF	I-AF-3	6.6		8.0		0.52		8.2	
	I-AF-4	–		0.0		0.00		0.0	
Series II	II-F-1	8.1	9.4	3.5	3.7	0.25	0.26	3.9	4.1
	II-F-2	15.0		0.5		0.07		1.1	
type F	II-F-3	7.3		4.6		0.28		4.5	
	II-F-4	8.0		6.3		0.44		7.0	
Series II	II-R-1	7.8	8.6	3.9	2.7	0.27	0.18	4.3	2.9
	II-R-2	8.2		2.8		0.20		3.2	
type R	II-R-3	11.0		0.3		0.03		0.4	
	II-R-4	7.5		3.6		0.24		3.8	
Series II	II-AF-1	11.1	9.0	2.6	3.5	0.23	0.25	3.7	4.2
	II-AF-2	6.6		3.7		0.23		3.7	
type AF	II-AF-3	9.0		4.5		0.31		5.3	
	II-AF-4	9.1		3.3		0.25		4.0	

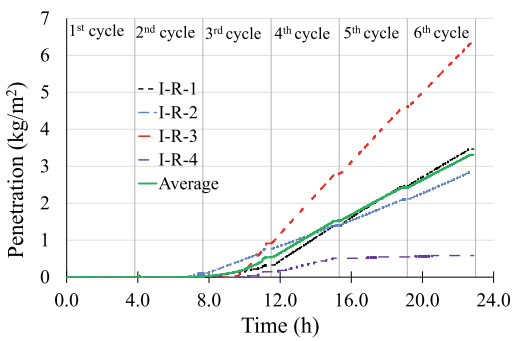

Fig. 5. Water penetration in the individual specimens of Series I type R.

3.2. Damp patches

Fig. 6 shows the time of emergence and location of the first visible dampness on the backside of the specimens. With some exceptions, the first visible dampness appears close to the brick–mortar interface in the vicinity of the head joint, as shown in Fig. 6. The obtained results indicate that the primary path for water to penetrate a brick masonry wall is through the brick–mortar interfacial zone due to the lower resistance of the brick–mortar interface, particularly at the head joint, to WDR [7,22,23,42]. The relatively low resistance of head joints to WDR may be related to the difficulty of workmanship to fill the head joints and to lower compaction compared with the bed joints [23].

Table 3 summarizes the time elapsed till the appearance of the first damp patch on the backside of the masonry triplets. On average, the first damp patch appears during the first test cycle, when the water content level of the specimens is approximately half of the saturation capacity (Fig. 7). Similar results were obtained by Kahangi Shahreza et al. [22] though the water spray rate varied between 1.7 and 3.8 l/m^2/h, indicating that the buffering capacity of masonry postpones the emergence of dampness on the sheltered side of masonry. Moreover, a considerable difference exists between the time elapsed till the emergence of dampness and the start of water penetration. In other cases, such as in specimen I-AF-4, the emergence of dampness (3.1 h) is not followed by any water penetration, an observation in line with the results obtained in Fishburn [19] and [20]. Once the first damp patch appears, mainly in the vicinity of the head joint, it typically spreads on the entire second course, including the head joint. The damp area then spreads over the bottom course and finally to the top course. The absorption, penetration, and dampness are illustrated together in Fig. 7.

4. Numerical analyses

4.1. Numerical model

Hygrothermal analysis of an external wall assembly in Gothenburg is conducted for the period 2000–2009 with WUFI Pro 6.5, commercial software for hygrothermal analysis of multi-layer building components. WUFI is based on hygrothermal models developed by Künzel [43], where coupled heat and moisture transport differential equations are solved by finite volumes. In WUFI, the liquid transport is limited to taking into account capillary conduction and surface diffusion mechanisms. As a limitation, hydraulic flow through pressure differentials has not been included. In this software, the temperature and relative humidity are the driving potential for heat and moisture transport through the material.

In this study, Gothenburg was chosen because it is one of the cities in Sweden with the highest exposure to WDR [1,44]. The studied period 2000–2009 was chosen because it is the period with relatively few missing segments of climate data. This analysis determines the moisture content variation in a common type of masonry wall assembly and demonstrates the effect of employing the suggested criterion for analyzing WDR penetration. The material properties used for simulating the bricks are based on a combination of values measured in this study (see Table 5, Brick type I) and are complemented with data from the literature.

For simplicity, the masonry wall is modeled as a homogenous layer, as suggested by Vereecken and Roels [45]. While this simplification comes with certain limitations [1], the corresponding analysis verifiably reproduces the general hygrothermal conditions of clay brick walls with

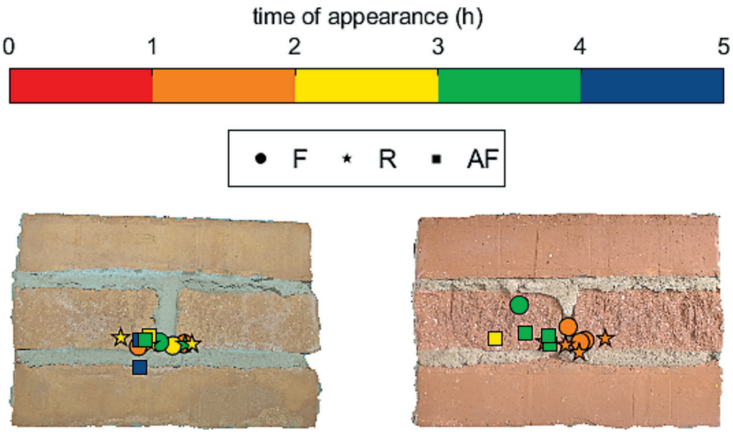

Fig. 6. Time and place at which the first dampness appears on the backside of the specimens.

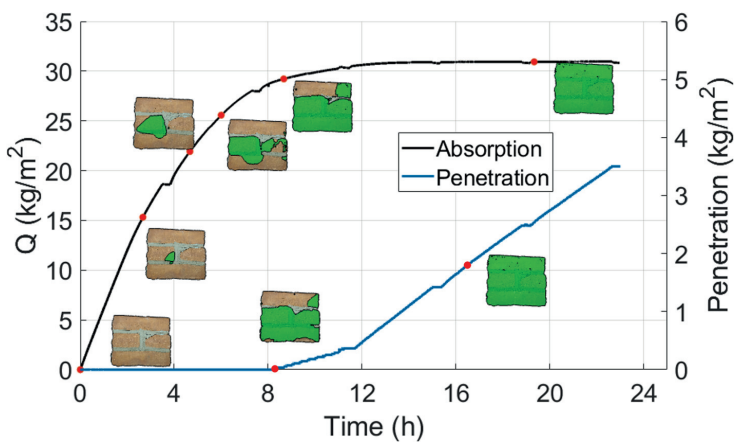

Fig. 7. Appearance and growth of dampness (green marking) on the backside of specimen I-R-1 at different times. (For interpretation of the references to color in this figure legend, the reader is referred to the web version of this article.)

Table 5
Material properties of the masonry used in the simulation.

Properties	Values for simulation
Bulk density (kg/m^3)	1800
Porosity (m^3/m^3)	0.293
Thickness (m)	0.12
Free water saturation (kg/m^3)	258
Water absorption coefficient (kg/m^2.s$^{1/2}$)	0.193
Thermal conductivity (W/mK)	0.6

acceptable accuracy [45,46]. Moreover, the 1D WUFI model of masonry used in this study is validated using the test results in terms of water absorption (water content), as shown in Fig. 8.

Fig. 9 shows the considered wall assembly. A constant airflow of 30 air changes per hour (ACH) [47,48] is considered for the air gap layer behind the masonry cladding.

4.1.1. Climate input

In this study, the hourly climate data, including rain intensity and

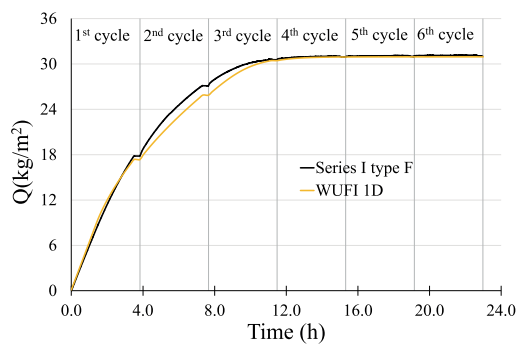

Fig. 8. Validation of the 1D WUFI model of masonry with respect to moisture absorption.

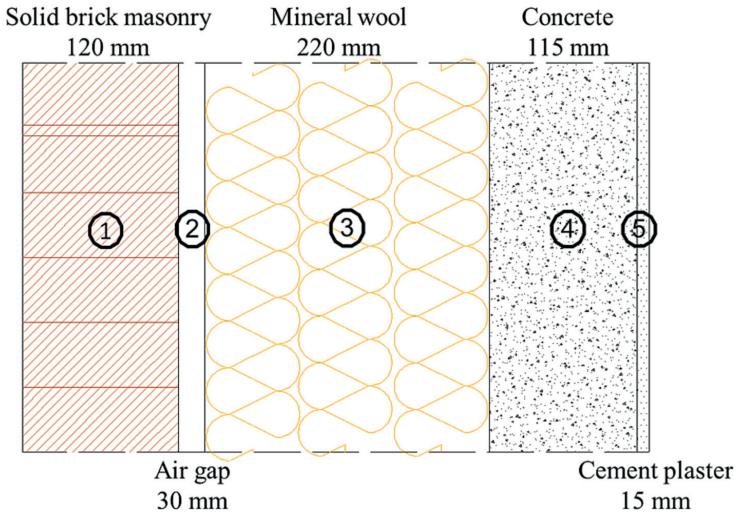

Fig. 9. Layers of the modeled wall in WUFI from outside (left): 1) solid brick masonry (120 mm), 2) air gap with ACH = 30 [1/h] (30 mm), 3) mineral wool insulation with thermal conductivity of 0.04 [W/m^{2}K] (220 mm), 4) concrete C 35/45 (115 mm), and 5) cement plaster (15 mm).

wind velocity, is obtained from the Swedish Meteorological and Hydrological Institute (SMHI) [49]. Since only the global radiation is available in the SMHI database and the numerical model also requires diffuse radiation, the latter was estimated based on a method proposed in [50], where the ratio of diffuse to global radiation is described as a set of stepwise linear functions for different intervals of global radiation. In general, the ratio of diffuse to global radiation decreases with increasing global radiation.

The wind-driven rain deposited on a façade is estimated as;

$$R_{WDR} = R_h(R_1 + R_2 U_w \quad (2)$$

where R_{WDR} is the driving rain intensity (mm/h), R_h is the hourly average rainfall intensity (mm/h), R_1 is a parameter for considering the wall angle relative to the vertical (-), R_2, WDR coefficient, is a wall factor for considering the effects related to the surroundings of the building and the building façade itself, and U_w is the orthogonal component of the mean wind velocity (m/s) incident on the wall surface. The wall orientation varies between the south and north, corresponding to high and low exposure to WDR, respectively. For vertical surfaces, R_1 is zero. The wall factor R_2 is estimated according to the ISO model [51], assuming the upper part of a 15 m high building with a flat roof is located in a terrain that is flat and free of obstructions. With these assumptions, R_2 for the given building façade is estimated to be 0.12 s/m. A more detailed description of how the WDR coefficient was calculated can be found in [22].

The WDR intensity calculated according to Eq. (2) is reduced by 10 % considering the fact that some water will bounce off the wall surface. While the default value used by WUFI is 30 %, the value used here is consistent with the observations in Section 3.1. The initial moisture content is set to the value of the typical built-in moisture according to the material database. The heat resistance of the exterior surfaces is set as wind-dependent. The average cloud index for the considered city is equal to 0.66 [49]. A time step of 1 h is used during the entire calculation period for the simulation.

4.1.2. Water content

Fig. 10 shows the water content of the simulated masonry façade between 2000 and 2009. Note that the considered wall facing south, the most exposed orientation to WDR, reaches capillary saturation during

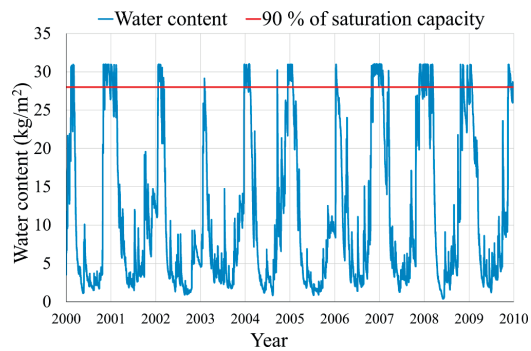

Fig. 10. Water content of masonry cladding in Gothenburg facing south according to simulation with WUFI 1D.

most of the winter periods. This result suggests a high probability of WDR penetration during winter, considering that a water content above 90 % of the saturation capacity is considered necessary for water penetration. As aforementioned, only masonry without imperfections is considered. Under real conditions, penetration may increase due to the poor contact between bricks and mortar as well as the presence of cracks.

Fig. 11 shows the water content in the wall facing north, the orientation with the lowest exposure to WDR in Gothenburg. As opposed to the south-facing wall (Fig. 10), the water content, in this case, exceeds 90 % of the saturation capacity only for a couple of days. Since the water content of the wall facing the least critical orientation concerning WDR rarely exceeds 30 % of the saturation capacity, a low probability exists of water penetration during the studied period, highlighting the benefit of the water absorption capacity of brick masonry.

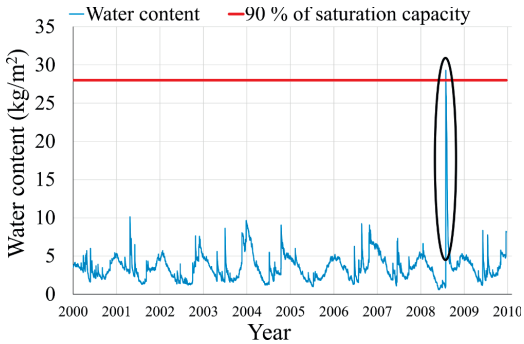

Fig. 11. Water content of clay brick masonry façade facing north in Gothenburg between 2000 and 2009 according to simulation with WUFI 1D.

5. Discussion

5.1. Influence of test parameters

5.1.1. Brick absorption properties

As mentioned in Section 2.1.1, two types of bricks with different absorption coefficients of 0.19 kg/(m^2.s$^{0.5}$) and 0.13 kg/(m^2.s$^{0.5}$) as well as water absorption capacities of 16.0 % and 8.6 % are used to study the effect of brick absorption properties on water absorption and water penetration in clay brick masonry. The obtained results show the significant effect of these brick properties on the water absorption behavior of masonry triplets. The water absorption coefficient of bricks influences the time it takes to reach surface saturation [1,12,22,30]. Furthermore, the total amount of absorbed water in masonry specimens is consistent with the water absorption capacity of the bricks. For example, the average amount of water absorption in the specimens of Series I with the average size of 255 mm × 215 mm is approximately 31.0 kg/m^2. Hence, on average, each masonry triplet with a thickness of 120 mm absorbed approximately 1700 g of water, equivalent to absorbing approximately 550 g in each brick (neglecting the amount of water absorption in mortar), which is consistent with the properties of bricks from type I (Table 1). Consequently, the water absorption properties of bricks are the dominant parameter in the water absorption response of masonry exposed to WDR.

On average, the water penetration in both Series starts when the water content is approximately 92 % and 93 % of the saturation capacity (Table 3), indicating the independence of the initiation of water penetration from brick absorption properties. Although the results indicate the usability of water saturation level as a criterion for initiating WDR penetration, the proposed criterion needs to be validated for a larger combination of bricks, mortars, and bricklaying methods.

Table 4 lists the water penetration rate for individual specimens. The average water penetration rate equals approximately 0.23 kg/m^2/h in both Series, but a large scatter exists on the individual level. The water penetration rate on individual levels varies between 0 and 0.52 kg/m^2/h despite using the same type of bricks. Several factors may contribute to the large scatter in the results: a) the quality of the workmanship to completely fill the joints may differ between specimens, and b) the contact between the brick and mortar may be inadequate in some specimens. Hence, the compatibility between the brick and mortar is important to ensure adequate bonding during design and bricklaying [22,23]. Moreover, the variability in the structure of bricks, e.g., the presence of cracks and defects, is an influential factor. Consequently, two bricks used in this study are saw cut to observe the structure of the bricks and the probable presence of cracks. Fig. 12 shows that several cracks and numerous voids exist in the structure of the bricks themselves, providing possible paths for water to penetrate. It should be noted that the primary pathway for water to penetrate is the brick–mortar interface, consistent with the visual observations made during both the present tests and other research studies [7,22,23]. However, deficiencies or cracks in the structure of the bricks might create additional pathways for moisture transport in masonry specimens; thus, water penetration might occur in a shorter period of time if saturation along the pathway is reached earlier. Although it was mentioned that the brick–mortar interface is the least resistant pathway,

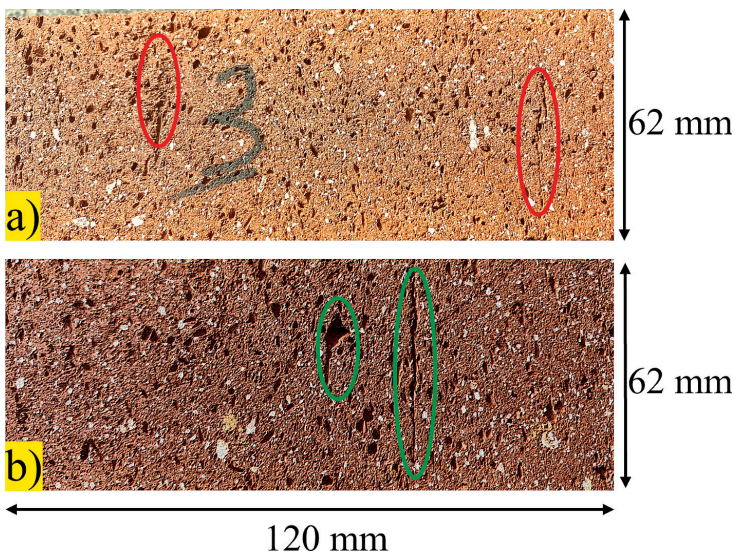

Fig. 12. Presence of micro-cracks in the structure of a) brick type I (saw cut perpendicular to the bed face along the length) and b) brick type II (saw cut perpendicular to the bed face along the width).

it is not the only possible one for water to penetrate.

5.1.2. Mortar joint profile

The experimental results indicate that no considerable difference exists between the amount of absorbed water in specimens prepared with different joint profiles. Furthermore, the mortar joint profile limitedly impacts both the water content level and initiation of water penetration (Table 3). Regardless of the type of joint profile, water penetration starts when the water content level exceeds 90 % of the saturation capacity.

Table 4 indicates that the rate of water penetration is not dependent on the joint profile. These results contradict previous findings [31,41], claiming that the effect of mortar joint profile on water penetration in masonry is substantial. This could be related to the fact that the test conditions of the mentioned studies, conducted as per ASTM E 514 standard [52] (water spray rate of 138 l/m^2/h and a pressure difference of 500 Pa), differ from the current study (water spray rate of 6.3 l/m^2/h without applying any air differential pressure). Furthermore, a comparison of the water penetration in specimens with raked joint profiles representing eroded mortar joints (type R) to the specimens with flush and after-pointed joint profiles (types F and AF) indicates that eroded mortar joints may limitedly affect the water absorption and water penetration in clay brick masonry exposed to WDR [22]. The depth of erosion is commonly used as a criterion for whether repointing is necessary [53], but the present results indicate that the depth of joint profile is a poor indicator of moisture performance.

5.2. Damp patches and water penetration

As shown in Fig. 6, there is a high concentration of points, representative of the appearance of the first dampness, in the vicinity of the head joint, indicating less resistance to moisture transport of head joints compared to the bed joints, as already observed by Slapø et al. [23]. This can be related to the difficulty of filling the head joint completely or less compaction than in the bed joint. After the first damp patch appeared, it grew on its surroundings and then usually spread over the bottommost course, which might be due to the gravitational forces. Eventually, dampness also appeared on the uppermost course and spread until the entire protected side of the specimen became damp.

The time elapsed till the emergence of the first damp patch on the backside of the specimens and the initiation of water penetration are summarized in Table 3; moreover, note that no correlation exists between the former and latter (Table 3 and Fig. 7), which is consistent with the results presented by Fishburn et al. [19] as well as Ritchie and Davison [42]. The Pearson correlation coefficient between the appearance of the first dampness and the timing of penetration start is 0.03 (p greater than 0.05), meaning that no significant correlation exists between the two metrics. For instance, the first dampness appears after 2.0 h and 3.3 h, and the first leakage is registered after 11.0 h and 9.9 h for specimens I-F-1 and I-F-2, respectively. Furthermore, the results indicate that the amount of water penetration is not associated with the emergence time of damp patches. Moreover, no water penetration is recorded for specimen III-F-3 though the first damp patch appears after only 0.3 h. In contrast, water penetration of specimen III-F-1 equals 0.9 kg/m^2, and the first dampness appears after 0.6 h on the backside of the specimen.

According to Table 4, the average percentage of leakage within each type of Series I and II varies between 2.6 % and 4.9 %. Herein, leakage is designated as the ratio between the amount of penetrated and sprayed water. The present results are consistent with the findings in a literature review conducted by Calle et al. [10] and Van Den Bossche et al. [12], indicating average leakage of approximately 0.005–3.3 %, with a minimum and maximum of 0 and 19.6 %. Comparing the leakage of individual specimens highlights the difficulty of quantifying water penetration in brick masonry, even when the same type of materials is used and bricklaying is accomplished by a skilled worker in a laboratory.

The difference between the time elapsed till the emergence of damp patches and the initiation of water penetration is that the former is predominately attributed to capillary transport from the exposed side to the backside; however, the latter is probably related to a laminar flow through larger pores and cracks with hydrostatic pressure as the driving force. Depending on the water saturation level, moisture transport in porous material may be generally governed by capillary suction or laminar flow [54]. As already mentioned in Section 3.2, dampness appeared on the backside of the specimens when the water content level was around half of the saturation capacity, indicating that capillary suction might have controlled the moisture transport. However, in the case of water penetration, it mostly occurred when the masonry specimens were nearly saturated (the water content level above 90 % of saturation capacity), highlighting that laminar flow might have governed the moisture transport. It should be noted that in the absence of a substantial air pressure difference, the occurrence of water penetration can be attributed to the gravitational effect of runoff and hydrostatic pressure as potential driving forces, which is consistent with findings in the experimental studies conducted by Calle et al. [10] and Straube and Brunett [16].

5.3. Use of the new criterion in hygrothermal analyses

The results stated in Section 4.1.2 show that there are several months during a year when the water content of the masonry cladding facing the most critical orientation with respect to WDR is greater than 90 % of saturation capacity, indicating a high risk of water penetration. Accordingly, if the climate does not favor drying or WDR events occur often, the masonry cladding will remain saturated or closely saturated; thus, the occurrence of rain penetration becomes more probable [29]. In contrast, the water content of the wall facing north, the least exposed side to WDR, rarely exceeds 30 % of its saturation capacity (Fig. 11); thus, a much lower probability of water penetration is expected compared to the south-facing masonry cladding.

According to the present study, water penetration starts when the water content of masonry exceeds 90 % of saturation capacity. Once water penetration starts, the average penetration rate for Series I and II specimens is approximately 3.8 %. In comparison, 1 % of the WDR penetrates through the cladding according to the ASHRAE Standard 160–2016 [14]. The amount of water penetration obtained from the ASHRAE Standard 160 and the criterion proposed in this study for the north-facing wall are shown in Fig. 13. According to the proposed criterion, the cumulative water penetration was close to zero from 2000 to 2009, except for a short period when the water content exceeded 90 % of saturation capacity (cumulative penetration of about 0.25 kg/m^2). In contrast, the cumulative penetration is approximately 3.5 kg/m^2 according to the ASHRAE Standard 160 (Fig. 13b). Thus, the ASHRAE Standard 160 may overestimate the water penetration in façades with limited exposure to WDR.

However, for the south-facing façade with the highest exposure to WDR at the studied location, the ASHRAE Standard 160 determines approximately 40 % lower cumulative water penetration compared to the proposed criterion, as shown in Fig. 14. In this case, the difference in estimated water penetration between the two criteria is rather limited. Yet, the proposed criterion in this study may provide a more differentiated moisture load, depending on the seasonal variation of the saturation level. Another sensitive difference between the ASHRAE Standard and the proposed criterion is the penetration rate, resulting in a stepwise pattern of the cumulative penetration when the latter is used. A more differentiated moisture load pattern may be important for designing wall assemblies that are susceptible to elevated moisture content.

5.4. Limitations and further considerations

The proposed criterion for water penetration is based on experimental results using two types of solid bricks and mortars, respectively. Clay brick masonry in real structures exhibits considerable variability

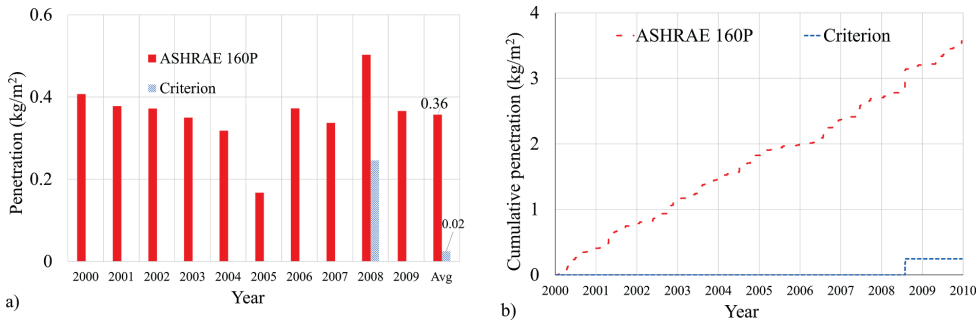

Fig. 13. a) Amount of yearly penetration and b) cumulative penetration for the studied north-facing wall during 2000–2009 according to the ASHRAE 160 standard and criterion introduced in this study.

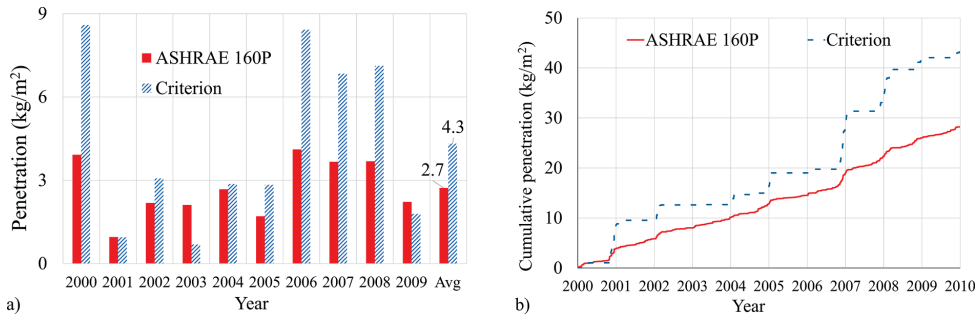

Fig. 14. a) Amount of yearly water penetration and b) cumulative water penetration according to ASHRAE 160 standard [14] and the criterion proposed in this study for the studied south-facing wall.

concerning the properties of raw materials, brick manufacturing, bond pattern, and workmanship during bricklaying. Thus, it is reasonable to assume that this variability significantly influences WDR-related water penetration. Clearly, the water penetration criterion proposed in this article must be seen as an attempt to explore the opportunities by using an easily accessible criterion for water penetration in clay brick claddings – average water content. It should be noted that the averaged total moisture content is not directly linked to local water penetration in the vicinity of joints. Yet, the strong correlation between the start of penetration and 90 % global water content suggests that water content can still be used as an indicator for the start of water penetration. Some limitations of the presented results and further considerations that might be clarified by future research are discussed below.

In the understanding of the authors, water penetration can take place when:

1. A pathway with a low resistance to laminar flow exists through the masonry.
2. The pathway and its surroundings are saturated.
3. There is a driving force that makes water stream through the pathway.

Concerning the first requirement, the results in this and previous research indicate that the interfacial zone between the bricks and mortar joints is often the primary pathway for water penetration. Head joints are specifically identified as a pathway for water penetration since they are more difficult to fill and compact than bed joints. In the present research, the triplet specimens were built with only one head joint. Although this configuration probably lowered the incidence of undesired disintegration of the specimens, it also meant that the percentage of head joints was lower than in real-world masonry – regardless of the bond type. With more head joints, the water penetration rate per unit wall area would increase. In addition, increasing the mortar-to-brick ratio could potentially result in lower saturation levels at penetration, as the water absorption coefficient of mortar is lower than for brick. At the same time, increasing the number of head joints per specimen could lead to an increased saturation level at penetration by reducing the volume of moisture buffering material available per pathway. The 90 % figure can be considered an approximate value in this case.

Besides the interfacial zones, there might be additional pathways for penetration, such as cracks and voids in the bricks and in the mortar joints. Cracks may significantly change the response of masonry claddings to water penetration since they may create interconnected cavities with a low resistance to water flow. Thus, studying the resistance of cracked masonry against WDR may produce more conclusive results concerning the criteria for water penetration, which can be beneficial for the precision of hygrothermal simulations. Perforated bricks are often encountered in clay brick claddings. Perforations might further facilitate water penetration because the empty volume can easily be filled with free water.

The thickness of the specimens in the present research was 120 mm, which is a frequent dimension in older Swedish clay brick claddings. From an international perspective, the thickness of clay brick claddings varies considerably, typically between 85 and 140 mm. For thinner masonry claddings, the penetration may relate to an even higher level of water content rather than the water content level proposed in this study. In contrast, the increased wall thickness may reduce the saturation level

at the start of water penetration.

Concerning the second requirement, it is reasonable to expect that wetting of the surface of the pathway must take place before a laminar flow is established. Since the pathway goes through brick and mortar, water is absorbed by capillary suction. When penetration starts, the vicinity of the pathway might be close to full saturation. This assumption is underpinned by the results in the present research, where, once it started, an almost constant penetration rate was observed.

Keeping in mind the large variability in moisture transport properties of different types of bricks and mortars, the average saturation level in a wall at the start of water penetration might differ from the criterion proposed in this paper. One could expect that in masonry with bricks having a low absorption coefficient, water penetration might start at a lower average water content since volumes farther away from the immediate proximity of the pathway might get saturated more slowly.

Concerning the third requirement, hydrostatic pressure from the water film formed on the exposed surface of the specimens has reasonably acted as a driving force in the present research. This assumption is confirmed by the observation that the water penetration stopped within approximately 10 – 20 s after stopping the water spraying.

In the present research, a water spray rate of 6.3 $l/m^2/h$ was used. In a real-world situation, the intensity of WDR might vary in a considerably larger range. Under conditions prevailing in Northern Europe, the intensity of WDR events often would be lower [1,44]. At lower WDR intensities, a thinner water film is expected, which might generate a lower driving force. The opposite should apply for higher WDR intensities. Furthermore, it is expected that runoff is more intense in the lower parts of a facade than higher up, especially when the surface of the wall is saturated. To generalize the water penetration criterion proposed in this paper, more research needs to be carried out to elucidate the role of runoff intensity on water penetration.

The experiments in the present research were carried out without applying an external air pressure difference. Since a certain wind pressure is always present during WDR events, incorporation of its effect in water penetration models seems essential. In this context, the wind pressure is expected to increase the driving force created by the runoff.

6. Conclusions

The research presented in this paper investigates the water penetration in clay brick masonry, resulting in a proposal of a novel criterion for water penetration. Masonry triplets with varying brick properties and mortar joint profiles are exposed to a uniform water spray with a rate of approximately 6.3 $l/m^2/h$, using a test setup capable of: a) measuring water absorption and water penetration in masonry specimens and b) tracking damp patches on the backside of specimens. Based on the results, the following conclusions can be drawn:

1. Water penetration starts when the water content reaches 90 % of the saturation capacity of masonry.
2. For the two types of studied masonry, no significant differences are registered concerning either the saturation level at the start of water penetration or penetration rate.
3. The average water penetration rate is approximately 4 % of the applied spray rate, with individual rates varying between 0 and 8 %. Once started, the penetration rate remains constant during the exposure to water spraying.
4. No significant difference is registered concerning water absorption or water penetration in the masonry specimens prepared with flush, raked, or after-pointed joint profiles.
5. The dampness on the backside of masonry appears at 50 % saturation. No strong correlation is observed between the time elapsed till the appearance of dampness and the start of water penetration, indicating that they are governed by capillary transport and laminar flow, respectively.
6. In contrast to the widely used ASHRAE Standard 160, the proposed water penetration criterion provides a more differentiated water accumulation in masonry claddings, with a pattern that periodically may imply high moisture loads.

CRediT authorship contribution statement

Seyedmohammad Kahangi Shahreza: Methodology, Validation, Visualization, Writing – original draft, Data curation, Formal analysis, Investigation. **Jonas Niklewski:** Validation, Visualization, Writing – review & editing, Supervision, Investigation. **Miklós Molnár:** Conceptualization, Supervision, Writing – review & editing, Project administration.

Declaration of Competing Interest

The authors declare that they have no known competing financial interests or personal relationships that could have appeared to influence the work reported in this paper.

Data availability

Data will be made available on request.

Acknowledgments

The authors gratefully acknowledge the financial support from SBUF - The Development Fund of the Swedish Construction Trade (grant 13576) and TMPB - The Masonry and Render Construction Association.

References

[1] P. Johansson, S. Geving, C.E. Hagentoft, B.P. Jelle, E. Rognvik, A.S. Kalagasidis, B. Time, Interior insulation retrofit of a historical brick wall using vacuum insulation panels: Hygrothermal numerical simulations and laboratory investigations, Build. Environ. 79 (2014) 31–45.
[2] M. Abuku, H. Janssen, S. Roels, Impact of wind-driven rain on historic brick wall buildings in a moderately cold and humid climate: Numerical analyses of mould growth risk, indoor climate and energy consumption, Energy Build. 41 (2009) 101–110.
[3] K. Calle, N. Van Den Bossche, Sensitivity analysis of the hygrothermal behaviour of homogeneous masonry constructions: Interior insulation, rainwater infiltration and hydrophobic treatment, J. Build. Phys. 44 (6) (2021) 510–538.
[4] M. Vanpachtenbeke, J. Langmans, J. Van den Bulcke, J. Van Acker, S. Roels, Modelling moisture conditions behind brick veneer cladding: Verification of common approaches by field measurements, J. Building Phys. 44 (2020) 95–120.
[5] M.L.M. Nascimento, E. Bauer, J.S. de Souza, V.A.G. Zanoni, Wind-driven rain incidence parameters obtained by hygrothermal simulation, J. Building Pathol. Rehabil. 1 (2016) 1–7.
[6] M.H. Salonvaara, A.N. Karagiozis, The influence of waterproof coating on the hygrothermal performance of a brick façade wall system, ASTM Spec. Tech. Publ. 1314 (1998) 295–312.
[7] C.J.W.P. Groot, J.T.M. Gunneweg, The influence of materials characteristics and workmanship on rain penetration in historic fired clay brick masonry, Heron 55 (2010) 141–154.
[8] H.M. Künzel, D. Zirkelbach, J. Radon, Hygrothermal consequences of rainwater leaks investigated for different wall structures with exterior insulation, 1st Central European Symposium on Building Physics (CESBP), Cracow, Poland, 2010, pp. 209–213.
[9] H.M. Künzel, D. Zirkelbach, Influence of rain water leakage on the hygrothermal performance of exterior insulation systems, in: Proceedings of the 8th Nordic Symposium on Building Physics in the Nordic Countries, 2008, pp. 253–260.
[10] K. Calle, C. Coupillie, A. Janssens, N. Van Den Bossche, Implementation of rainwater infiltration measurements in hygrothermal modelling of non-insulated brick cavity walls, J. Build. Phys. 43 (6) (2020) 477–502.
[11] K. Carbonez, N. Van Den Bossche, H. Ge, A. Janssens, Comparison between uniform rain loads and point sources to simulate rainwater leakage with commercial HAM-models, In International Symposium on Building Pathology (ISBP 2015), FEUP Edições.
[12] N. Van Den Bossche, M. Lacasse, A. Janssens, Watertightness of masonry walls: an overview, 12th International Conference on Durability of Building Materials and Components (XII DBMC-2011), FEUP Edições, 2011, pp. 49–56.
[13] S. Van Linden, N. Van Den Bossche, Review of rainwater infiltration rates in wall assemblies, Build. Environ. 219 (2022), 109213.
[14] ASHRAE, Standard 160-2016. Criteria for Moisture-Control Design Analysis in Buildings, ASHRAE Atlanta, GA, 2016.

[15] H.H. Saber, M.A. Lacasse, T.V. Moore, M. Nicholls, Mid-rise wood constructions: investigation of water penetration through cladding and deficiencies, Report to Research Consortium for Wood and Wood-Hybrid Mid-Rise Buildings, 2014.
[16] J.F. Straube, E.F.P. Burnett, Rain control and screened wall systems, Proceedings of the 7th Conference on Building Science and Technology. Durability of Buildings. Design, Maintenance, Codes and Practices, Toronto, 1997, pp. 20–21.
[17] S. Kahangi Shahreza, M. Molnár, J. Niklewski, Water absorption and penetration in clay brick masonry exposed to uniform water spray, 14th Canadian Masonry Symposium, Montreal, Canada, 2021.
[18] T. Ritchie, W.G. Plewes, A review of literature on rain penetration of unit masonry, Technical Paper (National Research Council of Canada, Division of Building Research), 1957.
[19] C.C. Fishburn, D. Watstein, D.E. Parsons, Water permeability of masonry walls, US Department of Commerce, National Bureau of Standards, 1938.
[20] C.C. Fishburn, Water permeability of walls built of masonry units, US Department of Commerce, National Bureau of Standards, 1942.
[21] J.F. Straube, E.F.P. Burnett, Driving rain and masonry veneer, Water Leakage Through Building Facades, ASTM International, 1998.
[22] S. Kahangi Shahreza, J. Niklewski, M. Molnár, Experimental investigation of water absorption and penetration in clay brick masonry under simulated uniform water spray exposure, J. Building Eng. 43 (2021), 102583.
[23] F. Slapø, T. Kvande, N. Bakken, M. Haugen, J. Lohne, Masonry's resistance to driving rain: Mortar water content and impregnation, Buildings 7 (2017) 70.
[24] K.B. Anand, V. Vasudevan, K. Ramamurthy, Water permeability assessment of alternative masonry systems, Build. Environ. 38 (2003) 947–957.
[25] J.C.Z. Piaia, M. Cheriaf, J.C. Rocha, N.L. Mustelier, Measurements of water penetration and leakage in masonry wall: Experimental results and numerical simulation, Build. Environ. 61 (2013) 18–26.
[26] T. Ritchie, A small-panel method for investigating moisture penetration of brick masonry, Internal Report (National Research Council of Canada, Division of Building Research); no. DBR-IR-160, 1958.
[27] T. Ritchie, W.G. Plewes, Moisture penetration of brick masonry panels, ASTM Bulletin 249 (1961) 39–43.
[28] T. Ritchie, Rain penetration of walls of unit masonry, Canadian Building Digest no. CBD-6 (1960).
[29] J.F. Straube, Moisture control and enclosure wall systems, Doctoral Dissertation, University of Waterloo, 1998.
[30] J.I. Knarud, S. Geving, T. Kvande, Moisture performance of interior insulated brick wall segments subjected to wetting and drying–A laboratory investigation, Build. Environ. 188 (2021), 107488.
[31] T. Hines, M. Mehta, Effect of mortar joints on the permeance of masonry walls, Proceedings of the 9th International Brick/Block Masonry Conference, Berlin, Germany, 1991, pp. 1227–1234.
[32] H.J.P. Brocken, Moisture transport in brick masonry-the grey area between bricks, Doctoral dissertation, TU Delft, Delft University of Technology, 1998.
[33] C. Hall, W. D. Hoff, Water Transport in Brick, Stone and Concrete (3rd ed.). CRC Press (2021). https://doi.org/10.1201/9780429352744.
[34] H. Derluyn, P. Moonen, J. Carmeliet, Moisture transfer across the interface between brick and mortar joint. In Proceedings of the Nordic Symposium on Building Physics 2008 (Vol. 2, pp. 865-872).
[35] J. Knarud, S. Geving, T. Kvande, Experimental Investigation of Capillary Absorption Along Mortar-Brick Interface Plane, on Building Physics, Dresden, Germany, 2016.
[36] ASTM C67/C67M-20, Standard Test Methods for Sampling and Testing Brick and Structural Clay Tile, ASTM International, West Conshohocken, PA, 2020.
[37] ASTM C1403-15, Standard Test Method for Rate of Water Absorption of Masonry Mortars, ASTM International, West Conshohocken, PA, 2015.
[38] "Weber Saint-Gobain Sweden AB" [Online]. Available: https://www.se.weber/fasad-puts-och-murbruk-produkter-och-system/murbruk/weber-gullex-murbruk-m-25. [Accessed July 2022].
[39] "Målarkalk Sweden AB" [Online]. Available: https://www.malarkalk.se/produkter/kalkbruk/nhl-bruk/kalkbruk-nhl35. [Accessed July 2022].
[40] P. Jonell, T. Moller, Moisture Penetration of Solid Facing Brick Walls, Technical Translation (National Research Council of Canada); no. NRC-TT-618, 1956.
[41] Brick Industry Association, Water Penetration Resistance – Construction and Workmanship, Technical Notes on Brick Construction, Brick Industry Association, 12007 Sunrise Valley Drive, Suite 430, Reston, Virginia 20191.
[42] T. Ritchie, J.I. Davison, Factors affecting bond strength and resistance to moisture penetration of brick masonry, ASTM Spec. Tech. Publ. 320 (1963) 16–30.
[43] H. M. Künzel, Simultaneous heat and moisture transport in building components. One-and two-dimensional calculations using simple parameters, Doctoral Dissertation, IRB-Verlag Stuttgart 65 (1995).
[44] M. Kahangi, Resistance of Clay Brick Masonry Façades to Wind-Driven Rain - Repointing of Eroded Mortar Joints, Licentiate Thesis, Lund University (2021).
[45] E. Vereecken, S. Roels, Hygric performance of a massive masonry wall: How do the mortar joints influence the moisture flux? Constr. Build. Mater. 41 (2013) 697–707.
[46] V.M. Nik, S.O. Mundt-Petersen, A.S. Kalagasidis, P. De Wilde, Future moisture loads for building facades in Sweden: Climate change and wind-driven rain, Build. Environ. 93 (2015) 362–375.
[47] J. Falk, K. Sandin, Ventilated rainscreen cladding: Measurements of cavity air velocities, estimation of air change rates and evaluation of driving forces, Build. Environ. 59 (2013) 164–176.
[48] S.O. Mundt-Petersen, L.E. Harderup, Validation of a 1D transient heat and moisture calculation tool under real conditions, Thermal Performance of the Exterior Envelopes of Whole Buildings XII, 2013.
[49] https://www.smhi.se/data. (Accessed September 2020).
[50] S.O. Mundt-Petersen, P. Wallentén, Methods for compensate lack of climate boundary data, XIII International Conference on Durability of Building Materials and Components, 2014, pp. 632–639.
[51] EN ISO 15927-3, Hygrothermal Performance of Buildings-Calculation and Presentation of Climatic Data. Part 3: Calculation of a Driving Rain Index for Vertical Surfaces from Hourly Wind and Rain Data, European Committee for Standardization (2009).
[52] ASTM E514/E514M-14a, Standard Test Method for Water Penetration and Leakage Through Masonry, ASTM International, West Conshohocken, PA, 2014.
[53] B. Brief, Maintenance of brick masonry, Brick Industry Association, Technical Notes on Brick Construction, 46 (2017) 1–11.
[54] L. Mengel, H.W. Krauss, D. Lowke, Water transport through cracks in plain and reinforced concrete–Influencing factors and open questions, Constr. Build. Mater. 254 (2020), 118990.

Paper IV

Impact of different water penetration criteria and cavity ventilation rates on the risk of mold growth in timber frame walls with brick veneer cladding

S Kahangi Shahreza[1, a)], A Abdul Hamid[2]

[1] *Division of Structural Engineering, Department of Building and Environmental Technology, Lund University, John Ericssons väg 1 SE-223 63 Lund, Sweden*
[2] *Division of Building Physics, Department of Building and Environmental Technology, Lund University, John Ericssons väg 1 SE-223 63 Lund, Sweden*

[a)] *Corresponding author:* mohammad.kahangi@kstr.lth.se

Abstract. The present paper investigates the impact of different water penetration criteria on the risk for damage in a common type of building envelope in Nordic countries, timber frame walls with brick masonry veneer. The studied walls are evaluated based on one damage criterion, the risk of mold growth. The study investigates several parameters: water penetration criterion, type of moisture source (uniformly distributed or point source) and its position in the wall assembly, air change rate (ACR) (representing different workmanship scenarios), wind-driven rain (WDR) coefficient, and locations (Gothenburg and Rensjön, with different average annual rainfall and temperature). Two criteria on how to implement water penetration are compared: a) a commonly accepted reference model that assumes one percent of all wind-driven rain deposited on the façade to penetrate the clay brick cladding, and b) a new criterion stating that 3.8% of WDR penetrates when the water content of the brick veneer cladding is above 90% of its saturation capacity. The simulation is done for a thirteen-year period with WUFI Pro and WUFI 2D. The results indicate the greater importance of implementing water penetration compared to ventilation in cavities. Further, the findings suggest that the moisture source's location significantly impacts the mold growth risk. The results also show that the choice of the WDR coefficient affects the risks, which suggests that this factor needs accurate quantification for hygrothermal analyses. The results in this study suggest that an effective measure for the design/maintenance of such walls should incorporate: a) limiting the amount of water penetrating through the cladding, particularly stopping water from reaching the sensitive elements, i.e., timber studs, b) removing extruded mortar stemming from poor workmanship, if any, which may act as a capillary bridge.

Keywords: hygrothermal simulation, water penetration, brick masonry veneer, timber frame wall, mold growth

1. Introduction

Multifamily residential buildings with clay brick masonry cladding are common in Nordic countries. The design of walls with brick veneer cladding is done in a way that the cladding prevents the entry of rainwater deposited on the facade. In addition, a cavity is provided in the form of a ventilated air gap

which allows the drainage of penetrated water and minimizes the amount of water reaching the interior side of the wall assembly. Such ventilated cavity also results in pressure equalization, which should improve the hygrothermal performance of the wall and allow for air exchange and drying of the wall [1]. In Sweden, around one-third of the existing buildings were constructed as a part of the so-called million program housing project between 1965 and 1974, with timber frame walls with brick veneer cladding as a common wall type [2]. Although walls with brick cladding efficiently shield against wind-driven rain (WDR), exposure to WDR is associated with the risk of water penetration. Furthermore, such buildings can lack proper design and contain deficiencies, such as cracks and voids that facilitate rain penetration, a costly issue promoting microbiological growth and affecting the hygrothermal performance of building envelopes [3]. Many of the existing buildings from this era are in need of renovation, for instance, due to the presence of mold growth. As a general maintenance scheme in Nordic countries, repointing of clay brick masonry is done after 40-50 years from erection to reduce water penetration through the masonry. Further, repointing is often claimed to prevent water ingress [4, 5] and avert internal dampness [6]. However, there is a need to quantify better the impact of repointing on water penetration, which is an important factor in hygrothermal analyses.

Water penetration through masonry claddings depends on several parameters categorized into two groups. The first group of parameters consists of characteristics of rain and wind, including rain intensity, raindrop size, wind velocity, and wind direction. The second group is related to the characteristics of the masonry, including material properties (absorption properties of brick and mortar), mortar water content, and joint thickness. However, masonry walls with the same prescribed characteristics may differ widely in performance due to workmanship during construction. A review of existing experimental studies shows that water penetration may vary between 0 and 7.2% of the sprayed water when no pressure difference is applied [7]. This range increases to approximately 36% in the case of brick masonry walls built with poor workmanship [7]. Because of the high uncertainties and dependencies on a number of parameters, there is no broad agreement on how much water penetrates through a masonry veneer.

Rain penetration is an essential factor in hygrothermal simulations of external walls. A commonly accepted assumption is that one percent of the deposited wind-driven rain (WDR) penetrates through the façade following the North American Standard, ASHRAE 160–2016 [8]. However, with such an assumption, the moisture buffering capacity of the masonry, which can postpone water penetration in brick masonry, is neglected. In order to mitigate this shortcoming, a new penetration criterion based on comprehensive experimental studies was recently proposed by Kahangi Shahreza et al. [9] (abbreviated as the KS criterion in this study). The criterion is dependent on the moisture content of masonry, stating that water penetration starts when the water content level is above 90% saturation capacity; afterward, approximately 3.8% of the deposited rain is considered to penetrate the facade. Implementing the ASHRAE standard results in a more continuous pattern of cumulative penetration, whereas a more differentiated moisture load pattern is obtained when the KS criterion is used [4].

In contrast to the many attempts available in research studies to quantify water penetration in brick masonry cladding, there is no consensus on where to place the moisture source in hygrothermal models and how to distribute it over a modeled wall [10, 11]. In a study done by Calle et al. [11], the hygrothermal performance of brick cavity walls was investigated by considering penetration criteria, moisture source types, and locations of moisture sources within hygrothermal modeling. Further, an analysis of the influence of the position of the moisture source (uniform rain loads and point sources) conducted by Carbonez et al. [12] showed that the implementation of an accurately defined local moisture source might have the potential to replicate reality. Moreover, as mortar might be extruded during bricklaying connecting the veneer to the inner part and acting as a capillary bridge, simulation of a point moisture source compared to the uniformly distributed moisture load approach may provide more realistic information concerning the hygrothermal performance of walls with brick veneer cladding. The lack of agreement between previous studies shows a need for an explicit implementation method for hygrothermal simulations to evaluate the impact on walls with masonry veneer cladding.

The main aim of this study is to investigate the effect of rain penetration on the risk of damage in timber frame walls with brick masonry veneer cladding while considering other factors that might affect the results. The considered parameters are water penetration criterion (ASHRAE 160-2016 [3] or Kahangi Shahreza et al. [4]), type of moisture source (uniformly distributed or point source) and its position in the wall assembly, air change rate (ACR) (0 h^{-1}, 10 h^{-1}, and 40 h^{-1} – representing different workmanship scenarios), wind-driven rain (WDR) coefficient, and locations (Gothenburg and Rensjön, with different average annual rainfall and temperature). This is done through hygrothermal analysis of a common external wall in Swedish buildings. Since mold growth is commonly reported concerning such walls, the risk of mold growth is evaluated accordingly. This can provide a better understanding that might be used in the assessment of such walls.

2. Method

Since determining the presence and extent of damage related to mold growth usually requires destructive excavating investigations, accurate hygrothermal modeling of the wall may lead to a better understanding prior to costly reparations. Also, by providing knowledge regarding influential parameters on the risk of mold growth, a more rational action can be taken into account during the design of such walls. A schematic of a timber frame wall with brick veneer modeled in this study is shown in Figure 1. The wall exemplified in Figure 1 was typically built in Sweden during the 1960s and 1970s.

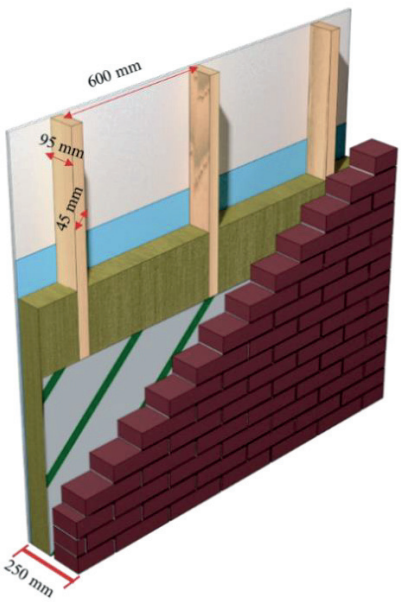

Figure 1. A typical schematic of a timber frame wall with brick veneer built in Sweden (thickness of ~ 250 mm) modelled in this study. Different layers of the wall assembly and their corresponding dimension from right side (exterior): brick masonry veneer (120 mm), air gap (20 mm), asphalt impregnated paper (1 mm), mineral wool insulation (95 mm), timber studs (95 mm × 45 mm) with center to center distance of 600 mm, vapor retarder (1 mm), and gypsum board (12.5 mm).

Three main damage criteria might be used to evaluate the performance of timber frame walls with brick veneer cladding: mold growth, decay of timber elements, and frost damage. This study evaluated the risk of mold growth at the surface of the timber studs, one of the most sensitive components in this type of wall. Since mold growth should be avoided, this is considered an absolute criterion. Two common models to determine the risk of mold growth are Viitanen's (VTT) model [13] and the mold resistance design (MRD) model. This study assessed all simulation results using the updated Viitanen's model implemented in WUFI. According to this empirical model, based on the obtained relative humidity and temperature, the growth level is expressed by the mold index M. A higher index indicates a higher risk of mold growth. Since the mold index was assessed at the surface of the timber stud element, the sensitivity class "sensitive" and decline class "relatively low decline" was assumed. The

different mold index classes that are used in the model are listed as follows: Mould index (M) of 0 ~ No mold growth, M = 1 ~ small amounts of mold on surface (microscope), M = 2 ~ <10% coverage of mold on surface (microscope), M = 3 ~ 10%–30% coverage of mold on surface (visual), M of 4 ~ 30%–70% coverage of mold on surface (visual), M of 5 ~ >70% coverage of mold on surface (visual), and M = 6 ~ tight and dense mold growth covers nearly 100% of surface.

3. Numerical model

The performance of the external walls was assessed using WUFI Pro [14] and WUFI 2D [15], two commercial software for hygrothermal analysis of multi-layer building components. Although modeling a brick veneer as a homogenous layer involves limitations, it has been shown that this simplification may provide acceptable results. Nevertheless, WUFI 2D was also used to calculate the two-dimensional heat and moisture flux through the construction and to analyze a more detailed moisture distribution and the interaction between the brick-mortar layer and the insulation-timber layer. In order to have a more appropriate long-term assessment of moisture accumulation, recent research studies suggest a minimum of ten years simulation period [16]. Thus, the analysis was carried out from 2000 to 2012. Two locations, namely Gothenburg and Rensjön, representative of different climate conditions in Sweden, were studied. As summarized in Table 1, the material properties used for simulating the walls are obtained from the literature [9] and the software database. In WUFI Pro (1D), the brick masonry cladding was modeled as a homogenous layer; however, in WUDI 2D, a head joint and a timber stud were also considered in the model. See Figure 2.a and Figure 2.b for illustrations of the WUFI Pro and WUFI 2D models of the wall. The 2D simulation considered a center-to-center distance of 600 mm between timber studs.

Table 1. Hygrothermal material properties.

Material	Thickness (mm)	Bulk density (kg/m^3)	Porosity (m^3/m^3)	Free water saturation (kg/m^3)	Vapor diffusion resistance (-)	Thermal conductivity (W/(mK))
Solid brick	120	1800	0.293	258.0	10	0.60
Lime cement mortar (used in WUFI 2D)	120	1880	0.280	210.0	50	0.60
Air cavity with moisture capacity (2 layers)	1	1.3	0.999	47.1	0.79	0.07
Air cavity-no additional moisture capacity	18	1.3	0.999	0.017	0.46	0.18
Asphalt impregnated paper	1	170	0.001	0.047	874	2.30
Mineral wool (used in WUFI 2D)	95	60	0.950	44.8	1.3	0.04
Spruce radial	95	455	0.730	600.0	130	0.09
Vapor retarder	1	130	0.001	0.047	10000	2.30
Gypsum board	12.5	850	0.650	400.0	8.3	0.20

The default value for the adhering fraction of rain, the fraction of the WDR available for capillary absorption, in WUFI Pro and WUFI 2D is 0.7, meaning that the WDR is reduced by 30% to account for the fact that some water would bounce off the wall surface. The value used in this study is 0.8, which is supported by experimental data [9, 17]. The initial conditions of the materials were assumed to be 17°C and 70% RH. The heat resistance of the exterior surfaces was set to be wind-dependent. A red clay brick façade was considered; thus, short-wave radiation was set according to red. The heat resistance of the interior surface was set to 0.125 (m^2.K/W). Nominally, a constant airflow (ACR) of 10 h^{-1} was considered to account for cavity ventilation. Since the climate file was prepared based on hourly data, the time step of 1 h during the calculation period was used for the simulation.

3.1. Climate input

Historical weather data, including hourly rain intensity, wind velocity, and wind direction, was obtained from the Swedish Meteorological and Hydrological Institute (SMHI) [18] for the studied locations. In order to compensate lack of data in the SMHI database for diffuse radiation, a method already presented in [19] was applied to estimate the diffuse radiation from global radiation. The average cloud index was considered to be equal to 0.69 and 0.70 for Gothenburg and Rensjön, respectively. The most critical

orientation with respect to WDR for walls in Gothenburg and Rensjön is south and north, respectively; thus, applied for each simulation.

Regarding the WDR coefficient, two methods are proposed in WUFI; the first one is dependent on the building height and the location on the façade, whereas the second model is per the ASHRAE 160-2016 standard [8]. Based on the former, for the upper part of a building with a height of more than 20m, the WDR coefficient is equal to 0.2 s/m. In contrast, in a building with severe exposure to WDR, according to the ASHRAE 160 standard [8], the coefficient equals 0.3 s/m. Nonetheless, according to the ISO model [20], an advanced and widely used semi-empirical model to quantify WDR, this value for a building located in a flat terrain free of obstructions is around 0.12 s/m [9]. Implementing different WDR calculation methods in the simulations of massive timber walls results in a significantly different indication concerning the risk of mold growth [21]. Moreover, long-term measurements of WDR indicate that results obtained by the ISO model [20] were 0.5–0.8 times that of the measured values, whereas the findings obtained by the ASHRAE 160–2016 standard [8] were 1.3–2.4 times greater than the experimental data (9). Thus, this study considers a WDR coefficient of 0.2 s/m, two-thirds of the value calculated by the ASHRAE 160-2016 standard and 1.7 times greater than that calculated by the ISO model in [9].

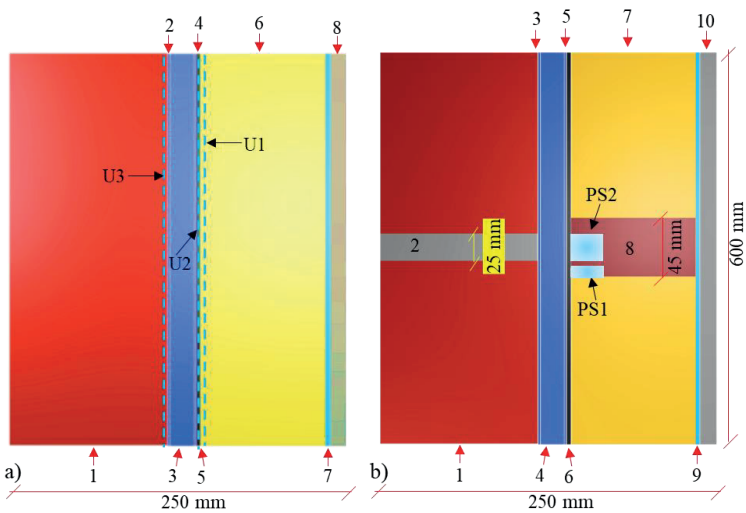

Figure 2. Layers of the modeled wall in **a) WUFI Pro**: 1) solid brick masonry, 2) air gap, 3) air gap without additional moisture capacity, 4) air gap, 5) asphalt impregnated paper (10 min paper), 6) mineral wool insulation, 7) vapor retarder, 8) gypsum board; **b) WUFI 2D**: from outside (left): 1) solid brick masonry, 2) cement lime mortar, 3) air gap, 4) air gap without additional moisture capacity, 5) air gap, 6) asphalt impregnated paper (10 min paper), 7) mineral wool insulation, 8) spruce stud, 9) vapor retarder, 10) gypsum board.
PS: The dotted lines (U1, U2, and U3) represent the uniform moisture sources, while the location of the point moisture sources is indicated with the surfaces (PS1 and PS2).

The internal climatic conditions were related to the outdoor temperature in Gothenburg and Rensjön, respectively, in accordance with the European Standard EN 15026 [22]. Accordingly, the indoor temperature was fixed at 20°C when the outdoor temperature was below 10°C and 25°C when it was above 20°C. While the ambient temperature varied between 10°C and 20°C, the interior temperature was set to alter linearly between 20°C and 25°C. Regarding the indoor relative humidity, a medium moisture load + 5% (a safety margin according to WUFI) was considered. The indoor relative humidity varied linearly between 35% and 65% when the ambient temperature was between −10°C and 20°C.

3.2. Parametric study

Different scenarios, as summarized in Table 2, assessing the impact of different parameters, were considered in simulations to investigate the effect on the hygrothermal performance of studied walls. The considered parameters are water penetration criterion (ASHRAE 160-2016 [8] or Kahangi Shahreza et al. [9]), type of moisture source (uniformly distributed or point source) and its position in the wall assembly, air change rate (ACR) (0 h^{-1}, 10 h^{-1}, and 40 h^{-1} – representing different workmanship scenarios), wind-driven rain (WDR) coefficient, and locations (Gothenburg and Rensjön, with different average annual rainfall and temperature).

In addition to the WDR coefficient of 0.2 s/m, a WDR coefficient of 0.3 s/m, according to the ASHRAE 160 standard [8], and a coefficient of 0.12 s/m, in accordance with ISO standard and taken from [17], were considered in order to investigate the effect of the WDR coefficient on the risk of mold growth. Since in 1-dimensional simulation, only a uniformly distributed moisture source can be implemented, 2D modeling was also considered to study the effect of a point moisture source.

Table 2. Overview of simulation methods and results in terms of mold growth index.

Scenarios	Location	Model	WDR Coeff (s/m)	Moisture source	Penetration criterion	ACR (h^{-1})	Time when M* reaches 3 (years)	Time at max M (years)	Max M (-)
A	Gothenburg	1D	0.2	-	0	10	6.81	12.82	3.36
B				U1	ASHRAE		0.93	8.21	5.28
C					KS**	0	0.91	8.90	5.30
D						10	0.92	8.90	5.30
E						40	0.96	8.22	5.30
F				U2	ASHRAE	10	4.82	12.89	3.75
G					KS		6.78	12.89	3.62
H				U3	ASHRAE		6.80	12.82	3.37
I					KS		6.81	12.82	3.36
J			0.12	U1	ASHRAE		1.76	7.06	5.01
K			0.3				0.83	8.21	5.30
L	Rensjön		0.2	-	0		-	1.73	1.06
M				U1	ASHRAE		-	4.77	2.30
N					KS		-	1.73	1.09
O	Gothenburg	2D	0.2	-	0	10	7.80	12.82	3.17
P				U1	ASHRAE		0.92	7.07	5.28
Q					KS		0.92	8.21	5.30
R				PS1	ASHRAE		1.13	7.06	5.13
S					KS		0.86	8.20	5.30
T				PS2	KS		0.41	7.06	5.30
U				PS2***		0	0.39	7.06	5.30
V	Rensjön			PS1	ASHRAE	10	-	4.77	2.03
W					KS		-	1.74	2.72

M*: mold index
U1: Uniformly distributed on the exterior surface of the timber stud – cut-off at max water content (3 mm)
U2: Uniformly distributed on the asphalt layer – no cut-off (1 mm)
U3: Uniformly distributed behind (on the interior of) the cladding – no cut-off (3 mm)
PS1: Point source on timber stud close to the contact zone with the insulation (10 * 3 mm^2)
PS2: Point source on timber stud in the same level as the extruded mortar joint (25 * 3 mm^2)
KS**: the criterion proposed by Kahangi Shahreza et al. [9]
0***: air gap partially filled with mortar to represent poor workmanship

As there is no agreement on where to place the moisture source in hygrothermal simulations, three locations within the wall assembly were considered in WUFI Pro (see Figure 2.a). In one case, a uniformly distributed moisture source was placed on the exterior of the insulation-timber stud layer with a width of 3 mm (U1), whereas in another case, it was placed on the asphalt-impregnated paper layer with a width of 1 mm (U2). In the third case, it was placed behind (on the interior of) the brick veneer with a width of 3 mm (U3). In WUFI 2D, a point moisture source (PS1 and PS2, see Figure 2.b) is implemented. In scenario PS1, a moisture source with a 10 mm × 3 mm surface was implemented close

to the interface zone between the timber stud and mineral wool insulation. Since mortar might be extruded behind the brick veneer, acting as a capillary bridge or filling the air gap, a localized moisture source (PS2) comprising an area of 25 × 3 mm^2 placed at the exterior of the mortar while modeling an extruded mortar joint was considered in the simulations. Further, two water penetration criteria, ASHRAE 160-2016 standard [3] and a recently proposed criterion by Kahangi Shahreza et al. [4], were implemented in the simulations (in the rest of the text, the latter is denoted by KS).

Despite the importance of the air change rate within the ventilated cavity on the hygrothermal performance of the building envelope [10, 23], its function in the case of masonry veneers can be impaired due to poor workmanship/extruded mortar. One way to incorporate the effect of workmanship thus can be applying different scenarios for the ventilation in the cavity or modeling extruded mortar joints, consequently acting as a capillary bridge in the wall and reducing the air change rate. Although an ACR of 400 h^{-1} was predicted numerically for air cavities behind the brick as an external cladding material [23], in most cases, the measured value of air change rates was lower than 50 h^{-1} (7). As a reference value, an ACR of 10 h^{-1} was considered in the simulations; however, in order to study the impact of air ventilation on the mold growth risk, ACRs of 0 h^{-1} and 40 h^{-1}, representing poor and good workmanship, were considered. In one scenario, denoted as PS2***, to represent poor workmanship, a point moisture source with a surface of 25 × 3 mm^2 was placed on the timber stud at the same level as the extruded mortar joint, while the air gap was partially filled with mortar, leading to an ACR of 0 h^{-1}.

4. Results and discussion

4.1. Mold growth assessment

The results of the maximum mold index (M) and its corresponding time for each simulation, and the corresponding time when the mold index reaches 3, are summarized in Table 2.

Generally, a high risk of mold growth can be seen in timber frame walls with brick masonry veneer, particularly those exposed to large amounts of WDR. Thus, the results suggest that the most influential parameter is exposure to WDR, which agrees with the findings of Hamid et al. [24]. An observation that supports this is that the mold index of walls in Renjsön (maximum: 2.72) is lower than that in Gothenburg scenario O (minimum: 3.17), which did not include any rain penetration. Further, during the first year, the walls in Gothenburg reached a mold index of 3. In contrast, the mold index was lower than 3 during 13 years of simulations for walls located in Rensjön.

The results indicate that the moisture source's position significantly affects the wall's risk of mold growth. The mold index of 5.30 is obtained when the moisture source is placed at the exterior of the timber stud (U1), whereas this value is equal to 3.75 when the moisture source is placed on the asphalt layer. Thus, although water penetration in walls should be reduced, particularly in locations with high exposure to WDR, close attention should be paid to preventing the water from reaching the moisture-sensitive element, timber studs in this case. Figure 3 shows no great difference between the ASHRAE 160 standard and KS criterion regarding the maximum mold index, comparing walls located in Gothenburg and modeled in WUFI Pro and WUFI 2D with two different water penetration criteria. In contrast, as shown in Figure 3, the maximum mold growth for wall V (located in Rensjön and based on ASHRAE 160) reaches 2.03 after 4.77 years, while the maximum mold growth equals 2.72, occurs only after 1.74 years for wall W (located in Rensjön and based on the KS criterion). This can be related to the fact that a sudden increase in moisture load pattern is obtained when the KS criterion is used, whereas implementing the ASHRAE standard results in a stepwise pattern of cumulative penetration [4]. Hence, the findings show that the hygrothermal performance of walls located in areas with relatively low exposure to WDR is affected by implementing different water penetration criteria.

In the case of Gothenburg, the results indicate that the impact of the ventilation rate in the air cavity on the maximum mold index is minimal. Interestingly, the maximum mold index was reached earlier, after 8.22 years, in wall E with an ACR of 40 h^{-1}, compared to the walls with ACR of 0 h^{-1} and 10 h^{-1}, where the maximum reaches after 8.90 years. The results, in this case, indicate that a high air ACR may lead to an increased risk for mold growth. However, this study analyzed the impact of different ACRs in simulations and considered only one position for the moisture source, U1. Other positions in the wall

might reduce the risk of mold growth by increasing the drying of the wall. However, the results obtained in this study agree with field and theoretical studies done by Salonvarra et al. [25], showing that cavity ventilation may not necessarily improve the drying of the wall.

Results in Table 2 suggest that the WDR coefficient impacts the mold growth rate. For wall J with the WDR coefficient of 0.12 s/m, it takes around 1.76 years to reach the mold index of 3. This time is reduced to 0.93 years and 0.83 years when the WDR coefficient of 0.2 s/m and 0.3 s/m is used, respectively. However, the difference between the maximum mold index when different WDR coefficients are implemented can be considered marginal, i.e., the maximum mold index equals 5.01 for wall J, while it is equal to 5.28 and 5.30 for B and K, respectively. The obtained results indicate that there is a high risk of mold growth in locations with high exposure to WDR, even when a lower value of rain load, a smaller value of WDR coefficient, is considered in simulations.

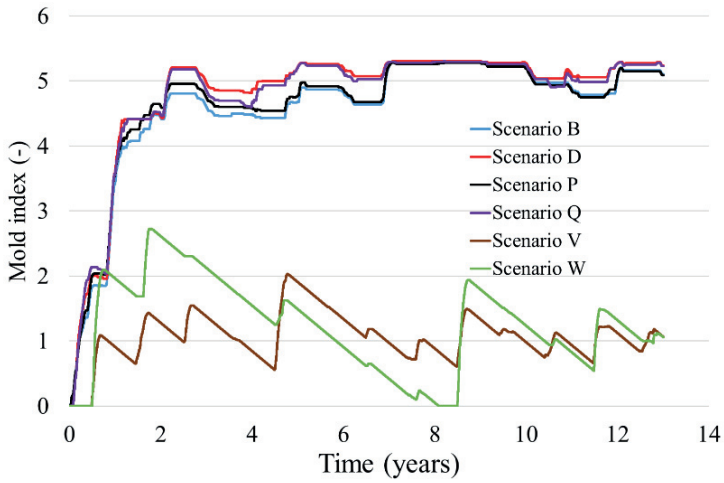

Figure 3. Mold index of scenarios B, D, P, Q, V, and W during the 13 years of the studied period.

A comparison of results from simulations for the wall in Gothenburg (Figure 3) conducted with WUFI Pro (scenario B) with simulations for the same wall but conducted with WUFI 2D (scenario P) shows a minuscule difference. However, the divergence in results between WUFI Pro and WUFI 2D is larger for Rensjön (V, W), a location with low WDR loads. Furthermore, the results in Table 2 indicate that placing a uniformly distributed moisture source (U1) is similar to modeling a point moisture source (PS1). However, the risk of mold growth is slightly lower when a point moisture source is considered in the simulations.

The impact of extruded mortar acting as a capillary bridge on the hygrothermal performance of the wall is noticeable. The mold index of 3 occurs in less than half a year for walls T and U, where the extruded mortar is in contact with the asphalt layer. In contrast, it takes approximately one year to reach the mold index of 3 for walls where the mortar is not extruded. Hence, it is vital to ensure that during the erection of a wall, mortar joints do not extrude to the extent that results in capillary bridges between the brick veneer and sensitive materials. For existing buildings, excess mortar should be removed during renovation. However, this is likely to be time-consuming and costly. Thus, at the erection of a building, it should be beneficial to ensure a wide air cavity that reduces the risk of issues due to extrusions.

It should be noted that the current study was an attempt to highlight the importance of influential parameters on the hygrothermal performance of a typical wall in Swedish buildings. Accordingly, this study has shown a high risk of mold growth for timber-frame walls with brick veneer in regions with high exposure to WDR, regardless of the choice of leakage model, simulation tool, or input parameters.

Thus, the results indicate that careful consideration should be made before designing/ constructing such walls within areas similar to the Gothenburg climate.

It should also be mentioned that providing realistic simulation parameters is often afflicted with practical difficulties and might imply high costs. For instance, assessing the factual state of an air gap behind a brick veneer or the integrity of an aged plastic sheet is practically difficult. Hygrothermal simulations as a risk-analysis tool should therefore be combined with reality checks. Regarding timber frame walls, such reality checks might imply monitoring moisture content or physical inspection of the wall.

4.2. Recommendations and limitations

The analysis of the results suggests that an effective measure for the design/maintenance of timber frame walls with brick masonry veneer should incorporate the following steps: a) limiting the amount of water penetrating through the cladding, particularly stopping water from reaching the sensitive elements, i.e., timber studs and b) removing extruded mortar, if any, which may act as a capillary bridge and reduce air ventilation within cavity due to poor workmanship.

Based on the obtained results in this study, rain penetration was shown to be the most influential among different parameters affecting the risk of mold growth on timber studs. Therefore, repointing, besides other maintenance techniques such as surface grouting and water repellent [26], can reduce leakage in brick masonry cladding. Thus, repointing can be an effective way to lower the risk of mold growth. However, there is a need to better quantify the effect of repointing on reducing water penetration in brick masonry. It should be noted that various uncertainties are included in the mentioned mitigation strategies, affecting their effectiveness and risk of mold growth which thus needs to be taken into consideration. However, it should be noted that as the risk of mold growth in such walls is high, particularly in regions with high exposure to WDR or constructed with poor workmanship, such as extruded mortar, repointing of mortar joints may not provide any significant improvement. Nevertheless, in the case of poorly constructed walls containing cracks or poor quality brick-mortar interface, facilitating water penetration as the least resistance pathway, maintenance techniques such as repointing or other surface treatments may improve the hygrothermal performance of such walls.

5. Conclusions

The present study has aimed to facilitate an understanding of the influential parameters on the hygrothermal performance of timber frame walls with brick masonry veneer. The obtained results indicate that the risk of mold growth in timber frame walls with brick masonry veneer is high in locations with high exposure to WDR. Further, among the considered parameters, the position of the moisture source considerably affects the modeled hygrothermal response of the studied wall in terms of mold growth index. The mold growth risk depends on the water penetration criterion implemented in the simulation, though the impact is more significant for the location with less exposure to WDR. The findings suggest a need to quantify better the amount of water penetrating the cladding and the portion reaching the sensitive elements such as timber studs.

Based on the obtained results, the following steps are recommended to be considered during the design/maintenance of such walls: a) reducing the amount of water penetrating cladding, particularly preventing water from reaching the sensitive elements, i.e., timber studs, and b) improving the workmanship by avoiding extruding the mortar during bricklaying or remove any extruded mortar joint during renovation, since it has a high potential to act as a capillary bridge.

The recently provided penetration criterion, KS, is provided for brick masonry cladding without any cracks/voids. In addition, the default value of water penetration in the ASHRAE 160-2016 standard does not distinguish between different cladding qualities. However, since cracks/voids may provide additional pathways with a low resistance to water penetration, there is a need to study the response of cracked masonry exposed to WDR, which may produce a more comprehensive criterion for water penetration. As many existing buildings contain cracks, a more accurate water penetration criterion can be beneficial for the precision of hygrothermal simulations.

6. Acknowledgments
The authors gratefully acknowledge the financial support from SBUF - The Development Fund of the Swedish Construction Industry (grant 13576), and TMPB - The Masonry and Render Construction Association.

7. References
[1] Van Linden S. Fourth Generation Watertightness: A Performance-Based Strategy to Control Rainwater Infiltration in Façade Systems: Ghent University; 2022.
[2] Janson U, Berggren B, Henrik S. Energieffektivisering vid renovering av rekordårens flerbostadshus. 2008.
[3] Gustavsson T, Gunilla B, Gustafsson E, Nilsson L-O, Persson M, Sikander E. Fuktsäkra byggnader: en nulägesbeskrivning. Malmö universitet; 2022.
[4] Fishburn CC, Watstein D, Parsons DE. Water permeability of masonry walls: US Department of Commerce, National Bureau of Standards; 1938.
[5] Wright E. Assessment of Water Damage in a Mass Masonry Wall Building. Building Science and the Physics of Building Enclosure Performance: ASTM International; 2020.
[6] Tc RHM. RILEM TC 203-RHM: Repair mortars for historic masonry. Materials and Structures. 2012;45(9):1295-302.
[7] Van Linden S, Van Den Bossche N. Review of rainwater infiltration rates in wall assemblies. Build Environ. 2022;219:109213.
[8] Standard A. Standard 160-2016: Criteria for Moisture Control Design Analysis in Buildings. American Society of Heating, Refrigerating and Air-Conditioning Engineers, Atlanta. 2016.
[9] Kahangi Shahreza S, Niklewski J, Molnár M. Novel water penetration criterion for clay brick masonry claddings. Construction and Building Materials. 2022;353:129109.
[10] Wang L, Defo M, Xiao Z, Ge H, Lacasse MA. Stochastic Simulation of Mould Growth Performance of Wood-Frame Building Envelopes under Climate Change: Risk Assessment and Error Estimation. Buildings. 2021;11(8):333.
[11] Calle K, Coupillie C, Janssens A, Van Den Bossche N. Implementation of rainwater infiltration measurements in hygrothermal modelling of non-insulated brick cavity walls. Journal of Building Physics. 2020;43(6):477-502.
[12] Carbonez K, Van Den Bossche N, Ge H, Janssens A, editors. Comparison between uniform rain loads and point sources to simulate rainwater leakage with commercial HAM-models. International Symposium on Building Pathology (ISBP 2015); 2015: FEUP Edições.
[13] Viitanen H, Ojanen T. Improved model to predict mold growth in building materials. Thermal Performance of the Exterior Envelopes of Whole Buildings X–Proceedings CD. 2007:2-7.
[14] Zirkelbach D, Schmidt T, Kehrer M, Künzel H. Wufi® Pro–Manual. Fraunhofer Institute. 2007.
[15] Zirkelbach D, Schmidt T, Künzel H, Kehrer M, Bludau C. WUFI® 2D. Fraunhofer Institute for Building Physics. 2007.
[16] Nath S, Dewsbury M, Künzel H, Watson P. Mould Growth Risks for a Clay Masonry Veneer External Wall System in a Temperate Climate. Atmosphere. 2022;13(11):1755.
[17] Kahangi Shahreza S, Niklewski J, Molnár M. Experimental investigation of water absorption and penetration in clay brick masonry under simulated uniform water spray exposure. Journal of Building Engineering. 2021;43:102583.
[18] https://www.smhi.se/data: SMHI, "SMHI Öppna data";
[19] Petersen SM, Wallentén P, editors. Methods for compensate lack of climate boundary data. XIII International Conference on Durability of Building Materials and Components, 2014; 2014.
[20] EN ISO 15927-3, Hygrothermal performance of buildings-Calculation and presentation of climatic data. Part 3: calculation of a driving rain index for vertical surfaces from hourly wind and rain data. European Committee for Standardization; 2009.

[21] Defo M, Lacasse MA, Snell N. Assessing the climate resilience of buildings to the effects of hygrothermal loads: impacts of wind-driven rain calculation methods on the moisture performance of massive timber walls. National Research Council of Canada. Construction; 2019 2019/04/30.
[22] 15026 E. Hygrothermal performance of building components and building elements. Assessment of moisture transfer by numerical simulation2007.
[23] Rahiminejad M, Khovalyg D. Review on ventilation rates in the ventilated air-spaces behind common wall assemblies with external cladding. Build Environ. 2021;190:107538.
[24] Hamid AA, Wallentén P. Hygrothermal assessment of internally added thermal insulation on external brick walls in Swedish multifamily buildings. Build Environ. 2017;123:351-62.
[25] Salonvarra M, Karagiozis AN, Pazera M, Miller W, editors. Air cavities behind claddings-what have we learned. Thermal Performance of the Exterior Envelopes of Whole Buildings Tenth International Conference; 2007.
[26] Ghanate K, Khanverdi M, Das S. Wind-driven rainwater penetration through brick veneer with and without surface treatments. Journal of Building Engineering. 2022;62:105347.

Paper V

Construction and Building Materials 420 (2024) 135631

Contents lists available at ScienceDirect

Construction and Building Materials

journal homepage: www.elsevier.com/locate/conbuildmat

Water penetration in cracked clay brick masonry before and after repointing

Seyedmohammad Kahangi Shahreza

Division of Structural Engineering, Department of Building and Environmental Technology, Lund University, John Ericssons väg, Lund 1 SE-223 63, Sweden

ARTICLE INFO

Keywords:
Clay brick masonry
Cracked masonry
Water penetration
Repointing
Saturation level
Dampness

ABSTRACT

This research study investigates the response of clay brick masonry with different crack widths before and after repointing subjected to water spray. In doing so, 3-course masonry prisms containing artificial cracks were exposed to a water spray during 23 hours of testing. Forty-nine cracked 3-course masonry prisms were prepared with a crack width varying between 0.3 mm and 0.9 mm, whereas thirteen specimens were built without known cracks for comparison. The results indicate a reasonable correlation between the crack width and the average water penetration rate. Compared to the reference specimens, those with crack widths of 0.3, 0.5, 0.7, and 0.9 mm showed average water penetration rates of 1.7, 2.4, 3.0, and 5.1 times higher, respectively. Further, a strong correlation was observed between the saturation level and the start of water penetration. In the reference specimens, water penetration started when the water content reached above 90% of the saturation capacity. Depending on the crack width, water penetration in the cracked specimens started when the saturation level was between 72 – 87%. The specimens were repointed and once again exposed to water spray. On average, the water penetration rate decreased by around 54% in the reference specimens and between 47 – 74% in the specimens with cracks. Raking of the specimens during repointing revealed that many head joints contained voids and gaps, confirming that head joints are probably the weakest part of clay brick masonry concerning water penetration. The results show that repointing has the potential to significantly reduce water penetration in clay brick masonry with and without known cracks exposed to water spraying.

1. Introduction

Clay brick masonry façades are widely used in Northern Europe and North America because of their high durability and reliable long-term performance. Although brick-cladding walls efficiently shield against wind-driven rain (WDR), exposure to WDR is associated with the risk of rain penetration. Further, such buildings can lack proper design and contain deficiencies such as cracks and voids, facilitating rain penetration. Rain penetration accounted for approximately half of the dampness problems in buildings [1,2], promoting microbiological growth [3,4], deteriorating timber-based wall elements, and compromising indoor air quality [1,5].

Water penetration due to WDR occurs as a result of several factors, including deposition, driving forces, and structures that permit its passage [6]. The deposited water on a masonry façade can be transported through the wall in several different ways; the brick-mortar interfacial zone is often cited as the path offering the least resistance [7–10]. Likewise, many masonry façades contain cracks stemming from moisture and temperature movements combined with frequent freeze-thaw cycles or dynamic loading, further facilitating leakage [4,11–14].

Since many real-world clay brick façades are far from flawless [11, 13], assessing the effects of defects such as cracks on water accumulation and penetration might provide a more risk-aware judgment of the moisture safety performance of the building envelope. Previous studies concerning water penetration through cracked concrete and masonry have shown that the amount of water passing through a crack is related to factors such as the crack width and the water pressure [11–13,15,16]. However, relatively few research studies are available in the literature investigating the impact of cracks on the resistance of clay brick masonry to water spraying [11,12].

Since cracks, in addition to the brick-mortar interface, provide paths for water to penetrate, there is a need for maintenance of such masonry façades. Repointing, the process of raking out the existing mortar up to around 25 mm and replacing it with a new mortar, is often claimed as a measure to reduce water penetration in masonry façades [10,12,17–19]. The decision on repointing is often taken without clear evidence that repointing will prevent water penetration in the renovated walls [20] and is carried out as part of a regular maintenance scheme 40–50 years

E-mail address: mohammad.kahangi@kstr.lth.se.

https://doi.org/10.1016/j.conbuildmat.2024.135631
Received 12 December 2023; Received in revised form 11 February 2024; Accepted 26 February 2024
Available online 2 March 2024

from the erection. While repointing of mortar joints is a commonly used long-term solution to improve the WDR resistance and the aesthetic condition of brick masonry claddings [21,22], this approach can be costly and may not necessarily result in improved permeability of the building façade [18,21,23].

Despite the importance of water penetration on the hygrothermal performance of building envelopes, it is generally simplified in research because of a lack of input data [4]. Currently, 1% of WDR deposited on a façade is considered to penetrate behind the cladding, in accordance with the North American Standard (ASHRAE 160–2021) [24]. However, Kahangi Shahreza et al. [25] conducted an experimental study on initially dry masonry where a criterion for water penetration in clay brick masonry is introduced. The moisture content equivalent to 90% of saturation capacity is considered a criterion for the start of water penetration. Yet, that study focused on masonry without any known cracks and deficiencies. Since cracks are accounted as a path facilitating water penetration in clay brick masonry, the current criteria for water penetration cannot be representative of many historical and existing façades containing cracks and deficiencies. Thus, similar to the introduced criterion in [25], this study aims to introduce a new benchmark, dependent on the moisture content level of masonry and water penetration rate, which can be used as an input for hygrothermal simulations.

The present paper aims to investigate the effect of crack width on the response of brick masonry exposed to uniform water spray. A 3-course masonry prism with an artificial crack located on a bed joint with a length of 50 mm, a nominal width size ranging between 0.3 – 0.9 mm, and a depth of 120 mm were prepared. For comparison, thirteen masonry specimens without cracks or known defects were tested in parallel. Subsequently, the specimens were repointed to study the impact of repointing on water penetration. The specimens were exposed to uniform water spray with an average rate of around 7 l/m^2/h without applying air differential pressure. Water absorption and penetration were measured continuously, providing information about the water content level of masonry, the time to start, and the amount of water penetration. A benchmark for water penetration in cracked masonry in relation to the crack width and water content of masonry is proposed, which can be further used in the hygrothermal assessment of existing and historical brickwork.

2. Material and methods

2.1. Material properties

A common type of solid clay brick in the Swedish construction market was used to build 3-course masonry prisms. The brick, identified as Röd Marktegel, is a red solid clay brick provided by Wienerberger AB. It possesses a compressive strength of 45 MPa, falls under durability class F2, indicating frost resistance suitable for various building conditions and exposure levels, and belongs to tolerance class T1. Tests were done according to the ASTM C67 [26] and ASTM C1403–15 [27] standards to determine the water absorption properties of bricks, including the initial rate of absorption (IRA), 24-hour water absorption capacity, and water absorption coefficient. Both the stretcher and bed face of the bricks were tested. In order to determine the water absorption coefficient (A_w), 15 bricks were tested in accordance with the ASTM C1403–15 standard [27]; the bricks were immersed in water at a depth of 3–5 mm for a specified period. The increase in mass due to water absorption was recorded at intervals of 1, 5, 10, 20, 30, 60, 120, 180, and 240 minutes. The amount of absorbed water per unit area of the brick Q [kg/m^2] is defined as the ratio between the difference of increased weight (w_i [kg]) and initial weight (w_0 [kg]) and the cross-sectional area of the brick A [m^2] (Eq. (1)).

$$Q = \frac{w_i - w_0}{A}[kg/m^2] \tag{1}$$

Q (kg/m^2) is plotted against the square root of time [t$^{1/2}$] to display the test results, as shown in Fig. 1. The tangent to the first linear branch of the Q – t$^{1/2}$ function is the mathematical definition of the water absorption coefficient A_w [kg/(m^2.s$^{0.5}$)].

Further, mortar M 2.5, a cement-based mortar, was used to build the specimens, whereas the repointing was done with mortar M 1, a widely used mortar for repointing brick masonry in Sweden. Mortar M 2.5, provided by Weber Saint-Gobain, consists of a binder comprising Portland cement and lime filler combined with natural sand ranging in size from 0 to 3 mm with a compressive strength of more than 2.5 MPa. Mortar M 1, provided by Finja Betong, features a binder with cement and lime, characterized by a lower cement ratio compared to Mortar M 2.5.

Ten 100-mm cubes were tested for each mortar type to determine their absorption properties using the same methods described for bricks. In order not to damage the mortar cubes and avoid cracking, specimens were dried out at a temperature of around 65°C in a climate box. Table 1 summarizes the material properties of the bricks and mortars used in this study.

The porosity of both brick and mortar is determined indirectly using an empirical equation (Eq. (2)) from [28,29], which establishes a strong correlation between sorptivity and material porosity:

$$S = 25.2 \bullet f^{2.3} \tag{2}$$

where S [mm/min$^{1/2}$] is the sorptivity and f [-] is the porosity. The sorptivity is calculated as the ratio between the water absorption coefficient, A_w [kg/(m^2.s$^{0.5}$)], and the density [kg/m^3] of water.

2.2. Masonry specimens

In total, 62 masonry prisms with length, height, and thickness of 250 ± 2 mm, 218 ± 2 mm, and 120 ± 2 mm were built by a professional bricklayer. The study involved constructing forty-nine specimens with a crack length of 50 mm and width ranging from 0.3 mm to 0.9 mm in their bed joint, whereas thirteen specimens without any crack were left as reference specimens for comparison. Since the bricks used in this study can be categorized as medium-suction bricks, the specimens were built without pre-wetting of the bricks, which is consistent with the recommendations given by the brick manufacturer. Fig. 2 shows different steps to prepare 3-course masonry prisms with different crack widths. Plastic strips with a width of 50 mm and a nominal thickness of 0.3, 0.5, 0.7, and 0.9 mm were placed on the first brick before mortar M 2.5 was applied to the bed joint. Two brick halves were laid on the first layer before filling the head joint from the top and front sides. In the next step, the bed joint was pointed with mortar, and the third course of brick was placed on the top. Eventually, a wooden stick was used to compact the mortar joints and have a flush joint profile. When removing the plastic strips, great care was taken to avoid damaging the specimens. A suitable time to remove the plastic strip was achieved by trial and error on a large number of dummy specimens. The appropriate time for taking out the strip is when the mortar is neither hardened nor loose. In the case

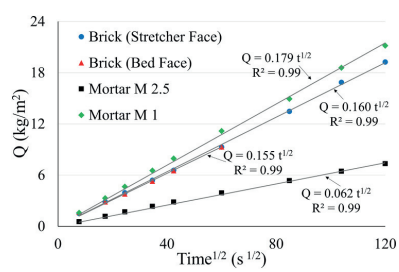

Fig. 1. Average water absorption per unit area, Q (kg/m^2) against the square root of time for stretcher and bed face of brick and for mortar M 1 and 2.5 during the initial stage of the test.

Table 1
Material properties of brick and mortars, including density, IRA, 24 h water absorption, and water absorption coefficient (A_w).

Materials	Dimensions (mm × mm × mm)	Density ρ (kg/m^3)	IRA (kg/(m^2. min))	CoV (%)	24-h water absorption (%)	CoV (%)	A_w (kg/(m^2. s$^{0.5}$))	CoV (%)	Sorptivity S (mm/min$^{1/2}$)	Porosity f (-)
Brick stretcher face	250 × 120 × 62	2029	1.51	11.4	8.6	11.1	0.160	13.2	1.239	0.268
Brick bed face			1.64	9.7			0.155	12.1	1.201	
Mortar M 2.5	100 × 100 × 100	1653	0.55	9.6	10.9	4.9	0.062	9.0	0.480	0.179
Mortar M 1	100 × 100 × 100	1607	1.59	9.4	14.0	1.1	0.179	4.8	1.386	0.283

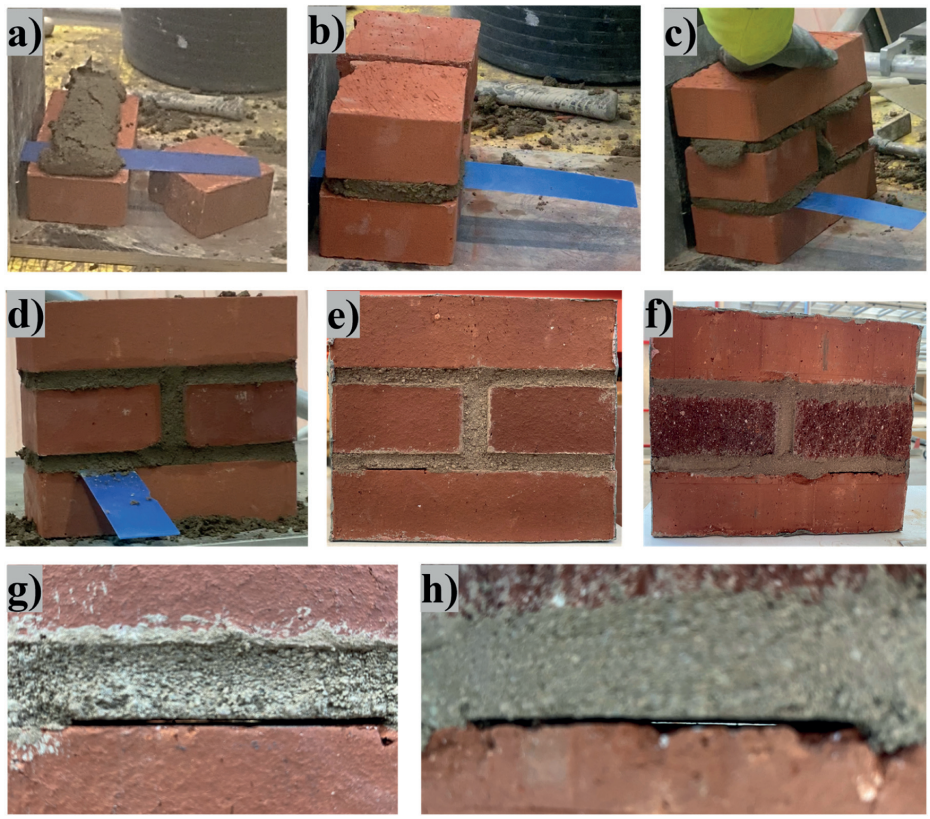

Fig. 2. Preparation of specimens with an artificial crack: a) laying the first brick course and placing a plastic strip to create the crack, b) applying mortar in the first bed joint, c) placing the third brick course, d) a 3-course masonry prism prior to removing the plastic strip, e & f) front view and backside, and g & h) close-up view of the created crack.

of hardened mortar, the mortar could loosen while removing the strip, whereas the crack could close in the case of loose mortar.

Specimens were categorized into groups G0, G03, G05, G07, and G09, depending on the width of the crack. Group G0 included thirteen masonry prisms manufactured without any known defects. Groups G03 and G05 consist of specimens with a crack width ranging between 0.25 – 0.35 mm (average 0.3 mm) and 0.45 – 0.55 mm (average 0.5 mm), respectively. Specimens with a crack width ranging between 0.65 – 0.75 mm (average 0.7 mm) and 0.85 – 0.95 mm (average 0.9 mm) belong to groups G07 and G09, respectively. Specimens were named following the notation X-N. For example, specimen G07–4 is the fourth specimen of group G07 with a crack width of around 0.7 mm. It is important to note that for the sake of simplicity, the term "cracked masonry" is used throughout the rest of the text to refer to masonry specimens with artificially created cracks. All masonry prisms were sealed in plastic bags in the laboratory for 28 days at a temperature of around 22°C. The specimens were wetted and then resealed during the curing process. Subsequently, in order to categorize the cracked specimens, a blade gap gauge was used to estimate the crack width.

The masonry specimens in this study were constructed with artificial cracks resembling voids or openings. It is important to note that these artificial cracks may not fully replicate the complicated nature of real

cracks in brickwork. Even though there was a trade-off in realism, the purpose of creating artificial cracks was to guarantee control and reproducibility. Unlike actual cracks, which can undergo dynamic changes in size and form over time due to environmental factors [12, 14], the introduced voids in the specimens were designed as a simplified representation. In order to simulate cracked structures more realistically, it is recommended that larger wall specimens be subjected to environmental movements or imposed loads to simulate real crack structures accurately. However, it should be noted that achieving precise control over crack size might pose challenges.

The masonry specimens were repointed after an experimental campaign involving exposure to water spraying approximately four months after the manufacturing. Firstly, the mortar was raked out up to a depth of around 25–30 mm. A mortar rake blade and a raking bit were used to rake out bed and head joints, respectively, as shown in Fig. 3.a and b. Subsequently, specimens were cleaned from dust and gently washed with water. A mortar type M 1 was used the day after to repoint the specimens. A skilled craftsman filled the joints manually, using a wooden stick to compact the joints. The repointed specimens were cured for 28 days in the laboratory before testing in a second exposure to water spray.

2.3. Test setup

As shown in Fig. 4, the test setup is equipped with two scales measuring the amount of absorbed and penetrated water, respectively. The occurrence and spread of dampness on the backside of the specimens were tracked using a digital camera. A ColorChecker was used for further color correction, and the camera recorded an image every 2 minutes. Water pressure regulators and a water flow meter were employed to adjust the water spray rate and minimize variations in the water flow.

The specimens were exposed to an average water spray rate of around 7 $l/m^2/h$ without applying any differential air pressure. Each test included six consecutive cycles, in total 23 h; each cycle lasted 210 min of water spraying with a subsequent 20 min of pausing. Before testing, a two-component sealant was applied on all sides of 3-course masonry prisms except the front face (exposed area) and the specimens' backside to avoid undesired water absorption.

Different test setups have been proposed in standards and research studies to investigate water penetration in masonry, where the ASTM E514 standard [30] is the most widely used test method. This standard has been established based on the early research done by Fishburn et al. [17] and Fishburn [31], where the test condition of the standard includes a water spray rate of 138 $l/m^2/h$ in combination with a differential air pressure level of 500 Pa, which represents infrequently occurring extreme weather conditions.

Despite being one of the most frequently used test methods in studies to investigate water penetration through masonry walls, the test conditions of ASTM E514 [30] standard represent extreme driving rain conditions that can only occur at specific locations (such as hurricanes in Miami), with very low frequencies, as analyzed by Cornick and Lacasse [32]. Furthermore, Ribar [33] suggests that current test standards need to be revised to incorporate a realistic exposure condition approach. Additionally, the range of WDR events in Sweden [10] indicates that the water application rate of 138 $l/m^2/h$ and differential air pressure of 500 Pa is extreme for the Swedish climate. Moreover, according to the field measurements and literature review by Straube and Burnett [34], driving rain deposition rates of more than 5 – 10 $1/m^2/h$ are rarely encountered, even on tall buildings.

Consequently, the first criterion for developing a test setup was lowering the water spray rate compared with the test conditions of ASTM E514 to represent a more realistic range of WDR events. In response to the limitations of ASTM E514, adjustments to the differential air pressure were made by Forghani et al. [35], reducing it from 500 Pa to 45 Pa. Other studies, such as those conducted by Anand et al. [36] and Lacasse et al. [37], carried out tests with a range of differential air pressures from 0 to 750 Pa. Rathbone [38] and Hens et al. [39] conducted experimental studies with masonry walls subjected to water spray rates between 2.0 and 6.4 $l/m^2/h$.

The second motivation for developing a new test setup was to address the need for continuous measurement of water absorption and moisture content in masonry throughout testing, a feature not feasible with the current ASTM E514 setup. Continuous measurement of water absorption (mass gain) provides valuable insights into the moisture content of masonry at the start of water penetration. While many research studies use high water spray rates and differential air pressure to study the resistance of saturated masonry, the developed test setup

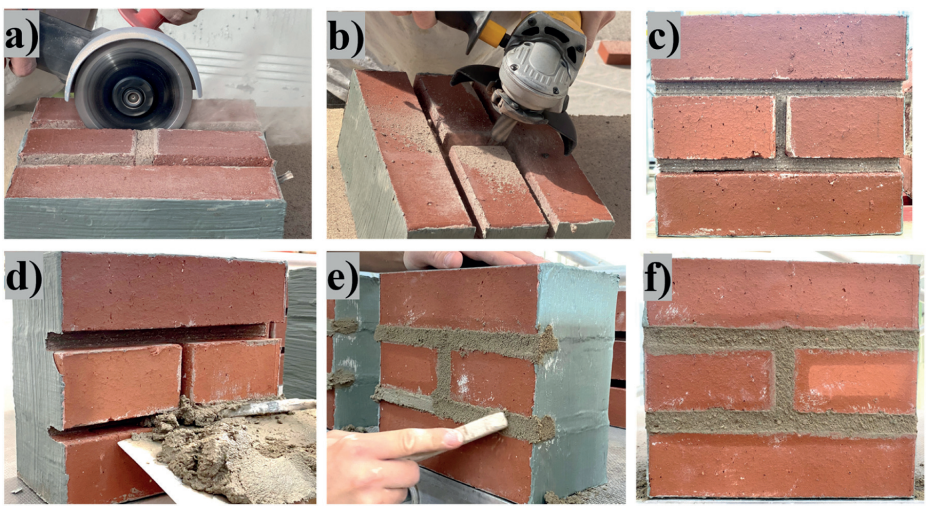

Fig. 3. Different steps of repointing a specimen: a) raking out bed joints, b) raking out the head joint, c) a gently washed specimen after raking, d) applying new mortar, e) compaction of the mortar, and f) a repointed specimen.

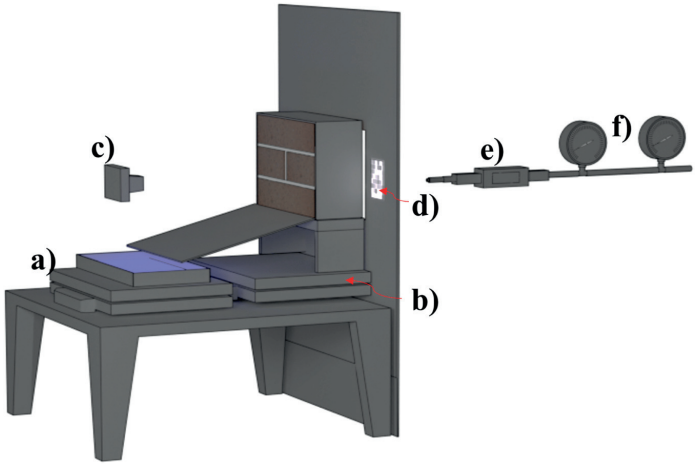

Fig. 4. Schematic of the test setup: a) scale measuring water penetration, b) scale measuring water absorption, c) digital camera, d) ColorChecker, e) water flow meter, and f) water pressure regulators.

allows for the investigation of initially dry brick masonry. A full description of how the test setup was developed is available in [9,25].

3. Results

3.1. Water absorption

Water absorption herein is expressed as the ratio between the amount of absorbed water (i.e., the difference between the increased weight and initial weight) and the exposed surface area. The results regarding water absorption (kg/m^2) for each group before and after repointing are shown in Fig. 5. Regarding the specimens before repointing, a constant absorption rate is observed because the exposed face is not yet saturated (the capacity of the specimens to absorb water was in balance with the water supplied to the surface) during the initial 2 h hours of the test. After repointing, the surface becomes saturated after around 1 h of exposure, indicating a reduction in the absorption rate of the masonry.

Prior to surface saturation, most of the sprayed water is absorbed, with a bounce-off of around 10 – 20%. The bounce-off can be calculated as the difference between the amount of sprayed water and absorbed water prior to surface saturation. Once the specimens attain surface saturation, the absorption behavior becomes nonlinear, and the slope of the absorption curve decreases until it approaches zero, indicating little to no water accumulation in the specimens. The water absorption rate in masonry specimens is mainly influenced by the spray rate, the water absorption coefficient of the bricks, and the mortar type, while the amount of absorbed water is primarily correlated with the absorption capacity of the bricks.

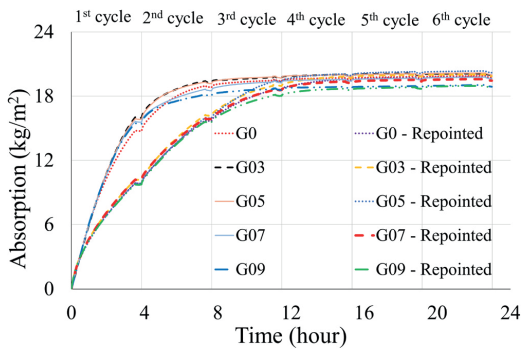

Fig. 5. Average water absorption vs. time response during 23 h of testing for all groups before and after repointing.

The absorption response is presented against time, despite the earlier mention that the absorbed mass of water is expected to be proportional to the square root of time (Section ↱2.1). This is because the experimental conditions did not align with the specific conditions under which cumulative absorption in a single-sided water absorption test shows an increase proportional to the square root of elapsed time ($t^{1/2}$) [28]. These conditions include (1) uniform initial water content, (2) strictly one-dimensional flow inside the material with freely available water at the inflow face (water should be available in unlimited supply), (3) material homogeneity, and (4) material remaining structurally and microstructurally unchanged by changes in water content. While conditions 1 and 4 are fulfilled in this study, it is important to acknowledge that meeting conditions 2 and 3 were not fulfilled due to test conditions. This implies that water was not freely available at the surface for absorption, given the water spray rate, and the masonry composed of brick and mortar is non-homogeneous.

3.2. Water penetration

Water penetration (kg/m^2) is defined as the amount of water collected from the backside of a specimen divided by its exposed surface, while the rate of water penetration is defined as the ratio between the total amount of water penetration and the time elapsed from the initiation of the water penetration. Fig. 6 shows the average water penetration within each group during the 23 hours of exposure, while Table 2 shows the corresponding results for individual specimens. As can be seen, there is a time lag between the start of tests and the start of water penetration. This indicates the moisture buffering capacity of brick masonry as an advantageous property in postponing water penetration. Once water penetration starts, it takes place at a constant rate, except for the 20-minute pause between each spray cycle when no penetration is registered. As can be seen, on average, the larger the crack width, the higher the water penetration rate.

On average, before repointing, the time to penetration was between

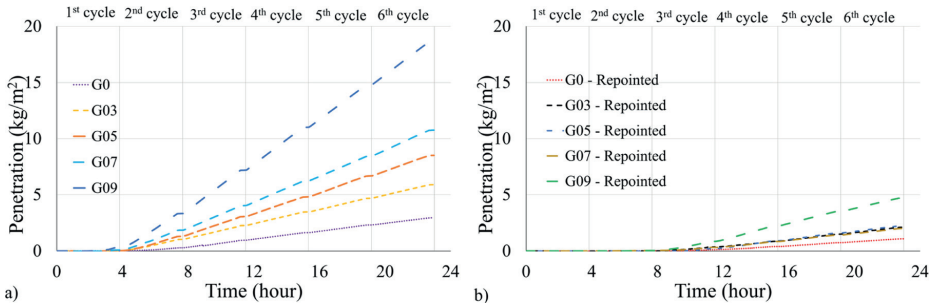

Fig. 6. Average water penetration during the 23 h of testing: a) before repointing and b) after repointing.

3.1 – 7.4 hours, with the shortest time in the specimens with the largest crack width (G09) and the longest time in the reference specimens (G0), i.e., those without any known defects. After repointing, the time to penetration was around 9.5 – 11.5 hours without a clear trend connected to the crack width. The results show that repointing postpones the start of water penetration, with 46% in the reference specimens and between 130 – 206% in the specimens with an artificial crack.

Before repointing, the average rate of water penetration was around 200 g/m^2/h in the reference specimens, while it increased from around 350 g/m^2/h in the specimens with the narrowest crack width (0.3 mm in group G03) to around 1050 g/m^2/h in those with the largest crack width (0.9 mm in group G09). After repointing, the penetration rate decreased by between 47 – 74%, without a clear trend in relation to the crack width. No penetration was observed in one specimen (G0–9) before repointing. After repointing, the penetration was zero in four specimens – G0–12, G05–5, G07–4, and G09–8. Interestingly, in specimen G0–9, penetration increased from zero to 66 g/m^2/h after repointing, showing that it is difficult to identify zones with a low resistance to water penetration unambiguously.

3.3. Damp patches

The location of the first damp patch that appeared on the backside of individual specimens within each group is shown in Fig. 7. Regarding group G0 (reference specimens), a high concentration of points around the head joint indicates that the first visible dampness consistently appeared on the bricks in the second course, close to the head joint. This highlights the low resistance of head joints, providing a primary pathway for water to penetrate. In the specimens with an artificial crack, in approximately 35% of the cases, the first damp patch appeared in the vicinity of the crack; otherwise, it appeared near the head joint. After repointing, initial dampness predominantly emerged in the vicinity of the head joint, with occasional occurrences near the bed joints or on the bricks. Notably, following repointing, the first damp patch did not appear proximate to the crack in any of the specimens.

The time to the appearance of the first dampness is summarized in Table 3. For all groups, the average time to the appearance of the first dampness varied in the range of 1.1 h – 1.5 h. While cracks can reduce the time it takes for the start of water penetration, there is no significant difference in the time it takes for the first dampness to appear between the reference specimens (group G0) and the cracked specimens (groups G03 – G09). After repointing, on average, it took around 4.0 h – 4.5 h to record the first damp patch on the backside of specimens, without a clear difference between the reference specimens and those with an artificial crack.

4. Discussion

The correlation coefficients, which measure the degree of correlation between two variables [40], have been calculated to indicate the correlation between crack width and different results, such as time to penetration start, saturation level at water penetration start, penetration rate, and leakage. While the statistical significance of the correlation coefficients has been verified, it should be noted that the upper and lower limits have not been checked. Further, the p-values for all coefficients were determined through the t-test to assess the probability of observing an equal or higher value under the null hypothesis. The correlation coefficient can assume any value in the interval from −1 to 1. The accepted guidelines for interpreting the correlation coefficient are as follows:

- 0 indicates no linear relationship.
- +1 indicates a perfect positive linear relationship.
- -1 indicates a perfect negative linear relationship.
- Values between 0 and 0.3 (0 and −0.3) suggest a weak positive (negative) linear relationship.
- Values between 0.3 and 0.7 (0.3 and −0.7) indicate a moderate positive (negative) linear relationship.
- Values between 0.7 and 1.0 (-0.7 and −1.0) signify a strong positive (negative) linear relationship.

4.1. The influence of crack width

4.1.1. Time to penetration and saturation level

The results in terms of time to penetration start for individual specimens are presented in Fig. 8 and Table 2. For group G0, the reference specimens, it took an average of 7.4 hours for the water to start penetrating, yet a large scatter exists in the results for individual specimens. For instance, the earliest penetration, 4.4 h, was recorded for specimen G0–8, whereas, for specimen G0–9, no penetration occurred during 23 h of testing.

There is a strong correlation between the time to water penetration start and crack width, as shown in Fig. 8, where the correlation coefficient is −0.781 with a p-value of less than 0.05. Considering only cracked specimens, groups G03 – G09, a correlation coefficient of −0.599 with a p-value of nearly zero was calculated, indicating a moderate negative correlation between time to water penetration start and crack width. However, a correlation coefficient of −0.425 with a p-value of 0.007 was obtained considering only groups G03, G05, and G07. Increasing the crack width from 0.3 mm to 0.9 mm resulted in reducing the average time to the start of penetration from 4.6 h to 3.1 h. The earliest water penetration within cracked specimens was recorded for specimen G09–1, after 1.7 h of water spraying, while the latest penetration occurred after 6.5 h in specimen G03–2, which is still shorter than the average time taken for water penetration in group G0. The results obtained indicate that in the absence of known cracks, the start of water penetration would vary significantly, which can be related

Table 2
Time to the start of penetration, water penetration, and penetration rate in individual specimens before and after repointing.

Specimens	Before repointing						After repointing			
	Time to penetration (h)	Avg (h) [CoV %]	Water penetration (kg/m^2)	Avg (kg/m^2) [CoV %]	Penetration rate (g/m^2/h)	Avg (g/m^2/h) [CoV %]	Time to penetration (h)	Avg (h) [CoV %]	Penetration rate (g/m^2/h)	Avg (g/m^2/h) [CoV %]
G0–1	7.5	7.4	3.1	3.0	223	204	9.7	10.8	175	94
G0–2	8.5	[20.4]	1.7	[88.9]	127	[83.1]	11.0	[22.2]	46	[97.2]
G0–3	5.4		6.3		394		11.0		30	
G0–4	8.7		0.1		9		13.8		9	
G0–5	5.4		7.3		461		10.4		163	
G0–6	8.3		0.4		31		5.4		37	
G0–7	7.9		3.0		222		13.7		44	
G0–8	4.5		5.9		382		11.8		114	
G0–9	-		0.0		0		8.3		66	
G0–10	10.1		0.7		58		13.8		142	
G0–11	6.3		7.1		472		9.1		331	
G0–12	6.1		2.9		191		-		0	
G0–13	8.1		1.0		77		11.0		63	
G03–1	4.1	4.6	2.4	5.9	137	348	-	10.6	0	186
G03–2	6.5	[21.2]	3.1	[64.7]	210	[61.3]	8.4	[28.8]	126	[82.3]
G03–3	3.2		10.6		593		12.6		116	
G03–4	4.6		5.2		311		8.1		390	
G03–5	5.9		3.5		226		8.2		126	
G03–6	4.5		3.3		199		15.6		205	
G03–7	4.0		13.8		795		7.9		378	
G03–8	5.5		1.4		90		9.7		68	
G03–9	4.9		5.8		352		9.5		305	
G03–10	4.2		6.9		403		10.4		116	
G03–11	3.2		9.2		517		13.9		479	
G03–12	5.5		2.2		138		7.6		32	
G03–13	4.4		9.3		552		15.9		74	
G05–1	4.1	4.3	15.9	8.3	924	488	9.7	11.5	181	194
G05–2	4.4	[17.4]	16.7	[67.6]	985	[66.3]	11.0	[22.5]	172	[88.3]
G05–3	5.0		7.0		427		9.9		528	
G05–4	4.6		2.8		170		13.2		145	
G05–5	4.5		2.9		171		-		0	
G05–6	3.3		15.9		898		10.2		62	
G05–7	3.0		5.3		293		9.9		428	
G05–8	5.6		4.4		280		12.9		123	
G05–9	4.2		4.5		261		17.4		27	
G05–10	4.4		8.0		475		9.3		269	
G07–1	3.1	3.8	8.7	10.8	488	619	11.0	10.3	195	161
G07–2	4.0	[17.8]	27.2	[62.2]	1573	[61.5]	8.5	[34.0]	421	[72.3]
G07–3	5.2		5.6		349		9.6		247	
G07–4	3.8		12.3		703		-		0	
G07–5	3.4		7.7		438		10.5		176	
G07–6	3.2		20.8		1169		6.3		183	
G07–7	4.4		4.8		287		8.8		242	
G07–8	4.5		3.0		179		18.5		21	
G07–9	2.9		13.5		743		13.5		245	
G07–10	3.3		11.5		647		7.0		131	
G07–11	3.6		7.2		416		13.9		40	
G07–12	4.4		7.3		438		9.7		144	
G07–13	3.4		10.8		612		6.8		53	
G09–1	1.7	3.1	13.8	18.6	714	1045	10.6	9.5	163	351
G09–2	2.0	[26.9]	13.0	[33.0]	684	[34.6]	8.8	[18.4]	583	[81.0]
G09–3	2.8		18.3		1004		10.3		65	
G09–4	4.1		19.3		1123		8.8		560	
G09–5	3.4		15.1		857		10.0		79	
G09–6	2.3		14.5		776		12.2		192	
G09–7	3.3		13.2		748		9.8		271	
G09–8	4.3		10.8		634		-		0	
G09–9	2.5		22.8		1234		12.0		316	
G09–10	3.3		27.1		1531		7.4		700	
G09–11	3.2		18.2		1023		7.3		469	
G09–12	3.2		30.4		1706		6.8		959	
G09–13	4.3		25.8		1546		10.1		207	

to the quality of the brick-mortar interface, which is counted as an important parameter in leakage. Similar results were obtained in studies done by Groot and Gunneweg [7], Slapø et al. [8], and Kahangi Shahreza et al. [25], where the penetration appeared to be mainly caused by brick-mortar interfaces, particularly in masonry built with low or medium suction bricks. Further, earlier water penetration would be expected in the case of cracked specimens, as cracks might exhibit low resistance to water penetration.

Table 3 and Fig. 9 collectively present the corresponding saturation level at the start of water penetration in individual specimens within each group. The saturation level (%) is expressed as the ratio between the amount of absorbed water at penetration start and the saturation

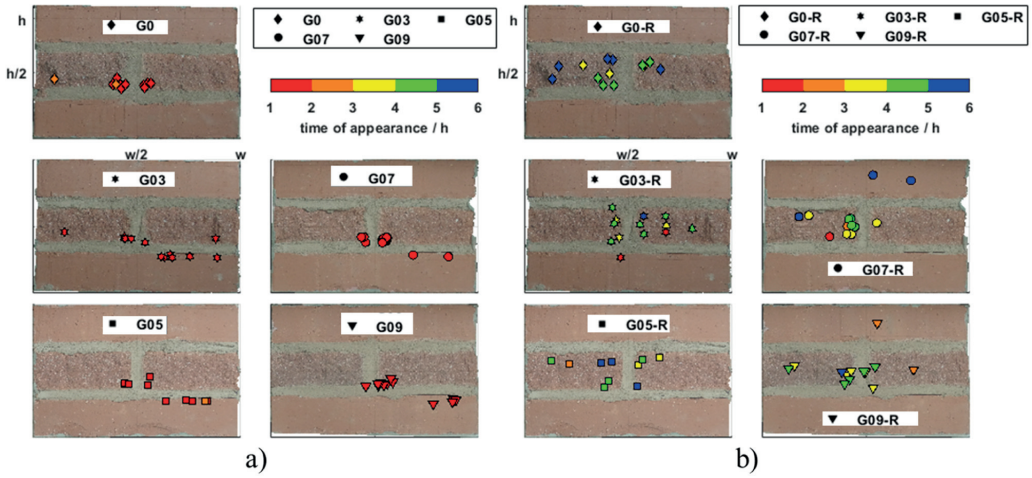

Fig. 7. The location and time of the first damp patch that appeared on the backside of individual specimens a) before repointing and b) after repointing.

capacity of masonry. In this study, the total absorption (final measured value after 23 h of exposure to water spray) corresponds to the saturation of the specimens, which is also confirmed by the fact that the final value was close to saturation based on the 24 h water absorption capacity of brick and mortar (see Table 1). On average, for group G0, water penetration started when the saturation level was 93.6%. Similar results were obtained by Straube and Burnett [34] and Kahangi Shahreza et al. [25], where in the latter, water penetration in uncracked masonry started when the absorbed water corresponded to around 93% of saturation capacity. Further, the average saturation levels of 87%, 84%, 81%, and 72% at the start of water penetration were recorded for specimens of groups G03, G05, G07, and G09, respectively. The obtained results indicate a strong negative correlation between the crack width and saturation level at the start of penetration; the larger the crack width, the lower the saturation level. The correlation coefficient was calculated to be around −0.72 with a p-value of less than 0.05.

It is noteworthy that water penetration commences once the amount of water surpasses the absorption capacity of the masonry along the pathway of least resistance, which is a crack in this study. Although the average saturation level in masonry is not directly linked to the saturation level along the pathway, cracks for groups G03 – G09, or brick-mortar interface for uncracked specimens, group G0, there is a considerable correlation between the start of penetration and overall saturation level for both uncracked and cracked specimens. Thus, the overall saturation level can still be considered an indicator of the start of water penetration.

4.1.2. Water penetration rate and leakage

The results in terms of leakage in individual specimens within each group are presented in Table 3 and Fig. 10. Leakage (%) herein is defined as the ratio between the amount of penetrated and sprayed water. The average leakage was equal to 2.2% for group G0, specimens without known cracks. In contrast, for the cracked specimens, the average leakage of 4.2%, 5.9%, 7.7%, and 13.3% were obtained for groups G03, G05, G07, and G09, respectively. The obtained results indicate a strong positive correlation between leakage and crack width, with a correlation coefficient of 0.70 and a p-value of less than 0.05.

The average leakage in specimens of group G07 and G09 is around 3.5 and 6 times larger than that of group G0, reference specimens. In individual specimens, a maximum leakage of 21.6% was obtained for specimen G09–12, indicating a great impact of crack width on leakage. It should be noted that comparing individual specimens within each group shows that leakage in specimens without cracks can be equal to those with a crack width of up to 0.7 mm. For example, leakage of 5.2% was recorded for specimens G0–5, which is approximately equal to specimens G03–10, G05–3, and G07–12. Similarly, comparing individual cracked specimens, it can be seen that leakage in specimens with a smaller crack width can be larger than those with a larger crack width. For instance, specimen G03–7, with a leakage of 9.8%, has a higher leakage than the average leakage of groups G05 and G07, specimens with a crack width of 0.5 mm and 0.7 mm.

The water penetration rate for individual specimens within each group is summarized in Table 2 and Fig. 11. A moderate positive correlation was observed between crack width and water penetration rate within each group, with a correlation coefficient of around 0.68 and a p-value of nearly zero. Regarding groups G03 – G09, the correlation coefficient is around 0.62, a moderate positive correlation, with a p-value of less than 0.05. However, it should be mentioned that considering only groups G03, G05, and G07, the correlation coefficient becomes 0.359 with a p-value of 0.025. This suggests a measurable difference not only between the reference specimens and cracked specimens but also among specimens with different crack widths.

Group G09 exhibited the highest average penetration rate, reaching 1045 g/m^2/h. A large scatter in the results of water penetration rate in individual specimens of each group can be seen. No penetration was registered for specimen G0–9, whereas this value reached up to 472 g/m^2/h in G0–11. For group G03, specimens with a crack width of 0.3 mm, the greatest and lowest penetration rates were obtained for specimens G03–3 and G03–8, 593 g/m^2/h and 90 g/m^2/h, respectively.

Several reasons exist attributed to the scattered results in terms of water penetration rate and leakage in the individual specimens despite the considerable correlation between the average penetration rate and leakage and the size of the crack (see Fig. 11). 1) Due to the difficulty in filling the head joints during bricklaying, the quality of the workmanship to fill the joints differed, as shown in Fig. 12, which could have the potential to provide a pathway for water to penetrate. In specimens with an artificial crack, if the head joint was poorly filled (Fig. 12.a), in addition to the crack, water could penetrate through the head joint. For example, a penetration rate of 90 g/m^2/h was obtained for specimen G03–8, which is around 5.2 times less than the penetration rate in specimen G0–11, 472 g/m^2/h. Similarly, the water penetration rate in specimen G03–3, 593 g/m^2/h, was nearly 3.5 times greater than that of

Table 3
Saturation level at the start of penetration, leakage percentage, and time to the first dampness and its corresponding saturation level for individual specimens.

Specimens	Before repointing							After repointing	
	Time until the first dampness (h)	Avg (h) [CoV %]	Location of the first dampness	Saturation level at the start of penetration (%)	Avg (%)	Leakage (%)	Avg (%)	Time until the first dampness (h)	Avg (h) [CoV %]
G0–1	2.5	1.5	h	94	93.6	2.2	2.2	4.2	4.5
G0–2	1.5	[42.1]	h	97		1.2		4.0	[17.0]
G0–3	1.1		h	80		4.5		5.2	
G0–4	1.3		h	97		0.1		5.3	
G0–5	1.5		h	94		5.2		3.8	
G0–6	1.0		h	96		0.3		4.8	
G0–7	1.3		h	97		2.1		4.4	
G0–8	1.8		h	89		4.2		5.0	
G0–9	2.9		b	-		0		5.5	
G0–10	0.9		h	98		0.5		4.5	
G0–11	1.2		h	92		5.0		5.0	
G0–12	0.8		h	93		2.1		3.2	
G0–13	1.2		h	95		0.7		3.2	
G03–1	0.9	1.4	c	82	87.2	1.7	4.2	1.8	4.0
G03–2	1.2	[27.1]	h	94		2.2		4.7	[28.4]
G03–3	1.8		h	81		7.5		2.0	
G03–4	1.3		h	83		3.7		3.7	
G03–5	0.8		c	95		2.5		4.8	
G03–6	1.6		h	82		2.4		3.8	
G03–7	1.5		c	88		9.8		3.5	
G03–8	1.7		c	91		1.0		4.3	
G03–9	1.0		c	88		4.1		4.0	
G03–10	1.2		h	83		4.9		4.8	
G03–11	2.0		h	84		6.5		4.3	
G03–12	1.1		h	91		1.6		6.0	
G03–13	1.6		c	91		6.6		4.8	
G05–1	1.7	1.5	h	90	84.1	11.3	5.9	4.0	4.4
G05–2	0.8	[29.1]	h	89		11.9		5.2	[24.4]
G05–3	1.5		c	85		5.0		4.7	
G05–4	1.5		c	85		2.0		5.0	
G05–5	1.9		c	85		2.0		5.1	
G05–6	1.5		h	77		11.3		2.8	
G05–7	1.5		c	75		3.7		4.5	
G05–8	2.5		c	89		3.1		5.8	
G05–9	1.2		h	84		3.2		3.3	
G05–10	1.3		h	82		5.7		3.3	
G07–1	0.9	1.4	c	76	80.7	6.2	7.7	3.3	4.0
G07–2	1.8	[23.9]	h	83		19.3		6.0	[32.6]
G07–3	1.2		h	91		4.0		4.2	
G07–4	1.6		h	81		8.8		4.3	
G07–5	0.9		h	78		5.5		1.7	
G07–6	1.3		h	76		14.8		2.0	
G07–7	1.6		c	84		3.4		3.3	
G07–8	0.8		h	90		2.1		5.5	
G07–9	1.5		h	77		9.6		4.9	
G07–10	1.5		h	76		8.1		3.0	
G07–11	1.5		h	77		5.1		4.0	
G07–12	1.7		h	86		5.2		4.5	
G07–13	1.3		h	76		7.7		5.3	
G09–1	1.1	1.1	c	49	72.3	9.8	13.3	4.2	4.0
G09–2	1.2	[31.8]	c	51		9.3		3.9	[16.7]
G09–3	0.9		h	74		13.0		3.8	
G09–4	1.2		h	84		13.7		3.5	
G09–5	0.8		c	73		10.7		5.3	
G09–6	1.0		h	65		10.3		3.5	
G09–7	0.9		h	85		9.4		4.4	
G09–8	0.7		h	86		7.7		3.7	
G09–9	1.2		h	73		16.2		4.1	
G09–10	0.9		h	77		19.3		3.0	
G09–11	1.7		c	76		12.9		3.0	
G09–12	1.2		h	79		21.6		4.8	
G09–13	2.0		h	68		18.3		4.3	

h: vicinity of the head joint
b: vicinity of the bed joint
c: close to the crack

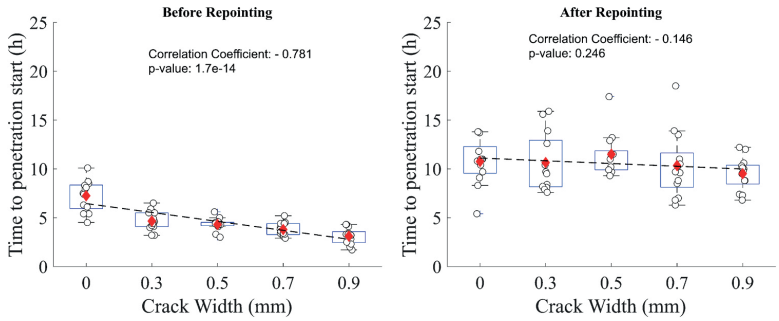

Fig. 8. Time to the start of penetration in individual specimens before and after repointing.

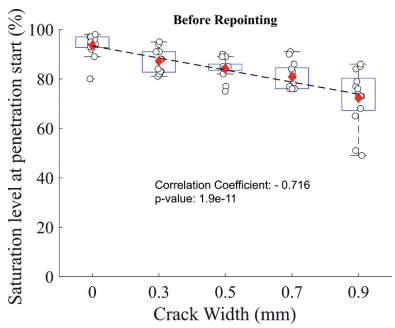

Fig. 9. Saturation level at the start of water penetration for individual specimens before repointing.

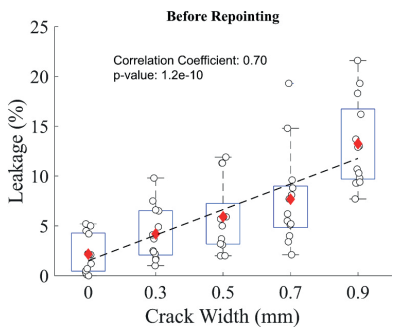

Fig. 10. Leakage (%) for individual specimens before repointing.

specimen G05–4, 170 g/m^2/h. Hence, if head joints are not filled completely, they may provide a similar pathway to the cracks, facilitating water to penetrate, since, for specimen G0–11, regardless of not having any known cracks, a large amount of water penetration was observed. 2) There is high uncertainty in the geometry of the cracks created in this study, where tortuosity or roughness of the wall of the crack could play an important role. After removing the plastic strips used to create the cracks, since the mortar did not get hardened completely, it could have filled some parts of the crack due to gravity. 3) Another uncertainty can be related to a tolerance in the nominal thickness of the plastic strips used to create cracks. Further, the plastic strips could be deformed unevenly during removal. This may lead to crack tortuosity, where in an experimental study conducted by Akhavan et al. [41], it was shown as a parameter that reduces the permeability in cracked mortar by a factor of 4–6 compared to Poiseuille's law. 4) Eventually, there is variability in the material properties of both brick and mortar. For instance, the water absorption coefficient of the brick and mortars had a coefficient of variation of roughly 10% (as shown in Table 1).

It should be mentioned that the variation in water penetration rate between individual specimens decreases as the crack width increases; group G0 with a CoV of 83%, groups G03, G05, and G07 with a CoV of around 60%, and group G09 with a CoV of 35%. Regarding group G0, specimens without known defects, similar results were obtained in experimental studies conducted in [25,31], in which the penetration rate varied significantly in specimens of the same type. This is further in agreement with a review of existing experimental studies done by Van Linden and Van Den Bossche [42]. As mentioned, water penetration is highly linked to the contact quality between brick and mortar, the brick-mortar interfacial zone, and how head joints were filled during bricklaying.

4.2. The effect of repointing

While the average total absorbed water remained similar for each group before and after repointing, indicating consistency with the water absorption capacity of the bricks, repointing led to a reduction in the absorption rate. As shown in Fig. 5, the amount of absorbed water after the first cycle in cracked specimens is as doubled as in repointed specimens. Despite the repointed mortar being a relatively small component of the masonry prisms, its impact on the absorption rate of masonry is noticeable. Interestingly, despite the higher water absorption coefficient of mortar M 1 used for repointing, compared to mortar M 2.5, the absorption rate of the masonry decreased after repointing. This can be related to the fact that, while raking out the mortar joints and subsequent washing, some of the pores in bricks might be filled with sawdust (clogged pores), which in turn results in lower absorption through bricks. Further, the applied mortar, M 1, was well compacted, resulting in a tightening of the joints. Prior to repointing, water could more easily permeate through the brick-mortar interface, but the compaction of the new mortar created a plugging effect, causing water absorption to occur primarily through the exposed brick face. This observation is further supported by the delayed appearance of the first dampness after repointing. Thus, the results indicate that repointing can be a part of the maintenance scheme in reducing the absorption of masonry exposed to WDR. Similar results were obtained in a study by Fusade et al. [19], where a reduction in water ingress depth in lime-mortar joints was reported.

Table 2 and Fig. 8 show the time to the start of penetration in individual specimens before and after repointing. Following repointing, groups G0 – G09 exhibit an average time to penetration start ranging from approximately 9.5 h to 11.5 h. There is a considerable delay in the

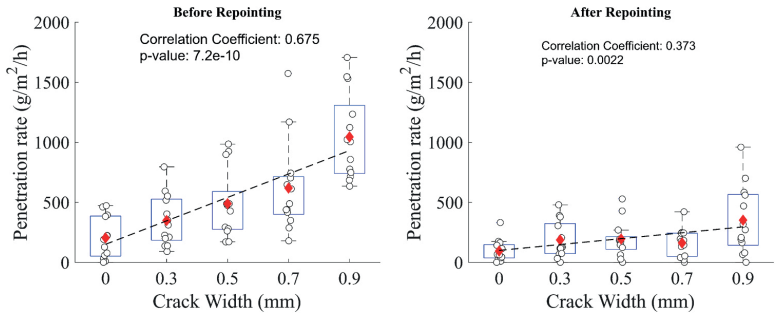

Fig. 11. Water penetration rate in individual specimens before and after repointing.

Fig. 12. Condition of head joints after being raked out to 25 mm – 30 mm: a) good/acceptable workmanship and b) poor workmanship.

average time to start water penetration within all groups after repointing. In group G0, the average time to the penetration start was postponed by around 3.5 h, from 7.4 h to 10.8 h. The t-test was conducted for each group before and after repointing to assess the statistical significance of the results. In all five groups, the p-value was less than 0.05, indicating that the results are statistically significant at a 95% confidence level. Contrary to expectations, repointing had an unfavorable impact on the time to water penetration initiation in specimens G0–6 and G0–9. However, the rate of water penetration did not show a considerable change when comparing these two specimens before and after repointing. In the case of cracked specimens, the results indicate that repointing is highly influential in postponing the start of water penetration by nearly 6.5 h; the larger the crack width, the more significant impact was obtained by repointing.

Regarding the water penetration rate, a reduction was observed in the average water penetration rate of each group after repointing (see Fig. 11). The t-test was performed for each group before and after repointing to evaluate the statistical significance of the results. In cracked specimens, groups G03 – G09, the p-value was less than 0.05, signifying the statistical significance of the observed effects. However, for group G0, a p-value of 0.0544 was obtained by comparing the before and after repointing.

The greatest reduction was obtained for group G07, specimens with a crack width of 0.7 mm; the average penetration rate decreased by 74%, from 619 g/m^2/h to 161 g/m^2/h. For group G09, specimens with a crack width of 0.9 mm, the average penetration rate decreased by 66%, from 1045 g/m^2/h to 351 g/m^2/h. A similar trend is observed in the case of reference specimens, group G0; the average penetration rate decreased by 54%, from 204 g/m^2/h to 94 g/m^2/h. However, it should be noted that repointing may not always result in decreasing the water penetration rate compared to individual specimens before and after repointing. For instance, the penetration rate increased by 46% in specimen G05–7 after repointing, yet the time to start penetration was postponed by around 7 h. Similarly, the effect of repointing on the water penetration rate was unfavorable in specimens G0–6, G0–9, and G0–10. This observation may be attributed to several factors: 1) the compaction, filling, and resistance of the mortar joints, including the head joint and bed joints, in these specimens were already optimal even before repointing, as evidenced by their initially limited water penetration rate. This suggests that repointing could not have significantly improved these specimens, and 2) during the raking process, some specimens might have been unintentionally damaged, leading to defects that might result in higher penetration. A comparison of individual specimens before and after repointing reveals that repointing might not always be an effective measure in reducing the penetration rate of masonry with a small crack width or uncracked masonry, particularly when the water penetration rate was already low prior to repointing.

Several reasons might contribute to the significant difference in the average water absorption and water penetration of each group before and after repointing. 1) Repointing resulted in filling the cracks to a certain depth (around 25–30 mm). Additionally, if the head joint had been inadequately filled, it was addressed during the repointing (see

Fig. 12.b). Since both cracks and head joints with gaps and voids might facilitate water penetration, properly filling these pathways can improve the moisture response of masonry and reduce the absorption rate and water penetration. 2) The compaction of mortar joints has the potential to enhance the resistance of masonry to water ingress. Through repointing, well-compacted joints can be achieved as bricklayers have the opportunity to apply a new mortar. Fishburn et al. [17] studied the performance of brick masonry walls before and after repointing, where a significant reduction in leakage was obtained.

4.3. Damp patches

As shown in Fig. 7, in the majority of specimens, nearly 80%, the first visible dampness was registered in the vicinity of the head joint; otherwise, near the crack. This can be further confirmed by observing the state of the head joint, particularly the brick-mortar interface, of representative specimens, as shown in Fig. 12. In contrast to water penetration primarily occurring through cracks as the path of least resistance, the first visible dampness appeared mainly in the vicinity of the head joint. This indicates that two different mechanisms, namely capillary suction and laminar flow, which is dependent on the water saturation, might have governed moisture transport. In the case of water penetration occurring under saturated or nearly saturated conditions, moisture transport might be governed by laminar flow. In contrast, the emergence of dampness can be attributed to capillary pressure dominating moisture transport. Fig. 13 shows three representative specimens, G09–2, G09–6, and G09–10, where, in all cases, water mainly penetrated through the crack, while the emergence of the first damp patch occurred in two different locations, dominated by capillary suction. Interestingly, the dampness appeared in the vicinity of the head joint and the vicinity of the crack nearly simultaneously for specimen G09–10, indicating that the brick-mortar interface at the head joint could provide a path similar to the crack for the emergence of the dampness.

Furthermore, as summarized in Table 2 and Table 3, comparing the time to the start of penetration and the time to the appearance of the first visible damp patch for individual specimens indicates that no significant correlation could be observed. The Pearson correlation coefficient between the appearance of the first dampness and the timing of penetration start is around 0.14 with a p-value greater than 0.05, meaning that no significant correlation exists between the two metrics. For instance, the first dampness appeared after 2.5 h and 1.5 h, and the first leakage was registered after 7.5 h and 8.5 h for specimens G0–1 and G0–2, respectively. A similar result was obtained by an experimental study by Fishburn et al. [31], where three failure criteria, namely dampness, visible water, and leakage, were recorded for brick masonry walls exposed to water spray. No strong correlation was found between the time to the first dampness and the time to the start of penetration. This is consistent further with the results presented by Kahangi Shahreza et al. [25] and Ritchie and Davison [43].

Table 3 presents the results in terms of time to the emergence of the first dampness after repointing. As can be seen, while the first dampness appeared after 1.1 h – 1.5 h of exposure to the sprayed water for specimens before repointing, the registered time increased to 2.5 h – 3 h

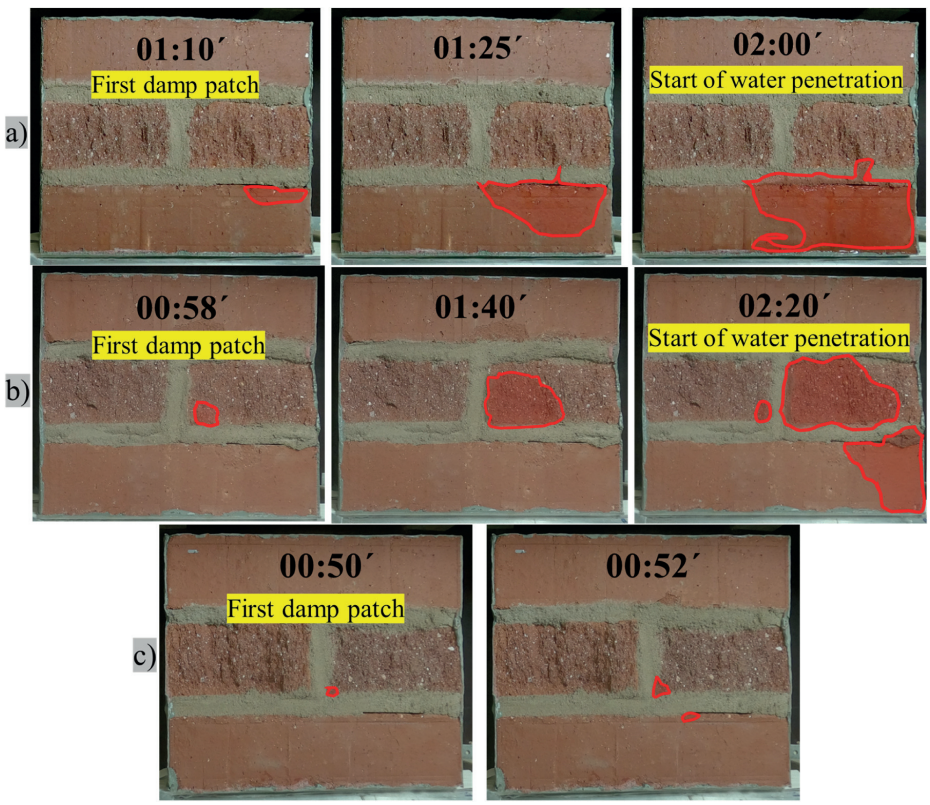

Fig. 13. The time and location of the first damp patch and time to the start of water penetration in specimens a) G09-2, b) G09-6, and c) G09-10.

after repointing. In contrast to the cracked specimens, where the first dampness could appear close to the crack (see Fig. 7.a), in none of the specimens after repointing, the first visible damp patch emerged in the vicinity of the crack (see Fig. 7.b), suggesting that repointing can be an effective measure for the maintenance of cracked masonry. The results highlight the importance of repointing to postpone the emergence of the first visible dampness, which can be related to filling the deficiencies/voids within the head joints and the extra compaction achieved by repointing. This can be further related to the reduction in the water absorption rate achieved by repointing, as it was shown in studies done by Kahangi Shahreza et al. [9,25] that a certain level of saturation is required for the emergence of the first dampness, i.e., a strong correlation existed between the saturation level and the emergence of the first dampness.

4.4. Input for hygrothermal analysis

The results obtained in this study might be further used in the hygrothermal analysis of walls with brick masonry as cladding. The penetrated water, referred to as leakage or moisture source, is an important input for hygrothermal analyses. Since water penetration as a major moisture source considerably affects the hygrothermal behavior of wall assemblies, it should be appropriately considered in hygrothermal analysis tools. Despite the significant impact of rainwater penetration on the hygrothermal performance of building envelopes, there is no general agreement on how much water penetrates through brick masonry claddings and how penetration should be implemented in hygrothermal analyses [42,44]. The current practice, as per the North American Standard (ASHRAE 160–2021) [24], is to assume that 1% of all WDR deposited on a façade penetrates behind the cladding. This assumption comes with some limitations: a) the buffering capacity of masonry is disregarded, and b) external claddings with different material properties and deficiencies are not differentiated. Recently, a new criterion for water penetration in brick masonry claddings was introduced by Kahangi Shahreza et al. [25], considering the moisture buffering capacity of masonry; yet, it is only applicable to masonry veneers without any known crack.

Based on the results obtained in the current study, a new benchmark that might be further used in the hygrothermal assessment of brick masonry claddings with different crack widths is proposed. For masonry without known cracks (Group G0), water penetration commences at a saturation level within the 90–95% range, with an average leakage rate of approximately 2.2%. For cracked specimens in Groups G03, G05, G07, and G09, water penetration starts at average saturation levels of nearly 87%, 84%, 81%, and 72%, respectively, with corresponding average leakage rates of 4.2%, 5.9%, 7.7%, and 13.3%. While mean values are used for simplicity, it is important to acknowledge the inherent uncertainty in these values. The hygrothermal analysis below aims to quantify the amount of water penetration that needs to be considered as the moisture source behind the cladding. While admitting the scattered results in this study, this analysis aims to improve the quantification of penetration for hygrothermal simulations in two ways: a) studying water penetration in brick masonry based on crack width, and b) implementing WDR penetration by accounting for leakage and saturation levels at the start of penetration stands in contrast to the ASHRAE 160 P standard [24], which only considers 1% leakage and overlooks the moisture buffering capacity of masonry. Thus, this section aims to investigate the impact of two parameters, saturation level and leakage, on hygrothermal analysis and compare it with the widely used ASHRAE 160 standard.

It should be noted that the actual WDR penetration in masonry walls remains generally unknown. Further, it is acknowledged that water penetration in real-world masonry façades may differ from what is quantified in this study, considering variations in crack types, lengths, and widths in brick masonry. Nevertheless, the study aims to highlight that varying water penetration occurs in masonry with different crack widths/deficiencies, suggesting the need for different water penetration criteria when simulating a brick masonry wall with different deficiencies rather than strictly adhering to the 1% criterion [24].

4.4.1. Numerical model

The hygrothermal performance of a timber frame wall with brick masonry cladding is analyzed with WUFI Pro 6.5, commercial software for hygrothermal analysis of multi-layer building components [45]. WUFI relies on hygrothermal models developed by Künzel [46], employing finite volume methods to solve coupled heat and moisture transport differential equations. The vapor transport mechanism included in WUFI is vapor diffusion, following the direction from higher to lower vapor pressure. The software considers liquid transport, accounting for capillary conduction and surface diffusion mechanisms. However, it has a limitation as it does not include hydraulic flow through pressure differentials. Regarding heat transport, WUFI takes into account thermal conduction, enthalpy flows through moisture movement, and solar radiation, while convective heat transport by air flows is disregarded. Temperature and relative humidity act as the driving potentials for heat and moisture transport within the material.

The simulation covers the period from 2000 to 2013 for two locations, Gothenburg and Rensjön, with different precipitation and temperature. While Gothenburg has the highest exposure to WDR in Sweden [47], Rensjön is located north of the Arctic Circle with a subarctic continental climate. Historical weather data, including hourly rain intensity, wind velocity, and wind direction, was obtained from the Swedish Meteorological and Hydrological Institute (SMHI) [48] for the studied locations. The average cloud index was assumed to be equal to 0.69 and 0.70 for Gothenburg and Rensjön, respectively. The most critical orientation concerning WDR was considered: south for walls in Gothenburg and north in Rensjön. The material properties used for simulating the bricks are based on a combination of values obtained in this study (see Table 4), complemented with literature and WUFI database data. Hygrothermal material properties used for simulating the walls are summarized in Table 4. The schematic of the studied wall is shown in Fig. 14. The masonry wall is represented in the model as a homogeneous layer. Although modeling a brick veneer in this way has its limitations, previous studies have demonstrated that this simplification can yield acceptable results, particularly when the wall is exposed to realistic climatic conditions [25,49,50]. Furthermore, the 1D WUFI model for masonry employed in this study has been validated through comparisons with test results in terms of water absorption, as shown in Fig. 15.

During a rain event, not all raindrops adhere to the wall surface; some bounce off upon impact. Understanding the phenomenon of bounce-off is needed when it comes to hygrothermal modeling, as it serves as an important input, the so-called "adhering fraction of rain." A study conducted by Künzel [46] found that about 70% of WDR adheres to vertical wall surfaces (whether the façade material is brick, timber, or any other material), whereas the remaining part takes the form of bounce-off, making it inaccessible for absorption. This, in turn, became the default value of the widely used WUFI and many hygrothermal simulation tools due to the lack of standards and measurements. Accordingly, in hygrothermal modeling, 30% of the WDR is usually assumed to bounce off the wall and is therefore unavailable for capillary suction. The remaining part, 70%, is considered to be available for absorption through liquid conductivity (capillary suction). Thus, the default value for "adhering fraction of rain" is considered 0.7. However, based on the results obtained in this study and other studies related to brick masonry [9,25], the bounce-off may vary between around 10% and 20%. Accordingly, the "adhering fraction of rain" was considered equal to 0.8, supported by experimental data in this study, indicating a 20% reduction in the amount of WDR rain hitting the façade to account for the fact that some water would bounce off the wall surface.

Several semi-empirical models have been developed to quantify WDR intensity [24,51]. These models typically rely on a straightforward

Table 4
Material properties of the masonry used in the simulation.

Material	Thickness (mm)	Bulk density (kg/m^3)	Porosity (m^3/m^3)	Free water saturation (kg/m^3)	Water absorption coefficient (kg/(m^2.s$^{0.5}$))	Vapor diffusion resistance (-)	Thermal conductivity (W/mK)	Specific heat capacity (J/kgK)
Solid brick	120	2029	0.268	175.0	0.16	10	0.60	850
Air cavity	20	1.3	0.999	0.017	-	0.46	0.18	1000
Asphalt impregnated paper	1	170	0.001	0.047	-	874	2.30	1500
Mineral wool	95	60	0.950	44.8	-	1.3	0.04	850
Vapor retarder	1	130	0.001	0.047	-	10000	2.30	2300
Gypsum board	12.5	850	0.650	400.0	0.287	8.3	0.20	850

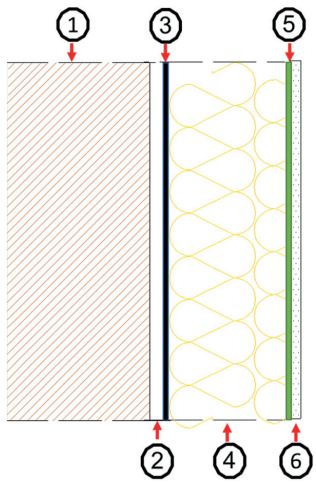

Fig. 14. Different layers of the wall assembly and their corresponding dimension from the left side (exterior): 1) brick masonry (120 mm), 2) air gap (20 mm), 3) asphalt-impregnated paper (1 mm), 4) mineral wool insulation (95 mm), 5) vapor retarder (1 mm), and 6) gypsum board (12.5 mm).

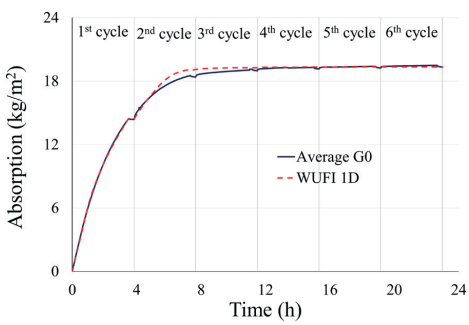

Fig. 15. Validation of the experimental results with 1D WUFI model in terms of water absorption.

analytical formula expressing that WDR intensity is proportionate to the product of the wind-velocity component normal to the wall and the horizontal rainfall intensity. The factor of proportionality in this WDR relationship is referred to as the WDR coefficient, which determines the amount of rainwater impinging on the building façades. This coefficient is dependent on several parameters, including the surrounding topography as well as the height of the building. This study considered a WDR coefficient of 0.2 s/m, a recommended value in WUFI for the upper part of the buildings with at least 20 m height.

A constant airflow (ACR) of 10 h^{-1} was considered to account for cavity ventilation, which is consistent with the findings in [52], where cavity ventilation behind brick veneer corresponds to an ACR between 1 and 10. Further, a review of existing studies on air cavities behind veneers indicates that measured values of the air change rates are lower than 50 h^{-1} in most cases [53]. The initial conditions of the materials were 18°C and 70% RH. The internal climatic conditions were related to the outdoor temperature in Gothenburg and Rensjön, respectively, following the European Standard EN 15026 [54]. Calculations were carried out using the time step of 1 h during the entire calculation period.

Fig. 16.a shows the variation in water content of the studied brick masonry cladding in Gothenburg during 2000 – 2012. As can be seen, the studied cladding was mostly saturated during winter periods, indicating that WDR would lead to water penetration. Hence, if the climate did not favor drying or WDR events occurred often, the occurrence of rain penetration became more probable as the masonry cladding would remain closely saturated [55]. In contrast, exposure to driving rain at levels below the threshold may not lead to water penetration. During warm periods, since the water content of masonry cladding is low, the simulated masonry veneer is capable of absorbing WDR due to its moisture buffering capacity.

The amount of possible water penetration obtained from the ASHRAE Standard 160 [24] and the criteria proposed in this study for different crack widths are shown in Fig. 16.b. As can be seen, exposure of a brick cladding having a crack width of 0.3 mm – 0.9 mm resulted in cumulative water penetration of around 150 kg/m^2 – 480 kg/m^2. Accordingly, the results suggest that in order to improve the hygrothermal analysis of brick masonry cladding with varying crack widths, it is important to account for the effect of cracks/deficiencies on water penetration. The ASHRAE Standard 160 thus may underestimate the amount of water penetration that should be considered as a moisture source behind the cladding for Gothenburg, a region with high WDR loads.

In contrast, there is an insignificant difference between the amount of penetrated water using the ASHRAE Standard 160 and the criterion proposed for group G0, reference specimens without known cracks. Accordingly, the obtained result suggests that in Gothenburg, a location with high exposure to WDR, ASHRAE Standard 160 may provide an acceptable amount of rain penetration to be used in the hygrothermal analysis for masonry without known cracks.

The variation in water content of the masonry cladding located in Rensjön during the studied period is shown in Fig. 17.a. As opposed to the wall located in Gothenburg (see Fig. 16.a), the wall reached saturation during the warm period, yet the number of times that the cladding became saturated was less than that of Gothenburg, which is related to the low exposure to WDR. Since the water content of the cladding seldom exceeds the saturation capacity, the probability of water penetration is low, highlighting the benefit of the water absorption capacity of clay brick masonry. Fig. 17.b shows the cumulative amount of water penetration during the studied period. The cumulative water

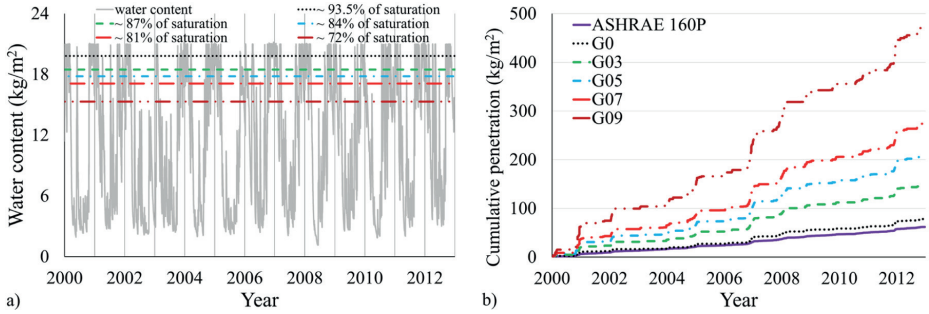

Fig. 16. a) Water content of the studied brick masonry cladding during 2000 – 2012 located in Gothenburg and b) using different penetration criteria.

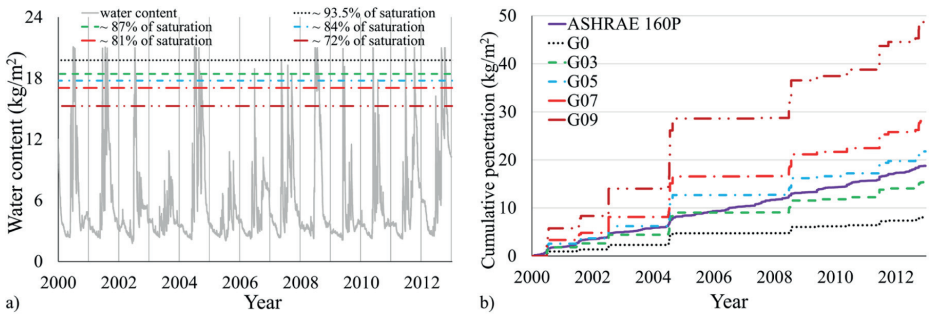

Fig. 17. a) Water content of the studied brick masonry cladding during 2000 – 2012 located in Rensjön and b) using different penetration criteria.

penetration ranges from 15 kg/m^2 to 50 kg/m^2 for masonry cladding with a crack width of 0.3 mm – 0.9 mm, around one-tenth of the wall in Gothenburg. Further, the total amount of penetration is around 8 kg/m^2 for masonry cladding without any known defects. The amount of penetration obtained by ASHRAE Standard 160 is close to that of cladding with a crack width of 0.3 mm – 0.5 mm, indicating that ASHRAE 160 may overestimate the water penetration in Rensjön, a location with limited exposure to WDR. As the saturation capacity of masonry is not considered in ASHRAE 160, this assumption may not provide a good picture of water penetration in claddings with low exposure to WDR. Since the number and intensity of WDR spells in Rensjön are lower than in Gothenburg, the absorbed water during WDR events can be easily distributed due to the moisture buffering capacity, postponing the start of water penetration.

Despite numerous research studies on water penetration in brick masonry, there is no general consensus on implementing water penetration in hygrothermal and moisture safety analyses [42,56]. This lack of agreement is evident in two aspects: 1) the amount of water that penetrates brick masonry and 2) the position for implementing a moisture source in hygrothermal models. While this study attempts to quantify water penetration in brick masonry and exemplify it for a commonly built building envelope type, the question of the latter remains open. While ASHRAE 160–2021 standard [24] recommends placing the moisture source on the water-resistive barrier behind the cladding, there are studies suggesting placing it on the protected side of the cladding or behind the vapor barrier. The varied recommendations highlight the significant impact of moisture source position on simulated hygrothermal performance, highlighting a lack of consensus [44,57].

The results highlight the need for an improved approach to moisture source incorporation, representative of rainwater penetration, in hygrothermal simulations. A method is suggested instead of a generic consideration of 1% of all WDR events deposited on a façade penetrating through claddings. While the presence of an air cavity and a vapor barrier in multi-wythe masonry walls may assist in draining penetrated water, it has been shown that water penetration in areas with high WDR loads may lead to moisture-related damages and significantly affect the hygrothermal response of the building envelopes [2,56].

Despite the benefit of ventilation and drainage of cavities, many existing masonry façades lack sufficient air cavity width [58]. Instances with limited air cavity width cause penetrated water to reach the backing system, which acts as a major moisture source, compromising the building envelope's durability and promoting a high risk of dampness and mold growth. Additional challenges include cases where extruded mortar joints act as capillary bridges [44,57], connecting the masonry veneer to adjacent layers. Since mortar bridges are found to influence the risk of mold growth, it is important to determine whether or not they arise in the cavity due to poor workmanship [44,57]. Additionally, water penetration becomes also important in cases where the vapor barrier is damaged or torn. In such scenarios, penetrated water may easily reach sensitive elements of building envelopes, such as timber or insulation [56].

4.5. Limitations and further considerations

It should be noted that the averaged saturation level may not have a precise physical basis to explain the onset of water penetration in masonry. However, the significant correlation established between the outcomes of this investigation underscores the viability of utilizing saturation level as an appropriate indicator for the initiation of water penetration. This correlation opens up new possibilities to be implemented in the hygrothermal analysis of masonry claddings. In the context of this research, the masonry prism specimens were constructed

with only a single head joint. This configuration was chosen to minimize the potential for undesired disintegration of the specimens. However, it is important to note that this design choice resulted in a lower percentage of head joints compared to typical real-world masonry, irrespective of the bond type. The water penetration rate per unit wall area would likely increase in practical masonry structures with more head joints.

Since cracks can be formed in any size or location in masonry veneers, the results of the current study can only be used for the hygrothermal analysis of masonry veneers with cracks through the bed joints. Cracks developed in the head joints of a masonry cladding might lead to substantial water penetration since considerable hydrostatic pressure can be built up. Further, the current study investigated the effect of cracks through masonry, whereas other types of cracks, such as hairline cracks, are often present in veneers. It should be noted that the 3-course masonry prisms used in this study had an exposed area (A_{sp}) of 55000 mm^2, while the area of the artificially created cracks (A_{cr}) ranged from approximately 15 to 50 mm^2, accounting for approximately 0.1% of the surface area of the specimens. The equivalent crack ratio may serve as valuable information through the assessment of brick masonry cladding.

It should be noted that the uncertainties in the results make it challenging to draw definitive conclusions or derive analytical equations for water penetration in brick masonry. Future efforts should focus on creating more representative cracks on large specimens induced by impact loads or moisture gradients and investigating different types of cracks with varying widths and positions to enhance the quantification of water penetration in cracked masonry.

While the main focus of this study was to quantify water penetration in cracked brick masonry and its implications for hygrothermal studies, it should be mentioned that cracks can serve as pathways for moisture ingress, leading to issues such as corrosion, frost damage, and microbiological growth. This study focuses on water penetration through cracks, yet it is important to consider the broader implications associated with cracks in massive masonry walls or masonry veneers.

While the primary emphasis in studies investigating water penetration in brick masonry has been on the brick-mortar interface as the pathway of least resistance for water, the significance of mortar and its microstructure should not be overlooked. This further plays an important role in determining the quality of the bond/contact formed between the brick and mortar. The microstructure of mortar and other mortar-related parameters [43], including mortar water content during bricklaying (flowability of the mortar) [8], mortar retention, and the type of workmanship in applying the mortar affect the contact zone between brick and mortar. However, it should be noted that water penetration predominantly occurs through the voids and gaps in the brick-mortar interface (which is mainly related to the workmanship), especially at head joints [7,8,25], rather than through the mortar or brick unless the brick has very high suction [7].

While the impact of pore size and microstructure on moisture transport in mortar is noteworthy, it should be highlighted that research studies centered on hygrothermal simulations of masonry walls to determine moisture variations in research studies have shown that modeling a brick masonry wall as a homogeneous layer (considering only the brick) can yield acceptable results under realistic weather conditions [49,50].

It should be noted that over 150 masonry specimens were initially prepared during this experimental campaign. Many specimens were excluded due to significant uncertainties in crack size and other difficulties during construction, handling, and repointing. The raking of bed joints was done with a blade, while a raking bit was used for head joints. Achieving precise control over the raking depth posed challenges, especially with the blade. Additionally, some mortar particles became loose during raking, resulting in uneven depths in certain parts of the joints. Similar challenges were encountered in head joints due to voids in some specimens, making achieving a uniform raking depth difficult, yet specimens not raked within the desired depth range of 25–30 mm were excluded from testing.

The aim of repointing mortar joints, a maintenance scheme of brick masonry claddings, is to preserve the integrity of the façade, improve aesthetics, and reduce moisture-related issues raised by WDR. During repointing, it is common practice to rake out joints to a depth of around 25 mm or 2.5 times the thickness of the mortar joint. However, considering that head joints typically provide the least resistance pathway for water to penetrate, it is worth exploring the possibility of increasing the raking depth, specifically in head joints. This raises the question of how much the reduction in water penetration could be correlated with the increased raking depth. Further, there is a need to study the effect of repointing on the long-term performance of masonry walls. In this study, repointing showed an improvement in reducing water penetration after a one-time exposure to water spray (short-term performance), yet there is a need to investigate the performance of repointed walls after several times of exposure to water spray (long-term behavior). In this study, masonry specimens were repointed four months after the initial preparation. However, considering the aging (erosion and deterioration) of the mortar as well as the time-dependent increase in mortar resistance, there is a need to conduct repointing at different time intervals, providing a more comprehensive assessment of mortar resistance to penetration and a deeper understanding of the impact of repointing. It is important to note that the current study involved specimens cured in a controlled laboratory environment without experiencing erosion or deterioration. Therefore, the results might vary if specimens were exposed to real weather conditions and subsequently followed by repointing.

While repointing can enhance the resistance of brick masonry cladding to WDR, there is a need to study the impact of repointing on the drying response of masonry walls. Since the water absorption behavior of masonry was influenced by repointing, i.e., a decrease in the absorption rate was obtained, it may further affect the drying of such walls. Thus, to have an accurate hygrothermal analysis of brick masonry after repointing, both absorption and drying properties need to be evaluated.

5. Conclusions

The study aimed to investigate the effect of repointing on water penetration in clay brick masonry, with and without cracks. In doing so, 3-course masonry prisms with artificial cracks with widths varying between 0.3 mm and 0.9 mm were exposed to uniform water spray. For comparison, reference specimens were built without any known cracks. After testing, masonry specimens were repointed to investigate the influence of repointing on reducing water penetration. Based on the obtained results, the following conclusions can be drawn:

- The average water penetration rate in specimens with crack widths of 0.3 mm, 0.5 mm, 0.7 mm, and 0.9 mm was 1.7, 2.4, 3.0, and 5.1 times more than in the reference specimens. Although there was a considerable correlation between the crack width and the average water penetration rate, the results showed a large variability comparing individual specimens, which might be due to crack tortuosity, quality of workmanship, and difficulties in controlling the actual width of artificial cracks.
- On average, it took around 1.1 h – 1.5 h for all groups until the appearance of the first damp patch on the backside of the specimens. In contrast to the effect of crack width on water penetration, crack width had a limited effect on the emergence of the first dampness.
- Water penetration in specimens without known defects started when the average saturation level was above 90%. The corresponding saturation level varied between 87% – 72% for cracked specimens. It was observed that larger cracks were associated with lower initial saturation levels prior to water penetration. Hence, a gained benefit in the case of brick masonry claddings, even if it is cracked, is the

moisture buffering capacity, postponing the occurrence of water penetration.

- Repointing can be an effective measure in reducing water penetration and postponing the start of water penetration. For specimens with a crack width of 0.7 mm, the average penetration rate decreased by 74% after repointing, from 619 $g/m^2/h$ to 161 $g/m^2/h$. Similarly, the average rate for reference specimens was reduced by 54%, from 204 $g/m^2/h$ to 94 $g/m^2/h$. While water penetration started after 7.4 h in reference specimens before repointing, the registered time for penetration increased to 10.8 h after repointing. In the case of cracked specimens, on average, it took 3.1 h – 4.6 h for water penetration to start, whereas, after repointing, the average time to start water penetration was around 9.5 h – 11.5 h.
- In addition to cracks, providing a pathway for water to penetrate, the brick-mortar interfacial zone has the potential to facilitate water penetration. Further, there is a need to highlight the importance of workmanship in filling the joints, particularly the head joints, which are probably the weakest part of clay brick masonry concerning water penetration.

Declaration of Competing Interest

The author declares that there is no known competing financial interests or personal relationships that could have appeared to influence the work reported in this paper.

Data Availability

Data will be made available on request.

Acknowledgments

The author gratefully acknowledges the financial support from SBUF – Development Fund of the Swedish Construction Industry (grant 14052) and TMPB - Masonry and Render Construction Association. I would like to thank Dr. Miklós Molnár and Dr. Jonas Niklewski for their feedback during the revision stage.

References

[1] I. Freeman, *Building failure patterns and their implications*. Building Research Establishment, Department of the Environment, 1975.
[2] N. Van Den Bossche, A. Blommaert, and B. Daniotti, "The impact of demographical, geographical and climatological factors on building defects in Belgium," *International Journal of Building Pathology and Adaptation,* no. ahead-of-print, 2022.
[3] M. Abuku, H. Janssen, S. Roels, Impact of wind-driven rain on historic brick wall buildings in a moderately cold and humid climate: Numerical analyses of mould growth risk, indoor climate and energy consumption, Energy Build. vol. 41 (1) (2009) 101–110. /01/01/ 2009.
[4] K. Calle, N. Van Den Bossche, Towards understanding rain infiltration in historic brickwork, Energy Procedia vol. 132 (2017) 676–681.
[5] I. Killip, D. Cheetham, The prevention of rain penetration through external walls and joints by means of pressure equalization, Build. Environ. vol. 19 (2) (1984) 81–91.
[6] G. K. Garden, "Rain penetration and its control, Can. Build. Dig. *1-100* (1963) 4, 4.
[7] C. Groot, J. Gunneweg, "The influence of materials characteristics and workmanship on rain penetration in historic fired clay brick masonry,", Heron *55* (2) (2010).
[8] F. Slapø, T. Kvande, N. Bakken, M. Haugen, J. Lohne, Masonry's Resistance to driving rain: mortar water content and impregnation, Buildings vol. 7 (3) (2017) 70.
[9] S. Kahangi Shahreza, J. Niklewski, M. Molnár, "Experimental investigation of water absorption and penetration in clay brick masonry under simulated uniform water spray exposure,", J. Build. Eng. vol. 43 (2021/11/01/ 2021) 102583.
[10] M. Kahangi, Resistance of Clay Brick Masonry Façades to Wind-Driven Rain: Repointing of Eroded Mortar Joints, Lund University, 2021.
[11] S. Selvarajah, A. Johnston, Water permeation through cracked single skin masonry, Build. Environ. vol. 30 (1) (1995) 19–28.
[12] C. Groot, J. Gunneweg, Water permeance problems in single wythe masonry walls: the case of wind mills, Constr. Build. Mater. vol. 18 (5) (2004/06/01/ 2004) 325–329.
[13] C.T. Grimm, "Masonry cracks: a review of the literature," *Masonry: materials, design, construction, and maintenance,* 1988.
[14] R.G. Drysdale and A. Kluge, "Performance of brick veneer steel stud wall systems subject to temperature, air pressure and vapour pressure differentials," 1990.
[15] C.-M. Aldea, S.P. Shah, A. Karr, Effect of cracking on water and chloride permeability of concrete, J. Mater. Civ. Eng. vol. 11 (3) (1999) 181–187.
[16] L. Mengel, H.-W. Krauss, D. Lowke, "Water transport through cracks in plain and reinforced concrete–Influencing factors and open questions,", Constr. Build. Mater. vol. 254 (2020) 118990.
[17] C.C. Fishburn, D. Watstein, and D.E. Parsons, *Water permeability of masonry walls*. US Department of Commerce, National Bureau of Standards, 1938.
[18] J.G. Stockbridge, Repointing masonry walls, APT Bull. vol. 21 (1) (1989) 10–12.
[19] L. Fusade, S.A. Orr, C. Wood, M. O'Dowd, H. Viles, Drying response of lime-mortar joints in granite masonry after an intense rainfall and after repointing, Herit. Sci. vol. 7 (1) (2019) 1–19.
[20] S. Kahangi Shahreza, M. Molnár, J. Niklewski, I. Björnsson, T. Gustavsson, Making decision on repointing of clay brick facades on the basis of moisture content and water absorption tests results–a review of assessment methods. in *Brick and Block Masonry-From Historical to Sustainable Masonry*, CRC Press,, 2020, pp. 617–623.
[21] A. Maurenbrecher, K. Trischuk, M. Rousseau, M. Subercaseaux, "Key Considerations for Repointing Mortars for the Conservation of Older Masonry (IRC-RR-225),". Canada: Institute for Research in Construction, National Research Council of Canada,, *Ottawa*, 2007.
[22] A. Maurenbrecher, K. Trischuk, M. Rousseau, M. Subercaseaux, "Repointing mortars for older masonry buildings–design considerations," *Construction Technology*, Update no. 67 (2008) 1206–1220.
[23] C.J.W.P. Groot, J.T.M. Gunneweg, "Choosing Mortar Compositions for Repointing of Historic Masonry Under Severe Environmental Conditions, in: J.J. Hughes, J. Válek, C.J.W.P. Groot (Eds.), Historic Mortars: Advances in Research and Practical Conservation, Cham: Springer International Publishing,, 2019, pp. 143–154.
[24] ASHRAE Standard, "Standard 160-2021: Criteria for Moisture Control Design Analysis in Buildings," *American Society of Heating, Refrigerating and Air-Conditioning Engineers, Atlanta,* 2021.
[25] S. Kahangi Shahreza, J. Niklewski, M. Molnár, "Novel water penetration criterion for clay brick masonry claddings,", Constr. Build. Mater. vol. 353 (2022/10/24/ 2022) 129109.
[26] ASTM International, "ASTM C67 / C67M-20, Standard Test Methods for Sampling and Testing Brick and Structural Clay Tile, ASTM International,, West Conshohocken, PA, 2020.
[27] ASTM International, ASTM C1403 - 15, Standard Test Method for Rate of Water Absorption of Masonry Mortars. West Conshohocken, PA, ASTM International,, 2015.
[28] C. Hall, W.D. Hoff, Water transport in brick, stone and concrete, CRC Press,, 2021.
[29] M. Raimondo, M. Dondi, D. Gardini, G. Guarini, F. Mazzanti, "Predicting the initial rate of water absorption in clay bricks,", Constr. Build. Mater. vol. 23 (7) (2009) 2623–2630.
[30] ASTM International, "ASTM E514 / E514M-14a, Standard Test Method for Water Penetration and Leakage Through Masonry, ASTM International,, West Conshohocken, PA, 2014.
[31] C.C. Fishburn, *Water permeability of walls built of masonry units*. US Department of Commerce, National Bureau of Standards, 1942.
[32] S. Cornick, M. Lacasse, An Investigation of Climate Loads on Building Façades for Selected Locations in the United States, J. ASTM Int. vol. 6 (2) (2009) 1–22.
[33] J. Ribar, "Water permeance of masonry: a laboratory study," in *Masonry: Materials, Properties, and Performance*, ASTM International,, 1982.
[34] J.F. Straube, E.F. Burnett, "Driving rain and masonry veneer," in *Water leakage through building facades*, ASTM International, 1998.
[35] R. Forghani, Y. Totoev, S. Kanjanabootra, A. Davison, "Experimental investigation of water penetration through semi-interlocking masonry walls,", J. Archit. Eng. vol. 23 (1) (2017) 04016017.
[36] K.B. Anand, V. Vasudevan, K. Ramamurthy, Water permeability assessment of alternative masonry systems, Build. Environ. vol. 38 (7) (2003/07/01/ 2003) 947–957.
[37] M. Lacasse, T. O'Connor, S. Nunes, P. Beaulieu, "Report from Task 6 of MEWS project: experimental assessment of water penetration and entry into wood-frame wall specimens-final report," (Feb), *Inst. Res. Constr.*, *RR 133* (2003) (Feb).
[38] A. Rathbone, *Rain and air penetration performance of concrete blockwork*. Cement and Concrete Association, 1982.
[39] H. Hens, S. Roels, and W. Desadeleer, "Rain leakage through veneer walls, built with concrete blocks," in *CIB W40 meeting in Glasgow*, 2004.
[40] B. Ratner, The correlation coefficient: Its values range between+ 1/− 1, or do they?,", J. Target., Meas. Anal. Mark. vol. 17 (2) (2009) 139–142.
[41] A. Akhavan, S.-M.-H. Shafaatian, F. Rajabipour, Quantifying the effects of crack width, tortuosity, and roughness on water permeability of cracked mortars, Cem. Concr. Res. vol. 42 (2) (2012/02/01/ 2012) 313–320.
[42] S. Van Linden, N. Van Den Bossche, "Review of rainwater infiltration rates in wall assemblies, Build. Environ. vol. 219 (2022/07/01/ 2022) 109213.
[43] T. Ritchie, J.I. Davison, Factors affecting bond strength and resistance to moisture penetration of brick masonry. " (in eng, ASTM Special Technical Publication, no. 320,, 1963, pp. 16–30.
[44] K. Calle, C. Coupillie, A. Janssens, N. Van Den Bossche, Implementation of rainwater infiltration measurements in hygrothermal modelling of non-insulated brick cavity walls, J. Build. Phys. vol. 43 (6) (2020) 477–502.
[45] D. Zirkelbach, T. Schmidt, M. Kehrer, and H. Künzel, "Wufi® Pro–Manual," *Fraunhofer Institute,* 2007.

[46] H.M. Künzel, "Simultaneous heat and moisture transport in building components: One-and two-dimensional calculation using simple parameters," PhD-thesis, IRB-Verlag Stuttgart, Fraunhofer Institute for Building Physics, 1995.
[47] P. Johansson, et al., Interior insulation retrofit of a historical brick wall using vacuum insulation panels: Hygrothermal numerical simulations and laboratory investigations, Build. Environ. vol. 79 (2014) 31–45.
[48] (accessed September 2023). ⟨https://www.smhi.se/data⟩.
[49] E. Vereecken, S. Roels, Hygric performance of a massive masonry wall: How do the mortar joints influence the moisture flux? Constr. Build. Mater. vol. 41 (2013) 697–707.
[50] V.M. Nik, S.O. Mundt-Petersen, A.S. Kalagasidis, P. De Wilde, Future moisture loads for building facades in Sweden: Climate change and wind-driven rain, Build. Environ. vol. 93 (2015/11/01/ 2015) 362–375.
[51] "EN ISO 15927-3, Hygrothermal performance of buildings-Calculation and presentation of climatic data. Part 3: calculation of a driving rain index for vertical surfaces from hourly wind and rain data," ed: European Committee for Standardization, 2009.
[52] J. Langmans, T.Z. Desta, L. Alderweireldt, S. Roels, Field study on the air change rate behind residential rainscreen cladding systems: a parameter analysis, Build. Environ. vol. 95 (2016) 1–12.
[53] M. Rahiminejad and D. Khovalyg, "Review on ventilation rates in the ventilated air-spaces behind common wall assemblies with external cladding," Build. Environ. vol. 190, p. 107538, 2021/03/01/ 2021.
[54] E. 15026, *Hygrothermal performance of building components and building elements. Assessment of moisture transfer by numerical simulation* . 2007.
[55] J.F. Straube, "Moisture control and enclosure wall systems," Doctor of Philosophy in Civil Engineering, University of Waterloo, 1998.
[56] S. Van Linden, "Fourth Generation Watertightness: A Performance-Based Strategy to Control Rainwater Infiltration in Façade Systems," Ghent University, 2022.
[57] S.K. Shahreza and A.A. Hamid, "Impact of different water penetration criteria and cavity ventilation rates on the risk of mold growth in timber frame walls with brick veneer cladding," in *Journal of Physics: Conference Series*, 2023, vol. 2654, no. 1, p. 012028: IOP Publishing.
[58] C.-M. Capener and K. Sandin, "Performance of a Retrofitted 1950's Multi-Unit Residential Building: Measurements and Calculated Transient Hygrothermal Behaviour," in *Thermal Performance of the Exterior Envelopes of Whole Buildings XII International Conference*, 2013.

Paper VI

Developments in the Built Environment 19 (2024) 100510

Contents lists available at ScienceDirect

Developments in the Built Environment

journal homepage: www.sciencedirect.com/journal/developments-in-the-built-environment

Towards rational decision-making on repointing to mitigate moisture damage in building envelopes: A probabilistic study

Seyedmohammad Kahangi Shahreza [a,*], Mohsen Bayat Pour [a], Akram Abdul Hamid [b]

[a] Division of Structural Engineering, Department of Building and Environmental Technology, Lund University, John Ericssons väg 1, SE-223 63, Lund, Sweden
[b] Division of Building Physics, Department of Building and Environmental Technology, Lund University, John Ericssons väg 1, SE-223 63, Lund, Sweden

ARTICLE INFO

Keywords:
Repointing
Building envelope
Brick masonry
Hygrothermal simulation
Mold assessment
Moisture content

ABSTRACT

Repointing is a prevalent maintenance practice in Northern Europe aimed at mitigating moisture-related damage in brick masonry buildings. Although commonly used, evidence of its effectiveness is limited. This study assesses repointing's role in reducing damage risks by conducting a probabilistic hygrothermal analysis of two wall types: timber frame walls and masonry cavity walls. Results indicate that repointing could reduce the mold index in timber frame walls and moisture content in the autoclaved aerated concrete (AAC) layer of masonry cavity walls, particularly in walls with visible defects. However, its impact is minimal on walls without significant deficiencies. Moreover, the study suggests that repointing, given its labor-intensive and costly nature, may not always be the most judicious maintenance strategy. It recommends a selective repointing approach, suiting the specific conditions and needs of the wall based on its location, orientation, and existing state, rather than a blanket application across all façade sections.

1. Introduction

1.1. Background

Brick masonry façades serve as critical barriers in protecting building envelopes from climatic factors such as wind-driven rain (WDR). Despite their notable longevity and durability, moisture-related deterioration remains a significant concern, with WDR identified as a primary moisture source (Briggen et al., 2009). The phenomenon of WDR is associated with increased moisture content in external masonry walls, creating a risk of water penetration (Johansson et al., 2014; Ott et al., 2015; Carmeliet and Blocken, 2004). Such infiltration can adversely affect building envelopes (Abuku et al., 2009), leading to compromised insulation, microbial growth (Abuku et al., 2009; Calle and Van Den Bossche, 2021), and the decay of timber components (Vandemeulebroucke et al., 2021a).

In Sweden, an estimated one-third of the building stock suffers from moisture-related damage (Boverket, 2010), resulting in material degradation, mold growth, the presence of unpleasant odors, and diminished indoor air quality. These issues are not only detrimental to the structural health of buildings but also have profound implications on construction practices (Bayat Pour et al., 2022). Similar challenges have been reported in Belgium and across various European nations, where excess moisture and inadequate water tightness are identified as predominant concerns. Analysis of damage cases in Belgium (De Vos, 2019; Van Linden and Van Den Bossche, 2022) revealed that the majority of these issues arise from water penetration through the building envelope. This observation is corroborated by findings in France, where 64% of all reported damage cases between 2018 and 2020 were linked to deficiencies in the building envelope's watertightness (Observatoire de la Qualité de, 2021), highlighting the critical need for effective rainwater management strategies.

The primary pathways for water penetration in brick walls are identified as imperfections at brick–mortar interfaces (Groot and Gunneweg, 2004; Groot and Gunneweg, 2010; Slapø et al., 2017; Kahangi Shahreza et al., 2021; Kahangi Shahreza et al., 2022; Kahangi Shahreza, 2024) and preexisting cracks or deficiencies (Groot and Gunneweg, 2004; Kahangi Shahreza, 2024; Calle and Van Den Bossche, 2017), which vary in terms of width and location. These vulnerabilities become increasingly significant over time, with crack formation in claddings exacerbated by temperature and moisture gradients, frost action, settlements, and dynamic loads. Prior research on water penetration through cracked masonry has established a direct correlation between

* Corresponding author.
E-mail addresses: mohammad.kahangi@kstr.lth.se (S. Kahangi Shahreza), mohsen.bayat_pour@kstr.lth.se (M. Bayat Pour), akram.abdul_hamid@byggtek.lth.se (A. Abdul Hamid).

https://doi.org/10.1016/j.dibe.2024.100510
Received 18 May 2024; Received in revised form 24 July 2024; Accepted 24 July 2024
Available online 25 July 2024

Abbreviations

(AAC)	Autoclaved aerated concrete
(WDR)	Wind-driven rain
(OSB)	Oriented strand board
(LHS)	Latin hypercube sampling
(CoV)	Coefficient of variation
(ACR)	Air change rate
(SMHI)	Swedish Meteorological and Hydrological Institute
(SC)	Simulation case

the volume of penetrated water and the width of cracks (Groot and Gunneweg, 2004; Selvarajah and Johnston, 1995; Grimm, 1988; Akhavan et al., 2012). An experimental investigation by Kahangi Shahreza (Kahangi Shahreza, 2024) revealed that water penetration rates could increase two to fivefold depending on the severity of deficiencies and crack widths, occurring at lower saturation levels compared to masonry without any known deficiencies.

Despite the considerable impact of rainwater penetration on the hygrothermal performance of building envelopes, the scope of research in this domain often remains limited by the scarcity of comprehensive input data (Van Linden and Van Den Bossche, 2022). The current practice, as per the North American Standard (ASHRAE 160–2021) (ASHRAE Standard, 2021), is to assume that only 1% of WDR deposited on a façade penetrates behind the cladding. Meanwhile, other studies have attempted to establish criteria for incorporating rainwater penetration into hygrothermal analyses (Kahangi Shahreza et al., 2022; Calle et al., 2020). However, these criteria may not accurately represent the conditions of many historical and existing façades, which often feature cracks and other defects (Calle and Van Den Bossche, 2017; Van Linden, 2022). A new proposed criterion, derived from an experimental study conducted by Kahangi Shahreza (Kahangi Shahreza, 2024), suggests that water penetration could vary depending on the extent of deficiencies and the width of cracks. Additionally, water penetration may occur at different saturation levels prior to full saturation.

Given the prevalence of imperfections in real-world clay brick walls, regular maintenance, such as repointing, is essential to mitigate water penetration risks and avoid the need for expensive remedial measures. Repointing, a common repair technique, significantly enhances the resistance of masonry walls to WDR (Groot and Gunneweg, 2004; Fishburn et al., 1938; Fusade et al., 2019; Kahangi, 2021; Nijland et al., 2024). Kahangi Shahreza's experimental study (Kahangi Shahreza, 2024) demonstrated a 70% reduction in water penetration for masonry with deficiencies after repointing.

Repointing is typically conducted 40–50 years after a building's construction, adhering to standardized checklists (Kahangi Shahreza et al., 2020). Beyond the time since construction, the degree of mortar joint erosion on different façade parts is crucial in deciding on repointing. Additional criteria for repointing include the presence of hairline cracks on mortar joint surfaces, large crack widths, and detected voids (Tindall, 1987; Stockbridge, 1989; Holland, 2012). However, the establishment of more rigorous criteria is necessary, as the rationale behind some existing recommendations may be subject to scrutiny (Kahangi Shahreza et al., 2020). Moreover, decisions regarding repointing frequently take into account the entire façade, even though only one side may be predominantly exposed to severe WDR or exhibit cracks and eroded mortar joints. In such instances, it may not be necessary to repoint all façade orientations. Therefore, an assessment of the repointing benefits in mitigating rainwater penetration damage is essential before any decision is made.

1.2. Objectives of the study

Recent reviews, such as those by Bayat Pour et al. (2024), have highlighted significant gaps in the field of probabilistic hygrothermal analysis, particularly regarding the treatment of modeling uncertainty and the stochastic nature of material properties and ambient conditions. The current study addresses these gaps by focusing on the effects of repointing, which is considered a detailed element within probabilistic hygrothermal models. The relevance of the model is enhanced by the incorporation of stochastic parameters that reflect the material properties of brick, which have been underemphasized in prior studies. The gap related to ambient and boundary conditions uncertainties is addressed by including different orientations in the probabilistic hygrothermal analysis, further highlighting the novelties of this research. This comprehensive approach is facilitated through an experimental design framework, wherein 96 simulation cases are structured, each comprising 100 scenarios, resulting in a total of 9600 simulations. This method promotes informed decision-making regarding repointing by facilitating the evaluation of building envelopes' performance in managing moisture-related challenges.

2. Materials

While timber frame cavity walls featuring brick masonry veneer are usually built in Sweden, the use of masonry cavity walls with an inner leaf constructed from AAC has not been as widespread in recent years. Timber frame walls are susceptible to mold growth (Vanpachtenbeke et al., 2017; Nath et al., 2022), especially in areas exposed to intense WDR, whereas AAC-based masonry cavity walls often suffer from moisture damage due to increased moisture content within the AAC element (Capener and Sandin, 2013). The presence of mold on timber components or insulation not only poses health risks to occupants but also necessitates immediate detection and remediation efforts, which can incur substantial economic impacts over the building's lifecycle (Bayat Pour et al., 2022). Fig. 1 illustrates a schematic of the timber frame wall with brick veneer as modeled in this study.

Moisture damage within masonry cavity walls featuring AAC as the inner leaf is primarily due to increased moisture levels in the AAC layer (Capener and Sandin, 2013). This issue may arise from the inadequacy

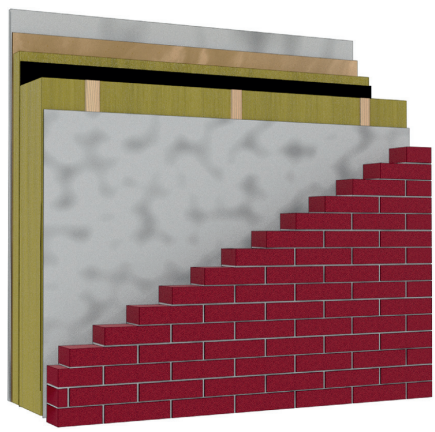

Fig. 1. Schematic of a modern timber frame wall with brick veneer constructed in Sweden (total thickness of approximately 415 mm). The composition from the exterior to the interior includes brick masonry veneer (120 mm), an air gap (30 mm), gypsum board (16 mm), wood fiber insulation (170 mm), a vapor retarder, additional wood fiber insulation (50 mm), oriented strand board (OSB) (12 mm), and another layer of gypsum board (16 mm).

of the air gap provided within these wall types, which compromises water drainage and impedes the wall's ability to dry effectively. Consequently, this type of wall is more susceptible to moisture damage, including dampness and indoor mold growth, particularly in regions experiencing high levels of WDR. Fig. 2 depicts a schematic of a masonry cavity wall constructed between 1940 and 1970 in Sweden, as modeled in this study. As shown in Fig. 2, the model includes a 10 mm air gap, which was not originally designed to serve as a drainage cavity for water penetration or to facilitate wall drying. Instead, this gap was introduced primarily to simplify the bricklaying process during construction and may be partially filled with extruded mortar.

It should be noted that repointing is primarily effective in reducing rainwater penetration through the outer leaf of masonry cavity walls but does not alter the properties of the brick itself, including pore structure and moisture absorption capacity. Consequently, the deterioration of the outer brick layer, including issues related to moisture content and susceptibility to frost damage, remains relatively unaffected by repointing. While repointing is considered a moisture management strategy, its impact on the outer layer is limited to aesthetic improvements.

3. Methods

This study utilizes probabilistic hygrothermal simulations to examine the efficacy of repointing to mitigate the risk of damage due to WDR-induced water penetration. It evaluates two types of wall constructions: timber frame walls with brick veneer exteriors and masonry cavity walls comprising AAC as the inner leaf with a brick masonry outer leaf. The analysis incorporates a range of variables, such as geographic location and façade orientation, and integrates empirical data on water penetration gathered from experimental studies on masonry conducted both before and after repointing (Kahangi Shahreza, 2024).

In the domain of building physics, deterministic modeling was traditionally the preferred technique, treating inputs such as material properties and climatic conditions as fixed quantities. However, despite its widespread application, this method could not be effective in adequately addressing uncertainties inherent in these variables. Consequently, deterministic modeling often depends on a single or limited set of simulations to determine if a design satisfies or violates the specified analysis criteria. In contrast, probabilistic modeling treats these inputs as stochastic variables, acknowledging and incorporating the uncertainties associated with them. Adopting a probabilistic approach

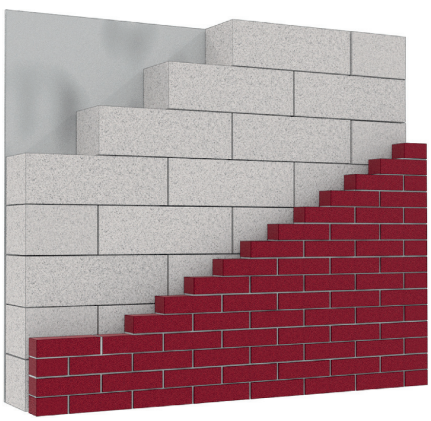

Fig. 2. Schematic of a masonry cavity wall built between 1940 and 1970 in Sweden, featuring brick as the outer leaf and autoclaved aerated concrete (AAC) as the inner leaf (total thickness of approximately 345 mm). From the exterior to the interior, the layers include brick masonry (120 mm), an air gap (10 mm), AAC (200 mm), and gypsum board (16 mm).

facilitates estimating the likelihood of failure, thereby providing more reliable insights for the decision-making process. To this end, the present study utilizes a probabilistic approach for 96 distinct simulation cases.

The investigation into convergence is needed to determine the required number of simulations for the probabilistic analysis. Bayat Pour et al. (Bayat Pour et al., 2023) introduced an equation aimed at facilitating convergence analysis within probabilistic hygrothermal analysis. This involves systematically increasing the number of simulations. The convergence criterion involves tracking the change in the target variable, expressed as the average of maximum mold index and the average of moisture content in this study, over the previous ten iterations. Each iteration consists of 10 distinct scenarios, with an additional 10 scenarios added in each subsequent iteration. As per (Bayat Pour et al., 2023), the simulation process continues until the convergence value drops below the predefined threshold of 0.005. Equation (1) is utilized to compute the convergence value:

$$\varepsilon_i = \frac{\left|\sum_{i-9}^{i-5} OF_i - \sum_{i-4}^{i} OF_i\right|}{\sum_{i-4}^{i} OF_i} \tag{1}$$

Here, i represents the current iteration number (greater than 10), OF_i denotes the ith iteration of the objective function, and ε_i signifies the convergence value of OF_i (i.e., average of maximum mold index and average of moisture content in this study). In this research, the convergence study demonstrated that all 96 case studies require a minimum of 100 scenarios (10 iterations; each has 10 scenarios), collectively amounting to 9600 simulations.

3.1. Simulation

The hygrothermal simulations are conducted using Delphin 6.1 1D (Delphin), a commercial software designed to simulate the transport of heat, air, and moisture through porous building materials and envelopes. The validity of this software has been established through field measurements and experimental studies (Laukkarinen and Vinha, 2011; Alkan and Yazıcıoğlu, 2023; Scheffler, 2008). Although it would be preferable to conduct specific experimental validations for each scenario in this study, this was not feasible due to the extensive range of scenarios and practical constraints such as time and cost. Instead, key simulation parameters, including brick absorption properties and water penetration, were derived from robust experimental data (Kahangi Shahreza, 2024), ensuring reliability within the defined scenarios and providing a solid empirical basis. This investigation limits its focus to a typical wall cross-section, excluding specific construction details such as corners or joints. Although modeling a brick veneer as a homogeneous layer introduces certain limitations, prior research has shown that this simplification can produce satisfactory results under realistic climatic conditions (Vereecken and Roels, 2013). It should be noted that this study explicitly focuses on the random nature of the moisture properties of brick without studying the moisture behaviors at material boundaries (such as mortar layers) or at the air film on both surfaces of the wall.

The study examines three locations within Sweden—Gothenburg, Rensjön, and Uppsala—each representing distinct climate zones. Gothenburg, located on the southwestern coast, experiences an oceanic climate. Rensjön, situated in northern Sweden, has a subarctic climate, while Uppsala, in the south-central eastern part, features a humid continental climate. These geographical locations are depicted in Fig. 3.

The simulations utilize material properties (Table 1) sourced from existing literature (Kahangi Shahreza, 2024; Bayat Pour et al., 2023) and the Delphin software database (Delphin). For the timber frame wall configuration, a vapor barrier with an Sd-value (equivalent diffusion air layer thickness) of 5 m is incorporated between the two layers of wood fiber insulation. To prepare for the probabilistic hygrothermal analysis, a finite set of scenarios is generated using the Latin hypercube sampling (LHS) technique (Wyss and Jorgensen, 1998). LHS is a well-known sampling method, considered for its efficiency when dealing with

Fig. 3. Geographical locations of the three cities evaluated in this study.

limited sample sizes (Zhao, 2012; Helton and Davis, 2000; Macdonald, 2009). This method is particularly favored in research, especially for complex model analyses, due to its significant reduction in computational demands (Helton and Davis, 2003; McKay et al., 2000). Supporting this, Macdonald's work (Macdonald, 2009) highlights the superiority of LHS in comparison to traditional Monte Carlo sampling under analogous conditions.

The results of the hygrothermal simulations are exported in accordance with postprocessing requirements. These outputs include temperature and relative humidity data pertinent for evaluating mold growth potential in timber frame walls, as well as moisture content information for the AAC layer in masonry cavity walls. In examining the impact of repointing on the mold index and moisture content, the decision to model certain parameters as normal distributions while treating others deterministically is based on the unique attributes and relevance of each factor. Given that this study primarily aims to explore the effects of repointing, which directly influences water absorption and penetration rates in brick masonry, only the properties related to brick absorption and water penetration rates are modeled as distributions, as detailed in Tables 1 and 2. Conversely, the properties of other materials involved in this study are represented by their mean values.

The Delphin database (Delphin) was employed to establish the outdoor convective heat exchange coefficient, set at 12 W/(m^2·K). The outdoor vapor diffusion coefficient is calculated using the Lewis relation based on the convective heat exchange coefficient through the built-in feature in the simulation settings. While a value of 0.7 was considered for the solar absorption coefficient, the long-wave emissivity, influenced by surface color and texture, was determined to be 0.9. The reduction/splash factor, set at 0.8, quantifies the proportion of rainwater that is available for capillary absorption by the wall, indicating that WDR is diminished by 20% to account for water that splashes away and does not contribute to moisture penetration. Additionally, the interior surface heat transfer coefficient was established at 8 W/(m^2·K). These parameters are summarized in Table 2. Initial conditions for the materials assumed a temperature of 20 °C and a relative humidity of 80%, consistent with the default settings in Delphin. The resistance to heat transfer at the exterior surfaces is represented by a coefficient that captures both convective and radiative heat exchange. This coefficient, termed the heat transfer coefficient, is adjusted to be wind-dependent, varying according to wind speed to more accurately reflect environmental conditions. In the simulation model, the outer layer of the wall was set to represent the properties of red brick, specifically the solar absorption coefficient and long-wave emissivity.

Table 2
Values for indoor and outdoor conditions applied in this study.

Variable	Value
Outdoor convection heat exchange coefficient [W/(m^2 K)]	12
Solar absorption coefficient [−]	0.7
Long-wave emissivity [−]	0.9
Reduction/splash coefficient of WDR [−]	0.8
Indoor surface heat transfer coefficient (convective + radiative) [W/(m^2 K)]	8
Indoor surface vapor diffusion coefficient [s/m]	2.5 × 10^{-8}
Air change rate (ACR) [h^{-1}]	10

Table 1
Material properties used in hygrothermal simulations, where N(μ, σ) denotes normal distribution with μ and σ as mean and standard deviation, respectively, and CoV stands for coefficient of variation.

	Bulk density (D_B $\left[\frac{kg}{m^3}\right]$)	Specific heat capacity (C_p $\left[\frac{J}{kg \cdot K}\right]$)	Porosity (θ_{por} $\left[\frac{m^3}{m^3}\right]$)	Thermal conductivity (λ_{dry} $\left[\frac{W}{m \cdot K}\right]$)	Water absorption coefficient (A_w $\left[\frac{kg}{m^2 \cdot s^{0.5}}\right]$)	Vapor diffusion resistance factor (μ_{VDR} [−])	Saturation point (θ_{eff} [m^3/m^3])
Brick (Kahangi Shahreza, 2024; Zhao, 2012)	N(2029.1, 43.9) CoV = 2.2%	N(889, 10.67) CoV = 1.2%	N(0.268, 0.035) CoV = 13.1%	N(0.548,0.077) CoV = 14%	N[a](0.16, 0.021) CoV = 13.1% N[b](0.14, 0.021) CoV = 19.1%	N(18.01, 0.018) CoV = 0.1%	N(0.166, 0.022) CoV = 13.0%
Air cavity (Calle et al., 2020)	1.3	1050	1	0.138	0.0000001	0.4	0.017
AAC (Delphin)	390	850	0.77	0.12	0.08	8	435
Gypsum board (as a water-resistive barrier) (Bayat Pour et al., 2023; Delphin)	745.07	1825.94	0.72	0.18	0.18	10.95	574.9
Wood fiber insulation (Delphin)	160.85	1661.87	0.89	0.039	0.0029	3.45	550
OSB (Bayat Pour et al., 2023; Delphin)	630	1880	0.4	0.13	0.0019	467	350
Gypsum board (Delphin)	745.07	1825.94	0.72	0.18	0.18	10.95	574.9

Two values for brick's water absorption coefficient (A_w) were reported.
[a] A_w before repointing and.
[b] A_w after repointing.

Cavity ventilation was factored into the model by assuming a constant air change rate (ACR) of 10 h^{-1}. This assumption is supported by findings from a study by Langmans et al. (2016), which suggest that cavity ventilation rates behind brick veneers typically range from 1 to 10 h^{-1}. The choice of an ACR of 10 h^{-1} is employed in other studies (Calle et al., 2020; Kahangi Shahreza and Abdul Hamid, 2023), which consider it a realistic value for walls constructed with brick masonry. While a recently published study (Bayat Pour and Kahangi Shahreza, 2024) underlines the impact of varying ACRs (0–20 h^{-1}) on mold growth, this study focuses specifically on the effect of repointing on moisture-related issues, narrowing the probabilistic input variables to the brick material properties and water penetration before and after repointing.

3.1.1. Initial input values

For the studied locations, historical climate data, including temperature (°C), relative humidity (%), rain intensity (mm/h), wind direction (degrees), wind velocity (m/s), air pressure (hPa), shortwave diffuse radiation (W/m^2), and shortwave direct radiation (W/m^2), were sourced from the Swedish Meteorological and Hydrological Institute (SMHI). Due to the absence of long-wave counter radiation data in the SMHI database, this variable was acquired from the Meteonorm meteorological database (Remund et al., 2020), which provides hourly climate data generated from measurements taken over a typical year. Hygrothermal analyses spanned a period of five years, from 2018 to 2023. To mitigate the potential impact of initial conditions on the results, the climate data for the year 2018 was replicated for an additional two years before commencing the primary simulations. Over this five-year span, the annual average rainfall in Gothenburg, Rensjön, and Uppsala was recorded at 879, 491, and 488 mm, respectively. The average yearly temperatures were 9.85, −0.70, and 7.97 °C for Gothenburg, Rensjön, and Uppsala, respectively.

The semi-empirical model outlined in ASHRAE Standard 160–2021 (ASHRAE Standard, 2021) was considered to determine the WDR coefficient, which determines the amount of rainwater impinging on the building façades. This coefficient is derived by multiplying the rain exposure factor (F_E), the rain deposition factor (F_D), and an empirical constant (F_L). The F_E, influenced by local topography and building height, varies from 0.7 for sheltered sites with buildings under 10 m to 1.5 for areas with severe exposure and buildings over 20 m tall. For this study, an F_E of 1.4 was selected, applicable to buildings 10–20 m in height exposed to severe weather conditions. The F_D takes on values of 0.35 for walls under steep-slope roofs, 0.5 for walls beneath low-slope roofs, and 1 for walls experiencing direct rain runoff, the latter being the assumption for this analysis. F_L, an empirical constant, is set at 0.2 s/m, resulting in a WDR coefficient of 0.28 s/m for the purposes of this model.

Indoor climatic conditions are correlated with outdoor temperature in accordance with the adaptive indoor climate model presented in standard EN 15026:2008 (EN 15026, 2007) and WTA leaflet 6.2 (WTA 6, 2014). When the outdoor temperature falls below 10 °C, the indoor temperature is maintained at 20 °C, and at outdoor temperatures above 20 °C, it is set to 25 °C. Between outdoor temperatures of 10 and 20 °C, indoor temperature exhibits a linear variation between 20 and 25 °C. A normal moisture load with an added 5% safety margin is assumed for indoor relative humidity, varying linearly between 35% and 65%, as outdoor temperatures range from −10 to 20 °C. This climate condition aligns with the recommended design climate for residential spaces according to DIN 4108-3 (DIN 4108, 2018). Thus, within this study, the sole part where a 5% margin is considered is interior relative humidity according to the model since reaching the proposed relative humidity values (35%–65%) is challenging in existing buildings.

3.2. Water penetration criteria

In the experimental study conducted by Kahangi Shahreza (Kahangi Shahreza, 2024), water penetration caused by WDR and the corresponding saturation levels at the onset of penetration were measured for brick masonry specimens. These specimens included those with deficiencies (featuring a crack length of 50 mm and widths ranging from 0.3 to 0.9 mm) and those devoid of any known deficiencies. The effect of repointing on water penetration in masonry was evaluated through repointing these specimens. For the purpose of the present study, the experimental findings from Kahangi Shahreza (Kahangi Shahreza, 2024) are integrated into the probabilistic hygrothermal analyses, providing foundational data needed for accurately assessing the impact of repointing on masonry walls.

Visual inspection is employed to assess the wall conditions; however, identifying walls with substandard workmanship, which may include voids, cracks, and extruded mortar joints, poses challenges. Additionally, in real-world scenarios, accurately determining the width and length of deficiencies or cracks poses difficulties since they can be in the form of voids, hairline cracks, cracks through the thickness of the wall, vertical cracks at head joints, and may entail other uncertainties related to their shape and tortuosity. Consequently, the current study categorizes brick masonry cladding into two distinct groups that can be easily distinguished through visual inspection: group G – façades in good standard condition and group D – façades in deficient condition. The former denotes walls with high-quality workmanship and without major erosion, cracks, or deficiencies, whereas the latter encompasses walls exhibiting deficiencies, cracks, and relatively poor workmanship.

The experimental results related to specimens with cracks and deficiencies from Kahangi Shahreza (Kahangi Shahreza, 2024) are applied in simulating walls classified under condition D. In contrast, simulation cases depicting walls in good standard condition (condition G) utilize results for brick masonry without noted deficiencies or cracks (Kahangi Shahreza, 2024). Table 3 presents the probability distributions for the saturation level threshold and leakage (the fraction of WDR penetrating the wall) for brick masonry both before and after repointing. These distributions suggest that water penetration in masonry walls may not occur if the moisture content of the brick veneer remains below the saturation threshold. Beyond this threshold, a portion of the WDR, depending on the wall's condition, is likely to penetrate. As outlined in Table 3, the Weibull distribution (W) provided a good fit for all datasets regarding saturation level as well as leakage. It is important to highlight that in instances where the saturation level threshold in sampling exceeded 100%, it was constrained to a maximum of 100%.

Furthermore, it has been demonstrated that repointing could reduce the water absorption rate of brick masonry (Fusade et al., 2019). To factor this reduction into the modeling in this study, a decrease in the water absorption coefficient (A_w) of bricks after repointing is considered, as detailed in Table 1.

The placement of the moisture source within hygrothermal simulations, representing water penetration, is a subject without a unified approach in the literature (Kahangi Shahreza et al., 2022; Calle et al., 2020; Van Linden, 2022). ASHRAE Standard 160–2021 (ASHRAE Standard, 2021) suggests that the moisture source should be uniformly distributed across the water-resistive barrier. However, in scenarios lacking such a barrier, a technical justification for the moisture source's location is required. Introducing the moisture source into a layer with moisture storage capability can lead to saturation of that layer, with any

Table 3
Probability distributions of experimental data concerning water penetration as moisture source; Weibull(λ, k): Weibull distribution with λ and k representing scale parameter and shape parameter, respectively.

	Saturation level threshold [%]	Leakage [%]
Condition G before repointing	W(95.95, 29.23)	W(2.44, 1.12)
Condition D before repointing	W(84.55, 12.02)	W(8.80, 1.57)
Condition G after repointing	W(93.53, 17.93)	W(0.89, 1.18)
Condition D after repointing	W(94.52, 17.39)	W(2.29, 1.13)

excess moisture being automatically adjusted out of the moisture balance in the subsequent time step, as per the Delphin software's functionality (Calle et al., 2020; Van Linden, 2022). Notably, when specifying a precise limited location, the rate of water penetration within a single time step may exceed the storage capacity of that layer, causing quick saturation of grid cells and consequently restricting water penetration due to an automated cut-off process. Attempting to address this, the moisture source in this study is strategically distributed across a broader area. The moisture source was positioned across a 10 mm section of the gypsum board layer for timber frame walls with a brick veneer, serving as a makeshift water-resistive barrier. For masonry cavity walls, in the absence of a designated water-resistive barrier, the moisture source was uniformly distributed across a 10 mm section of the AAC layer. This approach helps moderate the water penetration rate and moisture distribution more effectively, reducing the likelihood of quick saturation.

3.3. Damage risk indicators

3.3.1. Mold index

Three primary damage criteria are commonly used to evaluate the performance of timber frame walls with brick veneer cladding: the potential for mold growth, the decay of timber elements, and susceptibility to frost damage. This study focuses on evaluating the risk of mold growth on the outermost surface of the timber studs, which are among the most vulnerable components in this type of construction. The Finnish mold growth model (Finnish mould growth model, 2023), originating from the VTT model (Viitanen and Ojanen, 2007; Viitanen et al., 2015), is utilized to assess the risk of mold growth. The selection of this mold model is based on its comprehensive applicability across various material types, effectively accounting for the influences of different surface conditions and treatments through sensitivity and degradation classifications. A higher mold index correlates with an increased risk of mold growth. The mold index classifications utilized in this model are detailed in Table 4.

The mold index values are employed for comparative analysis across different conditions and wall types, facilitating the evaluation of relative risks associated with mold growth. These values enable the comparison of the effectiveness of repointing to reduce these risks by highlighting areas where the risk may be comparatively higher or lower. It is important to note that while these indices help quantify the impact of repointing, they are not absolute values of damage risks within the walls (Vandemeulebroucke et al., 2021b, 2023).

3.3.2. Moisture content

As previously discussed, AAC has a high moisture retention capacity, necessitating efficient strategies for the expulsion of excess moisture. Elevated moisture content within AAC leads to a significant increase in its thermal conductivity, highlighting the critical need for effective drying measures (Sandin, 1984). Additionally, increased moisture levels across the wall assembly can pose health hazards, primarily through the promotion of mold growth on interior surfaces and the prevalence of damp conditions within the structure (Bayat Pour et al., 2022). Therefore, this study assesses the moisture content in AAC under various scenarios, both before and after the repointing process, to serve as an indicator of wall performance and potential damage risk.

Table 4
Mold index classifications of the Finnish mold growth model (Finnish mould growth model, 2023).

Index M	mold growth	Notes
0	No mold growth	Spores not activated
1	Growth (microscope)	Initial stages of growth
2	Clear growth (microscope)	Coverage 10% of the studied area (microscope)
3	Growth (naked eye)	Growth covers less than 10% of the studied area (visual)
	Clear growth (microscope)	Growth covers less than 50% of the studied area (microscope)
4	Clear growth (naked eye)	Coverage of more than 10% (Visual)
	Rich growth (microscope)	Coverage of more than 50% (microscope)
5	Rich growth (naked eye)	Coverage more than 50% (Visual)
6	Very rich growth	Coverage around 100%

4. Results and discussion

4.1. Timber frame wall

The analysis of maximum mold indexes is presented through probability distributions for each simulation case (SC) in Table 5. Notably, the mold index is consistently higher for all cases prior to repointing. This index diminishes after repointing, influenced by the wall's condition, location, and orientation. Specifically, before repointing, SC 4, representing walls in a deficient state in Gothenburg facing south, recorded the highest mold index of 4.04. The lowest pre-repointing mold index of 0.16 was observed for SC 13, depicting walls in good condition located in Rensjön facing west. After repointing, the maximum and minimum mold indexes were noted as 3.29 and 0.15 for SC 4 and SC 13, respectively. Fig. 4 shows the simulation cases exhibiting the highest mold index under each wall condition across all evaluated locations.

The most significant decrease in mold index was realized in SC 6, dropping from 3.48 to 2.66. The smallest reduction was observed in SCs 9 and 13, where the post-repointing decrease was marginal, at 0.01. These results suggest that repointing is particularly beneficial for walls identified as being in deficient condition. In comparison, the mold index reduction for walls already deemed in good condition was minor. For instance, in SC 18 (deficient walls in Uppsala facing north), the mold index decreased by 0.79, from 1.76 to 0.97 after repointing. This reduction contrasts with a mere 0.09 decrease observed in SC 17 (good condition walls in Uppsala facing north), indicating that repointing may offer limited improvements for walls already in satisfactory condition. Similarly, for SC 22 (deficient walls in Uppsala facing west), the mold index dropped from 1.50 to 0.83, whereas SC 21 (good condition walls in Uppsala facing west) saw a negligible reduction of 0.03. These findings highlight repointing's efficacy in enhancing the performance of walls with cracks and deficiencies, attributed primarily to its significant impact on reducing water penetration.

Figs. 5–7 illustrate the variation in mold index over a five-year period for selected timber frame walls in different locations, both before and after repointing. Specifically, Fig. 5 presents data for SC 2, a timber frame wall in Gothenburg facing north, representative of a deficient condition before and after repointing. Fig. 6 details SC 10, situated in Rensjön, facing north, and in a deficient condition. Fig. 7 focuses on SC 20, located in Uppsala, facing south, also in a deficient condition, before and after the repointing. The shaded areas in these figures represent the range of possible mold indexes across all scenarios, with the solid red line indicating the average mold index. The results exhibit a broader range of discrepancies before repointing, particularly for walls in deficient conditions in Gothenburg, as summarized in Table 5. This variation is attributed to several factors: a) the limitation of water penetration, considered as a moisture source in hygrothermal simulations, after repointing; b) the potential for significant variance in water penetration in walls in deficient conditions (as detailed in Table 3), a phenomenon that is less pronounced in walls in good condition; and c) the higher WDR load in Gothenburg, relative to Rensjön and Uppsala, which contributes to increased water penetration and, consequently, a greater discrepancy in mold index results, as depicted in Figs. 5–7.

In Sweden, swift action is mandated by building regulations and practical considerations upon mold detection due to the associated

Table 5
Results (mean, standard deviation, CoV) in terms of maximum mold index [−] on timber element for different simulation cases (SCs) before and after repointing.

Simulation case	Location	Orientation	Condition	Index before repointing	Index after repointing	Difference in mold index [−]
1	Gothenburg	N	G	(2.04, 0.033, 1.63)	(1.87, 0.034, 1.83)	0.17
2			D	(2.39, 0.102, 4.26)	(2.03, 0.032, 1.59)	0.36
3		S	G	(3.33, 0.137, 4.12)	(3.08, 0.140, 4.54)	0.25
4			D	(4.04, 0.211, 5.22)	(3.29, 0.124, 3.78)	0.75
5		W	G	(2.71, 0.102, 3.76)	(2.47, 0.100, 4.04)	0.24
6			D	(3.48, 0.121, 3.47)	(2.66, 0.095, 3.57)	0.82
7		E	G	(3.22, 0.213, 6.60)	(3.00, 0.217, 7.24)	0.22
8			D	(3.76, 0.123, 3.28)	(3.20, 0.204, 6.37)	0.56
9	Rensjön	N	G	(0.76, 0.031, 4.13)	(0.75, 0.031, 4.20)	0.01
10			D	(0.98, 0.112, 11.46)	(0.76, 0.030, 4.02)	0.22
11		S	G	(0.78, 0.055, 7.05)	(0.73, 0.053, 7.28)	0.05
12			D	(1.03, 0.123, 11.84)	(0.77, 0.050, 6.53)	0.26
13		W	G	(0.16, 0.010, 6.22)	(0.15, 0.010, 6.65)	0.01
14			D	(0.29, 0.014, 4.80)	(0.16, 0.010, 6.24)	0.13
15		E	G	(0.81, 0.025, 3.15)	(0.78, 0.024, 3.12)	0.03
16			D	(0.90, 0.048, 5.36)	(0.80, 0.025, 3.16)	0.10
17	Uppsala	N	G	(0.99, 0.148, 15.02)	(0.90, 0.143, 15.84)	0.09
18			D	(1.76, 0.181, 10.28)	(0.97, 0.146, 15.02)	0.79
19		S	G	(2.40, 0.066, 2.73)	(2.19, 0.067, 3.04)	0.21
20			D	(3.01, 0.113, 3.74)	(2.36, 0.064, 2.69)	0.65
21		W	G	(0.84, 0.040, 4.80)	(0.81, 0.037, 4.57)	0.03
22			D	(1.50, 0.056, 3.73)	(0.83, 0.040, 4.81)	0.67
23		E	G	(0.78, 0.045, 5.79)	(0.75, 0.045, 6.04)	0.03
24			D	(0.86, 0.048, 5.60)	(0.77, 0.044, 5.76)	0.09

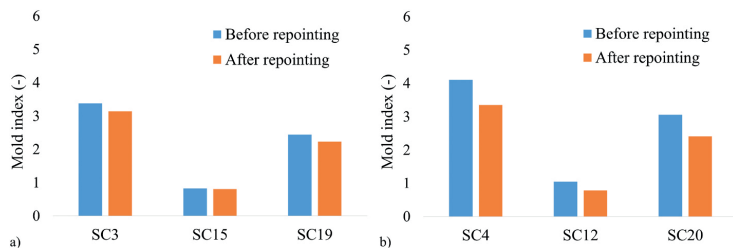

Fig. 4. Mold index before and after repointing for simulation case with the maximum mold index in each location for walls in a) good standard condition and b) deficient condition.

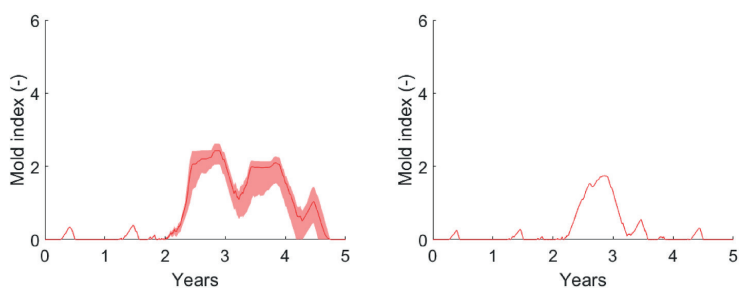

Fig. 5. Interval for possible mold index of 100 scenarios for SC 2 – timber frame wall in Gothenburg, facing north, in deficient condition before (left) and after (right) repointing.

health risks (Heseltine and Rosen, 2009). Several studies consider mold growth exceeding a mold index of one on the interior face of the wall as a failure threshold (Bayat Pour et al., 2023), as it poses health concerns. However, this mold index level may not have practical applicability, as a general building inspection may not detect mold growth at this index. Mold indexes below three are usually not visible to the naked eye and thus are not typically considered in regular visual inspection processes unless building users report or complain, potentially leading to a more detailed visual inspection. ASHRAE Standard 160–2021 (ASHRAE Standard, 2021) recommends that to mitigate mold growth issues, the mold index should not exceed three. The probability of failure for each SC, where the mold index exceeds one and three, is summarized in Table 6.

While the results suggest that repointing can diminish the risk of mold growth in timber frame walls with masonry veneer—particularly for walls in deficient conditions—the decision to undertake repointing should be guided by a thorough benefit analysis. When adopting a mold index of one as the failure threshold, the probability of failure for all SCs

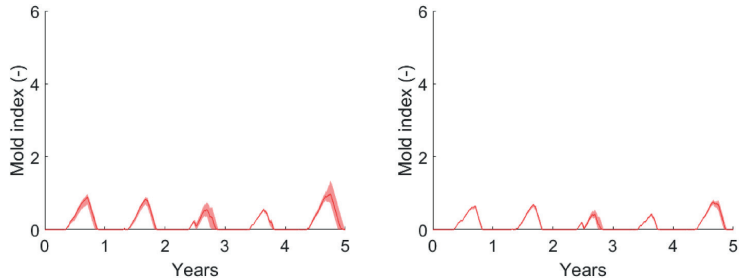

Fig. 6. Interval for possible mold index of 100 scenarios for SC 10 – timber frame wall in Rensjön, facing north, in deficient condition before (left) and after (right) repointing.

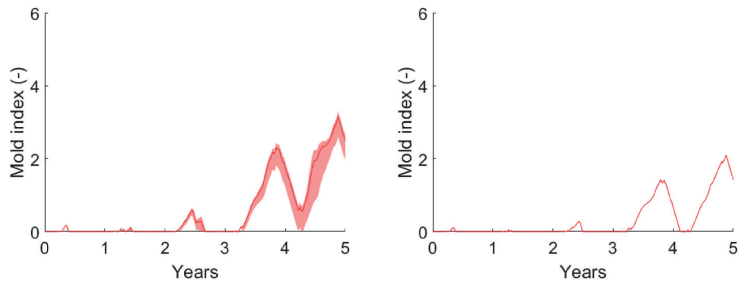

Fig. 7. Interval for possible mold index of 100 scenarios for SC 20 – timber frame wall in Uppsala, facing south, in deficient condition before (left) and after (right) repointing.

Table 6
Probability of failures for each simulation case (SC) where the mold index is above 1 and 3.

Simulation case	Index before repointing	Failure 1* [%]	Failure 3** [%]	Index after repointing	Failure 1* [%]	Failure 3** [%]
1	(2.04, 0.033, 1.63)	100	0	(1.87, 0.034, 1.83)	100	0
2	(2.39, 0.102, 4.26)	100	0	(2.03, 0.032, 1.59)	100	0
3	(3.33, 0.137, 4.12)	100	98	(3.08, 0.140, 4.54)	100	73
4	(4.04, 0.211, 5.22)	100	100	(3.29, 0.124, 3.78)	100	97
5	(2.71, 0.102, 3.76)	100	2	(2.47, 0.100, 4.04)	100	0
6	(3.48, 0.121, 3.47)	100	100	(2.66, 0.095, 3.57)	100	0
7	(3.22, 0.213, 6.60)	100	87	(3.00, 0.217, 7.24)	100	64
8	(3.76, 0.123, 3.28)	100	100	(3.20, 0.204, 6.37)	100	83
9	(0.76, 0.031, 4.13)	0	0	(0.75, 0.031, 4.20)	0	0
10	(0.98, 0.112, 11.46)	41	0	(0.76, 0.030, 4.02)	0	0
11	(0.78, 0.055, 7.05)	0	0	(0.73, 0.053, 7.28)	0	0
12	(1.03, 0.123, 11.84)	49	0	(0.77, 0.050, 6.53)	0	0
13	(0.16, 0.010, 6.22)	0	0	(0.15, 0.010, 6.65)	0	0
14	(0.29, 0.014, 4.80)	0	0	(0.16, 0.010, 6.24)	0	0
15	(0.81, 0.025, 3.15)	0	0	(0.78, 0.024, 3.12)	0	0
16	(0.90, 0.048, 5.36)	6	0	(0.80, 0.025, 3.16)	0	0
17	(0.99, 0.148, 15.02)	53	0	(0.90, 0.143, 15.84)	36	0
18	(1.76, 0.181, 10.28)	100	0	(0.97, 0.146, 15.02)	45	0
19	(2.40, 0.066, 2.73)	100	0	(2.19, 0.067, 3.04)	100	0
20	(3.01, 0.113, 3.74)	100	67	(2.36, 0.064, 2.69)	100	0
21	(0.84, 0.040, 4.80)	0	0	(0.81, 0.037, 4.57)	0	0
22	(1.50, 0.056, 3.73)	100	0	(0.83, 0.040, 4.81)	0	0
23	(0.78, 0.045, 5.79)	0	0	(0.75, 0.045, 6.04)	0	0
24	(0.86, 0.048, 5.60)	0	0	(0.77, 0.044, 5.76)	0	0

Failure 1*: Probability of failure where mold index is above 1.
Failure 3**: Probability of failure where mold index exceeds 3.

in Gothenburg remains at 100% both before and after repointing. Using a mold index of three as the failure threshold reveals that repointing does not substantially reduce the probability of failure in most SCs in Gothenburg, with the exception of SC 6. In this particular case, repointing significantly decreases the probability of failure from 100% to 0%. For SC 4, despite a reduction in the average mold index from 4.04 to 3.29, the mold index exceeds the visibility threshold for the naked eye, with the probability of failure marginally dropping from 100% to 97%. In such cases, repointing alone may not suffice to enhance the wall condition effectively.

In Rensjön and Uppsala, most SCs exhibit a mold index below three prior to repointing, suggesting that mold presence might not be readily detectable visually. Although repointing results in mold risk improvements across all SCs, the mold index both before and after repointing remains below the visual detection threshold, with the exception of SC 20. In SC 20, the probability of failure is notably reduced from 67% to 0%. Consequently, in most situations, opting for repointing may not be a judicious choice unless explicit damage is reported by building occupants or mold is observed upon visual inspection.

4.2. Masonry cavity wall

The simulation results concerning the AAC layer's moisture content are detailed in Table 7, encompassing the average moisture content (%), calculated as the mean of all simulation results for each case from 2018 to 2023. Prior to repointing, the highest average moisture content was observed in SC 28, which involved walls in a deficient state located in Gothenburg facing south, recording a value of 6.93%. The lowest average moisture content before repointing was noted in SC 37 (walls in good condition located in Rensjön facing west) at 2.44%. After repointing, these values adjusted to 5.01% for SC 28 and 2.30% for SC 37.

The analysis further suggests that repointing notably enhances the condition of walls identified as deficient rather than those in good condition. For instance, SC 30 experienced a 1.46% decrease in moisture content from 4.90% to 3.44% following repointing. In comparison, SC 29 exhibited a modest reduction of 0.76% in average moisture content after repointing, indicating a slight improvement for walls previously in good condition. Additionally, SC 48, which involved deficient walls facing east in Uppsala, exhibited a moisture content decrease from 5.18% to 3.79%. Meanwhile, SC 47, representing walls in good condition in the same location, showed a 0.64% decrease in average moisture content after repointing. These results highlight repointing's efficacy for walls with deficiencies, primarily attributed to its significant impact on mitigating water penetration, evidenced by an average leakage reduction from 7.9% to 2.2% (Kahangi Shahreza, 2024).

Fig. 8 illustrates the variation in water content over a five-year span for SC 28, a masonry cavity wall situated in Gothenburg, facing south, and identified with deficient conditions, both before and after repointing. Similarly, Fig. 9 shows the water content variations for SC 33, positioned in Rensjön, facing north, and categorized in good standard condition through the same period, before and after the repointing process. Meanwhile, Fig. 10 presents the water content changes for SC 48, a masonry cavity wall in Uppsala, facing east, also under deficient conditions, before and after repointing. The shaded areas within these figures denote the range of maximum and minimum potential water content, while the solid red lines represent the average outcomes derived from scenarios.

As discussed earlier, while moisture content alone does not directly signify a damage risk, sustained dampness or prolonged exposure to moisture can lead to decreased thermal comfort, the emergence of unpleasant odors, and significant damage to wall components. Although there is no definitive failure threshold based on the moisture content of the AAC layer, exceeding the permissible moisture levels for solid masonry walls, as summarized in Table 8, necessitates remedial actions (Hola, 2017). The masonry cavity wall configuration analyzed in this study resembles a solid masonry construction, with the brick façade and AAC layer positioned next to each other without an adequate intervening air gap. The mentioned threshold levels can offer a preliminary framework for critical values, aiding in the decision-making process regarding the necessity of repointing. While repointing has proven to be beneficial in lowering the AAC layer's moisture content, in areas characterized by a subarctic climate with minimal WDR exposure, such as Rensjön, repointing might involve undue expenses if the moisture content falls within acceptable limits prior to intervention.

4.3. Influence of parameters

4.3.1. Wall condition

As indicated in Tables 5 and 6, repointing significantly enhances the condition of walls classified as deficient, demonstrating reductions in both mold index and moisture content, regardless of the wall's location or orientation. The efficacy of repointing depends on the initial condition of the wall, particularly its susceptibility to water penetration, which in turn is influenced by the saturation level in the brick masonry veneer and the wall's overall condition. Walls with existing cracks and deficiencies exhibit water penetration at lower saturation levels and with greater leakage than those considered to be in good standard

Table 7
Results (mean, standard deviation, CoV) in terms of average moisture content [%] of AAC layer for different simulation cases before and after repointing.

Simulation case	Location	Orientation	Condition	MeanSum[a] Before repointing	MeanSum After repointing	Difference in MeanSum [%]
25	Gothenburg	N	G	(2.71, 0.016, 0.59)	(2.48, 0.002, 0.08)	0.23
26			D	(3.18, 0.060, 1.89)	(2.65, 0.015, 0.57)	0.53
27		S	G	(5.26, 0.362, 6.88)	(4.30, 0.252, 5.86)	0.96
28			D	(6.93, 0.569, 8.21)	(5.01, 0.328, 6.55)	1.92
29		W	G	(3.68, 0.089, 2.42)	(2.92, 0.018, 0.62)	0.76
30			D	(4.90, 0.178, 3.63)	(3.44, 0.076, 2.21)	1.46
31		E	G	(4.19, 0.131, 3.13)	(2.94, 0.010, 0.34)	1.25
32			D	(5.42, 0.329, 6.07)	(3.89, 0.126, 3.24)	1.53
33	Rensjön	N	G	(2.92, 0.094, 3.22)	(2.64, 0.042, 1.59)	0.28
34			D	(3.33, 0.180, 5.41)	(2.82, 0.079, 2.80)	0.51
35		S	G	(2.87, 0.101, 3.52)	(2.57, 0.028, 1.09)	0.30
36			D	(3.35, 0.154, 4.60)	(2.73, 0.111, 4.07)	0.62
37		W	G	(2.44, 0.030, 1.23)	(2.30, 0.006, 0.26)	0.14
38			D	(2.66, 0.046, 1.73)	(2.43, 0.035, 1.44)	0.23
39		E	G	(2.77, 0.040, 1.44)	(2.42, 0.004, 0.17)	0.35
40			D	(3.27, 0.139, 4.25)	(2.74, 0.050, 1.82)	0.53
41	Uppsala	N	G	(3.58, 0.062, 1.73)	(3.20, 0.022, 0.69)	0.38
42			D	(4.26, 0.095, 2.23)	(3.48, 0.066, 1.90)	0.78
43		S	G	(4.04, 0.147, 3.64)	(3.29, 0.031, 0.94)	0.75
44			D	(5.09, 0.251, 4.93)	(3.84, 0.136, 3.54)	1.25
45		W	G	(3.12, 0.020, 0.64)	(2.84, 0.009, 0.32)	0.28
46			D	(3.67, 0.041, 1.12)	(3.05, 0.012, 0.39)	0.62
47		E	G	(4.05, 0.075, 1.85)	(3.41, 0.094, 2.76)	0.64
48			D	(5.18, 0.139, 2.68)	(3.79, 0.088, 2.32)	1.39

[a] This is the average of the sum of all results for scenarios run for each simulation case.

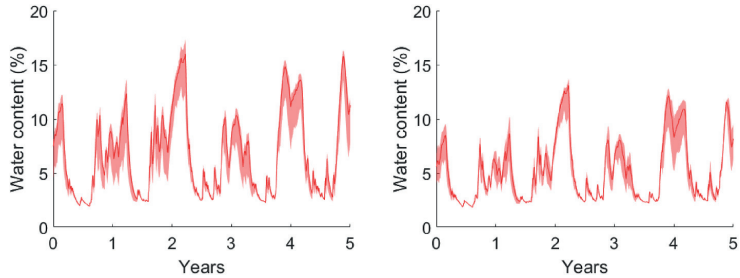

Fig. 8. Range of possible water content for SC 28—a masonry cavity wall in Gothenburg facing south in deficient condition—before (left) and after (right) repointing.

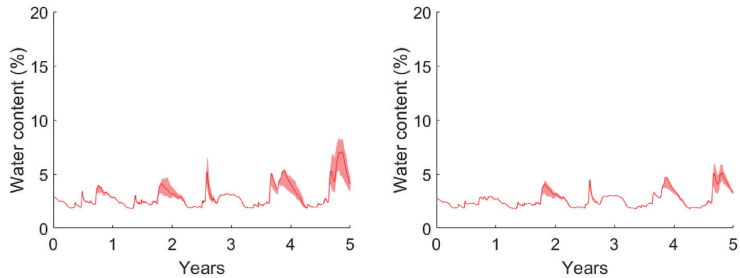

Fig. 9. Range of possible water content for SC 33—a masonry cavity wall in Rensjön facing north in good standard condition—before (left) and after (right) repointing.

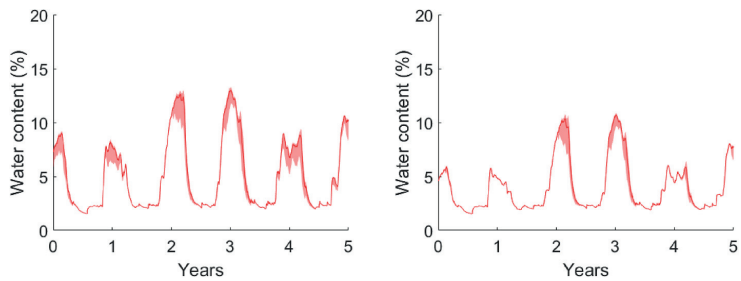

Fig. 10. Range of possible water content range for SC 48—a masonry cavity wall in Uppsala facing east and in deficient condition—before (left) and after (right) repointing.

Table 8
Classification of moisture content of brick walls (Hola, 2017).

Moisture content [%]	Classifications	Notes
0–3	Masonry wall with permissible moisture content	
3–5	Masonry wall with elevated moisture content	There is a need to undertake action to reduce moisture content
5–8	Medium damp masonry wall	
8–12	Very damp masonry wall	
>12	Wet masonry wall	

condition.

After repointing, the mold index reduction averages 0.28, with a more pronounced decrease of 0.45 observed in deficient walls compared to 0.11 in walls in good condition, as depicted in Fig. 11a. For masonry cavity walls, repointing leads to a 0.95% reduction in the AAC layer's average moisture content for deficient walls, while walls in good standard condition see a decrease of 0.53%, as illustrated in Fig. 11b. The most substantial change in mold index after repointing, a reduction of 0.82, occurs in SC 6 for deficient walls, whereas the minimal difference, 0.09, is noted in SC 24. For walls initially in good standard condition, the largest and smallest reductions in mold index are 0.25 (SC 3) and 0.01 (SCs 9 and 13), respectively. For walls in deficient condition, the maximum and minimum differences in average moisture content for the AAC layer in masonry cavity walls are observed in SC 28 (a 1.92% reduction) and SC 38 (a 0.23% reduction), respectively. The greatest and least differences in average moisture content for walls in good condition are 1.25% (SC 31) and 0.14% (SC 37), respectively.

These findings underscore that repointing yields marginal benefits for walls already in good condition, especially in low WDR areas. Conversely, repointing significantly mitigates mold risk and enhances

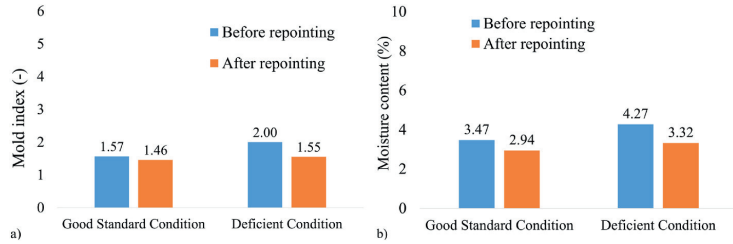

Fig. 11. Impact of repointing on walls classified as good standard and deficient, focusing on a) mold index and b) AAC layer's moisture content.

overall wall performance by reducing moisture content for walls with cracks or voids.

4.3.2. Location

Three studied locations were considered: Gothenburg, Rensjön, and Uppsala, each characterized by distinct average rainfall and temperature profiles. Fig. 12 illustrates the average annual WDR intensity, I_A [l/m^2], for these locations across various orientations from 2018 to 2023. Gothenburg experiences the highest WDR, averaging approximately 600 l/m^2, significantly more than Rensjön and Uppsala, which have average WDRs of about 200 and 150 l/m^2, respectively. Consequently, an increased damage index is expected for Gothenburg, correlating with the higher WDR exposure—a finding that aligns with the results summarized in Tables 5 and 6 Notably, the most significant mold index and average water content were recorded for SCs 4 and 28, respectively, with a mold index of 4.04 (SC 4) and a water content of 6.93% (SC 28).

The impact of repointing is markedly more significant in Gothenburg than in Rensjön and Uppsala. The reduction in mold index across Gothenburg, Rensjön, and Uppsala after repointing averages 0.42, 0.10, and 0.32, respectively, as shown in Fig. 13a. When evaluating timber frame walls deemed in good standard condition, repointing results in mold index reductions of 0.22, 0.02, and 0.09 for Gothenburg, Rensjön, and Uppsala, respectively; for walls identified as deficient, repointing leads to more substantial mold index reductions of 0.62, 0.18, and 0.55 for the respective locations. In terms of masonry cavity walls, the average water content of the AAC layer after repointing decreases by 1.08%, 0.37%, and 0.76% for Gothenburg, Rensjön, and Uppsala, respectively, as shown in Fig. 13b. For walls in deficient condition, the decrease in water content following repointing is 1.36%, 0.47%, and 1.01% for Gothenburg, Rensjön, and Uppsala, respectively, whereas walls in good standard condition see corresponding reductions of 0.80%, 0.27%, and 0.51%.

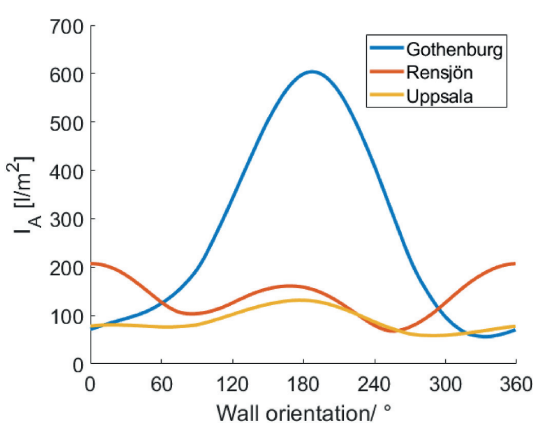

Fig. 12. Average annual WDR for three examined locations, considering different wall orientations (0° north, 90° east), between 2018 and 2023.

These results highlight the effectiveness of repointing in mitigating mold risk in timber frame walls and reducing moisture content in masonry cavity walls, particularly in regions with high WDR exposure. The benefits are most pronounced for walls in poor condition.

4.3.3. Orientation

While there is a noted correlation between the effectiveness of repointing and factors such as wall condition and location, the relationship between repointing and wall orientation presents further complexity. This complexity arises from the interaction between exposure to WDR and solar radiation. Orientations that expose walls to higher amounts of solar radiation with subsequent rain events may generate different hygrothermal behaviors compared to those with less solar exposure. Moisture absorption into the wall occurs primarily through capillary action during rain events, particularly in absorbent cladding materials. Moisture transport into the wall through vapor is compounded when such events are followed closely by periods of intense solar radiation. The rapid heating of the wall's surface accelerates the evaporation process, creating a significant vapor pressure gradient. Depending on the materials ' permeability and buffering capacity, this gradient can drive moisture deeper into the wall or pull it toward the interior. The elevated temperatures on the exterior surface can increase water vapor pressure within the wall, enhancing outward and inward moisture transport. Without adequate ventilation in the cavity, this dual-direction drying process results in significant amounts of moisture transported to the inner surfaces, potentially increasing the risk of high relative humidity, interstitial condensation, and, thereby, associated damage. Consequently, it becomes challenging to ascertain the necessity of repointing solely based on orientation.

The impact of façade orientation on mold index and average water content varies across different locations. As depicted in Fig. 12, walls in Gothenburg facing south are the most exposed walls concerning WDR, whereas, in Rensjön, the north-facing orientation experiences the highest WDR exposure. In Gothenburg, south-facing walls, being critically exposed to WDR, showed the most substantial reduction in average water content (1.44%) after repointing. Moreover, repointing led to significant reductions in the average maximum mold index for walls facing west and south by 0.53 and 0.50, respectively. Although the difference in mold index reduction between south and west orientations is minimal, the greater decrease in south-facing walls may be attributed to the exposure to solar radiation, which is more pronounced in the south.

In Rensjön, the variation in average annual WDR across orientations is less pronounced compared to that in Gothenburg. In Rensjön, walls facing both north and south are predominantly exposed to WDR, as shown in Fig. 12. Following repointing, the most notable reductions in mold index were observed for walls facing south and north, with reductions of 0.16 and 0.12, respectively. For masonry cavity walls, differences in average water content after repointing were relatively small across orientations, with the most significant decrease (0.46%)

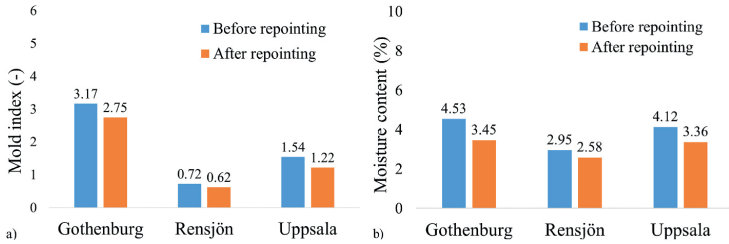

Fig. 13. Results before and after repointing in terms of a) mold index and b) AAC layer moisture content for three studied locations.

occurring in south-facing walls.

These findings highlight that while repointing can reduce mold index and water content depending on the wall condition and location, outcomes related to wall orientation are less predictable. For deficient walls, expected higher water penetration rates render repointing a more effective measure for mitigating mold risk and moisture content. Specifically, in Gothenburg, the substantial WDR load and the resulting high level of leakage lead to a more significant anticipated enhancement in wall performance following repointing. In Rensjön and Uppsala, where WDR exposure is lower, anticipated benefits from repointing are diminished. The interplay between solar radiation and WDR exposure complicates a definitive assessment of repointing's impact based on orientation, particularly in areas with minimal WDR.

4.4. Limitations and further considerations

This research investigated the impact of repointing on the hygrothermal performance of building envelopes, focusing on two wall types across three distinct locations. In Sweden, various wall configurations with brick masonry are prevalent, including masonry cavity walls with both inner and outer leaves of brick, masonry cavity walls with a brick outer leaf and lightweight aggregate concrete as the inner leaf, and mass masonry walls with a thickness equivalent to one and a half brick lengths. Moreover, timber frame walls incorporate diverse insulation materials such as glass wool, rock wool, cellulose, and wood fiber, resulting in various wall types. This study aimed to include locations representative of Sweden's varied climatic conditions comparable to those found in many other Northern European regions. However, it is important to note that WDR conditions in some regions, including the west coast of Norway and Scotland, can be more severe than those considered in this study. While some locations experience extreme WDR loads where repointing could be notably beneficial, others are subject to minimal WDR, thus diminishing the potential hygrothermal performance benefits of repointing. These considerations aim to enhance the comprehension of repointing's effects across two wall types and three climatic scenarios.

The study's primary objective was to assess the impact of repointing in reducing damage risks across various wall types. A probabilistic hygrothermal assessment was conducted, considering a distribution for brick properties and water penetration criteria. Despite identifying water penetration as a key factor, the necessity to assess the influence of additional parameters on the damage risk, including the mold index and moisture content, remains. The material properties of layers, such as brick, AAC, gypsum board, OSB, and wood fiber insulation, exhibit variability due to manufacturing differences and brand diversity, introducing a wide array of potential wall compositions in the construction sector.

The utilized WDR coefficient was set at 0.28 s/m, yet there is a need to be aware of its complex dependence on numerous factors such as local wind flow, topography, building layout, and the spatial arrangement of surrounding structures and urban features. Given that the default value in Delphin is 0.07 s/m, the amount of WDR deposited on the simulated walls will be four times less than what has been considered in this study. This, in turn, can significantly impact the moisture content of the wall and water penetration amount since implementing different WDR calculation methods in the simulations could considerably alter the perceived risk of mold growth (Defo et al., 2019). While the current study focuses on the isolated effects of repointing to understand its impact more clearly, future research could benefit from a stochastic approach where variables like the WDR coefficient are treated as probabilistic to capture the range of possible real-world conditions.

Additionally, this study integrated an ACR of 10 h^{-1} in simulations, contrasting with real-world observations, which indicate that the ACR within ventilated cavities could reach approximately 50 h^{-1} (Rahiminejad and Khovalyg, 2021). Factors such as poor workmanship or design flaws could severely restrict the air cavity's functionality, leading to much lower ACRs.

The experimental study by Kahangi Shahreza (Kahangi Shahreza, 2024), which utilized masonry specimens with artificially induced cracks to investigate the impact of repointing on water penetration, serves as an important input for the probabilistic hygrothermal analyses done in this study. While providing controlled conditions for systematic research, these simulated cracks might not fully replicate the varied characteristics and types of cracks in real-world masonry. Such differences might affect the direct applicability of these findings, especially when considering buildings where cracks can be irregular, vary widely in size, and evolve over time. Therefore, although the results from Kahangi Shahreza (Kahangi Shahreza, 2024) form a fundamental part of our probabilistic hygrothermal analyses, the translation of these results to practical scenarios must be approached cautiously, acknowledging the potential variations in real-life cracks. It is important, thus, to consider the possible discrepancies between simulated and actual crack characteristics. In this study, to facilitate a nuanced understanding of the discrepancies between simulated and real-world cracks, masonry specimens were categorized into two groups: Category D, which represents façades in deficient condition with cracks, and Category G, which denotes masonry without noticeable cracks, signifying good standard condition.

In this study, the water penetration criteria for repointing were based on an experimental study employing a single mortar type for the repair of cracked masonry. The choice of repointing mortar can significantly influence the degree of water penetration both before and after repointing. Additionally, this study attempted to differentiate between wall conditions, identifying façades without substantial cracks or erosion and those with evident cracks and defects. This differentiation may complicate the visual inspection process, as buildings might externally appear in good condition (lacking visible cracks or erosion) while internally suffering from substandard workmanship that leaves numerous voids in the head joints.

The inclusion of a moisture source to represent rainwater penetration in hygrothermal analysis software presents its own set of challenges. Though this study considered the total water penetration on the water-resistive barrier in accordance with ASHRAE Standard 160–2021, it is important to consider that a fraction of penetrated water may drain

away from the cavity. Moreover, in walls with a brick masonry veneer, water ingress primarily occurs through the brick-mortar interface, especially at head joints, which are the primary paths of least resistance for water entry. Accurately modeling such localized ingress in simulation tools, particularly those restricted to one-dimensional analysis, is difficult. These tools generally require the ingress to be uniformly distributed despite experimental evidence indicating more localized penetration patterns.

Another challenge involves determining the appropriate size for the moisture source within a layer. Many hygrothermal simulation tools do not account for free water transport, leading to the automatic expulsion of excess water once a layer reaches saturation. For instance, in software such as Delphin, excess water is swiftly removed if the moisture allocated to cell grids causes cell saturation. WUFI offers a solution to this issue by integrating a cut-off feature, which allows for the retention of excess water in saturated materials.

The decision concerning whether the moisture source should cover the entire material layer in the model or be restricted to the surface layer also raises questions. Assigning a moisture source to a narrowly defined area, represented by a limited number of cells, can lead to premature saturation from leakage, necessitating the removal of subsequent water. In this study, the moisture source was distributed over a broader area to enhance its impact, thereby preventing early saturation and the subsequent elimination of excess water.

5. Conclusions

This study aimed to investigate the impact of repointing clay brick walls on reducing mold growth in timber frame walls and decreasing water content in the AAC layer of masonry cavity walls. Through a comprehensive probabilistic hygrothermal analysis encompassing 9600 simulations, the study explored variables such as wall condition, location, and façade orientation. The findings yield several key insights.

- Repointing as a maintenance strategy: Repointing emerges as a viable repair technique for mitigating mold growth risk in timber frame walls and reducing moisture in the AAC layer, particularly for walls in deficient condition and in locations with high WDR exposure, such as Gothenburg. The study revealed a notable average mold index reduction of 0.45 following repointing for walls in deficient condition, compared to a 0.11 reduction for walls in good condition. Similarly, masonry cavity walls experienced an average water content decrease of 0.95% for deficient walls and 0.53% for walls in good condition after repointing.
- Impact by location: The effectiveness of repointing varied significantly across the studied locations. In Gothenburg, repointing led to an average decrease of 0.42 in the mold index for timber frame walls, whereas in Rensjön and Uppsala, the reductions were 0.10 and 0.32, respectively. For masonry cavity walls, Gothenburg saw the most substantial decrease in average water content (1.08%), highlighting repointing's potential to enhance wall performance in regions with high WDR load. The corresponding decrease for Rensjön and Uppsala were 0.37% and 0.76%, respectively.
- Orientation and performance enhancement: The relationship between wall orientation and performance improvement following repointing is nuanced and influenced by the interaction between solar radiation and exposure to WDR. This complicates the establishment of a straightforward relationship between orientation and after-repointing performance enhancement, especially in regions with low WDR loads.

The findings of this study provide a valuable foundation for decision-making regarding repointing, advocating for a more informed approach beyond the conventional maintenance schedule of 40–50 years after construction. This approach, which often lacks a detailed evaluation based on objective condition indicators, can lead to unnecessary expenses and environmental impacts. The insights gained from this research suggest that targeted repointing, focusing only on those wall sections and orientations where significant performance improvements are evident, can optimize cost and resource efficiency. Such a strategy encourages a shift towards partial repointing, offering a solution for optimizing building envelope maintenance while conserving resources.

CRediT authorship contribution statement

Seyedmohammad Kahangi Shahreza: Writing – original draft, Visualization, Software, Methodology, Investigation, Formal analysis, Data curation, Conceptualization. **Mohsen Bayat Pour:** Writing – review & editing, Software, Methodology, Formal analysis, Data curation, Conceptualization. **Akram Abdul Hamid:** Writing – review & editing, Supervision, Formal analysis.

Declaration of Generative AI and AI-assisted technologies in the writing process

While preparing this work, the authors did not use Generative AI. The authors reviewed and edited the content as needed. Readability and language were improved by Elsevier Language Editing Services.

Declaration of competing interest

The authors declare that they have no known competing financial interests or personal relationships that could have appeared to influence the work reported in this paper.

Data availability

Data will be made available on request.

Acknowledgements

The authors gratefully acknowledge the financial support from SBUF - the Development Fund of the Swedish Construction Industry [grant number 14052]; and TMPB - the Masonry and Render Construction Association.

References

Observatoire de la Qualité de la Construction: Édition 2021," 2021.
Abuku, M., Janssen, H., Roels, S., 2009. Impact of wind-driven rain on historic brick wall buildings in a moderately cold and humid climate: numerical analyses of mould growth risk, indoor climate and energy consumption. Energy Build. 41 (1), 101–110.
Akhavan, A., Shafaatian, S.-M.-H., Rajabipour, F., 2012. Quantifying the effects of crack width, tortuosity, and roughness on water permeability of cracked mortars. Cement Concr. Res. 42 (2), 313–320.
Alkan, S.N., Yazıcıoğlu, F., 2023. An analysis on hygrothermal behaviour of traditional timber framed brick infill exterior wall. A|Z ITU J. Fac. Archit. 20 (2), 333–345.
Bayat Pour, M., Niklewski, J., Naghibi, A., Hansson, E.F., 2024. A literature review of probabilistic hygrothermal assessment for building envelopes. Build. Environ., 111756
Bayat Pour, M., Niklewski, J., Naghibi, A., Thöns, S., 2022. Mould reliability analysis combined with mould health risks for decision support. In: Proceedings of the 5th Central European Symposium on Building Physics. CESBP, Bratislava Slovakia, p. 8.
ASHRAE Standard, 2021. Standard 160-2021: Criteria for Moisture Control Design Analysis in Buildings. American Society of Heating, Refrigerating and Air-Conditioning Engineers, Atlanta.
Bayat Pour, M., Kahangi Shahreza, S., 2024. Impact of extruded mortar joints on the hygrothermal performance of brick veneer walls: a probabilistic study. J. Build. Eng., 109936.
Bayat Pour, M., Niklewski, J., Naghibi, A., Hansson, E.F., 2023. Robust probabilistic modelling of mould growth in building envelopes using random forests machine learning algorithm. Build. Environ. 243, 110703.
Boverket, 2010. Teknisk Status I Den Svenska Bebyggelsen - Resultat Från Projektet BETSI.
Briggen, P., Blocken, B., Schellen, H., 2009. Wind-driven rain on the facade of a monumental tower: numerical simulation, full-scale validation and sensitivity analysis. Build. Environ. 44 (8), 1675–1690.
Calle, K., Van Den Bossche, N., 2017. Towards understanding rain infiltration in historic brickwork. Energy Proc. 132, 676–681.

Calle, K., Van Den Bossche, N., 2021. Sensitivity analysis of the hygrothermal behaviour of homogeneous masonry constructions: interior insulation, rainwater infiltration and hydrophobic treatment. J. Build. Phys. 44 (6), 510–538.
Calle, K., Coupillie, C., Janssens, A., Van Den Bossche, N., 2020. Implementation of rainwater infiltration measurements in hygrothermal modelling of non-insulated brick cavity walls. J. Build. Phys. 43 (6), 477–502.
Capener, C.-M., Sandin, K., 2013. Performance of a Retrofitted 1950's Multi-Unit residential building: measurements and calculated Transient hygrothermal behaviour. In: Thermal Performance of the Exterior Envelopes of Whole Buildings XII International Conference.
Carmeliet, J., Blocken, B., 2004. Driving rain, rain absorption and rainwater runoff for evaluating water leakage risks in building envelopes. In: 9th International Conference on Performance of Exterior Envelopes of Whole Buildings (Buildings IX).
Defo, M., Lacasse, M.A., Snell, N., 2019. Assessing the Climate Resilience of Buildings to the Effects of Hygrothermal Loads: Impacts of Wind-Driven Rain Calculation Methods on the Moisture Performance of Massive Timber Walls. National Research Council of Canada. Construction2019/04/30.
Delphin, "https://bauklimatik-dresden.de/delphin/index.php?aLa=en," Accessed August 2023.
DIN 4108-3 - Thermal Protection and Energy Economy in Buildings - Part 3: Protection against Moisture Subject to Climate Conditions - Requirements, Calculation Methods and Directions for Planning and Construction, 2018.
EN 15026, 2007. Hygrothermal Performance of Building Components and Building Elements. Assessment of Moisture Transfer by Numerical Simulation.
Finnish mould growth model, 2023. Building Physics. Tampere Universities.
Fishburn, C.C., Watstein, D., Parsons, D.E., 1938. Water Permeability of Masonry Walls. US Department of Commerce, National Bureau of Standards.
Fusade, L., Orr, S.A., Wood, C., O'Dowd, M., Viles, H., 2019. Drying response of lime-mortar joints in granite masonry after an intense rainfall and after repointing. Heritage Science 7 (1), 1–19.
Grimm, C.T., 1988. Masonry cracks: a review of the literature. Masonry: Materials, Design, Construction, and Maintenance.
Groot, C., Gunneweg, J., 2004. Water permeance problems in single wythe masonry walls: the case of wind mills. Construct. Build. Mater. 18 (5), 325–329.
Groot, C., Gunneweg, J., 2010. The influence of materials characteristics and workmanship on rain penetration in historic fired clay brick masonry. Heron 55 (2).
Helton, J.C., Davis, F.J., 2000. Sampling-based Methods for Uncertainty and Sensitivity Analysis. Sandia National Lab.(SNL-NM), Albuquerque, NM (United States). Sandia.
Helton, J.C., Davis, F.J., 2003. Latin hypercube sampling and the propagation of uncertainty in analyses of complex systems. Reliab. Eng. Syst. Saf. 81 (1), 23–69.
Heseltine, E., Rosen, J., 2009. WHO Guidelines for Indoor Air Quality: Dampness and Mould.
Hola, A., 2017. Measuring of the moisture content in brick walls of historical buildings–the overview of methods. IOP Conf. Ser. Mater. Sci. Eng. 251 (1), 012067. IOP Publishing.
Holland, M., 2012. Practical Guide to Diagnosing Structural Movement in Buildings. John Wiley & Sons.
Johansson, P., et al., 2014. Interior insulation retrofit of a historical brick wall using vacuum insulation panels: hygrothermal numerical simulations and laboratory investigations. Build. Environ. 79, 31–45.
Kahangi, M., 2021. Resistance of Clay Brick Masonry Façades to Wind-Driven Rain: Repointing of Eroded Mortar Joints, vol. 1055. Lund University.
Kahangi Shahreza, S., 2024. Water penetration in cracked clay brick masonry before and after repointing. Construct. Build. Mater. 420 (2024/03/22), 135631.
Kahangi Shahreza, S., Abdul Hamid, A., 2023. Impact of different water penetration criteria and cavity ventilation rates on the risk of mold growth in timber frame walls with brick veneer cladding. J. Phys. Conf. 2654 (1), 012028. IOP Publishing.
Kahangi Shahreza, S., Molnár, M., Niklewski, J., Björnsson, I., Gustavsson, T., 2020. Making decision on repointing of clay brick facades on the basis of moisture content and water absorption tests results–a review of assessment methods. In: Brick and Block Masonry-From Historical to Sustainable Masonry. CRC Press, pp. 617–623.
Kahangi Shahreza, S., Niklewski, J., Molnár, M., 2021. Experimental investigation of water absorption and penetration in clay brick masonry under simulated uniform water spray exposure. J. Build. Eng. 43, 102583.
Kahangi Shahreza, S., Niklewski, J., Molnár, M., 2022. Novel water penetration criterion for clay brick masonry claddings. Construct. Build. Mater. 353, 129109.
Langmans, J., Desta, T.Z., Alderweireldt, L., Roels, S., 2016. Field study on the air change rate behind residential rainscreen cladding systems: a parameter analysis. Build. Environ. 95, 1–12.
Laukkarinen, A., Vinha, J., 2011. Comparison of Calculated and Measured Values of Wall Assembly Tests Using Delphin 5.
Van Linden, S., 2022. Fourth Generation Watertightness: A Performance-Based Strategy to Control Rainwater Infiltration in Façade Systems. Ghent University.
Van Linden, S., Van Den Bossche, N., 2022. Review of rainwater infiltration rates in wall assemblies. Build. Environ. 219 (2022/07/01), 109213.
Macdonald, I.A., 2009. Comparison of Sampling Techniques on the Performance of Monte-Carlo Based Sensitivity Analysis.
McKay, M.D., Beckman, R.J., Conover, W.J., 2000. A comparison of three methods for selecting values of input variables in the analysis of output from a computer code. Technometrics 42 (1), 55–61.
Nath, S., Dewsbury, M., Künzel, H., Watson, P., 2022. Mould growth risks for a clay masonry veneer external wall System in a temperate climate. Atmosphere 13 (11), 1755.
Nijland, T.G., Lubelli, B., van Zundert, K., van Hunen, M., 2024. On the necessity of new hydrophobic treatment after repointing of water repellent masonry. Construct. Build. Mater. 411, 134732.
Ott, S., Tietze, A., Winter, S., 2015. Wind driven rain and moisture safety of tall timber houses–evaluation of simulation methods. Wood Mater. Sci. Eng. 10 (3), 300–311.
Rahiminejad, M., Khovalyg, D., 2021. Review on ventilation rates in the ventilated air-spaces behind common wall assemblies with external cladding. Build. Environ. 190, 107538, 2021/03/01.
Remund, J., Müller, S., Schmutz, M., Graf, P., 2020. Meteonorm Version 8. METEOTEST meteotest. com.
Sandin, K., 1984. Fuktens Inverkan På Energiflödet Genom Ytterväggar.
Scheffler, G.A., 2008. Validation of Hygrothermal Material Modelling under Consideration of the Hysteresis of Moisture Storage.
Selvarajah, S., Johnston, A., 1995. Water permeation through cracked single skin masonry. Build. Environ. 30 (1), 19–28.
Slapø, F., Kvande, T., Bakken, N., Haugen, M., Lohne, J., 2017. Masonry's resistance to driving rain: mortar water content and Impregnation. Buildings 7 (3), 70.
Stockbridge, J.G., 1989. Repointing masonry walls. APT Bull. 21 (1), 10–12.
Tindall, S.M., 1987. Repointing Masonry—Why Repoint. Old-House Journal, pp. 24–31.
Vandemeulebroucke, I., Caluwaerts, S., Van Den Bossche, N., 2021a. Factorial study on the impact of climate change on freeze-thaw damage, mould growth and wood decay in solid masonry walls in Brussels. Buildings 11 (3), 134.
Vandemeulebroucke, I., Caluwaerts, S., Van Den Bossche, N., 2021b. Factorial study on the impact of climate change on freeze-thaw damage, mould growth and wood decay in solid masonry walls in Brussels (in English). Buildings 11 (3). Art. no. 134.
Vandemeulebroucke, I., Kotova, L., Caluwaerts, S., Van Den Bossche, N., 2023. Degradation of brick masonry walls in Europe and the Mediterranean: Advantages of a response-based analysis to study climate change. Build. Environ. 230, 109963.
Vanpachtenbeke, M., Langmans, J., Van den Bulcke, J., Van Acker, J., Roels, S., 2017. Hygrothermal behaviour of timber frame walls finished with a brick veneer cladding. Energy Proc. 132, 363–368.
Vereecken, E., Roels, S., 2013. Hygric performance of a massive masonry wall: How do the mortar joints influence the moisture flux? Construct. Build. Mater. 41, 697–707.
Viitanen, H., Ojanen, T., 2007. Improved model to predict mold growth in building materials. Thermal Performance of the Exterior Envelopes of Whole Buildings X–Proceedings CD, pp. 2–7.
Viitanen, H., Krus, M., Ojanen, T., Eitner, V., Zirkelbach, D., 2015. Mold risk classification based on comparative evaluation of two established growth models. Energy Proc. 78, 1425–1430.
De Vos, J., 2019. Building Defects in the Belgian Construction Industry: Trend Analysis. Ghent university, Faculty of Engineering and Architecture. *master's thesis*.
WTA 6, 2014. 2 Leaflet - Simulation of Heat and Moisture Transfer.
Wyss, G.D., Jorgensen, K.H., 1998. A Users Guide to LHS: Sandias Latin Hypercube Sampling Software. Sandia National Lab.(SNL-NM), Albuquerque, NM (United States).
Zhao, J., 2012. Development of a Novel Statistical Method and Procedure for Material Characterization and a Probabilistic Approach to Assessing the Hygrothermal Performance of Building Enclosure Assemblies. Syracuse University.

Colleagues' perspectives

"Since 2019 I have had the pleasure of working with Mohammad in his PhD-project on clay brick masonry's response to wind-driven rain. With talent, intellectual sharpness and hard work he managed to advance our knowledge on a valuable part of our building stock. His open-mindedness and kindness have made him a highly appreciated colleague and teacher. Thank you, Mohammad!"
Dr. Miklós Molnár, Associate Professor, Main Supervisor

"It has been a pleasure to follow your journey as co-supervisor over the years, and I truly hope that we continue working together. This thesis is a testament to your excellence in research, but your dedication to teaching and your critical perspective on current challenges in academia are no less important. Congratulations on this outstanding achievement!"
Dr. Jonas Niklewski, Associate Professor, Co-Supervisor

Lund University
Faculty of Engineering
Division of Structural Engineering
Report: TVBK-1059
ISBN: 978-91-8104-062-3 (print)
ISBN:978-91-8104-063-0 (electronic)
ISSN: 0349-4969